

Project ID N°: **101036449**

Call: **H2020-LC-GD-2020-3**

Topic: **LC-GD-8-1-2020** - Innovative, systemic zero-pollution solutions to protect health, environment, and natural resources from persistent and mobile chemicals



Preventing Recalcitrant Organic Mobile Industrial chemicals for Circular Economy in the soil-sediment-water System

Start date of the project: **1st November 2021**

Duration: **42 months**

D2.4 – Guidance document on fate, transport and exposure for PMT's in the environment

Main authors:

Zessner Matthias, Baldwin Dwight, del Val Alonso Laura, Derx Julia, Devau Nicolas, Janssen Gijs, Jou Claus Sònia, Kittlaus Steffen, Knoche Franziska, Liu Meiqi, Markus Arjen, Valstar Johan, Meesters Joris, Meijers Erwin, Obeid Ali A.A., Oudega Thomas James, Pathak Devanshi, Sprenger Christoph, van Gils Jos, Wicke Daniel, Wintersen Arjen, Zhiteneva Veronika, Groot Hans

Lead Beneficiary: **TU Wien**

Type of delivery: **R**

Dissemination Level: **PU**

Filename and version: **PROMISCES_D2.4_Guidance-document (Version 1.0)**

Website: **<https://promiscses.eu/Results.html>**

Due date: **31/10/2024**

This project has received funding from
the European Union's Horizon 2020
research and innovation programme
under grant agreement N°101036449



Authors and their affiliations:

Zessner Matthias¹, Baldwin Dwight⁷, del Val Alonso Laura⁶, Derx Julia², Devau Nicolas³, Janssen Gijss⁴, Jou Claus Sònia⁶, Kittlaus Steffen¹, Knoche Franziska⁷, Liu Meiqi¹, Markus Arjen⁴, Valstar Johan⁴, Meesters Joris⁵, Meijers Erwin⁴, Obeid Ali A.A.², Oudega Thomas James², Pathak Devanshi⁴, Sprenger Christoph⁷, van Gils Jos⁴, Wicke Daniel⁷, Wintersen Arjen⁵, Zhiteneva Veronika⁷, and Groot Hans⁴

¹TU Wien, Institute of Water Quality and Resource Management, Karlsplatz 13, Vienna, Austria

²TU Wien, Institute of Hydraulic Engineering and Water Resources Management, Karlsplatz 13, Vienna, Austria

³BRGM, French Geological Survey, 2 avenue Claude Guillemin, Orléans France

⁴Deltares. Boussinesqweg 1, Delft, the Netherlands

⁵National Institute for Public Health and the Environment (RIVM), Bilthoven, the Netherlands

⁶Eurecat, Plaça de la Ciència 2, Manresa, Catalonia, Spain

⁷Berlin Centre of Competence for Water (KWB), Grunewaldstr. 61-62, Berlin, Germany

Authors of annexes are named at the beginning of the annexes.

© European Union, 2025



This work is licensed under Creative Commons Attribution 4.0 International. To view a copy of this license, visit <https://creativecommons.org/licenses/by/4.0/>

No third-party textual or artistic material included on the publication without the copyright holder's prior consent to further dissemination by other third parties.

Reproduction is authorized provided the source is acknowledged.

Disclaimer

The information and views set out in this report are those of the author(s) and do not necessarily reflect the official opinion of the European Union. Neither the European Union institutions and bodies nor any person acting on their behalf may be held responsible for the use which may be made of the information contained therein.

Document History

This document has been through the following revisions:

Version	Date	Author/Reviewer	Description
0.1	13.01.2025	Matthias Zessner et al.	First draft for review
0.2	31.01.2025	Matthias Zessner et al.	Second draft for validation
0.3	06.02.2025	Steffen Kittlaus et al.	Third draft for quality control
0.4	14.02.2025	Steffen Kittlaus et al.	Fourth draft for approval
1.0	25.02.2025	Matthias Zessner	Final Version for distribution

Authorisation

Authorisation	Name	Status	Date
Review	Dominique Guyonnet	Reviewer	20.01.2025
Validation	Hans Groot	WP2 leader	05.02.2025
Quality Control	Floriane Sermondadaz	IEIC Manager	10.02.2025
Approval	Julie Lions	Project Coordinator	27.02.2025

Distribution

This document has been distributed to:

Name	Title	Version issued	Date of issue
TU Wien	WP2 partner	Version 1.0	03.03.2025
BRGM	WP2 partner	Version 1.0	03.03.2025
Deltares	WP2 partner	Version 1.0	03.03.2025
RIVM	WP2 partner	Version 1.0	03.03.2025
Eurecat	WP2 partner	Version 1.0	03.03.2025
KWB	WP2 partner	Version 1.0	03.03.2025

Executive Summary

Models are used in exposure assessment for a number of reasons. They can help map the temporal and spatial variability of exposure, exposure pathways and exposure routes, and support risk assessment for water bodies where monitoring is lacking. They can be used to identify sources and pathways responsible for current exposures and to assess the impact of potential future developments of persistent, mobile, and toxic chemicals (PMT) exposures in surface water and groundwater. Such scenario assessment may include changes in PMT use, effects of pollution control measures, accidental spills or climate change.

The scope of this document, produced as part of the H2020 PROMISCES project, is to provide guidance for applications of models with a specific focus on model trains for the assessment of exposure to PMTs as part of the predictive risk assessment related to surface and groundwater. This document explains the basic concepts of specific models and how best to use them in model trains in the framework of a tiered approach. The intention is to inform users and interested stakeholders about what needs to be considered when using different methods, what is the best use of specific models, what are the best combinations in model trains and what are their current limitations.

The guidance document presents (i) “screening level” models for the assessment of regional exposure of groundwater from soil pollution and for the assessment of general exposure of air, soil and water at local, regional or global scales, (ii) spatial and temporal explicit approaches for the identification of pollution plumes in the soil-groundwater continuum and (iii) model train applications for the catchment – river – river bank filtration – drinking water continuum.

Exposure of surface water and groundwater to PMT depends on the use patterns and the environmental fate of the chemicals. Emission, fate and transport models incorporate driving factors into documented algorithms. The extent to which a substance persists in surface water can, for instance, be calculated with the “SimpleBox - Aquatic Persistence Dashboard”, based on its physical-chemical characteristics. The presented approach for deriving generic risk limits for soils shows that, depending on regional variations in geo(hydro)logical conditions, the high mobility of some PFAS could lead to strict requirements for materials applied on soil.

For the soil-groundwater continuum, a novel model train is presented which accounts for the main physical and chemical processes controlling the fate and transport of PFAS. For sorption and degradation reactions, several formalisms can be used, allowing one to select the most appropriate according to the PFAS molecular properties and the characteristics of the simulated domain. The results issued from these modelling applications indicate the key role of correctly identifying the main physical, chemical and biological processes controlling fate and transport of PFAS in the studied domain to build a robust conceptual model. To increase the robustness of the model, a thorough model calibration must be performed, preferably using time series measurements of the PFAS concentration in the pore solution at different locations of the contaminated site.

The results confirm the key role of the unsaturated zone in the transfer and long-term migration of PFAS. Nonlinearity and nonideality of sorption reactions were expected for a broad range of PFAS, suggesting using more complex numerical formalism than linear isotherms. Considering the key role of capillary fringe displacement on PFAS transport in the unsaturated zone, the model train seems to be very efficient in performing PFAS simulations, as it can explicitly describe water flow and solute transport at the interface between the unsaturated and saturated zones, avoiding the main pitfall encountered in other numerical approaches.

The combination of stand-alone models in model trains expands the scope that can be covered in the context of a catchment – river – riverbank filtration – drinking water continuum for exposure assessment of surface waters and bank filtered drinking water. Model trains can combine individual models either in a complementary way or in a sequence. A complementary combination may either compare models of different complexity to find out which level of complexity (and associated effort) is needed to answer which questions, or may compare different models with their different strengths and weaknesses in parallel to assess uncertainties and/or use models for scenario evaluation according to their specific capabilities. A sequential combination facilitates a broader application in terms of content and at different spatial resolutions. Clearly defined interfaces are essential for a successful implementation.

Examples of model trains for selected PFAS are presented for the catchment-river interaction in the urban context of the Berlin case and for the whole catchment – river – riverbank filtration – drinking water continuum on the scale of the Upper Danube Basin. The Berlin case demonstrates the application of the sequential model train by combining a city emission model with a city surface water fate and transport model to assess the resulting exposure to PFAS in the city surface waters. The Danube case demonstrates the application of a sequential model train for exposure assessment of bank filtered drinking water by combining large-scale catchment-scale emission models with different types of bank filtration fate and transport models for specific locations in the catchment. In addition, it also demonstrates complementary application by comparing emission models with different strengths and weaknesses for the assessment of multiple scenarios on the catchment scale and different levels of complexity for the fate and transport modelling of bank filtration. The model train has been successfully applied for 10 different PFAS-substances including the assessment of a large range of scenarios.

Current limitations for exposure assessment of PFAS at river basin scale require improvement in scientific understanding as well as additional efforts in administrative data collection and inventory development. Current results of the exposure assessment show the very high relevance of legacy pollution from use of fire-fighting foams or from old municipal landfills. On the administrative level, there is a strong need for improved identification and harmonized inventorying of contaminated sites at national and international (EU) level. The lack of robust, openly available information on production, import-export and therefore use volumes of PFAS at national and EU level is strongly hampering exposure assessment. A major effort is urgently needed to provide this information, as it is decisive for a sound environmental exposure assessment, not only for surface water and groundwater.

In regard to scientific advances, there is a need for more and better understanding of the extent of local groundwater pollution, particularly due to the application of fire-fighting foams or to the presence of municipal landfills. Further improvement of the scientific knowledge about the fate of PFAS in the environment, including their partitioning between different phases (air, water, solids) and the transformation of the so called “precursors” into stable “end-products”

like PFOA, PFOS and short-chain substances is needed to enlarge the number of PFAS that can be included into the exposure assessment. A reproducible and standardised analytical parameter for “total PFAS” or even “total toxicity of PFAS” would be needed to address all relevant PFAS in a combined way as it is a focus of Workpackage 1 of the H2020 PROMISCES project (Togola et al. 2024; Behnisch et al. 2024).

Contents

1. Introduction	19
1.1. Emission, fate and transport modelling for exposure assessment	19
1.2. Scope of the guidance document	21
1.3. Basics of exposure assessment and environmental fate	24
2. Screening level models	27
2.1. Introduction	27
2.2. The SimpleBox - Aquatic Persistence dashboard	28
2.3. Deriving generic risk limits for soils	34
3. Soil - Groundwater interaction	40
3.1. General aspects	40
3.2. Model train combining Hydrus and MODFLOW/MT3DMS	42
3.3. General explanation of case studies	46
3.4. Application for the PluriMetric Pilot experiment	48
3.5. Application of the model train in the CS#7 AFFF-polluted aquifer	58
3.6. Limitations and further outlook	62
4. Catchment – river – riverbank filtration – drinking water	64
4.1. General aspects	65
4.2. Emission models on catchment scale in the context of model trains	66
4.3. Emission model in an urban context	71
4.4. Fate and transport modelling at bank filtration sites	73
4.5. Model train application in an urban setting of Berlin	79
4.6. Model train application in a large catchment	84
4.7. Limitations and outlook	107
5. Discussion and conclusions	111
5.1. Background and scope of the guidance document	111
5.2. Pollution plumes in the soil-groundwater continuum	112
5.3. Modelling of the catchment – river – riverbank filtration – drinking water continuum	112
Bibliography	115
Annexes	120
A. Substance properties to be used in the SB-AP Dashboard	121
B. PluriMetric Pilot experiments	125
B.1. Key concepts to simulate PFAS fate and transport in SGW continuum	125

B.2. Extended description of the PMP experiment	127
B.3. Hydraulic, solute transport and reactive properties for simulations of the CS#6	131
B.4. Simulations of the spatial and temporal pattern of the non-reactive tracer concentration during the PMP experiment	136
C. Large scale investigations in CS#7 AFFF-polluted aquifer	139
C.1. Conceptual model	139
C.2. Model set-up	140
C.3. Results from the unsaturated zone model	143
C.4. Results from fully saturated model	144
C.5. Conclusions	146
D. Catchment Model MoRE for the upper Danube basin	150
D.1. Overview	150
D.2. Modelled PFASs	151
D.3. Modelled Pathways	152
D.4. Basic Model Setup	153
D.5. Approach for Validating the Model	154
D.6. Model Validation	158
D.7. Modelled Pathway Contribution	164
D.8. Risk Maps	168
D.9. Acknowledgements	170
E. PROMISCES watershed model for PM substances (PPM)	173
E.1. Introduction	173
E.2. Methods	174
E.3. Results	185
E.4. Acknowledgements	194
F. CS#2: MODFLOW model of the Szentendre Island	197
G. Scenario modelling for the upper Danube basin	203
G.1. General Considerations	203
G.2. Reference situation	204
G.3. Baseline for Scenarios	204
G.4. Accidental spill scenario (AC)	206
G.5. Water pollution control 1 (WPC1)	209
G.6. Water pollution control 2 (WPC2)	210
G.7. Summary of Scenarios	213
G.8. Scenario results	214

List of Figures

1.1.	Losses of chemicals to the environment via stages of the products life-cycle . .	24
1.2.	Conceptual multimedia box model for environmental fate and exposure	26
2.1.	Aquatic persistence for eight selected substances occurring as dissolved species or the sum of dissolved and sorbed species on a regional, continental and global scale as calculated with the SB-AP Dashboard	31
2.2.	Overview of sensitivity plots for substances with NFBS, 6:2 FTOH and 6:2 FTAB for aquatic persistence (s) vs water degradation rate constant ($\log s^{-1}$) and $\log K_{OW}$	32
2.3.	Conceptual model for the groundwater variant	38
2.4.	Conceptual model for the surface water variant	38
3.1.	Sketch of the model train developed to simulate fate and transport of PFAS in soil-groundwater continuum.	46
3.2.	Measured and simulated concentrations in 6:2 FTSA, 6:2 FTAB and 6:2 FTSAam over time in pore solutions at five depths below the infiltration square during the PMP experiment.	54
3.3.	Measured and simulated concentrations in 6:2 FTSA, 6:2 FTAB and 6:2 FTSAam over time in pore solutions at three depths in the saturated zone in two locations downstream to the infiltration square in the main flow path during the PMP experiment.	56
3.4.	Vertical distribution of main HYDRUS 1D modelled variables in the unsaturated profile	59
3.5.	Downgradient distribution of most abundant PFAS at the site in the saturated groundwater.	60
4.1.	Schema of the circular economy route “semi-closed water cycle”	66
4.2.	Overview of riverine load (Tier 2), pathway-oriented (Tier 3) and source-oriented (Tier 4) approaches.	68
4.3.	Considered substance sources and input paths of watercourse pollution	72
4.4.	Generic PMT substance attenuation heatmaps and breakthrough curves	77
4.5.	Left side: Monthly PFOA loads by path into Berlin’s surface waters, right side: Contributions of the separate sewer system (Sep. sewer), wastewater treatment plants (WWTP) and combined sewer overflows (CSO) to annual rainwater and wastewater discharges.	80
4.6.	Layout of the Berlin surface water model	81
4.7.	Schematic representation of the Flughafensee as a column model	82
4.8.	Simulated concentrations of PFOA in Berlin watercourses	83
4.9.	Map of the Danube catchment upstream of Budapest	85
4.10.	Map of bank filtration sites at Budapest	86

4.11.	Map of bank filtration site at Vienna	87
4.12.	Model validation for the MoRE model	88
4.13.	Modelled contribution of different emission pathways to PFAS loads	89
4.14.	Risk of exceedance of drinking water standards and proposed (E)QS for sum of PFAS in the rivers of the upper Danube catchments	90
4.15.	Attenuation heatmaps and breakthrough curves simulated by the generic bank filtration model at Vienna and Budapest case study sites.	93
4.16.	Box plots of measured versus simulated concentrations of all 10 substances in monitoring wells (MWs) and the pumping well (PW) from 2022–2024	97
4.17.	Development of a PFAS-peak from an accidental spill with AFFF observed at the bank filtration site at Vienna	103
4.18.	Development of a PFAS-peak from an accidental spill with AFFF observed at the bank filtration site at Tahi	104
4.19.	Development of a PFAS-peak from an accidental spill with AFFF into river Danube observed at the bank filtration site at Surány, Budapest.	105
B.1.	Measured and simulated concentrations in bromide and total organic fluoride (orange) over time in pore solution at five depths in the unsaturated and saturated zones below the infiltration square during the PMP experiment. . .	136
B.2.	Measured and simulated concentrations in bromide and total organic fluoride over time in pore solution at three depths in the saturated zone in two locations downstream to the infiltration square in the main flow path during the PMP experiment	137
C.1.	Concentrations of most abundant PFAS in the soil matrix. Black lines represent contact between different lithologies	139
C.2.	Interpolation of PFAS concentration groundwater represented in a map view of the CS#7 site.	141
C.3.	Geometry of the 2D vertical transport model of the fully saturated zone. . . .	142
C.4.	Vertical distribution of main HYDRUS 1D modelled variables in the unsaturated profile	144
C.5.	Fluxes and heads at top and bottom boundaries.	145
C.6.	Downgradient (from the source) distribution of most abundant PFAS at the site. Data obtained during a sampling campaign in autumn 2021. Dashed line represents modelled concentrations of PFOS.	146
C.7.	PFOS concentration distribution at 6 modelled times (days). Concentrations in g/m3.	147
C.8.	Evolution of concentrations of PFOS in groundwater at different depth for the two boreholes close to the source and for the river	148
D.1.	Overview map showing the Danube catchment and the case study #2 area– Upper Danube catchment, including smaller catchment units.	150
D.2.	Map of surface water monitoring sites in subtask 2.2.4.	155
D.3.	Validation graph of the modelled and observed discharge value at each monitoring sites, in area-specific form.	158
D.4.	Validation graph of the modelled load and monitored load for selected PFAS at each validation sites, in area-specific form.	159

D.5.	Validation graph of the modelled load and monitored load for selected PFAS at each validation sites excepts for Alz, in area-specific form.	160
D.6.	Validation graph of the modelled concentrations and monitored concentrations for selected PFAS at each validation sites.	161
D.7.	Validation graph of the modelled concentrations and monitored concentrations for selected PFAS at each validation sites excepts for Alz.	161
D.8.	Validation graph of the PFAS-sum calculated according to DWD (EU 2020) and drafted EQS (EC COM(2022) 540 final) using the modelled concentrations and monitored concentrations at each validation sites.	163
D.9.	Validation graph of the PFAS-sum calculated according to DWD (EU 2020) and drafted EQS (EC COM(2022) 540 final) using the modelled concentrations and monitored concentrations at each validation site excepts for Alz.	163
D.10.	Modelled PFAS emission from each pathway shown in cumulative form in absolute amount. Black dots indicate the load calculated from monitored data.	165
D.11.	Modelled PFAS emission from each pathway shown in proportional form compared to the load calculated from monitored data. Red dashed lines indicate the level of monitored river load, set as 100%.	166
D.12.	Modelled PFAS concentrations from each pathway shown in cumulative form in absolute amount. Black dots indicate the river concentrations monitored at each site.	167
D.13.	Modelled PFAS concentrations from each pathway shown in proportional form compared to the river concentrations monitored at each validation site. Red dashed lines indicate the level of monitored river concentrations, set as 100%.	168
D.14.	Map of risks of model catchments exceeding the standard levels of PFAS-sum for DWD (EU 2020) and drafted EQS (EC COM(2022) 540 final).	170
E.1.	Schematic overview of hydrological processes included in the Wflow model of the upper Danube catchment.	176
E.2.	Model domain.	177
E.3.	Comparison of ERA5 annual precipitation and blended Spartacus-ERA5 annual precipitation	178
E.4.	Spatially variable initialization of the concentration of PFOA in top soils.	181
E.5.	Linear regression plots to predict soil K _d values using EPA and QSAR model data	184
E.6.	Location of specific monitoring sites considered for model evaluation	186
E.7.	Modelled versus observed concentrations at the Inn monitoring site	187
E.8.	Modelled versus observed concentrations at the Morava monitoring site.	188
E.9.	Modelled versus observed concentrations at the Isar monitoring site.	189
E.10.	Modelled versus observed concentrations at the Budapest north monitoring site.	190
E.11.	Relative subdivision of total emissions aggregated over the Danube River catchment upstream of Budapest, averaged over simulated years 2012–2021.	191
E.12.	Relative surface water compartment balances	192
E.13.	Maximum value of the sum of concentrations of 10 modelled PFAS (top) and the duration of exceedance of the 100 ng/L threshold included in the EU drinking water directive (DWD) (bottom).	193
E.14.	Risk of exceedance of the proposed EU Water Framework Directive environmental quality standard based on PFOA equivalent weighted concentrations of 10 PFAS	194

F.1.	The first image on the left shows the layout of the Danube river and the volume of surface water (m^3/d) that flows into the subsoil. It also shows the location of the extraction wells, and particularly those for Surány and Tahi. The other images show the average computed groundwater levels at different depths. . .	198
F.2.	Timeseries of measured and computed groundwater levels for Tahi and Surány.	199
F.3.	Showing the overall statistics of the residuals of the compute heads minus the measured heads. Upper row: including all measurements. Lower row: excluding the measurements at the pumping well locations. Left column: entire model. Middle column: extent of Tahi cut-out model. Right column: extent of Surány cut-out model.	200
F.4.	Schematized streamline pattern for the cut-out models	201
G.1.	Evaluation of historic river gauge data at the Danube downstream of Vienna for critical flow conditions. The black line presents long-term average conditions (1977–2006 for Hainburg and 2000–2021 for Thebnerstraßl).	205
G.2.	Flow time-series for AC-lowflow (2018) and AC-highflow (2013) scenarios, highlighting the spill period of 7 days	207
G.3.	BF model results for reference period (top), scenario base line for post climate change conditions (middle) and scenario WPC1, post climate change (bottom)	218

List of Tables

1.1. Exposure, pollution sources/emissions, fate and transport considered in different model trains and related case studies.	23
2.1. Derived physicochemical property values inserted in the SB-AP Dashboard as input	29
2.1. Derived physicochemical property values inserted in the SB-AP Dashboard as input	30
2.2. Potentially relevant soil chemical and physical parameters to be collected for the purpose of deriving generic risk limits for leaching	36
2.3. Derived GLRLs for PFOS and PFOA for soil/sediment from the Dutch case study	39
3.1. Adjusted flow and transport parameters for the HYDRUS-1D unsaturated zone and for the MODFLOW6 2D saturated zone models	60
4.1. Compact comparative assessment of MoRE model and PPM model applied in the upper Danube Catchment.	69
4.2. Generic bank filtration model input parameters	77
4.3. Characterization of the catchment upstream bank filtration sites in Vienna and Budapest	85
4.4. Vienna and Budapest model parameters for the gBf model.	91
4.5. Mean Absolute Error (MAE, in m) and R^2 for all monitored wells in both cut-out models.	95
4.6. Sorption characteristics for the 10 modelled PFAS, using Hydrus' 1-site chemical nonequilibrium sorption model.	95
4.7. Overview of scenario assumptions to calculate potential changes of PFAS concentrations in river Danube and bank filtration wells at Vienna and Budapest.	99
4.8. Estimated concentrations and risk of exceedance of (E)QS in river Danube at Vienna and Budapest and after bank filtration for different scenarios for the 10 PFAS evaluated.	101
A.1. Derived biodegradability rate constants in water based on REACH Registration Dossier Information	121
A.2. Collection minimum and maximum dissociation constants for selected substances	123
B.1. Hydraulic properties for each layer of the 1D-vertical model and groundwater flow models	131
B.2. Solute transport and reactive properties for each layer of the 1D-vertical model and groundwater flow models	132
B.3. Model parameters for 6:2 FTSA sorption reactions for each layer of the 1D-vertical model and groundwater flow models	133

B.4.	Model parameters for 6:2 FTAB sorption reactions for each layer of the 1D-vertical model and groundwater flow models	134
B.5.	Model parameters for 6:2 FTSAam sorption reactions for each layer of the 1D-vertical model and groundwater flow models	134
C.1.	Calibrated parameters for the unsaturated and saturated models.	143
D.1.	List of modelled PFAS substances. The substance groups are classified according to the EPA Method 1633 (EPA 2024)	151
D.2.	List of pathways with abbreviations and corresponding numbers as referenced in the European Commission (EC) (2012) document, modelled in this study.	153
D.3.	List of PFAS substances selected for validation.	154
D.4.	Inhabitant-specific emission factors for calibration sites Isar and Svratka.	157
D.5.	Relative potency factors for the selected PFAS (drafted EQS (EC COM(2022) 540 final)).	162
E.1.	List of modelled PFAS substances	175
E.2.	Substance specific median concentrations, emission factors (EF) or loads considered to characterise some of the PFAS emission sources.	179
E.3.	Data sources for wastewater management parameters	182
E.4.	Input values of wastewater management parameters derived from ICPDR inventory (Kovacs et al. 2023)	182
E.5.	Input parameter values for FComSew and FrSldgRem	183
E.6.	Soil quality scores for PFAS substances	183
F.1.	Characteristics of the flow situation as derived from the particle tracking simulations	201
G.1.	Definition of sub scenarios for an accidental spill	208
G.2.	AFFF composition.	208
G.4.	PFAS Removal efficiency assumed for activated carbon application on municipal WWTP.	210
G.3.	Removal efficiencies for PFAS reported in literature for adsorptive wastewater treatment steps. BV: Bed volumes	211
G.5.	Summary of Scenarios	213
G.6.	Monitoring and modelled PFAS sum at two validation sites, Danube Vienna and Danube Budapest North, and relative changes compared to the monitoring PFAS-sum.	216
G.7.	PFAS sum and risk at two validation sites, after applying relative changes calculated in Table G.6	217

List of Abbreviations

α (alpha)	the inverse of the air entry suction head	Alpha	First order rate coefficient for nonequilibrium adsorption
λ (lambda)	substance specific decay constant	AR	Activity Rate
ρ (Rho)	bulk density of the soil	AWI	Air-Water Interface
(v)P(v)M	(very) persistent, (very) mobile chemicals	BF	Bank Filtration
6:2 FTAB	Carboxymethyldimethyl-3-[[(3,3,4,4,5,5,6,6,7,7,8,8,8-tridecafluorooctyl) sulphonyl]amino]propylammonium hydroxide	BL	Baseline Scenario
6:2 FTOH	1,1,2,2-Tetrahydroperfluorooctan-1-ol	BTC	Break Through Curve
6:2 FTS	synonym of 6:2 FTSA	C604	Reaction mass of potassium difluoro{[2,2,4,5-tetrafluoro-5-(trifluoromethoxy)-1,3-dioxolan-4-yl]oxy}acetate with potassium fluoride and potassium carbonate
6:2 FTSA	6:2-fluorotelomersulfonic acid	CEC	Contaminants of Emerging Concern
6:2 FTSAam	6:2 fluorotelomer sulfonamido amine	CS	Case study
AA-EQS	Annual Average Environmental Quality Standard. Threshold for protection against chronic toxicity.	CSO	Combined sewer overflow
AC	Accidental Spill Scenario	D _x	longitudinal dispersivity
ADE	Advection-dispersion equation	Disp. L	Longitudinal dispersivity
ADONA	4,8-dioxa-3H-perfluorononanoic acid	Disp. T.	Transversal dispersivity
AFFF	Aqueous film forming foams	DWD	Drinking Water Directive (EU DWD)
		EC	European Commission
		EF	Emission Factor
		EPA	U.S Environmental Protection Agency

EQS	Environmental Quality Standards according to Environmental Quality Standard Directive	IMOD-WQ	iMOD-Water Quality; graphical User Interface + an accelerated Deltares-version of MODFLOW (see below)
EQSD	Draft of the environmental quality standard directive (EC COM(2022) 540 final)	K _d	Linear adsorption isotherm for soil or sediment
EU	European Union	K _f	Hydraulic conductivity
f _{OC}	Fraction of organic carbon	K _{oc}	organic carbon-water partition coefficient
FAO	Food and Agriculture Organization of the United Nations	K _{ow}	octanol/water partitioning coefficient
FP	floodplain attenuation model approach	KGE	Kling-Gupta model efficiency coefficient (Gupta et al. 2009)
Fract.	Dimensionless fraction of adsorption sites with instantaneous sorption	K _s	Saturated hydraulic conductivity
FTOH	Fluorotelomer alcohol	KW	kinematic wave model approach
FTSAAm	N,N-Dimethyl-3-((perfluorohexyl)ethylsulfonyl)aminopropanamine N-oxide	L	length
gBF	generic Bank Filtration Model	LOQ	Analytical Limit of Quantitation
GenX	Commercial name of HFPO-DA	M	mass
GLRLs	generic risk limits for soils	MAE	Mean Absolute Error
GW	Groundwater	mNSE	Modified Nash-Sutcliffe model efficiency coefficient
GWD	Draft of the groundwater directive (EC COM(2022) 540 final)	MODFLOW	Modular three-dimensional finite-difference ground-water flow model
HFPO-DA	hexafluoropropylene oxidizedimer acid / perfluoro-2-propoxypropanoic acid	MODPATH	a particle-tracking postprocessing package that was developed to compute three-dimensional flow paths using output from steady-state or transient ground-water flow simulations by MODFLOW
I	Tortuosity parameter in the conductivity function		

MoRE	Modeling of Regionalized Emissions	PFHxS	perfluorohexane sulfonic acid
MSL	Mean Sea Level	PFNA	perfluorononanoic acid
MT3DMS	Modular Three-Dimensional Multispecies Transport Model for Simulation	PFNS	perfluoronoane sulfonic acid
MW	Monitoring Well	PFOA	perfluorooctanoic acid
n	Parameter n in the soil water retention curve	PFOA-eq	PFOA toxicity equivalents of PFAS substances according to (EC COM(2022) 540 final)
N-EtFOSAA	N-ethyl perfluorooctane sulfonamido acetic acid	PFOS	perfluorooctane sulfonic acid
ne	effective porosity	PFOSA	perfluorooctanesulfonamide
NFBS	1,1,2,2,3,3,4,4,4-nonafluoro-N-methyl-1-Butanesulfonamide	PFPeA	perfluoropentanoic acid
nRMSE	Normalized root mean square error	PFPeS	perfluoropentane sulfonic acid
NSE	Nash-Sutcliffe model efficiency coefficient	PFSA	Perfluoroalkane sulfonic acid
Nu	Langmuir coefficient	PHS	Priority Hazardous Substances (WFD)
p.e.	Population equivalent	PM	Persistent and mobile chemicals
PFAA	polyfluoralkyls acids	PMP	PluriMetric Pilot
PFAS	Per- and polyfluoroalkyl substances	PMT	Persistent, mobile and toxic chemicals
PFBA	perfluorobutanoic acid	PPM	PROMISCES watershed model for PM substances
PFBS	perfluorobutane sulfonic acid	PS	Priority Substances (WFD)
PFCA	Perfluoroalkyl carboxylic acid	PSA	probabilistic sensitivity analyses
PFDA	perfluorodecanoic acid	PW	Pumping Well
PFDS	Perfluorodecane sulfonic acid	Q ₉₅	Low flow with an exceedance of 95 % of the flows of a period
PFHpA	perfluoroheptanoic acid	Q _r	Residual soil water content
PFHxA	perfluorohexanoic acid	QS	Quality standard according to the proposed Groundwater Directive (QS)

Q _s	Saturated soil water content	SWI	Soil-Water Interface
R	Retardation	SZ	Saturated zone
R ²	Coefficient of determination	t	Time
RBM	River basin management	UNZ	Unsaturated zone
RBSP	River Basin Specific Pollutants (WFD)	V	Velocity
REACH	Regulation concerning the Registration, Evaluation, Authorisation and Restriction of Chemicals	WFD	Water Framework Directive, EU regulatory instrument for water management
SB-AP	SimpleBox - Aquatic Persistence Dashboard	WHO	World Health Organization of the United Nations
SEAWAT	Three-dimensional variable density groundwater flow and transport model based on MODFLOW and MT3DMS	WPC1	Water Protection Control Scenario 1
		WPC2	Water Protection Control Scenario 2
SFA	Substance Flow Analysis	WWTP	Waste Water Treatment Plant
SGW	Soil-Groundwater	x	Distance

1. Introduction

Keymessages of the chapter

Quantitative models for exposure assessment are needed to provide information on locations and times where monitoring data are not available, monitoring is not even possible (e.g. scenarios), for improved understanding of reasons for exposure and as basis to evaluate effectiveness of measures.

Exposure of surface and groundwater to Persistent, Mobile and potentially Toxic substances (PM(T)) depends on use patterns and environmental behaviour of the chemicals. Emission, fate and transport models put driving factors in documented algorithms.

This document explains the basic concepts of selected models designed to answer different specific questions and how they can best be used in combination in so-called “model trains”. The objective is to inform users and interested stakeholders on what needs to be considered for their application, what output and support they can provide and what not. Theoretical background is supported with good practice examples from the H2020 PROMISCES project.

1.1. Emission, fate and transport modelling for exposure assessment

What is exposure assessment?

Exposure assessment is the process of quantifying the dose of a contaminant (or a mixture of contaminants) that reaches a target organism. This is commonly followed by a second step, which quantifies the subsequent effect on the target organism. The total process is then referred to as “risk assessment”. In the context of human health, humans are the target organisms, with specific groups, such as infants or workers in factories, being the subject of study in certain cases. In accordance with the definitions set forth by FAO and WHO, exposure assessment is defined as “the evaluation of the probable intake of biological, chemical or physical agents via food, as well as exposure from other sources, if relevant”. In the context of assessments of aquatic ecological status, conducted in accordance with the Water Framework Directive, the specific target organisms are aquatic species (e.g. algae, macro-invertebrates, fish). The precise definition of “dose” depends on the subsequent effect assessment. It may, for instance, be the average intake of a contaminant via food, the “internal” concentration of the contaminant in vital organs, or the concentration in the surrounding environment (“external concentration” or “environmental exposure” for aquatic organisms in the water body).

An exposure assessment requires a conceptual framework. It is necessary to carefully delineate the sequence of steps, from the source of the contaminant to the adverse effect on the target organism. This involves identifying sources of exposure, the behaviour of the contaminant in the environment, and the way in which the contaminant reaches the organism. The terms “Exposure Pathway” (the way the contaminant travels from the source to the target organism) and “Exposure Route” (the way the contaminant enters the target organism) are frequently employed. A commonly addressed aspect is also the uncertainty inherent in the exposure assessment.

Exposure assessments can have a diagnostic objective. If a target organism has been identified as being exposed (via biomonitoring), the implementation of effective mitigation strategies requires the unravelling of the exposure routes, pathways and sources that caused exposure. Exposure assessments may also be conducted with a prognostic objective. Let us consider a scenario in which an industry wishes to start producing and using a new chemical. Will the intended use volume and use types lead to unacceptable exposure and subsequent human health risks? It is incumbent upon the exposure assessment to answer this question.

Aim of modelling in exposure assessments

Models are used in exposure assessments for two main reasons. The first reason is to complement monitoring data: it is often impractical or prohibitively expensive to monitor the environmental exposure at all times and along all exposure pathways and routes. In this context, modelling can assist in mapping the temporal and spatial variability of exposure, exposure pathways and exposure routes. Further, modelling can be employed to conduct hypothesis testing: can the known sources along the known pathways indeed be responsible for the measured exposure along the known exposure routes? If the answer is no, the underlying conceptual framework requires reconsideration.

A second rationale for utilising models is to evaluate potential future developments. Will the proposed mitigation measure prove effective in achieving the required reduction in exposure? Or, as in the example mentioned in the previous section, will the intended introduction of a new chemical result in adverse human health effects? Or will climate change interfere with exposure pathways, and how?

Emission modelling versus fate and transport modelling

Fate and transport models calculate contaminant concentrations in the environment at a given location and at a given point in time. They are commonly “process-based”, meaning that they rely on mathematical equations reflecting our process understanding. Their input data comprise three main categories:

1. The characterization of the environment in which the contaminant under study needs to be simulated. This includes both the geometry of the environment and the fluxes of transporting media (air, water, fine particles).
2. The quantification of the emissions of the contaminant under study into the environment.
3. The definition of substance properties that control the fate and transport of the contaminant in question in the environment. This typically includes properties that determine the distribution of the contaminant over different media (air, water, organic matter, soil),

as well as the degradation or transformation that the contaminant undergoes in different media.

A fate and transport model may need to be expanded to calculate the required “dose” or environmental concentration. An example are so-called bio-accumulation models, which translate external concentrations into internal concentrations inside certain compartments/organs of the target organisms.

The above almost automatically defines an emission model: a model that quantifies the emissions of a certain contaminant into the environmental compartments included in the fate and transport model. Emissions are expressed as mass per time. Depending on the complexity of the model chain, estimations of emissions can vary in spatial and temporal resolution and in considered compartments. Emission models can follow a wide spectrum of approaches, varying from completely data-driven modelling to almost fully process-based modelling.

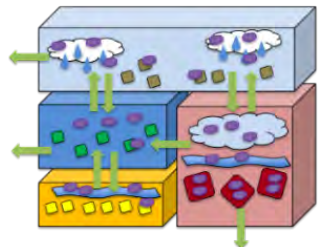
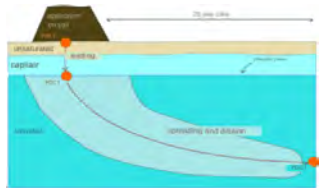
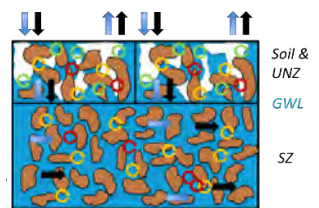
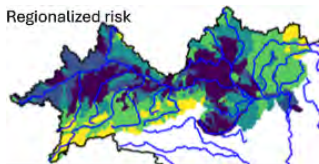
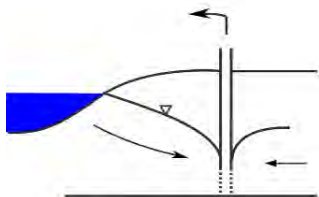
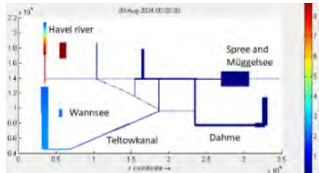
1.2. Scope of the guidance document

The scope of this document is to provide guidance for applications of models with specific focus on model trains for exposure assessment for persistent mobile and toxic chemicals (PMTs) as part of environmental risk assessment (specifically related to surface and groundwaters). This document explains the basic concepts of specific models and how these models can best be used in model trains in a tiered way. The term model train is used for a combination of standalone models to cover complex situations including several environmental spheres such as atmosphere, lithosphere, hydrosphere, biosphere, and anthroposphere, as well as their interfaces. Potential users are industries, utilities, environmental authorities, consultancies, and researchers. Further on, decision makers and regulators are addressed to increase the understanding of the potential policy implications and limitations of emission, fate and transport modelling in the context of environmental exposure assessment.

This guidance document is neither a handbook on a specific model nor a toolbox for explaining different models to users. A toolbox for fate and transport models of PMTs in the environment is provided by the PROMISCES-project in Deliverable D2.3 (Groot et al. 2025). The guidance provided by this document consists in assisting users to select appropriate methodological approaches (models and model trains) depending on which specific problem related to environmental exposure and related questions are posed, in order to identify and understand driving forces, potential future developments, and measures that could be taken to improve the situation in the light of European Green Deal including the Circular Economy Action Plan and of the Zero Pollution ambition of EU (EC COM(2019)640 final; EC COM(2020) 98 final; EC COM(2021) 400 final). The intention is to inform users and interested stakeholders on what needs to be considered for the application of different methods and on what can be expected and also what cannot be expected. In the guidance document we think more in terms of concepts rather than software/actual models. We focus on basic ideas, information requirements (data on regional circumstance and human activities, chemical properties, concentrations and loads in different media etc.), concepts of implementation, basic physical background, and comparison of different approaches to quantify processes by single models and on the role of single models in the context of a model train. Theoretical background is supported with good practice examples of model train applications from PROMISCES case studies.

The structure of the document follows specific exposure routes. We present (i) “screening level” models for the assessment of regional exposure of groundwater from soil pollution and for the assessment of general exposure of air, soil and water at local, regional or global scales, with less detail as more targeted approaches, (ii) spatial and temporal explicit approaches for the identification of pollution plumes from contaminated soil in groundwater and (iii) model train applications for the catchment– river – river bank filtration – drinking water interactions. For the latter we focus on the large scale in a river basin and on a medium scale in an urban context. Table 1 gives an overview on the considered exposure types, related emission routes and considered fate and transport processes.

Table 1.1.: Exposure, pollution sources/emissions, fate and transport considered in different model trains and related case studies.

Considered exposure	Considered compartments	Fate and Transport	Related case study	Graphic
Screening level Models				
Local, regional and global exposure of water, soil and air	Local, regional and global emissions into water, soil and air	Interaction of environmental spheres	-	
Generic risk levels for soil for protection of groundwater	Emissions into soils at regional scale	Soil to groundwater	-	
Soil – Groundwater				
Ground water	Contaminated soil sites	Plume development (time and space)	Large-scale experiment (CS#6) and Tordera aquifer (CS#7)	
Catchment – river – river bank filtration – drinking water				
Surface water	Terrestrial and man-made compartments in a large catchment	Transport, retention, degradation in surface waters	Upper Danube catchment (CS#2)	
Ground water & Drinking water	Surface water impacted by terrestrial compartments	Transport, sorption and degradation during bank filtration	Vienna and Budapest (CS#2)	
Surface water	Terrestrial and man-made compartments in an urban setting	Transport, retention, degradation in surface waters	Berlin (CS#1)	

1.3. Basics of exposure assessment and environmental fate

Chemicals are part of our life. Several hundred thousand are used in multiple applications in the European Union (Z. Wang et al. 2020) and as consequence may reach environmental spheres and water systems. Chemicals are used as pharmaceuticals, personal care products, pesticides/biocides or so-called industrial chemicals, which find application in manifold industrial processes or consumer products. Losses to the environment may occur throughout all stages of the life-cycle of products (i) from industrial production of chemicals, (ii) during finishing of consumer products, (iii) associated to consumptive use, (iv) from wear or ageing of products and materials and (V) during disposal from waste management (Figure 1.1). In the environment, these losses may lead to an exposure of aquatic life or humans via different emission pathways and exposure routes. The extent of the exposure depends on several factors determining the extent of emissions into the environment and the substances behaviour in the environment after their release. Emissions/releases into the environment in specific regions are driven by the amount of a chemical used (production plus import minus export) and the mode of use: private/industrial, use in closed systems, use resulting in inclusion into or onto an environmental matrix, non-dispersive or wide dispersive use.

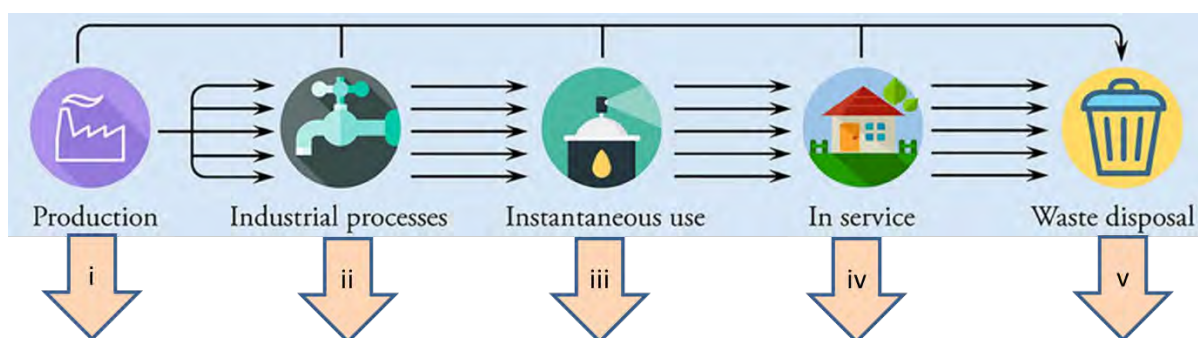


Figure 1.1.: Losses of chemicals to the environment via stages of the products life-cycle: (i) industrial production of chemicals, (ii) finishing of consumer products, (iii) consumptive use, (iv) wearing or aging of products and materials and (v) disposal from waste management (modified from Li et al. 2021)

Once released into the environment, distribution and hence the exposure of organisms at a certain place depends on the chemical-physical properties of a substance. These determine the processes relevant for distribution as advection or adsorption/desorption to soil or sediments, sedimentation/resuspension with sediment, degradation as well as diffusion and volatilisation (Figure 1.2). Already the characterisation of chemicals as persistent and mobile (PM) or very persistent and very mobile (vPvM) substances indicates most important factors of environmental behaviour: the persistence and the mobility.

Persistence describes the stability against degradation of a chemical under environmental conditions. While the mode of degradation/decay might differ between e.g. hydrolysis, photolysis or biodegradation and highly depends on the surrounding medium (e.g. soil, water, waste water treatment plants or soil), the shape of the degradation curve is typically considered to be a first order (exponential) decrease and can therefore be quantified by a first order rate constant/decay constant (λ [d⁻¹]) or a half-life time ($T_{\frac{1}{2}}$ [d]). Degradation may thus be described by the following

formula, where C_0 is the initial substance concentration in a medium and C_t the concentration after time t . $T_{\frac{1}{2}}$ and λ are quantitatively related to each other and are characteristic numbers for specific substances in specific media. Typically, they are determined under standardised test conditions. The higher $T_{\frac{1}{2}}$ and the lower λ is, the higher is the persistence of a substance.

$$C_t = C_0 e^{-t\lambda} \quad (T_{\frac{1}{2}} = \frac{\ln 2}{\lambda}) \quad (1.1)$$

A chemical is considered mobile in the environment, and more specifically in the water system, if it has a low affinity to be adsorbed to particles such as soil, sediments or suspended matter and is therefore transported by advection with the water flow. The adsorption in laboratory tests is frequently characterized by the octanol-water partition coefficient K_{OW} [-], the organic carbon-water partition coefficient K_{OC} [m^3/kg] or the linear adsorption isotherm for soil or sediment K_d [m^3/kg], where:

$K_{OW} = C_O/C_W$; (C_O ... concentration of a substance in octanol, C_W ... concentration in water)

$K_{OC} = C_{OC}/C_W$ (C_{OC} ... concentration of a substance in organic carbon)

$K_d = K_{OC} \times f_{OC}$ (f_{OC} ... fraction of organic carbon in soil)

In practice, K_{OW} and K_{OC} are often used as $\log K_{OW}$ and $\log K_{OC}$, where values below 3 indicate chemicals with a low tendency to adsorb onto organic carbon (contained in soils and sediments) and therefore with a high mobility in the environment, whereas values above 4 indicate chemicals with a high tendency to adsorb to organic carbon and therefore a low mobility in the environment.

While $T_{\frac{1}{2}}$ and λ as well as K_{OW} , K_{OC} and K_d are the most important parameters to characterize environmental behavior of a substance and are essential in many applications of emission, fate and transport modelling of environmental exposure, there are many other physico-chemical properties that might be used for specific cases. Among them, molecular weight [$g.mol^{-1}$], water solubility [$mg.l^{-1}$], vapour pressure [Pa] and boiling point [$^{\circ}C$] are worth being mentioned. A specific focus on methodologies from the field of chemo-informatics to assess substance properties relevant for environmental behaviour is given within the PROMISCES-project in deliverable D2.1 "Toolbox improved in silico models for PM(T) properties identification" (Sosnowska et al. 2024).

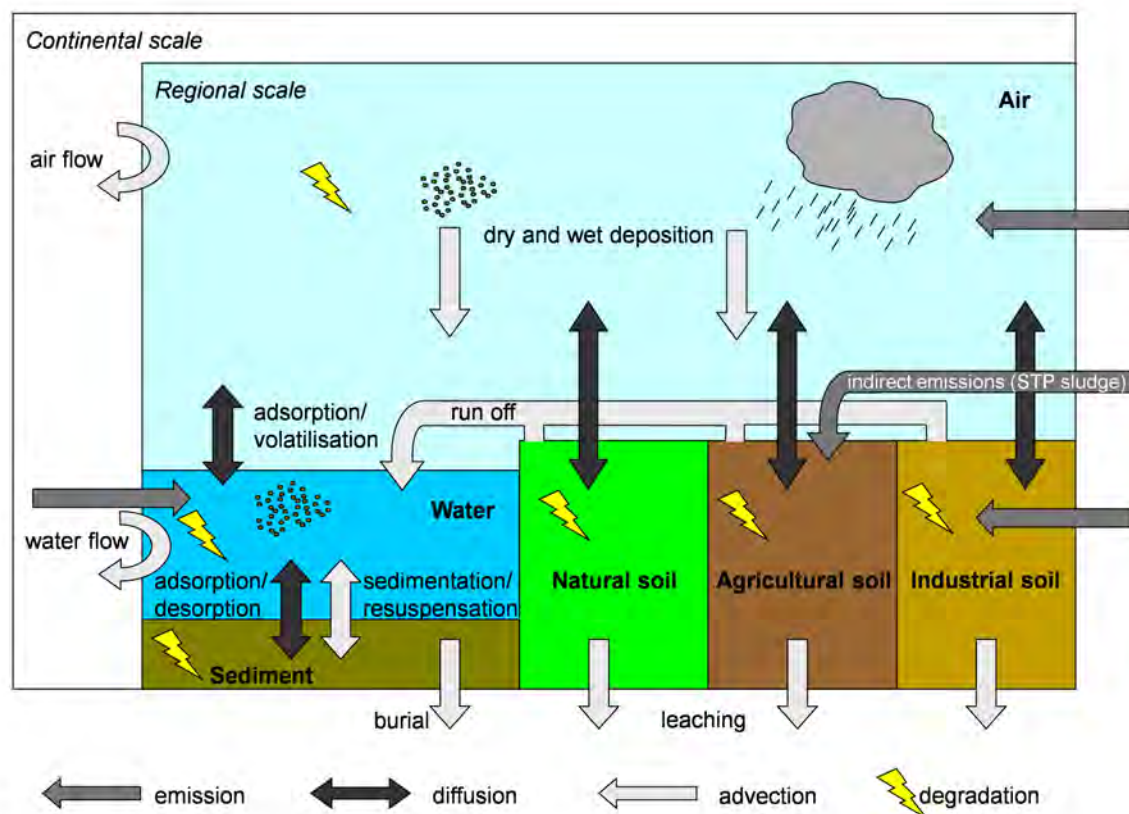


Figure 1.2.: Conceptual multimedia box model for environmental fate and exposure (EUSES 2024)

2. Screening level models

Key messages for screening level models

Screening level fate and exposure models are developed as tools to support decision makers, risk assessors, and policy makers that need to evaluate the environmental behaviour of chemical substances.

The SimpleBox - Aquatic Persistence dashboard (SB-AP Dashboard) is as such developed to evaluate the extent to which a substance remains in surface water bodies over a prolonged period of time, whereas the “generic risk limits for soils” (GLRLS) have been developed to evaluate the extent to which a substance is able to contaminate local surface and groundwater via leaching.

Such environmental behaviour is especially relevant for PMT substances as they are known to persist in aqueous environments and pose harm to organisms living in the environment due to their ecotoxic nature and humans via consumption of drinking water or recreation in water bodies.

The case study with the SB-AP Dashboard demonstrates the derivation of the aquatic persistence of eight different PMT substances, whereas the GLRLS case study demonstrates risk limits for PFASs in local soils.

2.1. Introduction

Using environmental fate and effect models for specific case studies of environmental pollution can be challenging, because they require specific data on substance properties, such as partitioning coefficients and reactive properties, but also emission quantities over a period of time, characteristics of the local landscape and the sensitivities of living (local) species towards ecotoxic effects. The aim of screening level models is to indicate potential environmental risks with relatively simple and conservative (worst-case) approaches in case monitoring data is absent or specific case study data is too limited. This guidance document includes (i) applications and developments of SimpleBox (*SimpleBox Website* 2024) and (ii) the development of a screening level approach for PMT substances leaching to soils by deriving generic leaching risk limit (GLRLs).

2.2. The SimpleBox - Aquatic Persistence dashboard

PMT substances are by definition poorly susceptible to (bio)degradation, and sorption, so that concentrations in water bodies can increase over time and/or substance mass can displace to remote regions via advective transport of streaming water. In addition, PM with low vapour pressure are poorly susceptible to volatilization to air, so that the substance tends to remain in surface waters even more (Meesters, J.A.J. 2024). Therefore, a dashboard has been developed within the EU-project PROMISCES as an additional module to SimpleBox (SB), which is a screening level multimedia environmental fate model for chemicals used for environmental exposure estimation as part of the chemical safety assessment for registration of chemical substances under the Registration Evaluation Authorisation and Restriction of Chemicals (REACH) program of the European Chemical Agency (ECHA) (European Chemical Agency (ECHA) 2016). Furthermore, the SB model has served as 'regional distribution module' in the European Union System for the Evaluation of Substances (EUSES). Potential users of the newly introduced SimpleBox - Aquatic Persistence (SB-AP) dashboard, such as policy makers or chemical risk assessors, can screen the extent to which substances persist in surface water compartments at a regional, continental or global scale (Meesters, J.A.J. 2024). Such aquatic persistence (P_{aq}) is calculated in the SB-AP Dashboard as the sum of all chemical mass present in water bodies ($\sum m_{water} \text{ in } g$) divided by the sum of the emissions to water ($\sum e_{water} \text{ in } g.y^{-1}$):

$$P_{aq} = \frac{\sum m_{water}}{\sum e_{water}} \quad (2.1)$$

Within PROMISCES (Meesters, J.A.J. 2024), it is demonstrated in detail how the SB-AP Dashboard can be used (i) to express aquatic persistence of emitted substances as a single value from deterministic input values for the chemical properties and emissions, (ii) to express probabilistic ranges for the aquatic persistence of emitted substances from ranges of input values for chemical properties and emissions and (iii) to perform probabilistic sensitivity analyses (PSAs) for investigation of the influence of one or more substance properties on the aquatic persistence of emitted substances.

2.2.1. Introduction to the SB-AP Dashboard case study

There are two types of studies that can be performed with the SB-AP Dashboard: (i) aquatic persistence as part of a dedicated fate evaluation study of specific substances and (ii) evaluation of aquatic persistence of substance emission pattern scenarios. Here, a dedicated fate evaluation case study is presented to assess the aquatic persistence of a PMT or vPvM substance on a screening level, by calculating the aquatic persistence of eight selected substances on a regional, continental and global level occurring as dissolved and/or sorbed species. Currently a substance is proposed by the European Commission (EC) to be (i) persistent (P) if its degradation half-life is larger or equal to 60 days in marine water, 40 days in estuarine water, 180 days in marine sediments, 120 days in estuarine sediments or 120 days in soil and (ii) very persistent (vP) if its degradation half-life is larger or equal to 60 days in marine, fresh or estuarine water or 180 days in marine, fresh or estuarine sediments or soil (EC C(2022) 9383 final). A substance is considered mobile (M) when the log K_{oc} is less than 3 and very mobile (vM) when the log K_{oc} is less than 2 (EC C(2022) 9383 final). PM and vPvM indexes have been derived with SB-AP

Dashboard as the calculated aquatic persistences a substance would have when inserting the EC proposed criteria as input parameter values. As such, the aquatic persistence of a PMT substance is calculated to be at least 131 days, 137 days and 140 days on a regional, continental and global scale respectively, while the aquatic persistence of a vPvM substance is calculated to be at least 187 days, 203 days and 215 days on a regional, continental and global scale respectively (Meesters, J.A.J. 2024). These (v)P(v)M index aquatic persistence indexes can be used to directly compare the aquatic persistence of a substance against those of substances meeting the proposed (v)P(v)M criteria.

2.2.2. SB-AP Dashboard case study approach

The SB-AP Dashboard case study evaluates the aquatic persistences of a selection of PMT substances included in PROMISCES. The physicochemical property data for these substances have been collected from the PROMISCES 'Phys Chem Properties' dataset (Sosnowska et al. 2024) which contains CAS numbers, molecular formulas, solubilities, vapour pressures and partitioning coefficients of 71 substances considered in PROMISCES. However, in order to perform a calculation with the SB-AP Dashboard, additional data on degradation half-lives and dissociation constants need to be collected. This data has been collected from REACH registration dossiers within ECHA's online substance database (ECHA 2024) and the USEPA CompTox Dashboard (US EPA 2024). First the availability of a REACH registration dossier comprising the additional degradation and dissociation test data was checked for each of the 71 substances. Such dossiers are found available for eight substances (Table 2.1). These substances – *C604*, *6:2 FTSA*, *PFBS*, *NFBS*, *6:2 FTOH*, *ADONA*, *FTSAAm* and *6:2 FTAB* – are selected for a fate evaluation case study dedicated to aquatic persistence. The other 63 substances in the dataset were not selected for a case study, because a REACH Registration Dossier was not available (ECHA 2024). The input parameter values inserted as physicochemical properties in the SB-AP Dashboard referring to the vapour pressure, solubility, octanol-water partitioning coefficient (K_{OW}) and the organic carbon -water partitioning coefficient (K_{OC}) are collected from the PROMISCES 'Phys Chem Properties' dataset (Sosnowska et al. 2024) comprises physicochemical property data that). The SB-AP Dashboard input fields also demand data for the substances' molecular weight, (bio)degradation rate constant in water and dissociation constants (pKa). The (ranges of) values inserted for these physicochemical properties (Table 2.1) have been collected from substance data REACH registration dossiers (ECHA 2024) and the USEPA CompTox Dashboard (US EPA 2024).

Table 2.1.: Derived physicochemical property values inserted in the SB-AP Dashboard as input

Trade or short name	CAS Number	Molecular weight g/mol	Vapour pressure at 25°C Log(pa)	Solubility Log(mg/l)	Log (K_{OW})	Log (K_{OC})	Log (pKa)	k.degwater log (s-1)
cC604	1190931-27-1	357.085	-1.2951	3.41	4.13 – 5.76	4.06	-1.96 - 23	-9.5 – - 9.38
6:2 FTSA	27619-97-2	428.16	-1.03	0.74	8.34 – 9.90	8.20	1.23	-6.65 – 6.7

Table 2.1.: Derived physicochemical property values inserted in the SB-AP Dashboard as input

Trade or short name	CAS Number	Molecular weight g/mol	Vapour pressure at 25°C Log(pa)	Solubility Log(mg/l)	Log (K_{OW})	Log (K_{OC})	Log (pKa)	k.degwater log (s-1)
PFBS	375-73-5	300.009	0.88	3.05	5.28	5.19	-1.61	-7.2
NFBS	68298-12-4	313.14	-1.28	3.49	5.13	5.04	-8.47 - 8.21	-7.58 – -6.81
6:2 FTOH	647-42-7	364.013	-0.81	1.96	6.12	6.02	9.74	-7.67 – -7.0
ADONA	919005-14-4	387.07	-0.31	2.97	5.51	5.42	-0.22	-7.46 – -7.24
FTSAAm	80475-32-7	528.33	-2.93	2.43	6.28	6.17	7.05	-7.46 – -7.24
6:2 FTAB	34455-29-3	570.37	-3.19	2.58	6.3	6.19	4.78	-9.5 – -9.38
PM Index	-	10,000	10^7	10^8	4	3	0.85	-6.7
vPvM Index	-	10,000	10^7	10^8	3	2	0.85	-6.87

The (bio)degradation rate constant in water is to be inserted in the SB-AP Dashboard as $\log (s^{-1})$, whereas degradation data in the corresponding REACH registration dossiers are qualitative descriptions of outcomes of different types of OECD and other degradation tests (Table A.1). Minimum and maximum degradation rate constants have been derived for each selected substance from the described durations of the tests and described mass fractions of the substance removed (Table A.1). The USEPA CompTox Dashboard (US EPA 2024) has been consulted to collect data for the molecular weights for eight substances and the dissociation constants for seven selected substances, because the registration dossiers only provided a dissociation constant for 6:2 FTAB (Table A.2).

The SimpleBox model in which the SB-AP Dashboard is plugged uses the K_{OW} to simulate the partitioning behaviour of the substance between water and the organic carbon content within environmental solid materials, such as suspended matter in the water column, sediments or soil grains. The PROMISCES 'Phys Chem Properties' dataset (Sosnowska et al. 2024) provides separate values for the a substance's K_{OW} and K_{OC} , whereas the SB-AP Dashboard calculates the K_{OC} as the product of K_{OW} and the fraction of organic carbon in solid materials ($K_{OC} = f_{OC} \cdot K_{OW}$, with $f_{OC} = 2\%$). However, the ratio between the K_{OC} and K_{OW} in the PROMISCES 'Phys Chem Properties' is not equal to this equation. Therefore, the K_{OW} s are inserted as probabilistic ranges with the K_{OW} given in the PROMISCES 'Phys Chem Properties' dataset as minimum and a K_{OW} derived as $\frac{K_{OC}}{f_{OC}}$ as maximum.

2.2.3. SB-AP Dashboard calculated aquatic persistence

The aquatic persistence calculated with the SB-AP Dashboard are compared with the PM and vPvM index substances which refer to hypothetical substances with properties matching the PM or vPvM criteria as defined in PROMISCES Deliverable D2.6 (Meesters, J.A.J. 2024) (Figure 2.1).

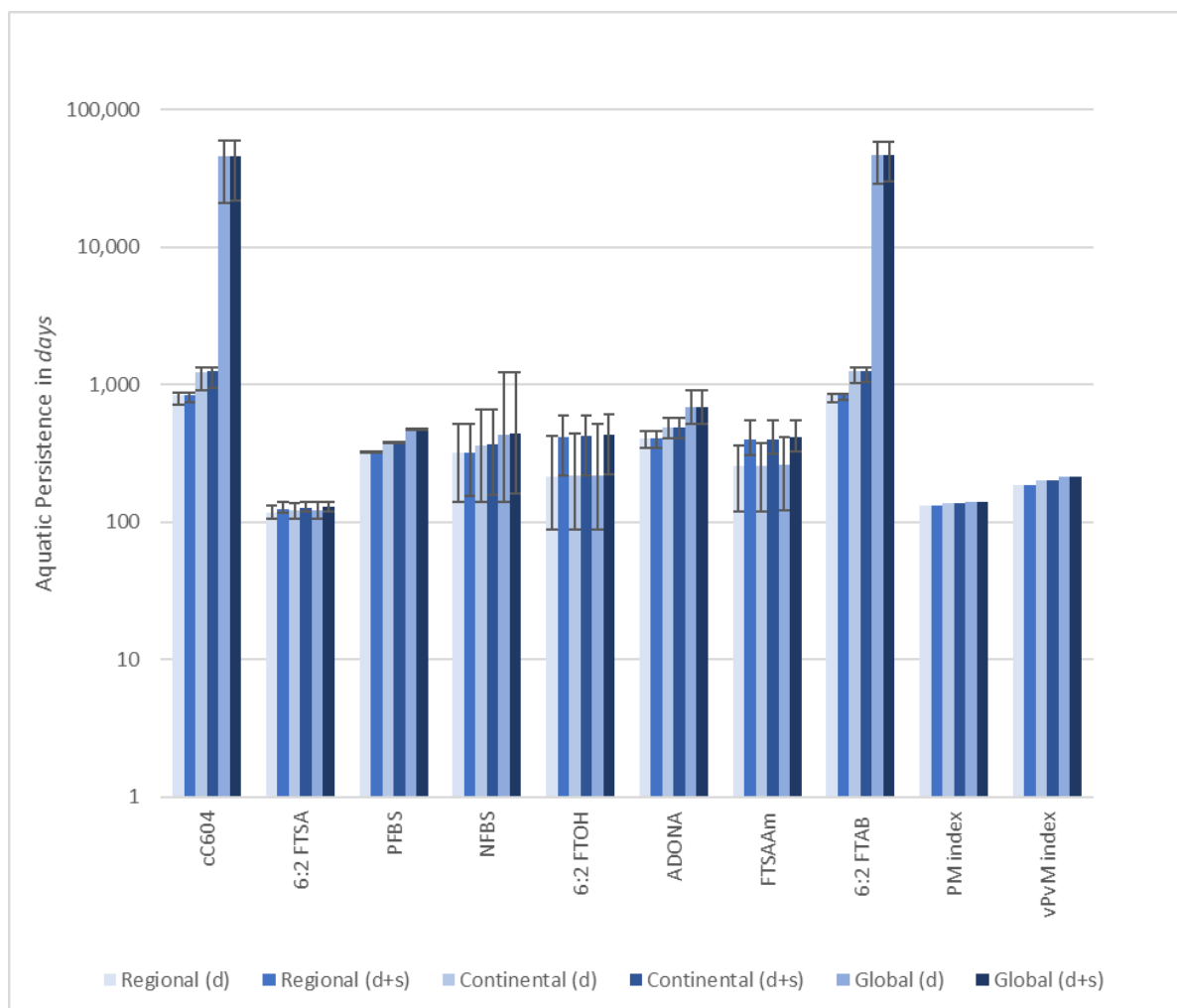


Figure 2.1.: Aquatic persistence expressed in days for eight selected substances occurring as dissolved species (d) or the sum of dissolved and sorbed species (d+s) on a regional, continental and global scale as calculated with the SB-AP Dashboard. Bars refer to median values, whiskers to minima and maxima.

The SB-AP Dashboard calculated that 6:2 FTSA is the only one of the eight selected substances that persists in surface waters comparably to the PM index, whereas the other seven substances persist comparably to the vPvM index or even stronger (Figure 2.1). The calculated aquatic persistence is most uncertain for NFBS, 6:2 FTOH and FTSAAm. For these substances the calculated maximum aquatic persistence is a factor of 1.8 to 8.8 larger than the respective minima (Figure 2.2). The degradation rate constant in water and the K_{OW} are input fields

which are inserted as ranges (Table 2.1), so that the relatively large uncertainty in aquatic persistence for these substances can be explained with the sensitivity plots that can be displayed in the SB-AP Dashboard (Meesters, J.A.J. 2024) (Figure 2.2).

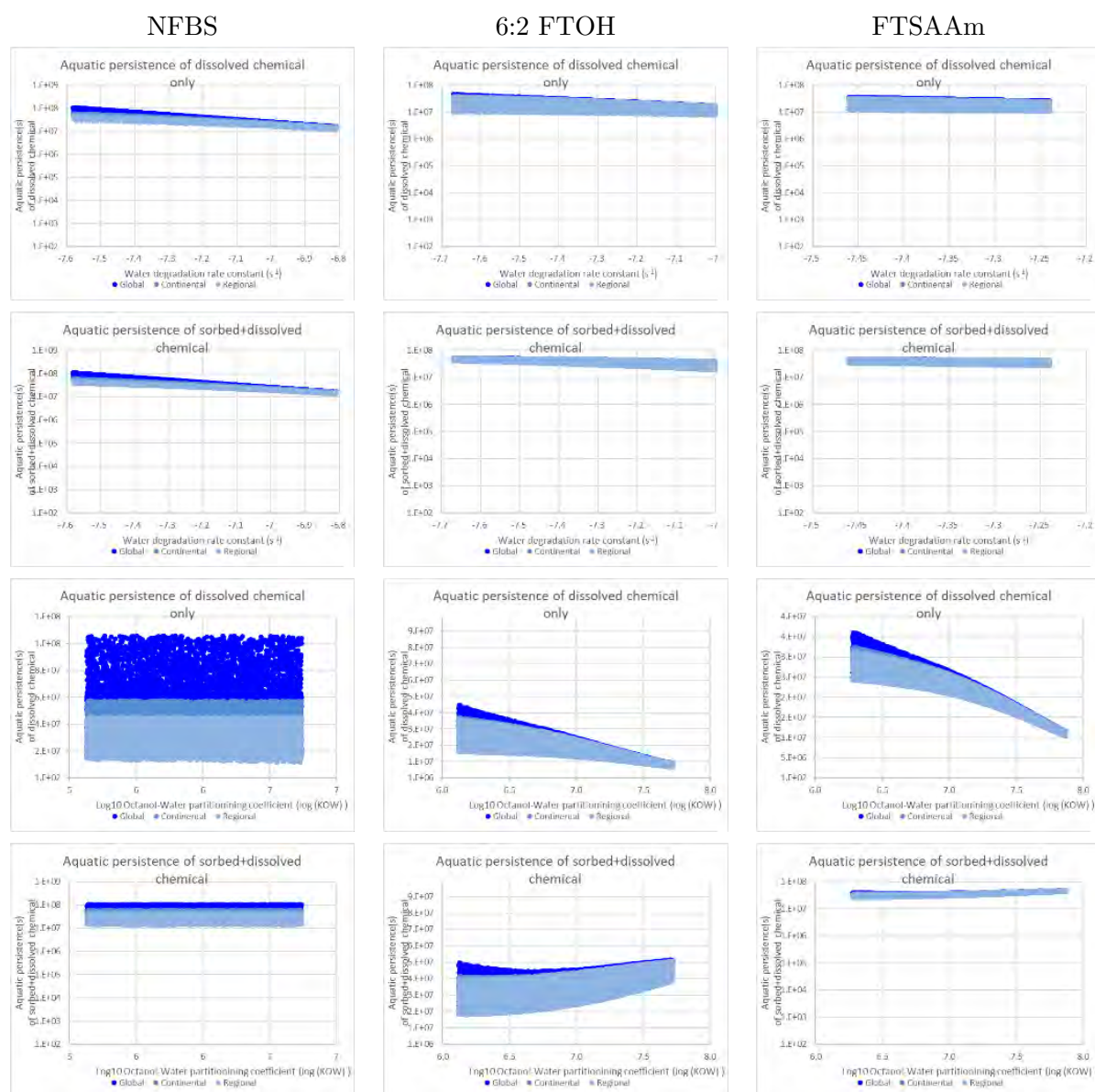


Figure 2.2.: Overview of sensitivity plots for substances with NFBS, 6:2 FTOH and 6:2 FTAB for aquatic persistence (s) vs water degradation rate constant ($\log s^{-1}$) and $\log K_{OW}$

For substance *NFBS* the uncertainty in the calculated aquatic persistence of dissolved species as well as the sum of dissolved and sorbed species is due to the rate constant for degradation in water. The respective plots show a clear linear decrease of aquatic persistence of *NFBS* with increasing water degradation rate constant, whereas the $\log K_{OW}$ plots only displays noise. For

6:2 FTOH and FTSAAm, there is a difference between aquatic persistence of the dissolved and sorbed species. The plots display clear decreases in aquatic persistence of dissolved species with increasing K_{OW} , whereas for the sum of dissolved and sorbed species the aquatic persistence increases with increasing K_{OW} . Within the SimpleBox model, where the SB-AP Dashboard is plugged into, the K_{OW} determines how strong substances sorb to the suspended matter, so that substance in dissolved species are removed from the water column. However, the SB model also calculates that sorbed substance mass is not prone for degradation in water, so that increasing K_{OW} leads to more sorption and hence less degradation. Such a simulation of chemical fate by SB can be seen in the sensitivity plots for 6:2 FTOH and FTSAAm, as (i) stronger K_{OW} decreases their aquatic persistence of dissolved species only, (ii) the sum of dissolved and sorbed species increases with increasing K_{OW} and (iii) an increasing water degradation rate constant affects the aquatic persistence of the sum of dissolved and sorbed species to a minor extent only. The SB model also simulates removal of substance out of the water column via sorption to suspended matter that settles to sediment layer at the bottom. Nonetheless, the aquatic persistence increases with increasing K_{OW} for 6:2 FTOH and 6:2 FTAB. It thus appears that the impact of blocking their degradation due to sorption is simulated to be stronger than the removal via sorption with settling suspended matter.

The substances *cC604* and 6:2 FTAB are calculated to be the most persistent in aquatic environments. Their aquatic persistence exceeds the vPvM index on a regional scale with a factor 4.6 (851 – 867 days *vs* 187 days), whereas on a continental scale this is a factor 6.5 (1270 – 1320 days *vs* 203 days) and even a factor of 270 on a global scale (43,686 - 58,000 days *vs* 215 days). For these two substances it can thus be concluded that their persistence in aquatic environments lasts for decades on a global level.

Key messages for the application of the SimpleBox - Aquatic Persistence Dashboard

The combined impact of (P)ersistent and (M)obile properties of a substance can be quantified with aquatic persistence as calculated with the SB-AP Dashboard.

This is useful in screening level substance evaluation by comparing the aquatic persistence

1. between different substances,
2. against PM or vPvM indexes or
3. between a substance' dissolved and/or sorbed form.

The impact of uncertain substance properties can be quantified and explained with sensitivity plots.

2.3. Deriving generic risk limits for soils

2.3.1. Model explanation

Soil contamination can lead to the degradation of groundwater quality in the long term, especially if the contaminants are persistent. Establishing risk-based soil quality criteria is a common approach for policy makers to deal with the effects of soil contamination on health and the ecosystem (Swartjes 2011). Most of these criteria are based on direct exposure however, whereas indirect effects, for instance through drinking water quality deterioration, stemming from soil pollution, are not part of the derivation of generic criteria. The following approach proposes a method to derive generic risk limits for soil (in situ or soil that is to be used, or ‘applied’ elsewhere) that can be applied on a national or a regional scale to underpin soil quality criteria. These risk limits based on leaching can be used alongside more traditional risk limits based on direct exposure.

Contaminants in soils are partitioned into an adsorbed phase and an aqueous phase. Under net infiltration, the contaminant will be transported towards the groundwater. In the simplest form, the partitioning is expressed as a partitioning constant K_p .

$$K_p = \frac{C_{soil}}{C_{aqueous}} \quad (2.2)$$

With C_{soil} being the total concentration in soil and $C_{aqueous}$ being the dissolved concentration in the aqueous phase.

The leaching of a contaminant is dependent on aspects that influence the partitioning of the (v)P(v)Ms and the transport of soil moisture. Partitioning is amongst others affected by the chemical properties of the (v)P(v)Ms as well as the chemical properties of the soil. The transport of soil moisture is a function of the hydrological balance and soil hydraulic properties.

Generic leaching risk limits (GLRL) for soil or sediment (that is to be re-used on land) can be derived using reactive transport modelling. These risk limits can aid in making decisions on applying soil or sediment in certain locations. This is especially important in the case of the re-use of material of a different origin than the location of application and as well in the case of vulnerable hydrogeological circumstances (e.g. shallow groundwater table, drinking water wells nearby).

Central to the derivation of generic leaching risk limits are standard scenarios. A standard scenario refers to the collection of (v)P(v)M properties, soil properties, both chemical and hydrological, climate data, starting conditions with regards to soil contamination and endpoints which are subsequently used to derive GLRL.

(v)P(v)M properties

The properties of the (v)P(v)Ms are of importance as these determine potential physicochemical transformations and interactions with soil components. Upon entering soils, compounds can undergo adsorption-desorption interactions with surfaces, degrade, volatilize or form precipitates.

Such reactions influence solute transport. Whilst (v)P(v)Ms are per definition persistent and mobile, which implies that they do not degrade readily and that adsorption interactions are limited, such processes need to be accounted as persistence and mobility are relative, and substantial differences may be present between substances.

To derive a GLRL, it is necessary to consider which physiochemical properties and interactions are relevant to describe solute transport accurately. Adsorption interactions should always be considered as part of the derivation as these can vary depending on the type of substance and soil, leading to differences in the derived GLRL's. The manner in which adsorption can be accounted depends on the modelling software used. It is unlikely that the requisite thermodynamic data to implement a mechanistic model is available for many (v)P(v)Ms and therefore only empirical models are suggested. Furthermore, for the derivation of GLRL, it is assumed that (v)P(v)M concentrations are well below the adsorption capacity of soils and that empirical models are therefore applicable. This holds almost without exception for soil contamination stemming from diffuse sources. When deriving and applying GLRL to be used in situations with higher contamination levels, e.g. near a point source, this condition should be explicitly verified. The model used per (v)P(v)M will vary depending on the information available. Ideally, a Freundlich isotherm that accounts for soil properties based on a multiple regression analysis is implemented. If this information is not available, a linear adsorption isotherm (K_d) that considers soil properties, or a K_{OC} in the case of hydrophobic compounds, can be used.

When using empirical models that account for soil properties, it is important that properties of the soil being modelled fall within the range of properties used to derive the relationship between the isotherm and properties. Furthermore, it is important that the concentration range of the (v)P(v)Ms being modelled, falls within the concentration range for which the empirical relationship was derived. If only a linear adsorption model is available for a (v)P(v)M, then it may be necessary to identify a K_d from literature and assign a generic decrease in the K_d with soil depth, to reflect the decrease in reactive surfaces (e.g. organic matter and clay content). In this case, a conservative approach is suggested, for instance by selecting a K_d from the lower end (e.g. a 5th or 10th percentile) of K_d values reported in literature for simulation purposes. It should be noted that selecting a specific K_d value from a distribution of curated values is in the end a matter of policy. If K_d values are not present in literature, then a value derived from a QSAR may be applicable.

Soil properties

Reactive surfaces in soils and soil solution chemistry influence (v)P(v)M transport. Variations in these factors therefore lead to differences in solute transport between soils. The hydraulic properties of soils influence waterflow and therefore well-draining, coarse textured soils, or soils characterized by macropores may facilitate contaminant transport to groundwater.

Due to the diversity in soil properties it is appropriate to derive GLRL using soil profiles representative of major soil types present in a state or country. If these profiles are not available, local soil experts should be consulted to identify representative soil profiles. For each soil profile, the average groundwater depth and relevant soil properties should be determined. The soil properties should be determined at intervals that capture the vertical heterogeneity of the

Table 2.2.: Potentially relevant soil chemical and physical parameters to be collected for the purpose of deriving generic risk limits for leaching

Soil property type	Parameters
Chemical	pH, organic carbon, soil texture, Fe-oxide, Al-oxide, CEC, AEC
Physical	Ks, θ_s , θ_r , n, ρ

soil profile. A list of potentially relevant soil chemical and physical properties is presented in Table 4. Note that because the depth of the groundwater table varies the depth to which soil property data needs to be collected may vary per soil profile. At the very least, the data needed to parameterize a single-porosity waterflow model is required with regards to soil hydraulic properties. If these parameters are not determined then the European pedotransfer functions (Szabó et al. 2021) can be used as an alternative until measurements have been conducted.

Climate

(v)P(v)M transport from the unsaturated to the saturated zone of soils is assumed to occur primarily by infiltrated precipitation. Downwards transport of water through a soil profile generally (i.e. in the absence of preferential flow) occurs when the field capacity is exceeded. Increased water transport implies an increased capacity for solute transport and therefore the balance between precipitation and evapotranspiration is an important factor to consider when deriving GLRL.

The balance between precipitation and evapotranspiration varies within and between countries. It is therefore necessary to use average daily precipitation datasets that are representative for the regions which the soil profiles represent. Ideally, data on the last 30 years of net precipitation input is used for the derivation of GLRL.

Initial conditions, boundary conditions and endpoints

The initial conditions refer to the depth of soil contaminated, the characteristics of contamination, the concentration of the contaminant and the groundwater depth. Together with policy makers, it is necessary to specify what portion of a soil profile is contaminated (e.g. top meter) and to characterize the distribution of contamination (e.g. homogenous or heterogenous) in the standard scenario. Furthermore, for simplicity, using a fixed groundwater depth as the lower hydrological boundary condition is suggested. Identical initial conditions should be used for each of the soil profiles for which GLRL are to be derived.

Endpoints are the points of compliance and associated environmental criteria. The point of compliance for GLRL is the upper meter of groundwater. Furthermore, the GLRL should be determined on the basis of peak concentrations reached with simulations. The environmental criteria the GLRL are based on human and/or ecological risk limits for the (v)P(v)Ms. The selection of appropriate risk limits in groundwater is a matter for policy.

2.3.2. Application cases of generic risk limits for soils and dredged material (sediment)

In this study, environmental quality criteria for PFAS in ground and surface water, e.g. based on WFD quality targets or drinking water protection, are the starting point for the calculation of corresponding concentrations in the soil or dredged material (sediment) to be used for the derivation of generic risk limits. Conceptual models have been drawn up for two main variants:

1. Groundwater. This main variant assumes that PFAS that are carried along with infiltrating rainwater end up completely in the groundwater. The standard used for groundwater in the baseline scenario is the health-based guideline value for drinking water. In this example a guidance value for PFAS of 4.4 ng/l PFOA equivalents was used (Schepens et al. 2023), a value that is based on the EFSA et al. (2020) health-based guidance. Three points or planes of compliance (POC) are defined (see Figure 2.3): POC 0, which is the point of infiltration in the unsaturated zone. POC1, an intermediate point at the phreatic plane. This point is located directly below the application and marks the transition from (the modelling of) vertical transport to horizontal transport). Finally, POC2 is located at a distance of 25-year transit time (based on groundwater flow) in the aquifer starting from POC0. Note that the selection of a certain transit time is a policy decision.
2. Surface water. This main variant assumes a relatively shallow aquifer in which complete mixing takes place of PFAS originating from the top soil layer (Figure 2.4). Note, that this is typical for many areas in the Western part of the Netherlands ('polders'), but in other areas combined systems of aquifers and surface water may run much deeper. An important outcome of this more or less typical 'Dutch variant' is that the dilution is relatively limited in comparison the other variant. The standard for surface water in the initial scenario is the current surface water standard in the Water Framework directive for PFOS (0.65 ng/l) and a similarly derived value for PFOA (48 ng/l, Verbruggen et al. 2017).

The groundwater variant is modelled using a Hydrus and Modflow modelling train (see chapter 3) whereas the surface water scenario is calculated using a simple dilution calculation based on the assumption of instantaneous mixing in the aquifer and a flux through POC2 that is equal to the net infiltration.

The risk limits are intended to substantiate generic standards that must apply to many different situations. It is therefore not operationally practical to establish criteria for a large number of different variants and scenarios. Depending on the spatial scale and variability of environmental conditions an appropriate number of generic risk limits may be derived. The variance of risk limits calculated for different cases can be used to aid in deciding the required amount of different values in relation to the scale and variability of the use case. As an example, a single baseline scenario has been chosen on the scale of the Netherlands for both of the above-mentioned main variants with the following characteristics:

- Based on an average concentration in the plane compliance POC 2, as opposed to setting a maximum concentration (only applicable to groundwater variant);
- Thickness of applied soil (soil that is to be re-used) layer of 1 meter;

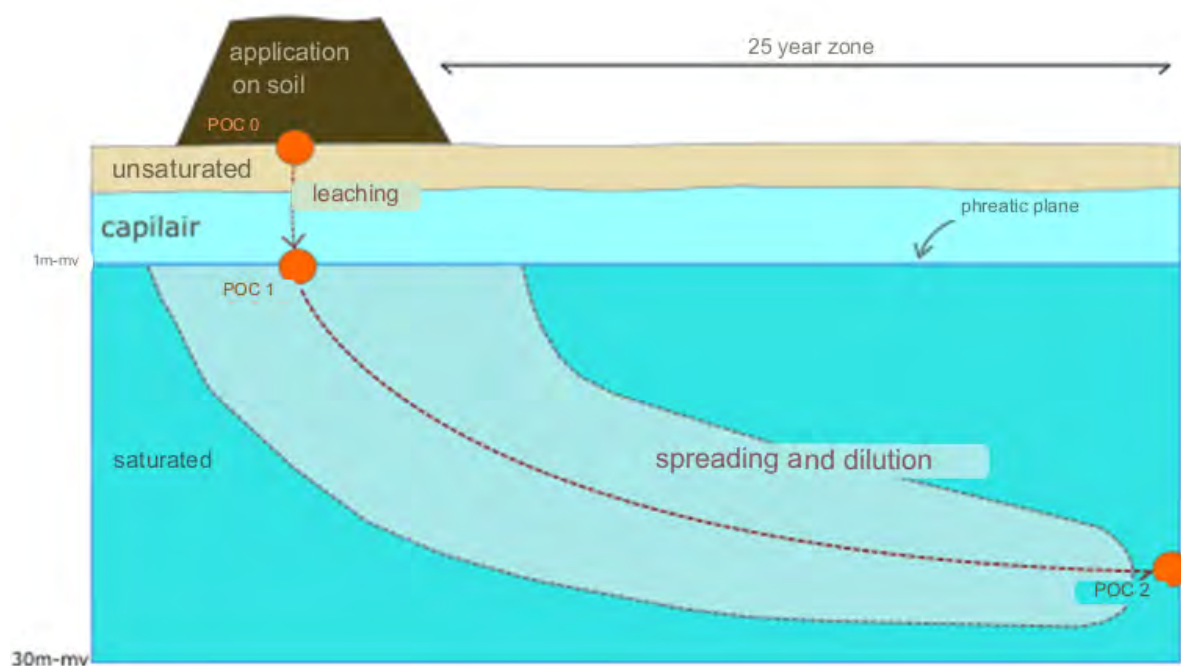


Figure 2.3.: Conceptual model for the groundwater variant

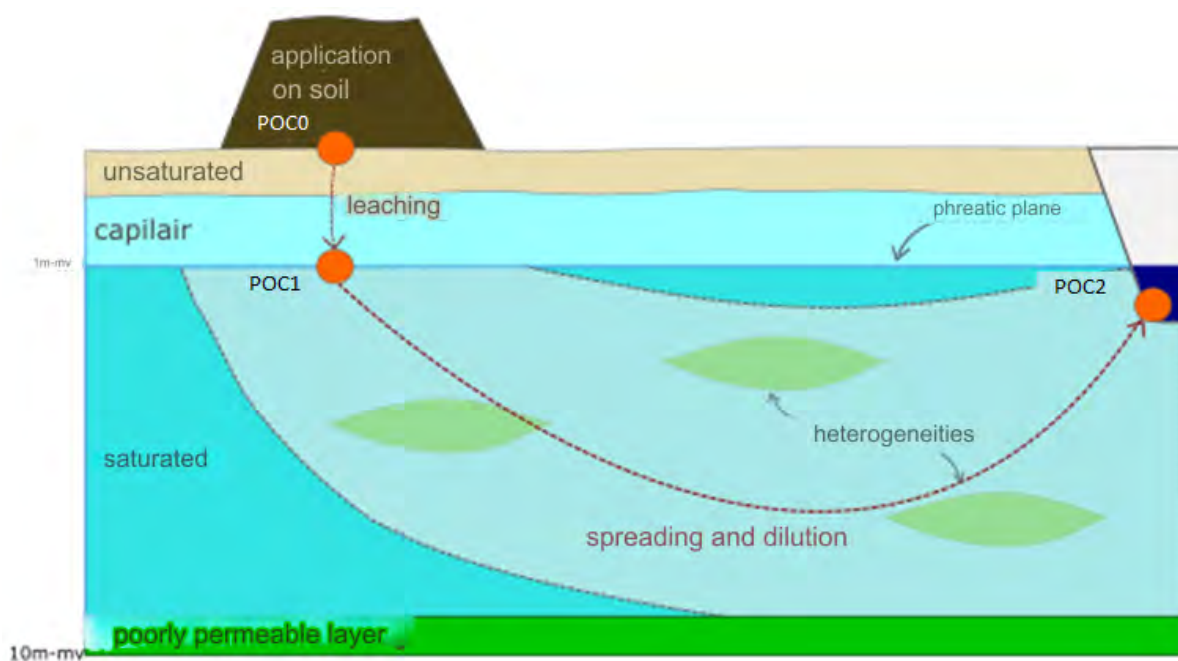


Figure 2.4.: Conceptual model for the surface water variant

- Surface area of soil application of 25 m × 25 m;
- Application of soil above the groundwater table (as opposed to below the surface);
- Groundwater level 1 meter below ground level (representative for large parts of The Netherlands);
- Not taking background concentrations in soil and groundwater into account;
- 10th percentile of the sorption coefficients from previous leaching research (Wintersen et al. 2020);

The criteria at POC2 in the groundwater variant are the drinking water guidance value of 4.4 ng/l for PFOA and 2.2 ng/l for PFOS and for surface water biota-based (human fish consumption) WFD(-type) criteria of 0.65 ng/l and 48 ng/l (Verbruggen et al. 2017) for PFOS and PFOA respectively.

The calculated risk limits for leaching associated with the baseline scenarios for the two main variants are shown in Table 2.3. These risk limits can be used to assess both in situ soil and soil that is to be applied (re-used) elsewhere.

These values should be considered as the result of a first proof of concept for the Dutch situation. Depending on further (policy) choices and local variations, different values can apply. The calculated risk limits expressed as concentrations in soil/dredged sediment based on the surface water variant are lower than the values calculated for the groundwater variant. This is caused by the combination of stricter risk limits in surface water and the smaller amount of dilution in this scenario.

Table 2.3.: Derived GLRLs for PFOS and PFOA for soil/sediment from the Dutch case study for different points or planes of compliance (POC) in groundwater and surface water.

Substance	GLRLs for soil/sediment [µg/kg ds]	
	Groundwater	Surface water
PFOS	48	0.14
PFOA	37	3.4

Key messages for deriving generic risk levels for soils

The relatively high mobility of some PFAS combined with low environmental quality criteria for ground and surface water can necessitate the derivation and enforcement of criteria that are to be applied on soil and sediment that is to be applied on land;

This case study provides generic guidelines for deriving such criteria. Regional variations in geo(hydro)logical circumstances, leading to variations in sorption, should always be considered when deriving such criteria;

As an example, generic criteria for Dutch soils and sediments are presented, based on a parameter set that is typical for Dutch situations (shallow groundwater table and close proximity to surface water).

3. Soil - Groundwater interaction

Key messages of exposure assessment in the soil groundwater continuum

The model train developed is efficient to simulate PFAS fate and transport in the soil-groundwater continuum from semi-real to aqueous film forming foams (AFFF) contaminated site scales

The simulation results highlight the key role of the unsaturated zone in the PFAS transport in the soil-groundwater continuum to correctly predict the extension of PFAS plume.

Capillary fringe displacement plays a key role in PFAS remobilisation by controlling water flow rate in the unsaturated zone and modifying PFAS sorption onto air-water interface.

Numerous processes are involved in PFAS transport in the soil-groundwater continuum. Most of them are interrelated.

3.1. General aspects

In many soils, measured PFAS are orders of magnitude greater than the health advisory level. A quantitative understanding of the fate of PFAS in soils and to other environmental compartments such as groundwater is therefore mandatory to develop effective remediation or mitigation strategies. PFAS migration in porous media is one of the most challenging as it needs to account for variably saturated media (soil and unsaturated zone) as well as fully saturated media (groundwater). Modelling the fate and transport of PFAS in this continuum are challenging due to the following several issues:

- Lack of knowledge on the physical, chemical and biological processes controlling fate and transport of PFAS in the soil-groundwater (SGW) continuum,
- Difficulty to assess spatio-temporal patterns of heterogeneities in SGW continuum and their consequences on PFAS reactive transport,
- Diversity of the numerical formalisms, from empirical ones to physically based, preventing to identify the most appropriate to simulate the processes controlling PFAS reactive transport,
- Uncertainties concerning the validity of upscaling simulation results and modelling tools from laboratory scale to contaminated site scale,

- Lack of modelling tools to build 3 dimensions (3D) PFAS reactive transport model in transient time conditions,
- Existence of a broad range of PFAS with contrasted molecular properties, implying to develop modelling tools that can be applied to all, or at least, most of these compounds,
- Spatial/temporal variability and uncertainty of PFAS monitoring at field scale, often preventing to conduct robust model calibration,
- Scarcity of the data used to estimate PFAS emissions at the top of the SGW continuum, questioning the boundary conditions selected as input data in the modelling tools,
- The broad range of PFAS concentration encountered from the hot spot of contamination (mg/L) to the fringe of the plume where the concentration is lower ($\mu\text{g/L}$),

Up to now, PFOA and PFOS are the most studied PFAS in the literature as they are the most used and older PFAS used. In addition, thresholds values have been defined in drinking water directives ($0.1 \mu\text{g/L}$ for each) or EPA is setting enforceable Maximum Contaminant Levels at 4.0 ng/l for PFOA and PFOS, individually. Although a growing number of research works have been conducted to simulate reactive transport of numerous PFAS in SGW continuum, developing a robust and efficient modelling tools whom results can be used by various stakeholders, policy makers or operating agents dealing with problems of PFAS contamination in groundwater is still a complex task not clearly defined up to now. To efficiently develop modelling tools to simulate fate and transport of PFAS in SGW continuum several steps must be conducted. Note that several of these steps are also found in the modelling framework developed for “screening level” models (see section 2) and model train applications for the catchment – river – riverbank filtration – drinking water interactions (see section 4). These steps are the following:

- Conceptualize a robust and comprehensive conceptual model describing the key processes controlling fate and transport of the studied PFAS in the studied SGW continuum,
- Build a model train combining several numerical tools/software that are efficient to simulate the processes identified during the first step,
- Selecting the most appropriate mathematical formalisms to simulate the processes controlling fate and transport of the studied PFAS in the studied SGW continuum
- Perform an efficient model calibration using a dedicated dataset,
- Analyse modelling results for each simulation to characterize and rank the main processes involved in reactive transport of the studied PFAS in the studied SGW continuum,
- Estimate origins (conceptual, numerical, calibration, etc.) of discrepancy between simulated and measured results,
- Identify the best improvements steps to update the model for improving its efficiency to simulate and forecast the reactive transport of the studied PFAS in the studied SGW system.

Considering the two first steps aforementioned, a solid knowledge on the processes controlling PFAS migration in SGW continuum is required. A brief review of the key concepts to simulate PFAS fate and transport in SGW continuum is provided in Annex B.1

3.2. Model train combining Hydrus and MODFLOW/MT3DMS

Several numerical tools have already been developed to simulate PFAS fate and transport. These numerical tools have been mainly applied to simulate PFAS migration at 1 or 2 spatial dimensions according either theoretical scenarios or laboratory and/or field-scale experiments. To the best of our knowledge, no 3D model has been developed to simulate PFAS fate and transport dealing with both unsaturated and saturated conditions. This lack of tools prevents to provide insightful simulations of PFAS migration in SGW continuum at large spatial scale such as watershed scale and over long-term.

For this purpose, a modelling framework based on coupling a 1D model for describing water flow and solute transport in unsaturated zone with 3D groundwater flow and transport models has been demonstrated as efficient to simulate water flow and solute transport in SGW continuum. One of the basic principles behind linking independent models for unsaturated and saturated zones is the exchange of information between them. For water flow, these information, at each time step, are the recharge water flux from the unsaturated zone to the saturated zone and the elevation of the water table. For solute transport, mass fluxes at the bottom of the unsaturated zone and the solute concentration at the top of the water table at each time step are required. A model train combining several software has been developed to simulate water flow and PFAS transport in the SGW continuum. This model train couples the following software: 1D-Hydrus, MODFLOW and MT3DMS, respectively (Figure 3.1). Considering the coupling scheme selected (see below), the model train can be used as a stand-alone executable program or built in Python environment by using the existing libraries for 1D-Hydrus (*Phydrus*) and MODFLOW/MT3D (*FloPy*) and developing scripts allowing exchange of output/input data between them.

3.2.1. Model train for water flow

To simulate water flow in the SGW continuum, the 1D-Hydrus software is coupled to the MODFLOW software. These two software are widely accepted numerical tools to simulate water flow in unsaturated and saturated zones, respectively. Their features have been widely described and their efficiency and robustness have been broadly demonstrated. Therefore, the software features are only shortly summarized.

1D-Hydrus variably saturated flow software

The 1D-Hydrus software solves the Richards equation to simulate variably saturated water flow in porous medium. An advanced formalism of the Richards equation dealing with (constant or time-varying) boundary conditions is solved. The Richards equation is highly nonlinear. Therefore, soil hydraulic functions have to be used to solve this equation. Several functions are available such as Brooks and Corey, Durner, Van Genuchten or Kosugi. The 1D vertical domain can be simulated as a complex layered system. The flow region may be composed of non-uniform layers with an arbitrary degree of local anisotropy. The code further implements a scaling procedure to approximate variability in the hydraulic properties along a soil profile using a set of linear scaling transformations. The scaling factors can be either normally or log-normally distributed. The boundary conditions are prescribed either as pressure head or

flux boundaries, as well as boundaries controlled by atmospheric conditions. Surface boundary conditions may change during the simulation from prescribed flux to prescribed head-type conditions (and vice versa), accounting for infiltration, ponding, surface runoff or actual soil evaporation processes. Seepage face boundary, through which water leaves the saturated part of the flow domain, and free drainage boundary conditions can also be used. In addition, a special boundary condition simulating plant water uptake as a sink term, with an explicit distribution of the root zone along the soil profile, can be used. 1D-Hydrus software also incorporates hysteresis, assuming that during scanning curves are scaled from the main drying curve and wetting curves from the main wetting curve. The governing equations are solved numerically by discretizing the simulated domain in several blocks (called cells). Galerkin-type linear finite element method is used to mesh the simulated domain. Integration in time is achieved using an implicit finite difference scheme. The equations are solved by: i) linearization and subsequent Gaussian elimination for banded matrices, ii) a conjugate gradient method for symmetric matrices or iii) the ORTHOMIN method for asymmetric matrices. To speed up resolution time, automatic time step adjustment and conservation of the Courant and Peclet numbers within pre-set levels are used.

MODFLOW software

Complex groundwater flow model can be built using the MODFLOW software. The core of the code is dedicated to solving the groundwater flow equation resulting from coupling the Darcy's Law and 3D mass conservation equation. This equation is solved using the finite-difference method, wherein the continuous partial-differential equation is replaced by a finite set of linear algebraic difference equations according to the features of the space and time discretisation. A regular block-centred discretization method is usually used to mesh the simulated domain. More advanced meshing option can be also used to simulate complex, irregularly shaped aquifer structure. Implicit finite difference scheme is used for time dimension. A broad range of boundary conditions (constant and transient) can be defined such as fixed pressure head, flux boundaries or atmospheric boundaries. In consequence, numerous phenomena impacting groundwater flow such as pumping/recharging wells, recharge, evaporation, flow to drains and flow through riverbeds or lake can be simulated. Three types of solvers can be used to solve the equation system, the most commonly used is the conjugated gradient methods with preconditioning steps.

Coupling scheme

Two options have been used to couple the 1D-vertical model for unsaturated zone and groundwater models built using 1D-Hydrus and MODFLOW 2005 software, respectively. The first option has been used in the model developed for CS#7 while the second option has been used in the model developed for CS#6. The two coupling options are the following:

- The first option is based only on input/output exchange data between the two models. More precisely, water fluxes at the bottom of the unsaturated zone calculated at the $n-1^{\text{th}}$ time step is used as input value for recharge in the groundwater flow model for the n^{th} time step while the groundwater table depth calculated by the groundwater flow model

at the $n-1^{\text{th}}$ time step is used as bottom boundary condition in the 1D-vertical model for unsaturated zone for the n^{th} time step

- The second option is also based on an input/output exchange data between the two models identical to option 1 plus a numerical scheme using an algorithm developed by Beegum et al. 2018 to eliminate inaccurate simulations of water flux at the bottom of the unsaturated zone due to sudden water inflow or outflow when the groundwater table depth changes. The algorithm updates the pressure head at the bottom of the 1D-vertical model for unsaturated zone at the beginning of the time step of the groundwater model by accounting for an equivalent pressure head profile that would exist if there was a continuous change in the water table elevation. In consequence, no unrealistic changes in flow rate are simulated preventing erroneous simulations of water flow, hence PFAS transport in the SGW continuum.

3.2.2. Model train for solute transport

For simulating PFAS transport, the transport module in the 1D-Hydrus software and MT3DMS software have been coupled for unsaturated and saturated zones, respectively. A short summary of the software features is provided below.

1D-Hydrus solute transport software

The advection and dispersion equations are used to simulate solute transport in unsaturated zone. The water flow rate calculated by the 1D vertical model is used as input to simulate advection. The dispersion process is simulated by accounting for dispersion tensor. It includes terms reflecting the contribution of molecular diffusion, tortuosity and longitudinal dispersion. The transport equation is modified to account for equilibrium and nonequilibrium sorption reactions between the solid and liquid phases, attachment/detachment theory, including filtration theory, linear equilibrium reactions between the aqueous and gaseous phases (allowing simulations of volatile chemicals), zero-order and two-first order degradations reactions, one of which can be used to represent parent-daughter degradation reactions. Chemical nonequilibrium sorption is simulated using a two-site adsorption model, which divides the sorption sites into two groups. Sorption on the first sorption sites is instantaneous (linear or nonlinear), while sorption on the remaining sites is kinetic (first order rate sorption equation). In addition, physical nonequilibrium solute transport can be simulated by assuming a two-region dual porosity domain that partitions the liquid phase into mobile and immobile regions. 1D-Hydrus software supports both (constant and time-varying) boundary conditions. Fixed concentration (Dirichlet) or concentration flux (Cauchy) boundary conditions can be used. The numerical method used to solve the reactive transport equation is like the one described for water flow (see above). A recent version of 1D-Hydrus software including an explicit simulation of the PFAS sorption onto air-water interface (AWI) according to changes in water saturation as well as surface tension-driven flow has been delivered. This version cannot be coupled to MODFLOW software, hence this modified version of 1D-Hydrus model has not been used.

MT3DMS software

Model simulating solute transport in saturated zone are built using MT3DMS software. This software solves a modified version of the advection dispersion equation accounting for sorption and degradation reactions in a fully saturated porous medium. Similar options to the ones mentioned above for 1D-Hydrus software can be used in the groundwater model built using MT3DMS software. A finite-difference approximation is used to solve the modified advective-dispersion-reaction equation. The simulated domain is then divided in a finite set of discrete blocks in space and time. The concentrations of solutes in aqueous phase and sorbed onto the solid phases are calculated in all the cells, allowing to replace the continuous partial derivatives by linear set of equations to simulate mass transfer between each cell and between aqueous and solid phases. The same discretization schemes available in MODFLOW can be used in MT3DMS. Dirichlet and Cauchy boundary conditions can be considered. These boundary conditions can remain fixed or evolved with time. A generalized conjugate gradient method is used to numerically solve the set of equations with preconditioning steps.

Coupling scheme

The two options previously mentioned are available to couple the 2 models developed using the 1D-Hydrus solute transport module and MT3DMS software, respectively. The first option has been used in the model developed for CS#7 while the second option has been used in the model developed for CS#6. The 2 options can be summarized as following:

- For option 1, a direct exchange of information is performed between the two models. More precisely, the simulated solute fluxes at the bottom of the unsaturated zone at the $n-1^{\text{th}}$ time step are used as input for the concentrations of the recharge fluxes in the groundwater solute transport model for the n^{th} time step. The simulated solute concentrations at the top of the saturated zone by the groundwater solute transport model at the $n-1^{\text{th}}$ time step are used as boundary condition of the 1D-vertical model at n^{th} time step.
- The option 2 for solute transport is linked to the option 2 for water flow simulations. This latter implies that the pressure head distribution in the 1D-vertical model for unsaturated zone is updated after each time step. Hence, solute concentrations have to be correspondingly adjusted to preserve mass balance. This is done by either lowering (diluting) or increasing (concentrating) solute concentrations, depending on changes in pressure head distribution. Concentrations in sorbed solutes are also updated. Data transfer between the 2 models is a “loose” coupling, which is only partially automatized using a post-processing step on the output of the 1D-Hydrus solute transport module.

3.2.3. Modelling framework

A dedicated framework has also been developed to use the model train. This framework is divided in the 4 following steps:

- Develop 1D vertical model dedicated to unsaturated zone using 1D-Hydrus software. In the case, the unsaturated zone properties and associated boundary conditions of the simulated domain are heterogeneous, the unsaturated zone of the simulated domain has to be splitted in different zones. The number of zones need to be defined by the modellers. For each zone, a 1D-vertical model has to be developed.
- Develop a 3D groundwater flow model using MODFLOW software. According to the option selected to couple the models, these two steps can be conducted iteratively (option 1) or simultaneously (option 2). In the case, the unsaturated zone of the simulated domain is divided in several zones, the groundwater flow model has to account for the same number of recharge zones. Information exchange is performed between each 1D-vertical model and the corresponding recharge zone,
- Develop a 1D-reactive solute transport model dedicated to unsaturated zone using 1D-Hydrus solute transport module. In the case, unsaturated zone is divided in several zones, a 1D-reactive solute transport model has to be built for each zone,
- Develop a 3D solute transport model for saturated zone using MT3DMS software. In the case, several recharge zones are defined in the 3D groundwater flow model, the same discretization has to be used in the 3D solute transport model.

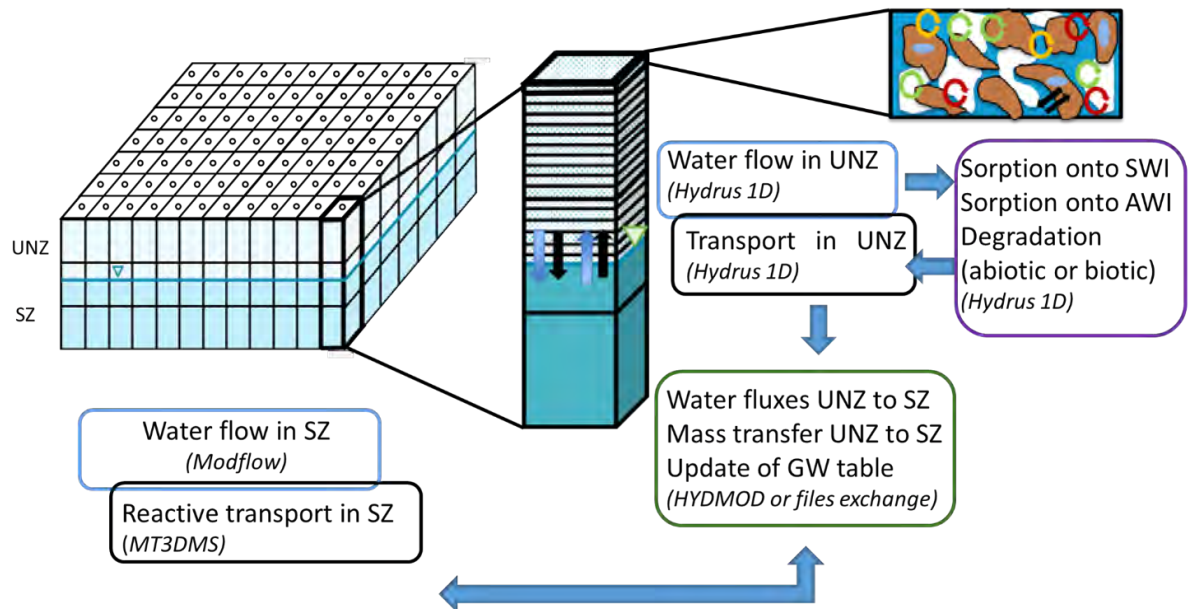


Figure 3.1.: Sketch of the model train developed to simulate fate and transport of PFAS in soil-groundwater continuum.

3.3. General explanation of case studies

To go beyond theoretical recommendations, examples to illustrate the use the model train to simulate fate and transport of PFAS in SGW continuum are provided. The model train has been applied to simulate the PFAS migration monitored in 2 case studies (CS#6 and CS#7, respectively). The 2 case studies are contaminated sites by the use of aqueous film forming

foams (AFFF) containing PFAS. This type of contaminated sites has been identified as one of the major sources of PFAS in environment due to the widespread uses of AFFF to extinguish hydrocarbon fuel fires since the 1960s (Anderson et al. 2016). AFFF are commonly used in airport and military fire-training areas and could be spread in environment due to accidental release. AFFF formulations are a complex proprietary mixture of chemicals with various hydrocarbon and fluorine-containing surfactants that include 1-4% (w/w) PFAS. According to AFFF formulations, various PFAS can be found. In legacy AFFFs produced prior to 2000s, PFOS, PFHxS and others PFASs and PFCAs can be found. Accordingly, PFOS is still the major species in older AFFF-impacted sites. During 2000s, manufacturers started to produce AFFF through the fluorotelomerization process, which generates fluorotelomers such as 6:2 FTAB, 6:2 FTAS or fluorotelomer alcohols (e.g. 6:2 FTOH). Many of these compounds are referred as precursor compounds of PFCAs through oxidation pathways or biotransformation in terrestrial invertebrates (Lyu et al. 2022), hence producing stable compounds such as PFOA and PFOS. To go beyond theoretical recommendations, examples to illustrate the use the model train to simulate fate and transport of PFAS in SGW continuum are provided. The model train has been applied to simulate the PFAS migration monitored in 2 case studies (CS#6 and CS#7, respectively). The 2 case studies are contaminated site using aqueous film forming foams (AFFF) containing PFAS. This type of contaminated sites has been identified as one of the major sources of PFAS in environment due to the widespread uses of AFFF to extinguish hydrocarbon fuel fires since the 1960s (Anderson et al. 2016). AFFF are commonly used in airport and military fire-training areas and could be spread in environment due to accidental release. AFFF formulations are a complex proprietary mixture of chemicals with various hydrocarbon and fluorine-containing surfactants that include 1-4% (w/w) PFAS. According to AFFF formulations, various PFAS can be found. In legacy AFFFs produced prior to 2000s, PFOS, PFHxS and others PFASs and PFCAs can be found. Accordingly, PFOS is still the major species in older AFFF-impacted sites. During 2000s, manufacturers started to produce AFFF through the fluorotelomerization process, which generates fluorotelomers such as 6:2 FTAB, 6:2 FTAS or fluorotelomer alcohols. Many of these compounds are referred as precursor compounds of PFCAs through oxidation pathways or biotransformation in terrestrial invertebrates (Lyu et al. 2022), hence producing stable compounds such as PFOA and PFOS.

Beside a similar source of PFAS contamination by AFFF, the two case studies differ in terms of complexity considering geological, hydrological, hydrogeological, climate and soil features. The first case study (CS#6) is a large-scale, long-term experiment conducted in a PluriMetric Pilot (PMP). This research infrastructure has allowed to reproduce an AFFF-contaminated site at semi-real scale in controlled condition. The PMP has been filled with a geomaterial specifically produced for the experiment. A vadose zone and groundwater continuum has been experimentally created in the PMP as well as an AFFF has been released at the top of the SGW continuum. This experiment has been held for 11 months. All the hydrogeological and mass transfer conditions such as water table depth, boundary conditions and mass of PFAS injected have been controlled during the experiment. A high-density monitoring set up as well as a high frequency monitoring of several physical and chemical parameters have been deployed to give a very precise vision of PFAS migration. However, results provided by PMP are still far from real site complexity. To highlight the capabilities of the model train, it has been applied to a real AFFF-contaminated site, CS#7. This aquifer is a complex structure with several layered solid materials. Furthermore, the thickness of the unsaturated zone is time-dependent, evolving in response to water regional flow and effective recharge as well as

interactions between groundwater and surface water. PFAS contamination has been induced by repeated use of AFFF for fire-fighting training activities. Field campaign measurements have been done to characterize groundwater flow, variably saturated flow in the unsaturated zone and PFAS contamination.

For each case study, an example on the use of the model train is provided. The main steps aforementioned for building a model to simulate PFAS fate and transport in the SGW continuum are explained below. More details on the PMP experiments and CS#7 are given in the Annexes (B.2 and C, respectively).

3.4. Application for the PluriMetric Pilot experiment

This section describes the model of the PluriMetric Pilot experiment that is described in detail in Annex B.2.

3.4.1. Conceptual model

Based on the interpretation of the results issued from the PMP experiment, a conceptual model explaining PFAS fate and transport during the PMP experiment has been built. The conceptual model considers four processes: i) water flow in both unsaturated and saturated zone controlled by different type of boundary conditions, ii) advection-dispersion, iii) sorption reactions onto soil-water interface (SWI) in both unsaturated and iv) saturated zone and sorption reactions onto air-water interface (AWI) in unsaturated zone. The magnitude of these processes, hence their role in controlling PFAS fate and transport, changes with distance to the AFFF infiltration area, named infiltration square, along the water flow path and time. In consequence, several hypotheses have been assumed to explain the spatio-temporal pattern in PFAS migration. These hypotheses are the following:

- At the beginning of the AFFF infiltration stage, pore volume in both unsaturated and saturated zone below the infiltration square has decreased compared to the values defined for the uncontaminated geomeia. This change in pore volume is assumed to be induced by foam formation.
- By sorbing onto soil-water and air-water interfaces, PFAS have modified the hydraulic properties of the geomeia, increasing water flow rate in both unsaturated and saturated zone below the infiltration square.
- Changes in pore volume and hydraulic properties have been stable during all the PMP experiment since starting AFFF infiltration
- The first centimetres of the unsaturated zone seems less impacted by foam formation, hence hydraulic properties and pore volume remained like the ones measured in the uncontaminated geomeia.
- At the top of the PMP, evaporation has impacted both water flow rate and has induced an increase of PFAS concentration in pore water.

- Water table depth as well as boundary conditions controlling water flow in the saturated zone remained constant during all the experiment
- Sorption reactions on soil-water interface have occurred in both unsaturated and saturated zones for the three main PFAS found in the AFFF solution (6:2 FTSA, 6:2 FTAB, 6:2 FTSAam)
- Sorption reactions on air-water interface have occurred for the three main PFAS in the unsaturated zone. The magnitude of this reaction seems to decrease along the depth of the unsaturated zone. More the geomedium was unsaturated, greater the sorption reactions onto AWI has been.
- The three main PFAS in AFFF can be classified according to their concentration in pore solution as following: 6:2 FTSA » 6:2 FTAB > 6:2 FTSAam.
- The three main PFAS were not affected by degradation reactions during the PMP experiment
- No competition between the three main PFAS was expected for the sorption sites either onto SWI or AWI.

3.4.2. Numerical model set up

Based on the conceptual model, a model train combining: i) a groundwater flow model developed using MODFLOW software, ii) 1D-vertical model for simulating water flow in the unsaturated zone developed using 1D-Hydrus variably water flow module, iii) a groundwater solute transport model developed using MT3DMS and iv) a 1D-vertical model for simulating solute transport in the unsaturated zone developed using 1D-Hydrus solute transport module. The numerical scheme used to couple the software is the option 2 (see the paragraph 'Coupling scheme' in section 3.2.2). For each model of the model train, 5 main steps have been performed. They are described below.

Spatial and temporal discretization

The first step has been to define geometry and meshing of the groundwater flow model. The PMP has been described as a full 3D space of 5.2 m long, 3.6 m width and 3.0 m depth. This domain is discretized in 7020 square cells, each square cell has a side of 0.2 m (0.2 long, 0.2 width and 0.2 depth), except for the first layer of cell whose thickness is greater (1.2 m). The number of layers in the groundwater flow model is equal to 10. The first layer corresponds to the unsaturated zone in the PMP experiment. In this first layer, water flow is simulated by a 1D-vertical model built using 1D-Hydrus instead of the recharge modules available in MODFLOW. The thickness of the first layer has been defined to be sure that the bottom of the 1D-vertical model is below the deepest possible water table level that can occur during the simulations. To keep the model as simple as needed, a 1D-vertical model was not built for each cell of the first layer of the groundwater flow model. Two groups of cells have been defined, the cells located in the square where AFFF has been infiltrated and the cells outside of the AFFF infiltration square. In each group, hydrodynamic, solute transport and reactive properties as well as the associated boundary conditions are assumed identical for all the cells. Therefore,

only two 1D-vertical models were built. For these two 1D-vertical models, the simulated domain is divided in 121 nodes, hence cell thickness is equal to 0.01 m. For the 1D-vertical model built to simulate water flow in the AFFF-infiltration square, the cells have been distributed between 6 layers to simulate heterogeneities of the hydraulic properties as well as the decrease of PFAS sorption onto AWI along depth. As the thickness of each layer cannot be characterized, these values have been determined by calibration. The same geometry and meshing were used for the groundwater solute transport model and the 1D-vertical models developed for simulating solute transport. The time length of the PMP experiment (205 days) has been divided into 4920 stress periods. Each stress period has therefore a length of 1 h. For each stress period, boundary conditions are defined (see below).

Boundary and initial conditions

In the PMP, water in the saturated zone flows from left side to right side. On left side, constant head boundary is prescribed. On right side, a pumping well is located. The pumping rate is kept constant as it has been done during all the PMP experiment. For the unsaturated zone, transient boundary conditions are considered. More precisely, recharge, potential evaporation and solute fluxes are simulated at the top of the 1D-vertical models simulating water flow and solute transport in the cells of the AFFF infiltration square. The amount of infiltrated water (with and without AFFF) during the PMP experiment is simulated. For potential evaporation, mean values have been calculated for each hour based on the data collect periodically on air temperature and air humidity at the top of the PMP during the experiment. The same pattern of evaporation has been reproduced for each simulated day. To simulate solute fluxes, transient conditions are also considered. Prior and after AFFF infiltration, the water infiltrated is PFAS-free. During the infiltration stage, the infiltrated water contains non-reactive tracer compounds (bromide) and the three main PFAS found in the AFFF (6:2 FTSA, 6:2 FTAB and 6:2 FTSAam). The concentrations of these compounds are assumed equal to the mean values calculated based on the time series measurements performed on the input solution. For the 1D-vertical model used for the cells outside the infiltration square, only potential evaporation has been fixed as boundary conditions. Concerning initial conditions, the water content profile at the starting of the PMP experiment cannot be measured. In order to obtain steady-state conditions prior to standard the simulations of the PMP experiment, a prior modelling stage was simulated. During this stage with a time length of 70 days, a weekly infiltration of 120 L of PFAS free water is simulated in the cells of the infiltration square. Evaporation is also simulated considering the same values that during the simulations of the PMP experiment.

Hydraulic properties

In the two 1D-vertical models built, the Van Genuchten-Mualem equations are used to predict changes in hydraulic properties according to changes in pressure head. The values for these hydraulic functions are defined for each layer of the model. For the 1D-model developed for the cells located in the infiltration square, these values have been calibrated as they cannot be measured directly. For the 1D-model developed for the remaining surface of the PMP, the values were calculated using the distribution of the granulometric fractions in the geomeia. To avoid any discrepancy between the 1D-vertical models and the groundwater flow model, the

same hydraulic properties in saturated conditions are considered in the cells at the bottom of the former model and in the cells of the latter. No longitudinal neither transversal anisotropy is assumed. Hence, values of longitudinal and transversal saturated permeability are equal. Specific yield is kept similar in all the layer and set equal to value determined for sandy materials (0.353).

Solute transport properties

The apparent density is fixed based on measurement and set equal to 1900 kg/m^3 . The longitudinal dispersion assumed in each layer of the 1D-vertical model developed for the infiltration square is calibrated (see below). For the 1D-vertical domain for the remaining part of the unsaturated zone, the longitudinal dispersion is assumed equal in the 6 layers and is set equal to 10. This value is similar to the ones used for sandy materials. The same values of longitudinal dispersion are set identical in the deeper layer of the 1D-vertical models (Layer 6) and the saturated layers in the groundwater solute transport model. In the groundwater solute transport model, longitudinal and transversal dispersion are set identical. Diffusion does not affect PFAS fate and migration during the PMP experiment, hence diffusion and tortuosity coefficients are fixed to 0.

Reactive properties

Prior experiments at laboratory scale have demonstrated that the sorption reactions of 6:2 FTSA, 6:2 FTAB and 6:2 FTSAam in the geomeia onto SWI and/or AWI are not linear and not ideal (data do not show). Furthermore, these experiments illustrated that sorption reactions on SWI and AWI occur for the three PFAS.

A non-equilibrium chemical approach accounting for two-site adsorption model is used to simulate PFAS sorption reaction in the unsaturated zone below the infiltration square. This approach approximates sorption reactions onto SWI and AWI in the unsaturated zone without distinguished them. The Langmuir isotherm is used to simulate instantaneous sorption reaction while a first order rate sorption equation is used for the kinetically controlled sorption reaction. The proportion of the two groups as well as the values for the Langmuir isotherm and the rate of the kinetically controlled sorption equation have been calibrated for each layer of the 1D-vertical model devoted to the unsaturated zone below the infiltration square.

For the groundwater solute transport model located below and downstream of the infiltration square, the Langmuir isotherm is used to simulate sorption of PFAS onto SWI. The parameters values for cells below the infiltration square are calibrated.

3.4.3. Calibration

As mentioned above, values of several model parameters have been calibrated. A calibration approach relying on fitting iteratively several objective functions (see below), minimizing the difference between simulated and measured values, was used to define the values of the model parameters. The metrics used to characterize the discrepancy between measurements and simulations are the normalized root mean square error (nRMSE) and the correlation coefficient

(R^2). Furthermore, calibration was conducted by assuming constraints. One of them is that the a priori distribution of values for model parameter is narrowed based on literature knowledge. Spatial changes in model parameter values are also constrained based on the interpretations of the results of the PMP experiment. Last, interrelation rules between model parameters were also set. The modelling framework mentioned in section 3.2.3 was used, hence four steps was considered during the calibration.

The first calibration step was dedicated to estimate values of pore volume, the hydraulic properties and the longitudinal dispersivity of the 1D-vertical model (both variably water flow and solute transport built using 1D-Hydrus) for the cells located in the unsaturated zone below the infiltration square were fitted first. The objective function relies on the Br concentration measured during the experiment for the three sampling points located to the unsaturated zone. Based on the interpretations of the PMP experiment (see Annex B.2), the pore volume decreases along depth in the unsaturated zone. Hence, the values of pore volume attributed to an upper layer cannot be lower than the one used for a deeper layer in the 1D-vertical model. For the permeability in saturated conditions as well as the parameters of the Van Genuchten and Mualem functions, the values are assumed similar all along the unsaturated zone, except in the first layer close to the surface where the pore network is assumed to be disturbed during the filling of the PMP.

The second calibration step had focused on estimating the hydraulic properties and the longitudinal dispersivity for the cells located below and downstream the infiltration square in the saturated zone. Similarly, to the step 1, the objective function is to fit the Br concentrations measured during the experiment in the sampling point located below and downstream the infiltration square. As previously mentioned (see above), the model parameters in the cells of the model at the top of the saturated zone below the infiltration square was assumed to be identical to the model parameters at the bottom of the 1D-vertical model to avoid inconsistency in the capillary fringe. Furthermore, the impacts of AFFF infiltration on hydraulic and solute transport properties are assumed to be fading drastically according to the distance from the infiltration square. Therefore, for each model parameter, the range of values used for cells not below the infiltration square were assumed to be narrow and centered on the mean values estimated for the uncontaminated geomeia. As the geomeia is assumed isotropic, the same values were used for longitudinal and transversal dispersivities in the saturated zone.

The third calibration step was devoted to estimate the values for the thickness of the 6 layers assumed in the 1D-vertical models, the distribution of the two sorption site groups, the partition coefficient of the Langmuir equation, the maximum amount of sorbing site available in the Langmuir equation and the rate of first order kinetically-controlled sorption reactions in the unsaturated zone. As sorption reactions onto the SWI and the AWI were not differentiated during the simulations, the model parameters for the Langmuir equation and the first order rate equations are combinations of the independent values for each one of the sorption reactions either on the SWI or the AWI. This calibration step was conducted independently for the three main PFAS present in the diluted AFFF solution (6:2 FTSA, 6:2 FTAB and 6:2 FTSAam) as no interactions between the three compounds were assumed. For each of the three compounds, the data used were the measured concentrations measured during the experiment in the three sampling points located below the unsaturated zone. As observed by interpreting the measured results, the intensity of the sorption reactions onto the AWI decreased with depth, i.e. more PFAS are sorbed onto the AWI in the upper part of the unsaturated zone below the injection

square due to the higher surface of the AWI in the zone of the PMP, this latter resulting from the lower water content.

The model parameters describing the sorption reactions onto SWI in the saturated zone were fitted during the last calibration step. As in the third calibration step, this step was performed independently for each one of the three main PFAS present in the diluted-AFFF solution. For each compound, data used are the concentrations measured during the experiment in the sampling points located below and downstream the infiltration square in the unsaturated zone. To avoid discrepancy between the 1D-vertical model and the groundwater solute transport model dedicated below the infiltration square, the same values for the parameters of the Langmuir isotherm were used for cells at the bottom of the 1D-vertical model and the cells at the top of the groundwater solute transport model. The geomeia is assumed to exhibit low heterogeneity. In consequence, sorption reactions onto the SWI are expected to be identical below and downstream from the infiltration square. Therefore, the same values for the model parameters mentioned above are used for all the cells in the saturated zone below and downstream the infiltration square, except for the cells at top of the groundwater solute transport model.

The fitted values for hydraulic properties, solute transport properties and sorption reaction can be found in the Annex B.3.

3.4.4. Results

The main demonstration issued from the modelling activities on CS#6 is that the model train was able to reproduce accurately the measured spatial and temporal changes in concentration of 6:2 FTSA, 6:2 FTAB and 6:2 FTSAam during the PMP experiment, even if measured PFAS concentrations were overestimated or underestimated by the model at different sampling points (see Figure 3.2 and Figure 3.3). The changes in Br concentrations were also correctly reproduced (Annex B.4). As an illustrative purpose, the modelling results obtained along the main water flow path, below and downstream the infiltration square, are discussed. The model goodness-of-fit illustrates that the model developed using the model train for SGW continuum developed in the PROMISCES project is able to simulate the main physical and chemical processes controlling the fate of 6:2 FTSA, 6:2 FTAB and 6:2 FTSAam during the PMP experiment. The comparison between modelled and measured concentrations for both non-reactive tracer and PFAS allows to validate or not the hypotheses of the conceptual model, improving our understanding of the main processes controlling PFAS fate and transport in the simulated domain.

By demonstrating the high goodness-of-fit of the model to simulate spatial and temporal changes in non-reactive tracer concentrations in pore solution, three main hypotheses of the conceptual model can be validated:

- Evaporation at the top of the PMP has impacted water flow and solute transport during the experiment. This process explains that the non-reactive tracer concentrations in the pore solution rose above the concentration in the infiltrated AFFF solution. These results highlight that an accurate description of the boundary conditions at the top of the simulated domain is a key step to correctly simulate the fate and transport of the PFAS. Considering a very long residence time for some reactive PFAS such as PFOS and

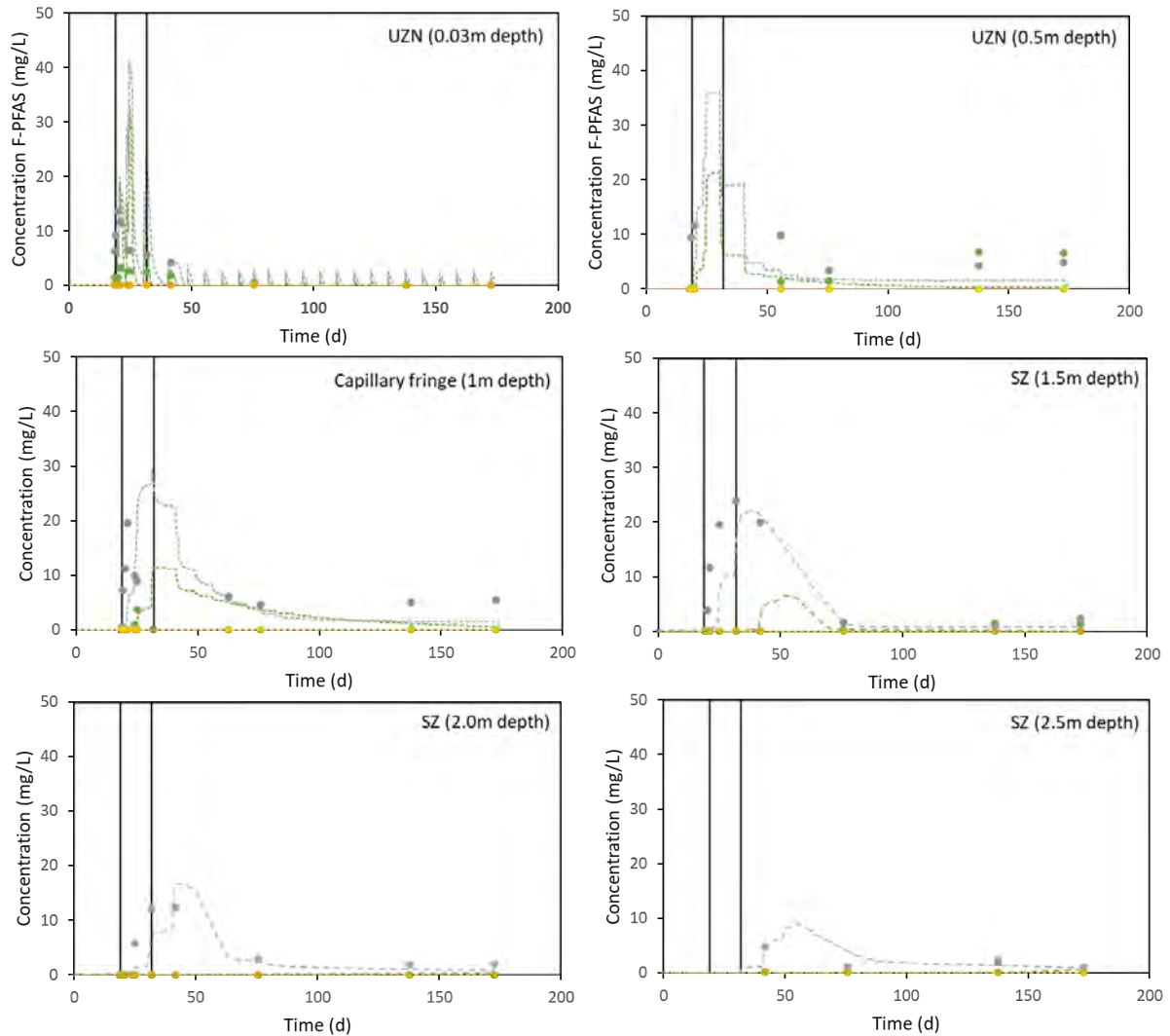


Figure 3.2.: Measured and simulated concentrations in 6:2 FTSA (grey), 6:2 FTAB (green) and 6:2 FTSAam (yellow) over time in pore solutions at five depth (0.03 m, 0.5 m, 1 m, 1.5 m, 2.0 m and 2.5 m depth) in the unsaturated and saturated zones below the infiltration square during the PMP experiment. Concentrations are expressed in mgF/L. Lines represent simulated concentrations over time while dots represent measured concentrations.

some hydrogeological context, this step could be complex as boundary conditions need to be reconstructed on several decades and data availability on such time length is rare.

- The decrease of the pore volume in the unsaturated and saturated zones below the infiltration square This phenomenon is induced by foam formation in the pore network during AFFF infiltration. Indeed, the calibrated values of the pore volume for the cells of the unsaturated and saturated zones below the infiltration square are lower than the values estimated in the uncontaminated geomeia (Annex B.3). This decrease of the pore volume is interpreted because of the foam formation during the AFFF infiltration stage, which blocks some pore throats in the porous network. This foam seems stable during the experiment as the same values of pore volume are used to simulate solute transport during the PFAS leaching stage. Furthermore, the PFAS sorbed onto the SWI has decreased the interfacial tension, promoting water flow in pore network. These changes in hydraulic and solute transport properties of the geomeia below the infiltration square induce preferential water flow and mass transfer, explaining the quick increase and decrease of the non-reactive tracer and PFAS concentration at the beginning of the AFFF infiltration and PFAS leaching stages, respectively.

Changes in hydraulic and non-reactive solute transport properties occurs only below the infiltration square and does not extend downstream. The calibrated values for the hydraulic and solute transport properties for the cells located downstream to the infiltration square in the saturated zone are similar to the ones estimated for the uncontaminated geomeia (Annex B.4).

The calibration approach by performing iterative steps to calibrate first the non-reactive tracer and then the PFAS concentrations allows to identify correctly the main characteristic of the sorption processes onto the SWI and AWI in the fate and transport of the three main PFAS present in the infiltrated AFFF. Four hypotheses of the conceptual model concerning sorption reaction have been validated.

- PFAS sorption reactions onto the SWI and AWI in the unsaturated zone as non-equilibrium should be used to simulate accurately the spatial and temporal changes in PFAS concentrations in this zone. The sorption reactions were non-ideal and non-linear as depicted using the Langmuir isotherm and a first-order rate equation. In consequence, the values of the model parameter cannot be compared with the partition coefficient values issued from existing literature or in silico approach as most of them account for a linear sorption reaction.
- As illustrated by the higher values of the Langmuir partition coefficient and rate of the kinetically controlled sorption reaction in the upper part of the unsaturated zone compared to the deeper part, PFAS sorption onto the AWI has a key role for the three main PFAS present in the AFFF. The intensity of this sorption reaction is higher when the water content is low as the surface of the AWI increases. The model outputs (data not shown) indicate that the three PFAS are mainly sorbed in the first 30 centimetres below the infiltration square, explaining the strong decrease of PFAS concentrations in pore solution compared to the infiltrated AFFF solution.
- In the saturated zone, PFAS sorption reactions are non-linear for the three main PFAS present in the infiltrated AFFF as Langmuir isotherm needs to be used to simulate

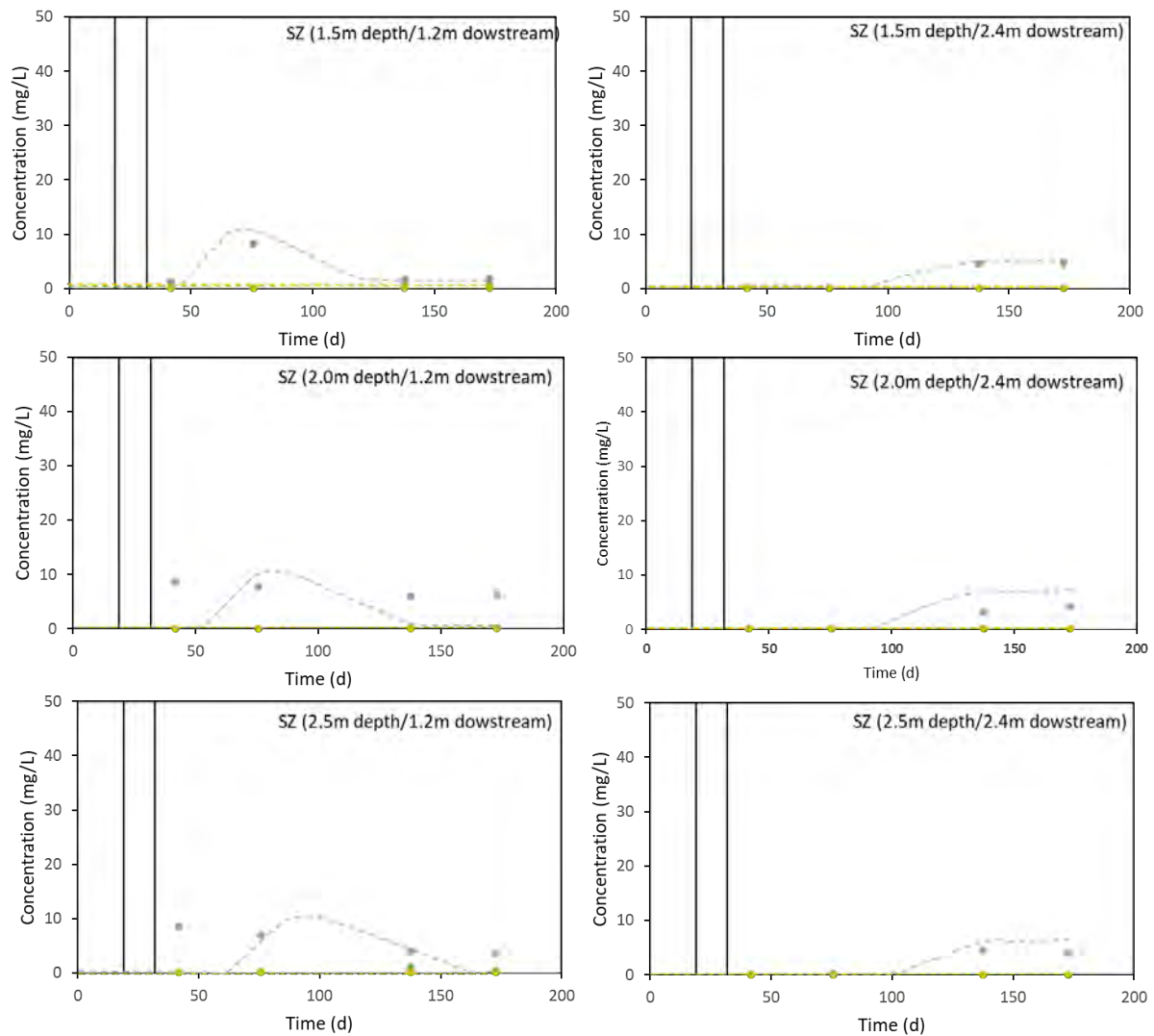


Figure 3.3.: Measured and simulated concentrations in 6:2 FTSA (grey), 6:2 FTAB (green) and 6:2 FTSAam (yellow) over time in pore solutions at three depths (1.5 m, 2.0 m and 2.5 m depth) in the saturated zone in two locations (1.2 m and 2.4 m far from the centre of the infiltration square) downstream to the infiltration square in the main flow path during the PMP experiment. Concentrations are expressed in mgF/L. Lines represent simulated concentrations over time while dots represent measured concentrations.

accurately spatial and temporal changes in the dissolved 6:2 FTSA, 6:2 FTAB and 6:2 FTSAam concentrations.

- The magnitude of the sorption reactions onto the SWI and AWI vary according to the PFAS present in the infiltrated AFFF. 6:2 FTSAam is the most-sorbed PFAS, followed by 6:2 FTAB. By comparison, 6:2 FTSA is less sorbed onto the SWI and AWI, explaining that this compound is the only one migrating downstream to the infiltration square. These results confirm that the molecular structure of the PFAS, including carbon chain length, hydrophobicity and nature of the functional group, are key data to understanding PFAS migration.

The conclusions from the modelling of the CS#6 can be used to highlight the key processes that need to be investigated in real AFFF-contaminated sites and demonstrate that the model train can be used to build models for real AFFF-contaminated sites dealing with natural complexity and heterogeneity in terms of water flow and reactive solute transport.

Key messages of the PluriMetric Pilot experiment

The model train developed in the PROMISCES project can be used to simulate PFAS fate and transport in the SGW continuum in a semi-real scale experiment in controlled conditions.

The selection of the key processes, that are considered in the model, is a complex task as a broad range of physical and chemical processes, and their spatial and temporal pattern in the simulated domain, had an impact on PFAS fate and transport, hence the building of the conceptual model based on available data is a key step.

The use of time series measurements of PFAS to calibrate the model increases drastically its robustness.

High frequency monitoring of PFAS fate and transport in the unsaturated zone is required as a sharp migration front can occur in this zone.

Interrelations between physical and chemical processes controlling fate and transport of PFAS should be considered in the model as illustrated by the changes in hydraulic and solute transport properties that are impacted by AFFF infiltration. IN the PMP experiment, the AFFF was locally present in the pores as a separate phase.

Water flow rate in the unsaturated zone should be carefully simulated to predict accurately migration front of the more mobile PFAS.

The sorption reactions of the monitored PFAS (6:2 FTSA, 6:2 FTAB and 6:2 FTSAam) onto the soil-water interface and the air-water interface are non-linear and non-ideal in the unsaturated zone.

Capillary fringe displacement plays a key role in the reactive transport of the three monitored PFAS by controlling water flow rate in the unsaturated zone and modifying PFAS sorption onto AWI.

3.5. Application of the model train in the CS#7 AFFF-polluted aquifer

To demonstrate a real-life application, the previously described approach and model train were tested on field scale, in the aquifer polluted with CS #7 AFFF. This area is of interest because of its relatively pristine aquifer, polluted exclusively by aqueous film forming foams (AFFF), rich in PFAS, which have been periodically released in fire-fighting training activities. Unfortunately, data outside the polluted site and the project implementation period are very scarce, forcing us to simplify the model geometry and scope, aiming only to roughly reproduce spatial distributions, rather than absolute exact magnitudes.

The aquifer is composed of alluvial and colluvial Quaternary sediments (10 m thickness), which lay unconformably over the bedrock (fractured granodiorite and granite). Soil data show that PFAS are retained at the sandy silt sediments present between minus 2 and minus 4 meters. The concentrations in groundwater for some PFAS extinguish close to the source, while others, such as PFOS, peak around 7.5 m downgradient. The most abundant PFAS at this site are PFBA, PFPeA, PFHxA, PFOA, PFHxS, PFOS and 6:2 FTS. 6:2 FTS has a complex degradation pathway under natural conditions that leads to PFBA, PFHxA, and PFPeA (Held and Reinhard 2020). The other three PFAS (PFOA, PFOS, and PFHxS) are known to be undegradable under natural conditions. From these, PFOS shows the highest concentrations in both the solid and liquid phases. Therefore, it was chosen for the modelling.

To analyze the fate and transport of PFAS, we set up a 2D vertical cross-sectional model in a two-step model train, as explained in previous sections. The unsaturated zone was modeled with *HYDRUS 1D* (*Phydrus*), while the saturated zone was modeled with *MODFLOW/MT3D* (*FloPy*). The model reflects the average flow path of groundwater flowing downhill through the polluted site towards the nearby river. The exact location of the site is not shown due to confidentiality issues.

A 1D vertical transport model was set with *Phydrus* (Python library to run HYDRUS 1D, Collenteur et al. 2019) for the unsaturated zone below the source. The vertical 600 cm domain was divided into 5 zones: anthropogenic fill (160 cm), fine silty sands (200 cm), gravels (120 cm), fine silty sands (30 cm) and gravels (90 cm). Initial hydraulic and transport parameters were obtained from lab experiments. Information on the quantity of product used in each firefighting event and its frequency was not available. Therefore, we assumed two events per month, in which 20,000 l of diluted foaming products were estimated to be used. PFOS concentrations in foaming products were approximated based on Høisæter et al. (2019).

A 2D flow model was set up in *FloPy* (Python library to run MODFLOW6 models, Hughes et al. 2023; Bakker et al. 2016; Bakker et al. 2024) to model fate and transport in the saturated zone. The modelled space is 700 m long and around 14 m depth. The top boundary is the average piezometric level. A constant head boundary was prescribed at the left side (up-gradient), and a drain boundary was set at the river location, while the bottom was assumed impermeable.

At the top, a recharge flux boundary condition was set using the bottom leachate of the unsaturated zone model. Three lithologies were defined, a high permeable sandy layer, a lower permeability weathered granite and a very low permeability granite layer at the bottom. Initial values for the hydraulic conductivity of the site were obtained from slug tests performed during the characterization phase.

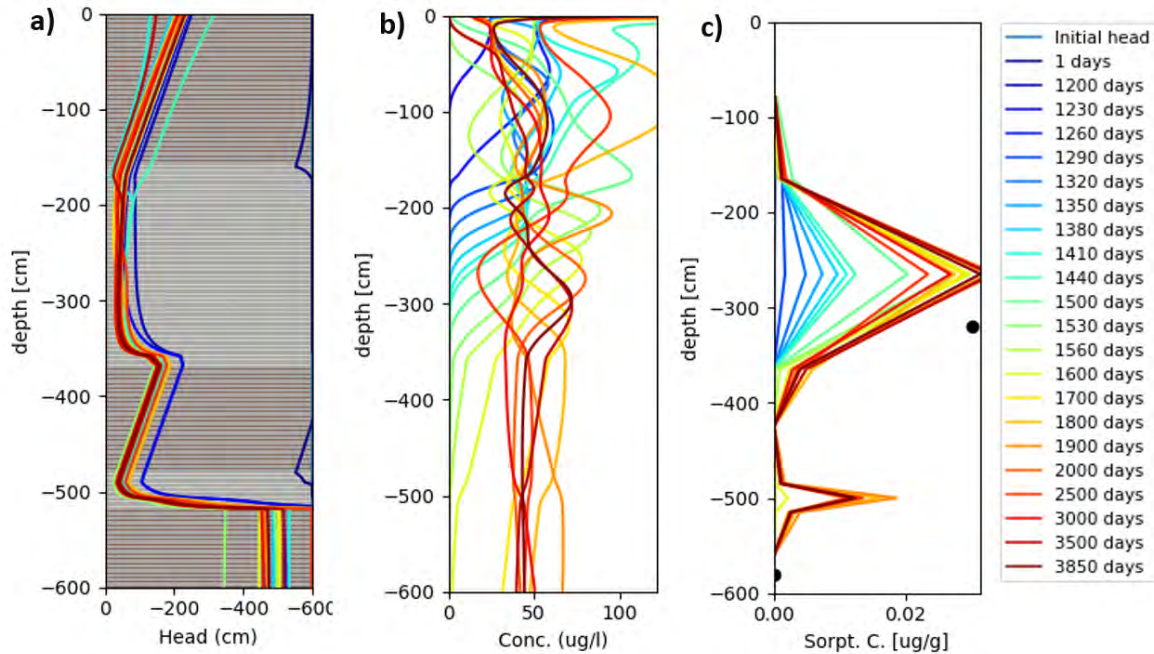


Figure 3.4.: Vertical distribution of main HYDRUS 1D modelled variables in the unsaturated profile: a) Head in cm and distribution of materials. b) Evolution of PFOS concentrations in liquid phase. c) Lines represent modelled sorbed concentration over time for each layer, while black dots represent measured PFOS concentrations in soil at the field site.

Both models were run over a period of 2146 days (starting in January 2016 ending in November 2021 when the field campaign took place). To reach a stationary initial state before the period of interest, the HYDRUS1D model was run for 1200 days with annual average precipitation and evapotranspiration values. Hydraulic conductivities (K_f), linear sorption coefficients (K_d) and PFOS input concentration through the top boundary, were calibrated by roughly matching field measurements (Figures 3.4.c. and 3.5).

For the HYDRUS1D model, calibrated hydraulic conductivities are larger than those measured in the field ($0.0003 - 1$ m/day), while linear sorption coefficients are a bit smaller, than those measured in the lab ($2.7 \cdot 10^{-6}$ m³/g) (Table 3.1). These deviations from the expected value do not come as a surprise. Hydraulic conductivities were estimated from soil samples, which may not be fully representative from the complete profile. Linear sorption coefficients may be overestimating sorption, since they were obtained in the lab with isotherms that did not reach saturation, and PFOS sorption does not behave linearly. PFOS input concentrations were also calibrated, since the PFAS pollution source term is not known.

The modelled PFOS concentrations in groundwater are in the order of magnitude of observed ones, though a bit higher. Oscillations in the concentration of the recharge flux at the source

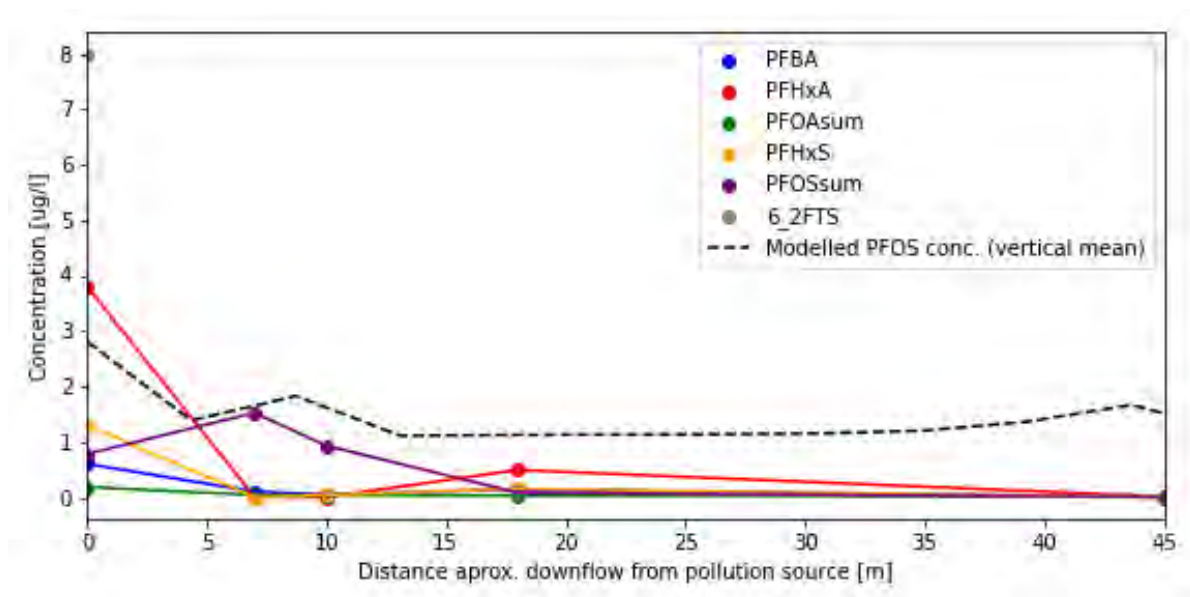


Figure 3.5.: Downgradient (from the source) distribution of most abundant PFAS at the site in the saturated groundwater. Data obtained during a sampling campaign in autumn 2021. Dashed line represents modelled concentrations of PFOS. Reported concentration in the field for PFOS and PFOA.

Table 3.1.: Adjusted flow and transport parameters for the HYDRUS-1D unsaturated zone and for the MODFLOW6 2D saturated zone models

Model layers (HYDRUS1D)	Kf (m/day)	Kd (m ³ /g)	Model layers (MODFLOW/MT3D)	Kf (m/day)	Kd (m ³ /g)
Anthropic fill	200	1 · 10 ⁻³	Anthropic fill	1	6 · 10 ⁻⁷
Buffer layer (10 cm)	2	3 · 10 ⁻⁴	Buffer layer (10 cm)	1	6 · 10 ⁻⁷
Fine silty sands	0.2	6 · 10 ⁻⁵	Fine silty sands	0.1	6 · 10 ⁻⁷
Buffer layer (10 cm)	2	3 · 10 ⁻⁴			
Rounded gravels	200	1 · 10 ⁻³			
Buffer layer (10 cm)	2	3 · 10 ⁻⁴			
Fine silty sands	0.2	3 · 10 ⁻⁵			
Buffer layer (10 cm)	2	3 · 10 ⁻⁴			
Rounded gravels	200	1 · 10 ⁻³			

are reflected as concentration pulses in the downflowing plume. Based on the model, it takes PFOS around a year to reach the groundwater level, and around 2 years to reach the river. Further description of the model implementation can be found in Annex C.

The modelling approach presented here combines *HYDRUS1D* and *MODFLOW/MT3D* to model PFAS fate and transport from the source at the soil surface, to the exfiltration point, in a downgradient river. The model uses a simple linear sorption to approximate observed PFOS concentration in soil and liquid phases. Based on the model a rough estimation of the time for the PFOS plume to reach the river was obtained.

Due to the lack of field data, the approach to model the behaviour of PFAS was simplified, in order to avoid an overfitting problem. In reality, sorption of PFAS at the soil matrix does not behave as a linear isotherm. Moreover, sorption at the air-water interface, which is very relevant for some PFAS, is also not incorporated in the Hydrus-1D code. As a result, the obtained K_d values are effective values of sorption. This approach is acceptable as long as the ratio of the soil-water content to the area of the water air interface remains constant. The complexity of the model should go in line with the amount and quality of the available data. Therefore, in the absence of lots of data, the combination of *HYDRUS1D* and *MODFLOW/MT3D*, through their Python libraries, could be a good starting point for modelling the fate and transport of PFAS.

In an optimal situation, in which sufficient spatial and temporal coverage of the data is available, the main limitations of this approach are, (a) the lack of a real coupling between both models, and (b) the lack of adsorption of PFAS at the air-water interface in Hydrus-1D. The effect of temporal changes in the water content on the ratio of adsorbed and dissolved PFAS is therefore not described. This assumes the fringe zone does not move, neglecting the contribution of draining and rewetting cycles to the leakage of PFOS to the groundwater. This is an important process for PFAS transport, as they are substances that concentrate at the interface between air and water.

Key messages of model applications at the CS#7 AFFF-polluted aquifer

Both HYDRUS-1D and MODFLOW/MT3D models are open-source codes freely available and ready-to-use through their Python libraries. Although their use in a detached manner (not-coupled) neglects the importance of the fringe zone oscillation in the sorption/desorption of PFAS, they are helpful for an initial assessment of the PFAS fate.

More complex modelling approaches require a corresponding amount of field data to calibrate the required number of parameters necessary to define the different sorption types, without overfitting.

If a detailed model needs to be implemented, it is necessary to perform several PFAS sampling campaigns in both solid and liquid phases including different moments of the hydrological year to catch oscillations in the fringe zone.

3.6. Limitations and further outlook

Despite the demonstration that the model train can be applied successfully to simulate PFAS fate and transport in both CS#6 and CS#7, three main limitations/recommendations in the use of this approach need to be mentioned:

- The work conducted in PROMISCES shows that PFAS fate and transport in the SGW continuum is mainly controlled by water flow in both unsaturated and saturated zone, advection-dispersion in the pore network, sorption reactions onto the SWI in both unsaturated and saturated zone, and sorption reactions onto the AWI in unsaturated zone. Nonetheless, a robust interpretation of the results obtained on the studied domain must be done to elaborate the conceptual and numerical model, to characterize the spatial and temporal variability of these four processes in the studied domain, as well as the boundary conditions that could impact them. This work can be mainly performed by conducting a comprehensive interpretation of the data collected on the studied domain. However, the often-limited number of data available hampers the construction of robust conceptual model. Among the key data that are the most difficult to obtain are the amount of AFFF, their composition, and the variation in time of the released concentrations. As boundary conditions of the studied domain such as regional groundwater flow, precipitations, evaporation or plant transpiration control strongly water flow and reactive solute transport, they have to be carefully collected. However, PFAS could exhibit a large residence time in porous media according to their molecular structure and porous media properties, implying that data to characterize the boundary conditions need to be collected over several decades and not only on recent years. This limit can be partially overcome by developing various version of the conceptual model, and the associated numerical model, to quantify the impact of various processes on PFAS fate and transport in the studied domain
- Despite a broad range of numerical formalisms to describe the main physical, chemical and biological processes controlling PFAS fate and transport in the SGW continuum, some numerical developments should still be conducted to include numerical formalism, allowing to describe some additional processes identified during the simulations of the CS#6 and CS#7. Among the identified process, PFAS sorption reactions onto the AWI has been demonstrated as a key process controlling PFAS fate and transport in the unsaturated zone, allowing complex PFAS retardation patterns during a long time period. Another numerical development could be done for allowing simulations of the water lateral fluxes and mass transfer in the unsaturated zone. These processes are currently not simulated. Such development could improve the understanding on the impact of the change in pore volume and hydraulic properties on PFAS transport in the unsaturated zone of SGW continuum strongly contaminated by PFAS. One should note that prior to any numerical developments, a review of the existing numerical formalism, including empirical and physically based formalism, should be conducted to identify the main advantages and limits of each one of them. This knowledge can be used to select the most appropriate formalism and avoid any unnecessary numerical development.
- In real PFAS contaminated sites, with scarce monitoring data, calibration step of a model built using the model train developed in PROMISCES can be a limiting step. The examples provided by simulating PFAS fate and transport in CS#6 and CS#7

illustrate that a limited dataset obtained during only one field campaign cannot be used in calibration step, as a broad range of model parameter values are estimated during this step. To improve model calibration, time series of PFAS concentrations should be acquired by performing monitoring field campaign over time. To be more efficient, different period of the hydrogeological cycle must be targeted to better quantify the role of the fringe zone in PFAS transport in the studied domain.

4. Catchment – river – riverbank filtration – drinking water

Key messages of the chapter

The combination of stand-alone models in model trains expands the scope that can be covered in the context of catchment – river - riverbank filtration - drinking water interaction. Model trains can combine stand-alone models either in a complementary way or in a sequence.

A complementary combination may either compare models of different complexity to find out which level of complexity (and associated efforts) is needed to answer which questions or may compare different models with their different strengths and weaknesses in parallel to assess uncertainties, and/or use models for scenario evaluation according to their specific capability.

A sequential combination facilitates a broader application in terms of content and a combination of approaches at different spatial resolutions. Clearly defined interfaces are essential for a successful implementation.

Examples of model trains for selected PFAS are presented for the catchment – river interaction in the urban context of the Berlin case and for the whole catchment – river – riverbank filtration – drinking water interaction on the scale of the upper Danube Basin.

The Berlin case demonstrates the application of the sequential model train by combining an emission model of the city with a fate and transport model of the city's surface waters.

The Danube case demonstrates the application of a sequential model train by combining large catchment scale emission models with different types of bank filtration fate and transport models for specific locations in the catchment. Further, it also demonstrates the complementary application by comparing emission models with different strengths and weaknesses for the assessment of multiple scenarios on the catchment scale and different levels of complexity for fate and transport modelling of bank filtration.

4.1. General aspects

In addition to water abstraction from groundwater via springs and wells or directly from surface waters, abstraction via riverbank filtration is a commonly used method to gain raw water for drinking water supply (see Figure 4.1). Riverbank filtration is a type of filtration that works by passing water to be purified for use as drinking water through the banks of a river or lake. It is then drawn off by extraction wells some distance away from the water body. Three filtration mechanisms are possible. Physical filtration or straining takes place when colloids and suspended particulates are too large to pass through interstitial spaces between alluvial soil particles. The second mechanism is biological degradation occurring when soil microorganisms remove, and digest dissolved or suspended organic material and nutrients. The last is chemical filtration including ion exchange that may take place when dissolved chemicals adsorb to alluvial soils when passing through with water movement. Many contaminants (microbial organisms and inorganic or organic pollutants) will be removed by bank filtration, either because they get filtered out by the solid phase of the bank, because the residence time (which may be days or potentially weeks) is sufficient to render them inactive or if they are adsorbed by the soil material. Therefore, abstraction via bank filtration is a preferred option of water supply over direct use of surface water in more downstream areas of larger rivers, in cases where the catchment of the water body cannot be sufficiently protected by protection zones and bank filtration offers a natural first purification step. For instance, 45%, 50% and 16% of the total drinking water supply are provided by bank filtration in Hungary, Slovakia and Germany, respectively (Handl et al. 2017).

Potential problems for water supply via bank filtration arise from the fact that filtration capacity of the riverbank is limited and depends on its width, the property of the soil as well as the physical-chemical properties of the pollutants. As water from a river (or a lake) is the source of riverbank abstraction, the whole catchment may contribute to impacts on drinking water quality, especially if persistent and mobile chemicals are considered. All different types of human activities in the catchment are potentially acting as sources or pathways of contamination of the river and connected water supply via bank filtration (industrial and agricultural activities, chemical use in households, waste and wastewater disposal...). Regarding circular economy routes, drinking water supply via bank filtration is considered as “semi closed water cycle” as industrial and urban waste waters are discharge into the rivers and indirectly and unintended reused for drinking water supply after mixing and dilution in the natural runoff of a region. Figure 11 shows the schema of circular economy route “semi-closed water cycle” in the context of catchment – river – riverbank filtration – drinking water interaction.

Exposure assessment of drinking water from bank filtration via emission, fate and transport modelling requires a model train covering the whole catchment – river – riverbank filtration – drinking water interaction. That means it should on the one hand consider the sources and pathways of pollutants in the catchment, the transport and fate of the chemicals in the river system, as well as the behaviour and fate during the filtration step in the riverbank of the river to the water abstraction. This offers the chance to explain reasons for pollution levels in drinking water and to calculate scenarios for potential future developments as implementation of measures, changes in chemical use, accidental spills or climate change. In the upcoming chapters we focus on emission models at catchment scale, on emission modelling in an urban

context, on fate and transport modelling at bank filtration sites and present application cases for Berlin and the upper Danube catchment.



Figure 4.1.: Schema of the circular economy route “semi-closed water cycle” in the context of catchment – river – riverbank filtration – drinking water interaction.

4.2. Emission models on catchment scale in the context of model trains

4.2.1. General

Emission models at the watershed scale are typically used by river basin management (RBM) authorities as part of the implementation of the Water Framework Directive (WFD), the main EU regulatory instrument for water management (2000/60/EC). Emission modelling can be used for Priority Substances (PS) and Priority Hazardous Substances (PHS), for which environmental quality standards (EQS) have been defined (EC, 2013) at the European level. Compliance with these EQS is required to achieve “good chemical status”. Emission modelling can also be used for pollutants of regional or local relevance (River Basin Specific Pollutants, RBSP), for which EQS need to be established and compliance achieved as part of achieving “good ecological status”. Finally, emission modelling can address various Contaminants of Emerging Concern (CEC), which are not (yet) regulated. The WFD requires the preparation of an inventory of emissions, discharges and losses of all PS and PHS that are found relevant. Such

inventories should inform RBM authorities on the loads discharged to the aquatic environment. In 2012, Guidance Document No. 28 on the Preparation of an Inventory of Emissions, Discharges and Losses of Priority and Priority Hazardous Substances was issued, as part of the Common Implementation Strategy for the European Commission (EC) 2012. This introduction is based on the information compiled in this Guidance.

An emission inventory should be seen as a tool, which may be used to:

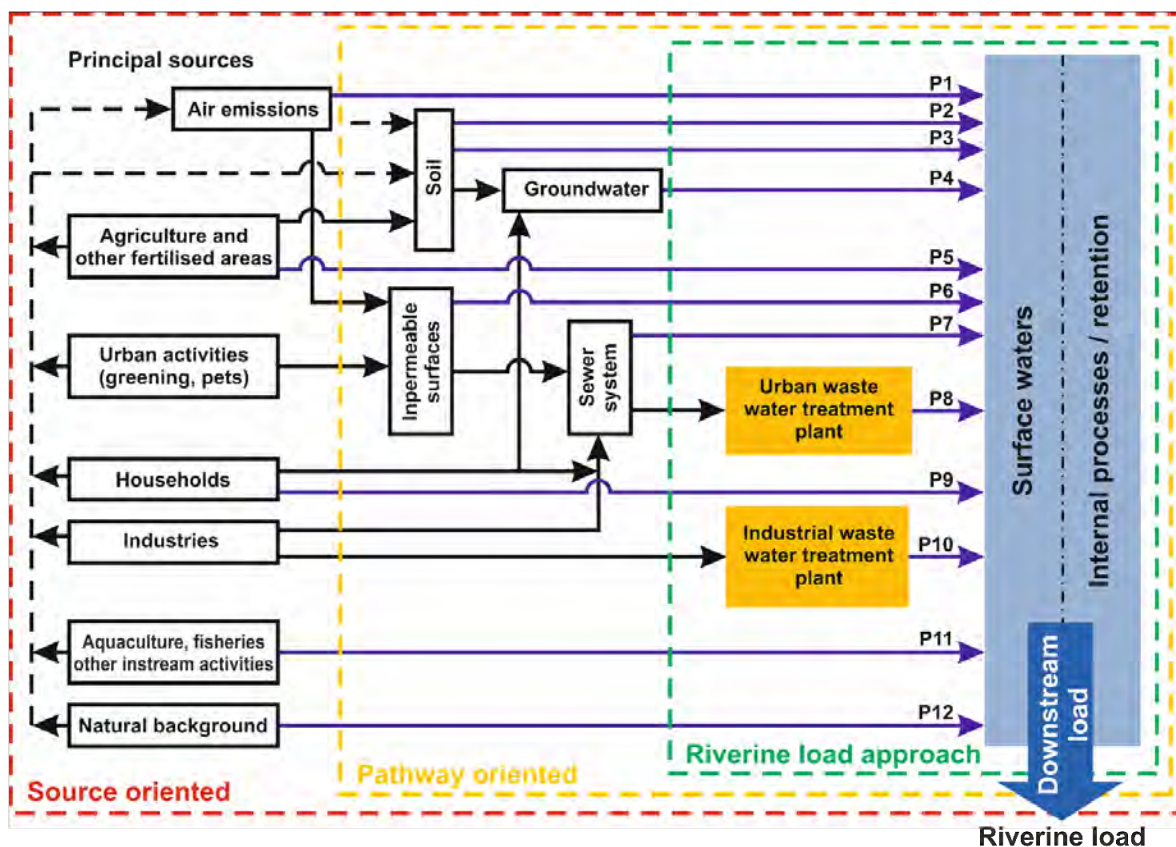
- provide quantitative understanding of present emissions (diagnosis), which is a prerequisite for defining (cost-)effective control measures;
- appreciate knowledge and data gaps and subsequently provide focus for future research and data collection;
- conduct scenario analyses (prognosis) to assess the efficacy of pollution control measures and/or the impact of external changes (e.g. climate change & adaptation measures).

Especially for the latter objective, emission modelling is combined with water quality (fate & transport) modelling, to translate the emission inventory into in-stream concentrations.

For the elaboration of the emission inventory, the Guidance discusses four so-called “tiers”:

1. Tier 1 comprises an inventory of point sources using statistical data including point source information reported under the European Pollution Release and Transfer Register (E-PRTR).
2. Tier 2 adds a quantification of in-stream loads, based on concentration and discharge data. The resulting riverine load, in combination with the information gained in tier 1 allows the allocation of observed loads to point and diffuse sources. A high contribution of diffuse sources is a reason to proceed to tier 3 or 4.
3. Tier 3 is a pathway-oriented modelling approach, using more specific information about land use, hydrology and basic transport processes of pollutants towards the surface water. Regionalized emissions for small catchments (analytical units) are calculated and subsequently aggregated to larger units.
4. Tier 4 is the source-oriented modelling approach, that sets up a mass balance or Substance Flow Analysis (SFA) and addresses the whole system starting from the principal sources of substance release.

Figure 4.2 provides a schematic overview of Tier 2, 3 and 4 and their inter-relation.



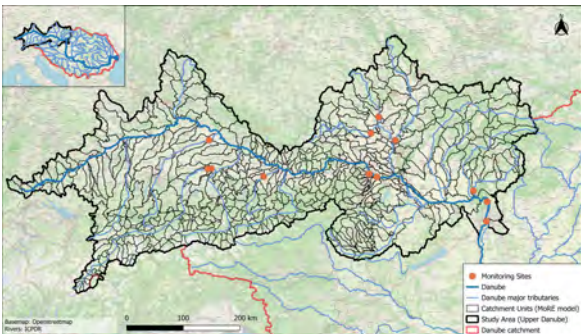
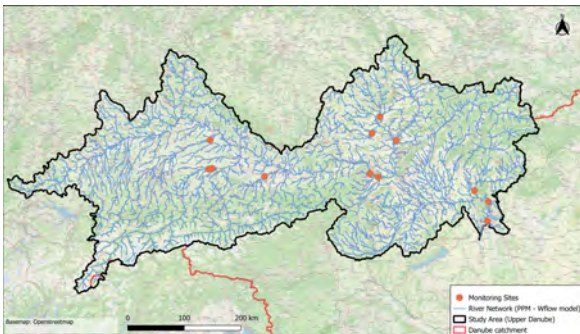
Pathways		
P1	Atmospheric deposition directly to surface water	P7 Storm water outlets and combines sewer overflows + unconnected sewers
P2	Erosion	P8 Urban wastewater treated
P3	Surface runoff from unsealed areas	P9 Individual – treated and untreated – household discharges
P4	Interflow, drainage and groundwater	P10 Industrial wastewater treated
P5	Direct discharges and drifting	P11 Direct discharges from aquaculture, fisheries and other instream activities
P6	Surface runoff from sealed areas	P12 Natural background

Figure 4.2.: Overview of riverine load (Tier 2), pathway-oriented (Tier 3) and source-oriented (Tier 4) approaches. Modified from Chorus and Zessner (2021) and European Commission (EC) (2012).

4.2.2. Modelling approaches

The PROMISCES project applied models in support to both Tier 3 and Tier 4 approaches, covering the Danube River Basin upstream of Budapest. A compact comparative assessment of the two approaches is shown in Table 4.1.

Table 4.1.: Compact comparative assessment of MoRE model and PPM model applied in the upper Danube Catchment.

Modelling of Regionalized Emissions (MoRE)	PROMISCES watershed model for PM substances (PPM)
	
Pathway-oriented (Tier 3; WFD Guidance)	Source-oriented (Tier 4; WFD Guidance)
526 analytical units with an average size of 350 km ² and a single (in specific cases two) outflow point and an upstream downstream connection	Regular grid consisting of 81,217 cells (~ 1500 × 1500 m)
Simulates annually/seasonally steady states	Simulates day-to-day variability
Operates on annually averaged hydrology information (generated by the Tier 4 model)	Calculates the time dependent hydrology using global and local weather data
Calculates average emission loads via different pathways (see Figure 4.2). For PFAS diffuse emissions from legacy pollution (PFAS production and inhabitant related pollution as firefighting grounds eg. at airports and landfills) have been implemented for the first time.	Calculates daily time series of emissions
Calculates annual average water quality with potentially using retention parameterized on hydrological indicators	Calculates water quality using a dynamic fate & transport model
Specific input data used: substance concentrations in simulated pathways	Specific input data used: substance flux (mass/time) released from simulated sources (see Figure 4.2)

MoRE	PPM
Model is validated on in-stream loads and concentrations	Model is validated on in-stream concentrations
Scenario assessment of the model mainly addresses measures focusing on specific pathways. In combination with climate driven water balance models, climate scenarios can be implemented	The model is capable of assessing scenarios focusing on reduction of emissions via source abatement, may calculate effects of accidental spills and implement climate scenarios.
Runs on Windows-based computers. Offers graphical user interface, but still technically challenging.	Runs on Windows-based personal computers. No graphical user interface available for less-experienced users. Technically more challenging.

Both models use the following spatial information and data (though they often express it differently): (a) catchment delineation and digital terrain model; (b) land use, population and settlement types; (c) soil loss; (d) water consumption; and (e) stormwater and wastewater collection and treatment infrastructure. Both models apply the principle of mass balances on (sub) catchment scale, which calculates the instream loads of the river net (I) along the flow tree based on the sum of emission loads (E) minus substance degradation (D) and retention (R) and the substance concentrations (c) based on instream loads (I) at a specific point subdivided by the river flow (Q):

$$I = \Sigma E - D - R \quad (4.1)$$

$$c = I/Q \quad (4.2)$$

Conceptual differences result in the fact that both models have complementary strengths and weaknesses. In respect to application by river basin management (RBM) authorities MoRE (Fuchs et al. 2017) is characterized by much stricter implementation and documentation requirements reducing the flexibility but making used input information, calculation steps and results more transparent, while the PPM model (Verseveld et al. 2024; DELTARES 2025; Smits and Beek 2013) as expert tool has its strength in a higher flexibility during application which reduces the transparency. In respect to resolution the focus of the PPM model clearly lies on the time resolution as it is driven by daily time steps of a hydrological model. The focus of MoRE model is much stronger on substance specific data of different pathways and therefore on the regional representation of these pathways on the level of analytical units. The complementary foci are of clear advantage for a combined application in a model train. While MoRE highly benefits from the PPM model by high resolution water balance modelling and resulting flow data including the possibility of climate driven runoff scenarios, the PPM model benefits from data on emission pathways from MoRE either for validation of its calculations of pathway emissions or for back-calculating emission factors of emission sources and is able to disaggregate this information to calculations of river concentrations with daily time step.

The latter is a requirement in case scenarios include more dynamic changes with time as it is the case in the accidental spill scenario presented in section 4.6.4. More details for the MoRE application in the context of this guidance document can be found in Annex D and for the PPM model in Annex E.

4.3. Emission model in an urban context

4.3.1. General aspects

Precipitation events can introduce large quantities of various pollutants, nutrients and pathogens into surface waters. Urban water bodies with densely populated and highly sealed catchments are often particularly affected by stormwater discharges from the separate sewer system and combined sewer overflows (CSOs). Quantitative estimates of the chemical loads in stormwater and wastewater runoff are an important basis for the assessment of water pollution. This chapter presents a method to assess the rain-related PMT/PFAS pollution situation of surface waters caused by urban drainage inputs via source-pathway and process descriptions.

Based on measured data and/or additional literature data with a monthly resolution, monthly loads of substances entering surface waters via the three pathways of stormwater discharges from separate sewer systems, wastewater treatment plants and combined sewer overflows are calculated (Figure 4.3). For this purpose, an emission model has been developed specifically for an urban catchment to calculate PFAS and PMT loads. The calculated loads are then used in a surface water model to predict the fate and transport of these substances in the surface water systems. As the substances may adsorb to particulate organic material, it is possible that in areas (or periods) with very low flow velocities, sedimentation of the organic material and the adsorbed pollutants occurs. Adsorption will likely not affect all PMTs and certainly not in the same amount, so that some variation has to be considered.

4.3.2. Emission model

A number of input parameters are required for the emission model to calculate the monthly load of pollutants entering various water bodies and watercourses via stormwater and wastewater via the separate sewer system, combined sewer overflows (CSOs) and wastewater treatment plant (WWTP) effluents:

1. Mean concentrations in stormwater runoff
2. Mean concentrations in wastewater (+ CSO)
3. Mean concentrations in WWTP effluent
4. Stormwater runoff volumes (separate sewer system), in m³/month for defined water bodies
5. Wastewater volumes (WWTP effluent & CSO* volumes) discharged to receiving water bodies, for defined water bodies

*CSO volumes are estimated at 0.3% of wastewater volumes

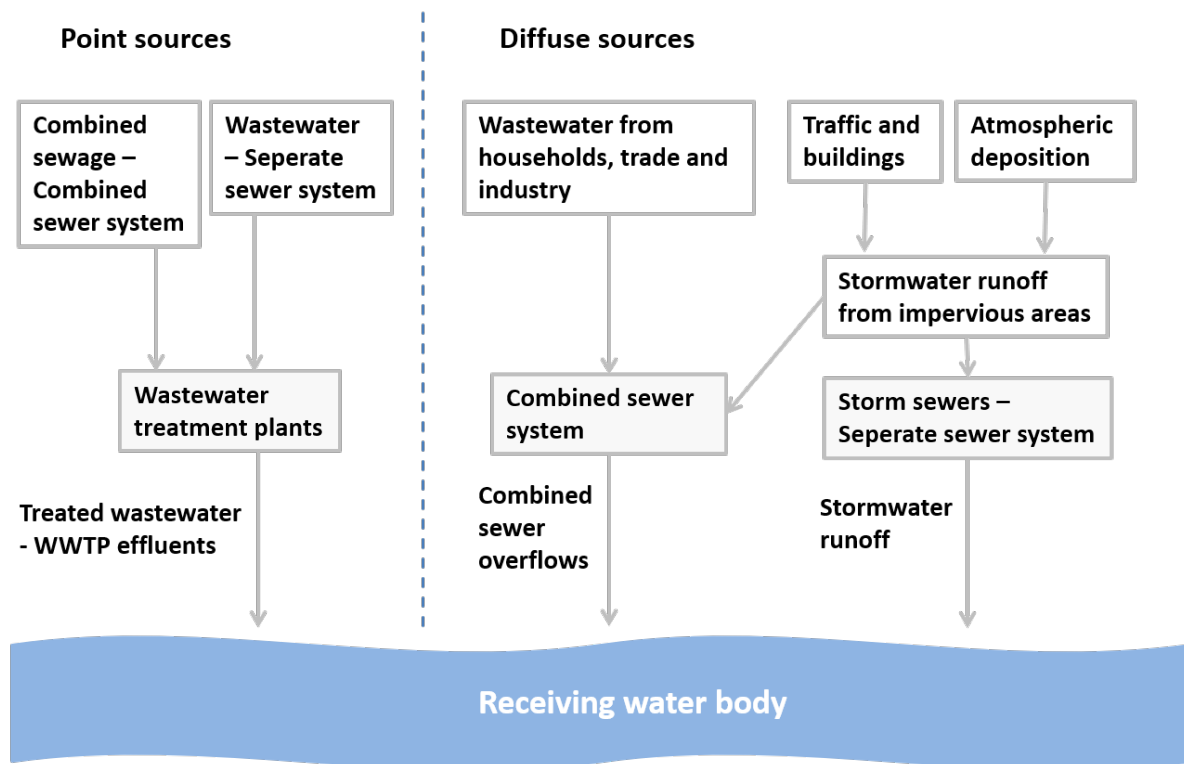


Figure 4.3.: Considered substance sources and input paths of watercourse pollution

Following the calculation of the monthly loads, the outputs of the model are total emission loads to each water body subdivided into different categories, depending on the source of pollution (stormwater or wastewater) and/or its pathway (separate sewer system, CSO or WWTP) with a monthly resolution. Thus, for each water body, the total monthly load of a substance in the stormwater runoff and in the wastewater is determined, as well as the proportion of these loads accounted for by combined sewer overflows, stormwater and treated wastewater discharges.

4.3.3. Surface water model

Following input is required for the subsequent surface water model:

1. The network of channels, rivers and lakes that form the surface water system of Berlin as an example for model application. This network is schematised so that it is useable by the water quality model.
2. The hydraulic information that makes up the flow regime.
 - a) Inflow from the rivers (in this case notably Spree and Havel) and the distribution of the water via the channels;
 - b) Groundwater abstraction for drinking water production, known per calendar month, in m^3/month ;
 - c) Bank filtrations shares, again known or estimated per calendar month, in m^3/month ;

- d) Stormwater runoff volumes (separate sewer system), in m³/month for defined water bodies
 - e) Wastewater volumes (WWTP effluent & CSO*, receiving water bodies)
3. Concentrations of the various substances in the wastewater effluent. Averages are deemed to be representative of typical circumstances. Nevertheless, if the storm events show significant contributions (in terms of the mass that enters the system during the event versus the average/typical mass in the same duration), a detailed time series which resolves the storm events and the associated pollutant concentrations might be a more appropriate approach. This presumes that data are available that allow us to draw such a conclusion.

For the PMT substances we need to consider different adsorption characteristics, as they exhibit a wide range of behaviours (Oudega et al. 2024). Adsorption of the PMT substances to organic or inorganic particulate matter means that under low flow-velocity circumstances, the adsorbed fraction can sediment onto the bottom of the water body along with the particulate matter. This could lead to a build-up of these substances in the sediment. By using various such characteristics, we get better insight in the role of sedimentation with regards to the transport and fate of PMT substances.

The expected output of the surface water model can be summarized as follows:

1. Concentration patterns as they evolve in the water system in place and time.
2. Indications of where the PMT substances end up in the sediment and how much.
3. Mass balances indicating the importance of storm water versus wastewater and background concentrations.

4.4. Fate and transport modelling at bank filtration sites

4.4.1. Basic ideas

The bank filtration (BF) models described in this chapter were devised to answer questions regarding PMT (here we focus on PFAS) transport and fate in riverbank filtrations systems (RBF). The focus herein lies in predicting PMT concentrations in drinking water wells in RBF systems. This is done by simulating infiltration of PMT into the riverbank and subsequent transport through the groundwater body towards the pumping well.

By doing this, a variety of questions might be answered:

- Future changes: How would PMT concentrations in a drinking water well change if ...
 - ... the pumping rate changes (population growth)?
 - ... PMT production increases (worst-case scenario)? *
 - ... certain legal requirements come into play (e.g. further treatment of wastewater)? *
 - ... other local changes are carried out (e.g. river water level changes)?

- Calamities: What PMT concentrations might I expect in a drinking water well, if ...
 - ... a fire in the catchment area requires application of large amounts of PFAS-containing firefighting foam? *
 - ... a PFAS spill (e.g. ...) happens close to my RBF system?

* To answer some of these questions (marked with an asterisk, *), the BF model should be used in tandem with a catchment-scale model, as the results will be affected by catchment-scale changes. Other questions can be answered with the BF model alone.

This chapter presents two different modelling approaches that, either together or independently, can be applied to study the above-mentioned questions. In the order of increasing complexity and data requirements these are: 1. A generic 1D bank filtration model, 2. A 3D physically-distributed numerical reactive transport model. The two approaches are subsequently explained in the following sections.

Information requirements

While the generic bank filtration model has very low requirements of the regional situation, for the 3D physically distributed reactive transport model specific information from the study site is needed. Because PMT transport is affected by local conditions (flow rate, water chemistry, aquifer composition), an accurate prediction of future concentrations requires on-site measurements.

Ideally, a sampling campaign might look something like this:

- Firstly, 1 or 2 “wide” sampling campaigns in the area, in which many different wells are sampled, preferably also wells in the “hinterland” behind the drinking water wells, as unknown terrestrial PFAS sources may occur (as shown in this case study).
- Secondly, when certain “hotspots” (i.e. sites of interest) have been identified, a more targeted campaign can be devised for these areas, where monthly or bimonthly samples are taken. This campaign should last over 1 year at minimum to be able to capture any seasonal changes.

It is advised that these sites of interest contain multiple monitoring wells to get a clear observation of PMT transport through the subsurface. A minimum of 1 monitoring well between the river and the pumping well, as well as 1 monitoring well behind the pumping well, and a monitoring well both upstream and downstream of the pumping well is advised, but more would be better, if funds allow it (e.g. to capture additional removal and clogging processes close to the riverbank). (Bi-) monthly samples should be then taken from the river, the pumping well and any monitoring wells along the transect.

The monitoring campaign best spans a range of varying states of the system, in order to be able to learn how the system responds to changes and to validate model behaviour on this. 'Varying states' refers to, for example, periods of high flow and low flow. Ideally periods of varying PFAS input concentration are monitored, for example in case of a calamity; it is valuable to be alert for such 'golden opportunities' and act upon them if they occur, to gain insights in system responses that otherwise would be hard to acquire.

The information from this sampling campaign can then be used to set-up and calibrate the model, before predictions are made for the future.

Basic physical background

PFAS groundwater transport is affected by many different groundwater and soil characteristics, e.g. (among others): advection (flow rate), dispersion, soil type (gravel, sand, silt, clay), presence of organic matter, other possible sorption sites (e.g. presence of the mineral goethite), redox conditions, PFAS degradation and transformation. The list of these characteristics and how they influence PMT transport and sorption is ever-evolving, and the latest literature should be consulted when creating and calibrating the model.

If it is deemed important, more measurements can be done so that all these physical processes can be modelled directly (e.g. gather information about PFAS concentration decrease over distance). Hydraulic conductivity and river conductance can be based on lithological measurements and then adjusted in order to fit the simulated to observed water levels, and sorption parameters can be assumed from the literature and then further adjusted within reported ranges to fit the simulated to observed PFAS concentration data in the monitoring wells and pumping wells.

4.4.2. Generic bank filtration model

Aquifer capacity for sorption and degradation to remove PMTs and other industrial compounds are often unclear along the flow path of bank filtrate. As first and least data demanding approach we present a generic bank filtration (gBF) model for PMT and other industrial compounds, considering advective and dispersive transport, degradation, and sorption mediated by the fraction of organic carbon. This gBF model is designed as a tool for the initial assessment of PMTs including PFAS contamination at riverbank filtrate sites. Moreover, it can be applied to a wide variety of aquifer properties to assess a large number of chemical constituents. A notable advantage to a generic approach for contaminant fate and transport calculation is the capability of the model to be adapted to nearly any riverbank filtration scenario with only basic input data.

The model was developed using an analytical equation for solute transport in porous media. The one-dimensional analytical solution accounts for advection, dispersion, linear isothermal sorption, and first-order decay as described in Bear (1979), solution given in Eq. 4.3 (West et al. 2007):

$$C_{(x,t)} = \frac{C_0}{2} \left\{ \exp \left(\frac{xv}{2D_x} \left[1 - \sqrt{1 + \frac{4\lambda RD_x}{v^2}} \right] \right) \times \operatorname{erfc} \left(\frac{x - \frac{vt}{R} \left[\sqrt{1 + \frac{4\lambda RD_x}{v^2}} \right]}{2\sqrt{\frac{D_x}{R}t}} \right) + \exp \left(\frac{xv}{2D_x} \left[1 + \sqrt{1 + \frac{4\lambda RD_x}{v^2}} \right] \right) \times \operatorname{erfc} \left(\frac{x - \frac{vt}{R} \left[\sqrt{1 + \frac{4\lambda RD_x}{v^2}} \right]}{2\sqrt{\frac{D_x}{R}t}} \right) \right\} \quad (4.3)$$

Where: $C_{(x,t)}$, and C_0 are resulting and initial concentrations, R is Retardation (calculated by equations 4.4 and 4.5), D_x is the longitudinal dispersivity, v is velocity, λ is the substance specific decay constant (Equation 4.6), x is the distance, and t is time.

$$R = 1 + \frac{\rho_b K_d}{n_e} \quad (4.4) \quad K_d = K_{oc} \times f_{oc} \quad (4.5) \quad \lambda = \frac{\ln(2)}{Dt50} \quad (4.6)$$

Where: ρ_b [g/g] is the bulk density of the soil, K_d is the specific sorption coefficient, n_e is the effective porosity [-], and DT50 is the substance specific half-life [t].

Using the equations 4.4, 4.5, and 4.6 the gBF model calculates retardation and degradation, then fate is simulated using equation 1. The gBF model generates breakthrough curves (BTC) calculated for a user-determined range of aquifer and substance specific parameters. Heat maps are then calculated by varying K_{oc} and half-life input parameters over a wide range. The heatmap computes a resultant concentration (C/C_0) for each parameter combination and generates a plot with K_{oc} parameters across the horizontal axis and half-lives along the vertical axis.

The advantage of the generic model, especially the heatmap is that the user may assess chemical attenuation even when large uncertainties exists on substance specific transport properties. The model is able to be used quickly with literature and field values and is suited towards exploratory research in uncertain conditions. The model script is written in the R programming language to maximize versatility and usability. The code contains parameter inputs and can be applied to any fate and transport problem fitting at least two criteria: (1) long-term exposure, and (2) travel times of the bank filtrate are known. Parameters that may not be known (i.e. aquifer f_{oc}) can be assumed directly or taken from literature, and then iteratively revised as new data is gathered. This model calculates resultant concentrations and breakthrough curves for steady-state conditions, and is not meant to simulate short-term transient exposure events. Model results should be verified on the basis of measured concentrations at BF sites. The model is intended as an early assessment tool for PMTs and PFAS and may be used before development of more detailed fate and transport. Table 4.2 presents the parameters used for the gBF model.

The generic model simulations were employed with common values for porosity, solid material density, organic carbon content (f_{oc}), dispersion, flow velocity, and substance parameters (K_{oc} and half-life) representing PMTs (Neumann and Schliebner 2019). The travel time of bank filtrate was varied by changing the flow distance to represent common bank filtrate conditions, one with short travel time of 10 d, medium travel time of 50 d, and elevated times of travel of 100 d.

Model outputs are plotted as heatmaps and breakthrough curves. The heatmap output shows equilibrium attenuation simulated for subsurface travel time of 10, 50, and 100 d for chemical species expressed as normalized concentration (C/C_0) with a half-life ranging from 0 to 700 days and log K_{OC} ranging from 0.1 to 6 (Figure 4.4). The black rectangle in each plot highlight the range of parameters (K_{oc} and half-life) corresponding to a generic PMT substance as defined by Neumann and Schliebner (2019).

Table 4.2.: Generic bank filtration model input parameters

Parameter	Porosity	Density solids [g/cm ³]	f _{OC} [g/g] ^[1]	Log K _{OC} [-]	Half-life [d]	Long. disp. [m]	Flow velocity [m/d]	Flow distance [m]	Time of travel [d]	C/C ₀ [-]
Break through curve	0.3	2.65	1.1 · 10 ⁻⁴	1 - 4	120 – 600 ^[2]	2	1	10, 50, 100	10, 50, 100	1
Heat map	0.3	2.65	1.1 · 10 ⁻⁴	0.1 - 6	1 - 700	2	1	10, 50, 100	10, 50, 100	1

¹ Fraction of organic carbon taken from ITRC (2015); ² Definition for PMT substances; the mobility criterion is met if the organic carbon water partitioning coefficient (K_{oc}) is lower than 4 in the pH ranges of 4 to 9 and the persistence criterion is met if the degradation half-life of the substance in soil is greater than 120 days (Neumann and Schliebner 2019).

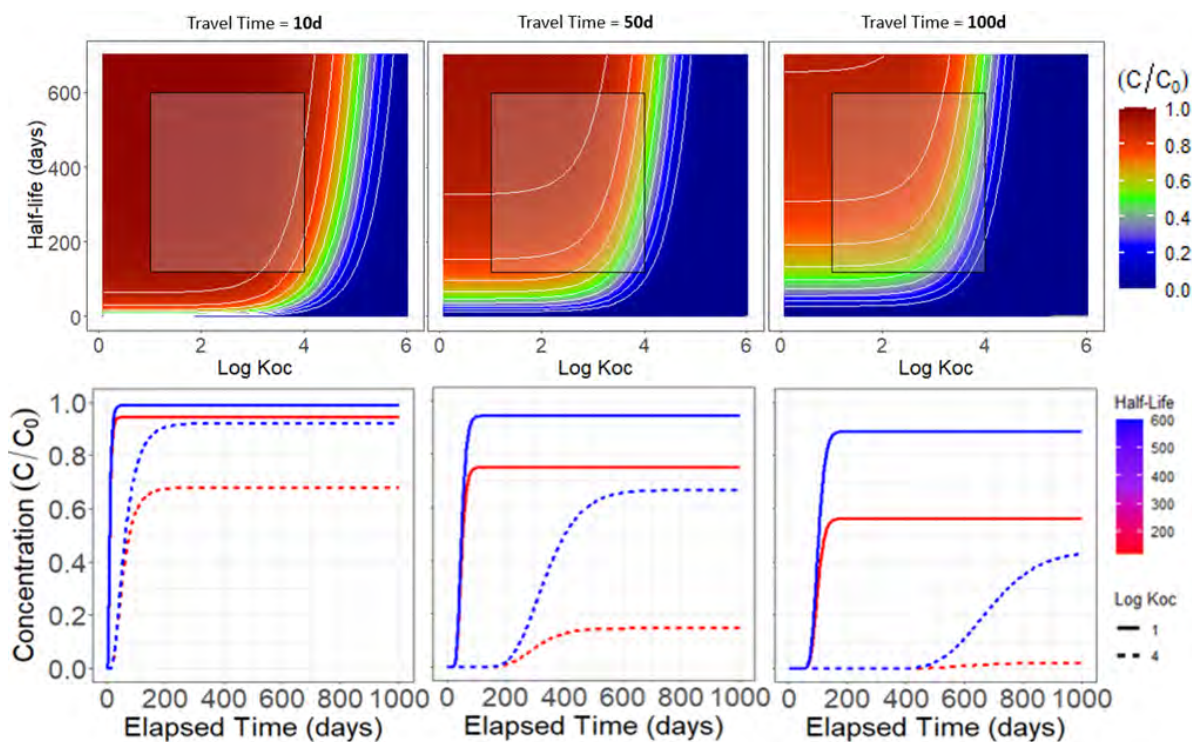


Figure 4.4.: Generic PMT substance attenuation heatmaps showing C/C_0 across varied half-life and log K_{oc} parameters (above) and breakthrough curves representing the minimum and maximum expected half-life and log K_{oc} parameters (below) for 10 d, 50 d and 100 d of travel time; white lines represent attenuation contours at intervals of 0.1 of C/C_0 ; black frame rectangle indicate log K_{oc} = 1-4 and half-life = 120-600 d corresponding to the definition of PMT substances (Neumann and Schliebner 2019).

As seen in the heatmap and breakthrough curves, the travel time has a high influence on attenuation of chemical substances undergoing riverbank filtration. Half-lives based on degradation rate constants for PFAS substances range from just over a month to nearly 70 years (see Table A.1). The half-life values presented here represent the sensitivity of the substances. As travel time increases the effect of degradation (half-lives) and sorption (K_{oc}) on the resulting concentration increases. At short travel times of 10 days, only substances with high sorption (e.g. $\log K_{oc} > 3$) and short half-lives (e.g. < 100 days) are attenuated significantly. The simulated BTCs indicate that PMT substances are attenuated to a maximum of $0.7 C/C_0$. This means that BF sites with short travel times have very limited attenuation capacity in terms of pollutant retention. In contrast, BF sites with travel times of 100 days enable significant attenuation for substances even with slow degradation and limited sorption. The simulated BTCs indicate that PMT substances of bank filtration sites with travel of 100 d can be attenuated to a maximum of $< 0.1 C/C_0$.

4.4.3. 3D physically-distributed flow and transport modelling

The second modelling approach consists of fully 3D numerical flow and reactive transport modelling. Groundwater flow is modelled with MODFLOW-2005 (Harbaugh 2005) and reactive transport is modelled using MT3DMS (Zheng and P. Wang 1999), both as implemented in the iMOD modelling environment (Vermeulen et al. 2024). MT3DMS reads the flow field as calculated by MODFLOW and calculates the reactive PFAS transport along this flow field. The numerical approach allows for fully dynamic reactive transport calculations, which in the bank filtration setting with highly fluctuating river levels and pumping rates is indispensable. The models are run on a daily time step, with transport step sizes determined automatically during runtime based on stability constraints.

The 3D physically-distributed transport models use a one-site nonequilibrium model to simulate sorption of PFAS species to the soil during BF. This model allows for more detailed reactive transport, which can differentiate between PMT species based on their characteristics. It uses two parameters to simulate sorption; first, the adsorption isotherm coefficient K_d [$M^{-1} L^3$], which controls equilibrium sorption to the solid phase, and second, the first-order kinetic rate coefficient Alpha [T^{-1}], which controls the speed in which equilibrium sorption is reached. The values for K_d and Alpha were found by modelling of column tests done with quartz sand, using Hydrus 1D (Simunek et al. 2013).

The model performs this calculation for every cell in the domain for every time step, thus allowing for detailed calibration and validation of the model with monitoring results not only from the pumping wells (PWs) but also from the monitoring wells (MWs), as well as allowing for the calculation of high-resolution PMT concentration distributions in scenarios.

4.5. Model train application in an urban setting of Berlin

4.5.1. Description of the study site

The city of Berlin, Germany was chosen as a study site for modelling the fate and transport of PM(T)-substances in an urban environment. Berlin has both a separate and a combined sewer system. The two systems carry stormwater runoff from an impervious, connected area of ~170 km² and wastewater from ~3.6 million inhabitants. Micropollutant loads from stormwater can enter surface water via three pathways: (i) treated at wastewater treatment plants (WWTPs) or untreated via (ii) storm sewers or (iii) combined sewer overflows (CSOs). There are ~176 combined sewer outfalls in the centre of Berlin, affecting the water quality of the Spree, Landwehrkanal, Panke, etc. Micropollutant loads from (dry weather) wastewater are either treated in WWTPs or can also reach surface waters untreated via CSOs.

In Berlin, surface waters cover more than 6% of the total area. These include lakes, rivers, river lakes, canals and ponds, which are used intensively by humans for various purposes; for drinking water extraction from groundwater and bank filtrate, as receiving waters for urban drainage, as waterways for shipping and as bathing waters and local recreation areas. Consequently, watercourses are exposed to many anthropogenic impacts, which have direct and indirect influences on watercourse structures, flow dynamics, biology and water quality. The main watercourses Spree, Dahme and Havel are regulated, partly dammed and very slow-flowing watercourses, in whose lake-like extensions - such as Müggelsee and Tegeler See - the water sometimes has very long residence times, which leads to little erosion and a high amount of sedimentation. As part of the PROMISCES project, two stormwater sewers were sampled during more than 20 rain events from April to October 2023 in Berlin. The stormwater runoff samples were analysed for various PMs. As the two sampling points are located in the catchment area of the Flughafensee, which is fed 100% by stormwater runoff and has no outflow, a particular focus is placed on this lake in the case study.

4.5.2. Application of the emission model for Berlin

To characterise the PMT pollution of Berlin's watercourses caused by inputs from urban drainage, the diffuse and point sources of stormwater discharges, CSOs and WWTP discharges were considered (see section 4.3). Therefore, in addition to the monitoring results of the sampling in the two stormwater sewers, further input data were required for the load calculations, such as the concentrations of the analysed parameters in wastewater and treated wastewater and the discharge volumes of stormwater and wastewater. Some of these data are actual Berlin data, such as the effluent volumes of the Berlin WWTPs (BWB 2024) and the monitoring results from the 'OgRe' project (Wicke et al. 2015). Urban runoff via impervious areas connected to the sewer system was simulated for the years 2014 - 2023 using the Berlin water balance model ABIMO for 28 surface water bodies in Berlin (Goedecke et al. 2019). In the absence of data on PMT concentrations in Berlin's wastewater and treated wastewater, monitoring results from the upper Danube River Basin (Liu et al. 2023) were used.

Subsequently, the probability distributions of the data were analysed. To implement uncertainties, a Monte Carlo simulation was conducted, generating 1000 random data points. The

monthly loads were then calculated for a range of 1000 random concentrations and volumes, and the results were summarised in statistical key figures.

As an exemplary result, Figure 4.5 shows the annual discharge volumes into Berlin's watercourses by source (rainwater and wastewater) and path (separate sewer system, CSO, WWTP) next to calculated monthly loads of PFOA. In terms of both volume and load, WWTP treated wastewater is the largest source.

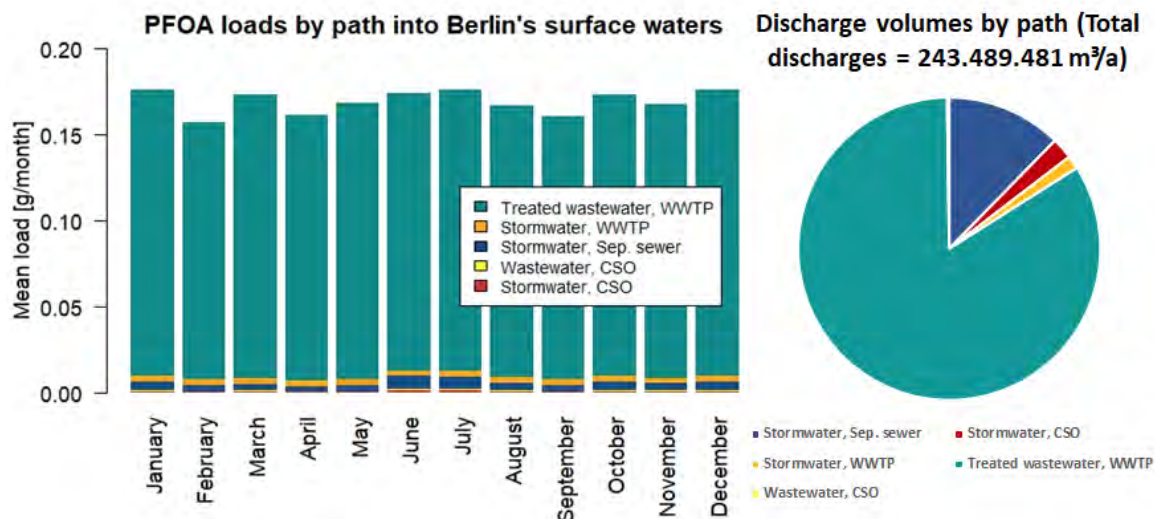


Figure 4.5.: Left side: Monthly PFOA loads by path into Berlin's surface waters, right side: Contributions of the separate sewer system (Sep. sewer), wastewater treatment plants (WWTP) and combined sewer overflows (CSO) to annual rainwater and wastewater discharges.

4.5.3. Explanation of the surface water model

Based on geometrical information of the components of the water system (length and width of branches, depth, size of the various lakes and the connections between the components), a somewhat simplified schematization was devised (see Figure 4.6).

The flow through the rivers and canals was estimated using available hydraulic data (Schumacher 2023). An important aspect of the flow field is that it must be volume-conserving: if two branches join up together, then the flow in the downstream branch should be the sum of the flows in the two upstream branches. When a branch splits up, a similar condition holds. To determine a consistent, volume-conserving flow field with the appropriate geometrical information and connections, an auxiliary program was used. Each branch consists of two or more grid cells, depending on the length of the branch. The various lakes were treated as if they were wide branches.

The exception to this set-up is the Flughafensee. As it is an isolated lake with a depth of up to 36 m, an alternative approach was used: it is assumed that the lake is well-mixed in the horizontal but exhibits concentration gradients in the vertical. While there are no detailed measurements regarding temperature available, it seems likely that the lake is not well-mixed in the vertical direction, see Figure 4.7.

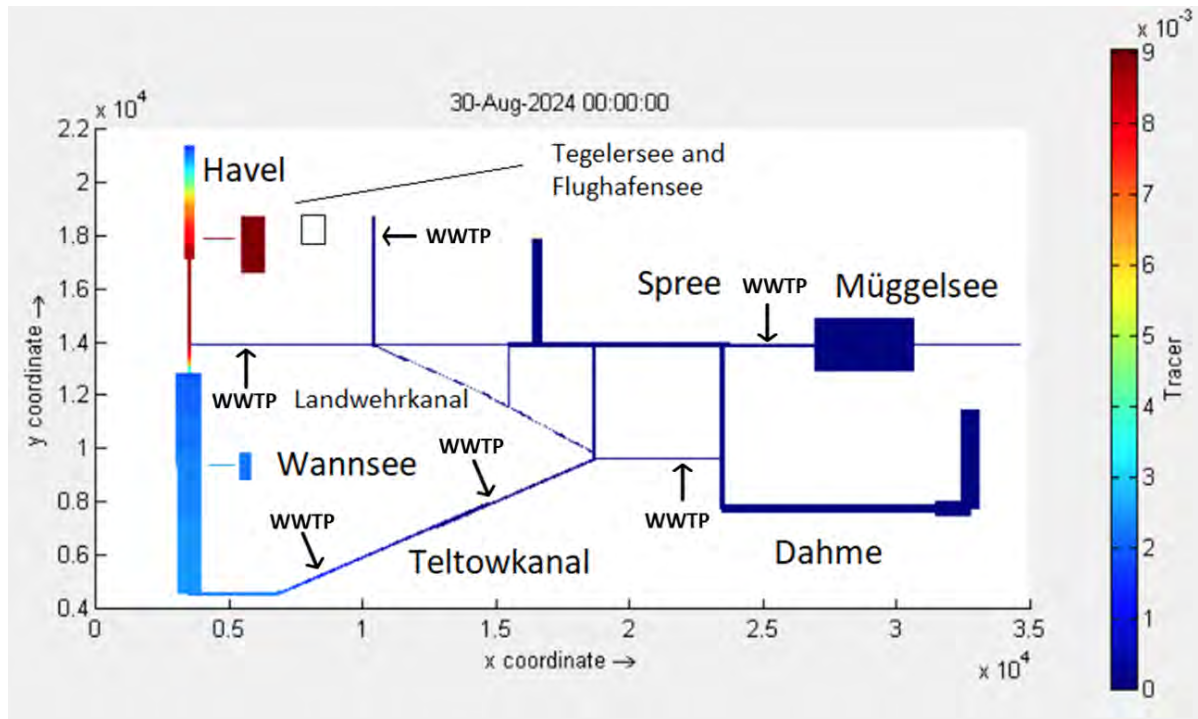


Figure 4.6.: Layout of the Berlin surface water model, visualized via the concentration of a tracer. (Note: not all connections are visible, notably the connection between the Wannsee and the Unterhavel, the lower part of the Havel.)

To illustrate the model the input of suspended sediment was kept constant in time and the concentrations resulting after a long time were plotted. The sediment will actually accumulate on the bottom, so there is no equilibrium there, but in the water column a steady distribution is reached.

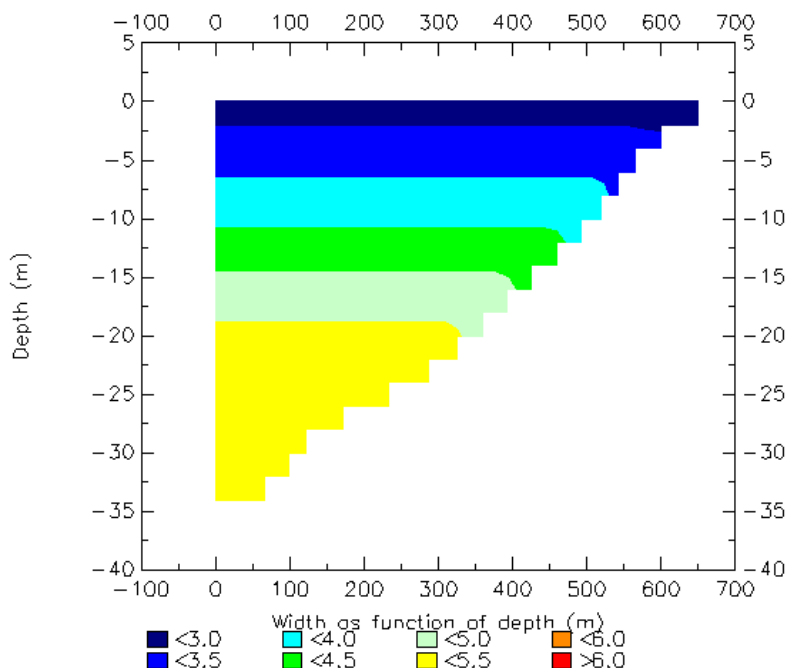


Figure 4.7.: Schematic representation of the Flughafensee as a column model. The quantity shown is the concentration of suspended solids (mg/L). The concentration at the surface is lower than near the bottom due to sedimentation.

4.5.4. Modelling the PMT substances

The approach to modelling the PMT substances in water and sediment is the same for both schematics: PMT behave as dissolved substances but can also adsorb to organic and to a lesser extent inorganic particulate matter. The following assumptions are made:

- PMT substances do not degrade and are not volatile, so that they persist in the water system.
- Adsorption to particulate matter can be described via a partition coefficient, so that one fraction is dissolved, and the other is adsorbed. The adsorption process is assumed to be fast, so that an equilibrium exists.
- The adsorbed fraction can sink to the bottom along with the particulate matter and accumulate there.

Thus, we need to include the following substances:

- Particulate matter in the water phase and at the bottom

- PMT concentration in the water phase and in the bottom sediments

The model for the Berlin surface waters was used to make a first, illustrative calculation for PFOA (see Figure 4.8). The results of the month July were used, assuming a constant influx. As the residence time of the system is rather long (several months, partly due to the lakes that are an integral part of the water system), the simulation time was set to 5 months.

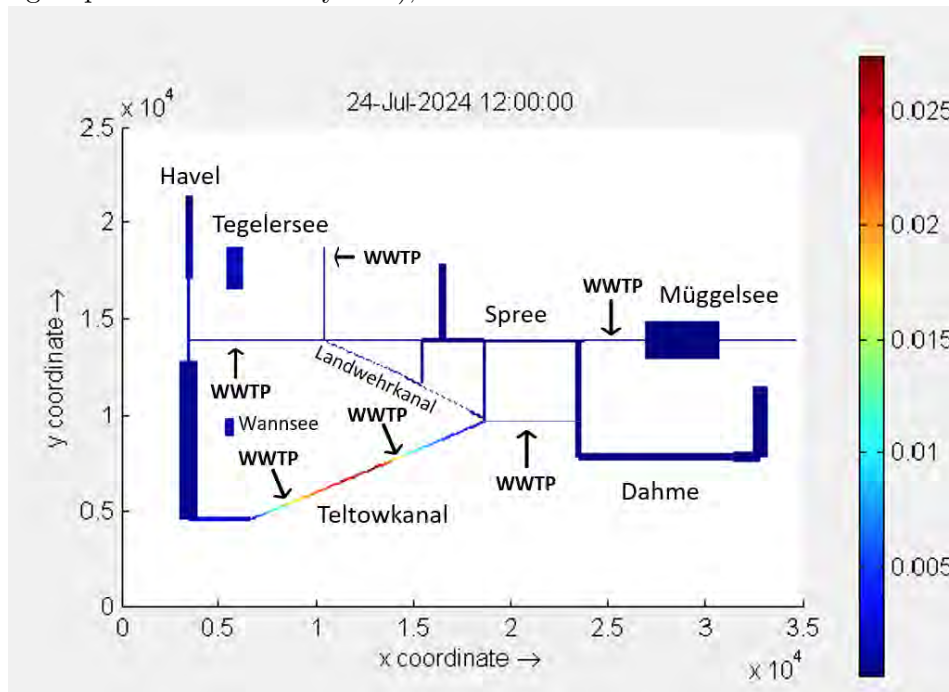


Figure 4.8.: Simulated concentrations of PFOA in Berlin watercourses as the result of rainwater, treated wastewater and raw wastewater discharges (in ng/L).

The calculation starts out with a concentration of zero and the inflow of the various rivers (Havel, Spree and others) into the system, as well as the discharges of (treated) wastewater at the various branches, cause the pollutant to enter the surface water. Due to the adsorption to particulate matter (organic and inorganic) of PFOA, part of it can reach the sediment layer. In the Berlin water system, the flow velocity is very low, which makes it likely that PFOA in the sediment continually accumulates over time.

Figure 4.8 shows the simulated PFOA concentrations in ng/L in Berlin's watercourses. Higher concentrations can be observed in the Rudower-Teltowkanal, which receives the effluent from two large sewage treatment plants. The high concentrations are partly due to the high discharge volumes of the WWTPs and partly to the low flow velocities in the Teltowkanal. The various treatment plants, for instance in the Teltowkanal, cause an increase in the downstream concentration. The magnitude of this increase depends on the flow rate and on the actual discharge.

Key messages of the Berlin Case Study

The largest emission loads of most PFAS and PMT substances analysed enter the water bodies via the treated wastewater discharges of the WWTPs.

While the concentrations of PFOA are in the order of 0.02 ng/L, this concerns a single PFAS species only. The total PFAS concentration is likely to be an order of magnitude larger.

Water systems like that of the city of Berlin are quite complex and it is inevitable that some simplifications are made when schematising them. Moreover, important data are often missing or are only approximately known, such as the typical concentration of particulate matter. One has to make informed assumptions, then, even if it introduces further uncertainties.

4.6. Model train application in a large catchment

4.6.1. Description of the study site

The study site for application of a model train for exposure assessment in the context of the catchment – river – riverbank filtration – drinking water interaction in a large catchment is the Danube catchment upstream of Budapest shown in Figure 4.9. Some basic data for characterization of the catchment are shown in Table 4.3. The main questions addressed in this study site are (i) what are the main sources and pathways of PFAS pollution in the catchment, (ii) how do different PFAS parameters behave during bank filtration, (iii) how could future changes in the catchment lead to changes in concentrations in pumping wells for drinking water abstraction, and (iv) is there a risk of failing to achieve standards for drinking water or (E)QS in surface or ground water now or in the future? The model train applied consists of the combination of the MoRE and PPM models for assessing sources and pathways of PFAS emissions in the catchment as well as 3D physically distributed reactive flow and transport models (MODFLOW/MT3DMS) for three bank filtration sites, namely one small-scale site (~10 m) in Vienna and two larger-scale (~100-2000 m) sites on Szentendre Island in Budapest.

The catchment models focus on the PFAS parameters: PFBA, PFPeA, PFHxA, PFHpA, PFOA, PFBS, PFHxS, PFOS, ADONA and HFPO-DA/GenX. These ten parameters are fully reflected in catchment modelling with MoRE and PPM model, with the possibility of validation against measurements. The models can calculate emission loads for PFNA, PFDA, PFPeS, PFNS, PFDS, 6:2 FTS PFOSA, N-EtFOSAA as well, due to quantifiable concentrations in some pathways. Nevertheless, concentrations of these parameters in rivers are mostly below limit of quantification. Therefore, modelled river loads cannot be validated by comparison to observations. The behaviour of the first ten substances is further investigated using bank filtration modelling.

While in Vienna most of drinking water is supplied from karstic springs, in Budapest Danube bank filtration is the dominant drinking water source. The bank filtration at Danube Island is a potential source to increase the water supply as a rising demand is predicted for the future. Water is abstracted from multiple wells groups on both the eastern and western bank

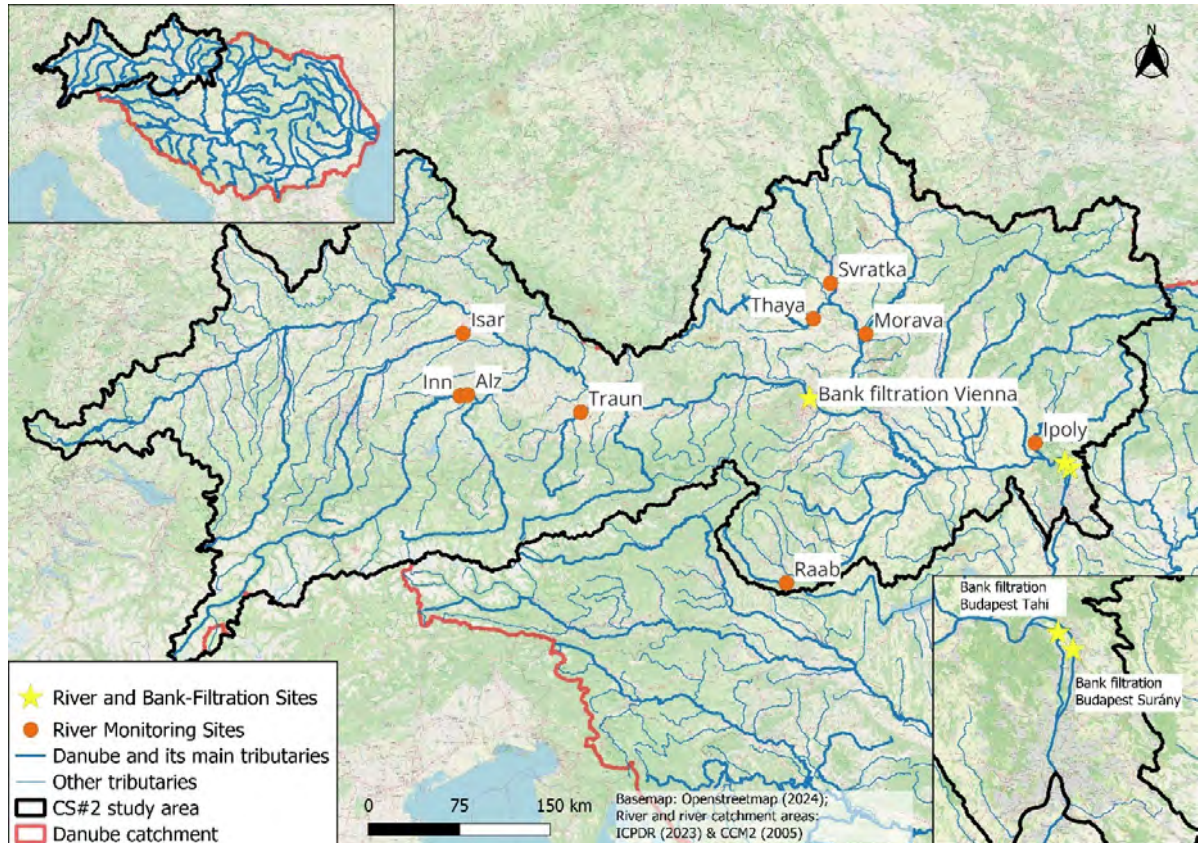


Figure 4.9.: Map of the Danube catchment upstream of Budapest, showing monitoring points for validation at Danube and its tributaries as well as bank filtration sites at Vienna and Budapest.

Table 4.3.: Characterization of the catchment upstream bank filtration sites in Vienna and Budapest

		Danube Island Vienna	Danube Island upstream Budapest
Catchment	km ²	101,527	183,293
Inhabitants	Inh.	15,577,100	23,858,775
Waste water from municipal and industrial WWTPs	p.e.	18,482,423	30,911,725
Waste water from municipal and industrial WWTPs	10 ⁶ m ³ /a	1,349	2,256
Average river discharge	m ³ /s	1,871	2,333
Average river discharge	10 ⁶ m ³ /a	59,004	73,573

of Szentendre Island. One abstraction well from the well group “Tahi” and one from the well group “Surány” have been chosen for detailed evaluation due to favourable conditions with respect to accompanying monitoring wells. Figure 4.10 shows a map of the local situation.

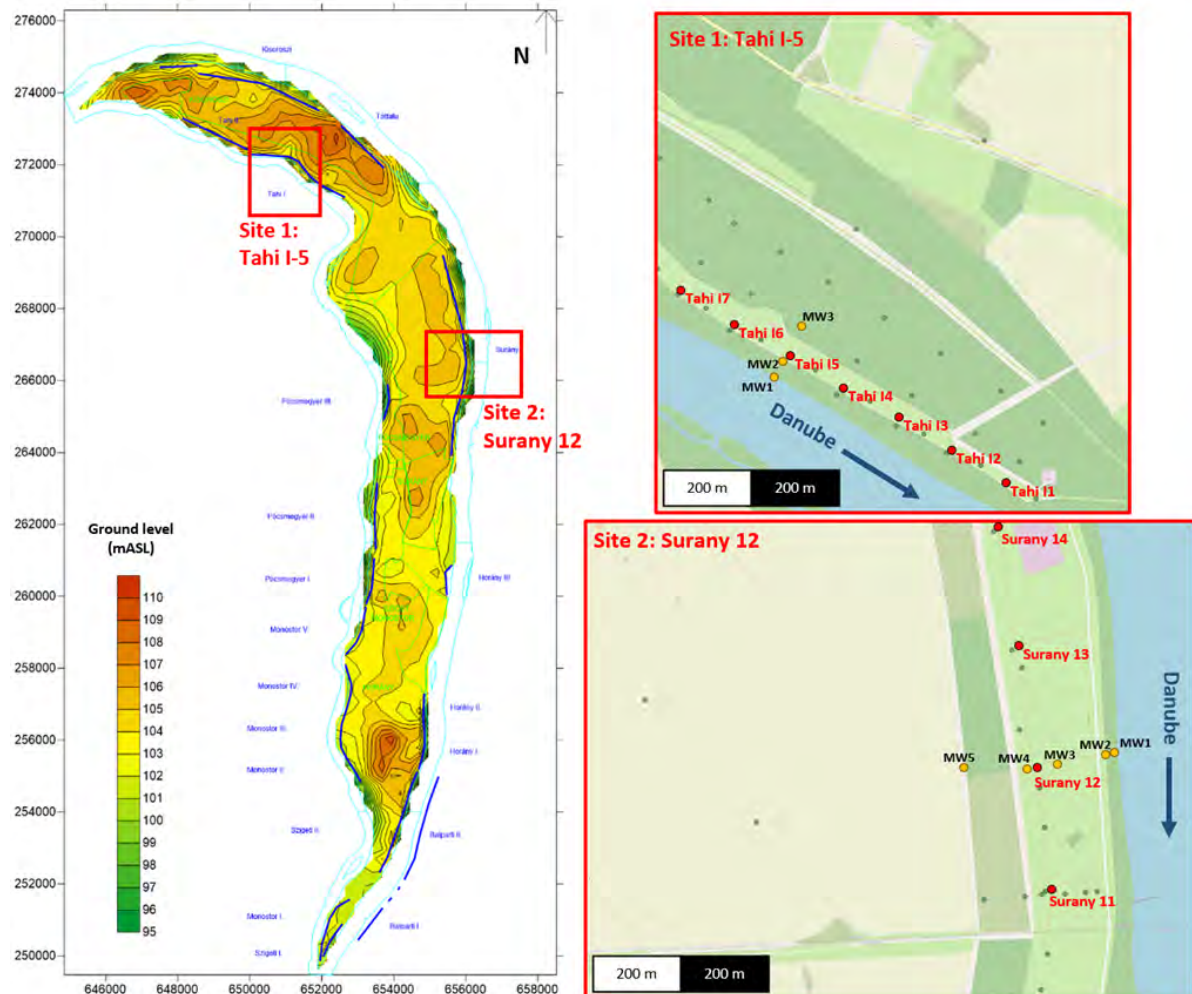


Figure 4.10.: Map of bank filtration sites at Budapest. Left: ground level [m.a.s.l.], Right: detailed map of Site 1 (Tahi I-5) and Site 2 (Surány 12). Extraction wells in red, monitoring wells (MW) in orange, unused monitoring wells in green.

For a smaller scale BF study, the Danube island in Vienna was chosen (Figure 4.11). This is an area close to where bank filtered water is used to produce drinking water. Three monitoring wells (MW) are located in a straight line at distances of 1, 15 and 28 m from the riverbank. Besides the smaller scale, another difference with the Budapest transects is the absence of a pumping well (PW) and the presence of a significantly clogged riverbank, potentially increasing the effectiveness of BF at the site.

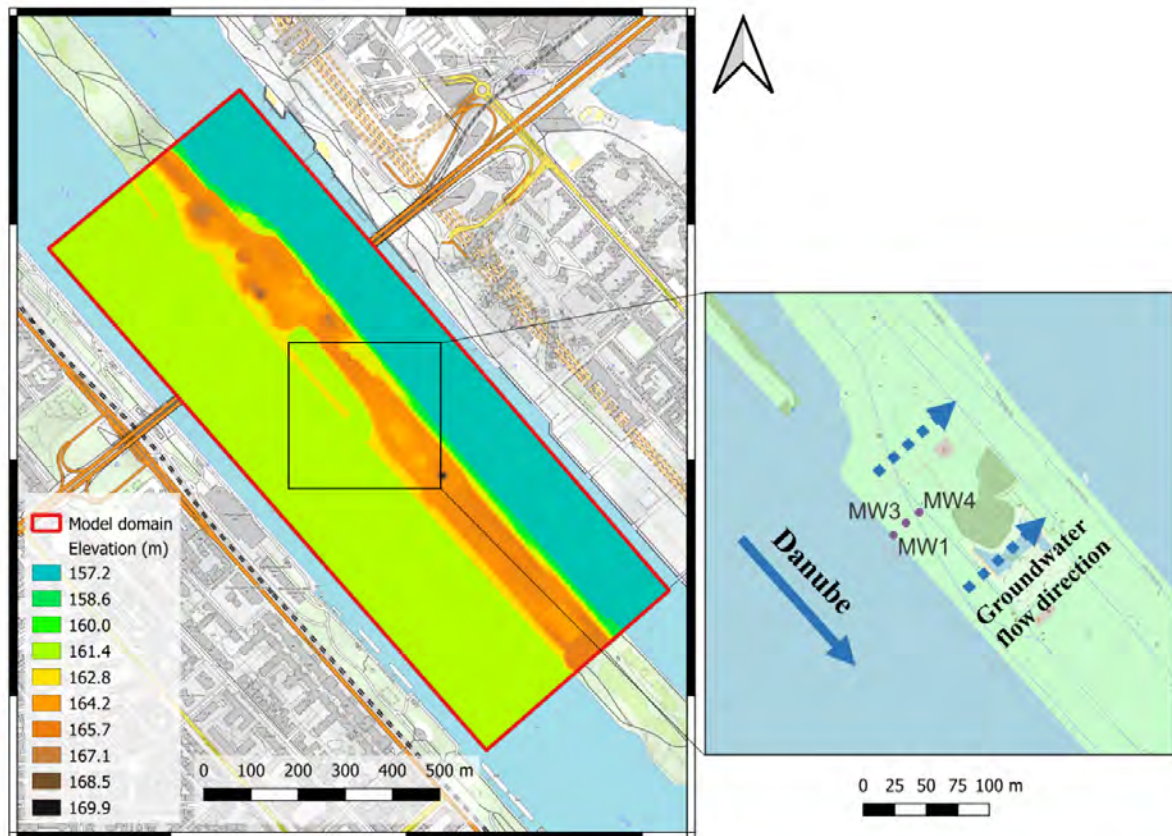


Figure 4.11.: Map of bank filtration site at Vienna. Left: model boundaries and absolute elevation (m.a.s.l.) of the Danube Island in the center of the city, Right: detailed map of the transect. Groundwater Wells (GW) 1, 3 and 4 were monitored. No extraction wells are present in the transect.

4.6.2. Catchment emission models

In the MoRE application for the upper Danube catchment, emission loads via different pathways are calculated at the level of 526 sub-catchments as analytical units with an average size of 350 km² and summed up along the flow tree to assess river loads at the outlet at each sub-catchment. If river concentrations are observed by monitoring, modelled concentrations can be compared to these observations to validate model calculation. In the upper Danube Basin, river concentrations have been observed at 11 locations (see Figure 4.9) and river loads have been calculated from that and associated flow data. Figure 4.12 shows model performance for the sum of 10 parameters covered by quantitative modelling (see above) calculated according to EU Drinking Water Directive (EU DWD) and the suggested procedure according to the proposed new groundwater and environmental quality standard directive (EC COM(2022) 540 final). Model efficiency coefficients (KGE and NSE) > 0.65 indicate high model performance, with a good agreement between modelled and observed loads. Due to the good model performance, it is justified to use model results for more detailed evaluation and scenario calculation.

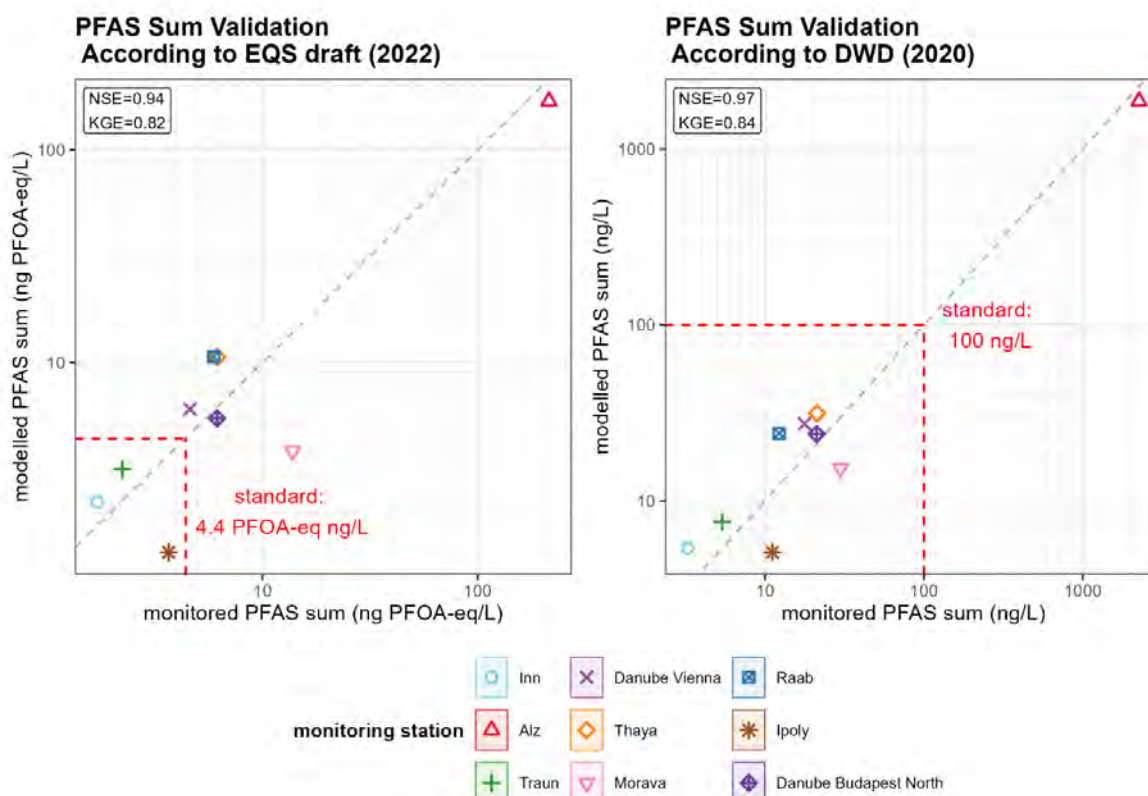


Figure 4.12.: Model validation for the MoRE model at outlets of 11 sub-catchments for different PFAS. X and Y axes in logarithmic scale. KGE and NSE indicate the model performance. Values > 0.65 indicating a good agreement between modelled and observed loads

The dominating emission pathways of the catchments upstream of each of the eleven validation points are shown in Figure 4.13. There is a clear dominance of industrial direct discharges into the rivers of the Danube catchment upstream of Budapest for most carbonic acids (PFBA, PFPeA, PFHxA and PFHpA as well as ADONA and GenX). These emissions are mostly associated to the emissions from 3M PFAS production in the Chemical-Park in Gendorf close to the Alz river. PFOA production at this location was stopped 15 years ago. Thus, PFOA point source emissions from this place are currently neglectable. Nevertheless, due to contamination of the surroundings, diffuse legacy pollution from this area is still the dominating pathway for PFOA. Another emission pathway with a potentially high share of emissions is the legacy pollution from urban areas (P4c: inhabitant-specific diffuse pollution via groundwater), which includes pollution from firefighting training grounds at airports or other locations as well as from former landfills. The estimates for this pathway are however still affected by high uncertainty due to lack of specific input data. The contribution of municipal wastewater treatment plant effluents is between 10 to 25% of the total emission of different PFAS substances. For some of the parameters also background loads via groundwater contribute with relevant shares. The overall assessment of emission pathways highlights the relevance of 3M PFAS production at the Chemical-park Gendorf as well as different types of legacy pollution for the overall loading of river Danube at the bank filtration sites at Vienna and Budapest.

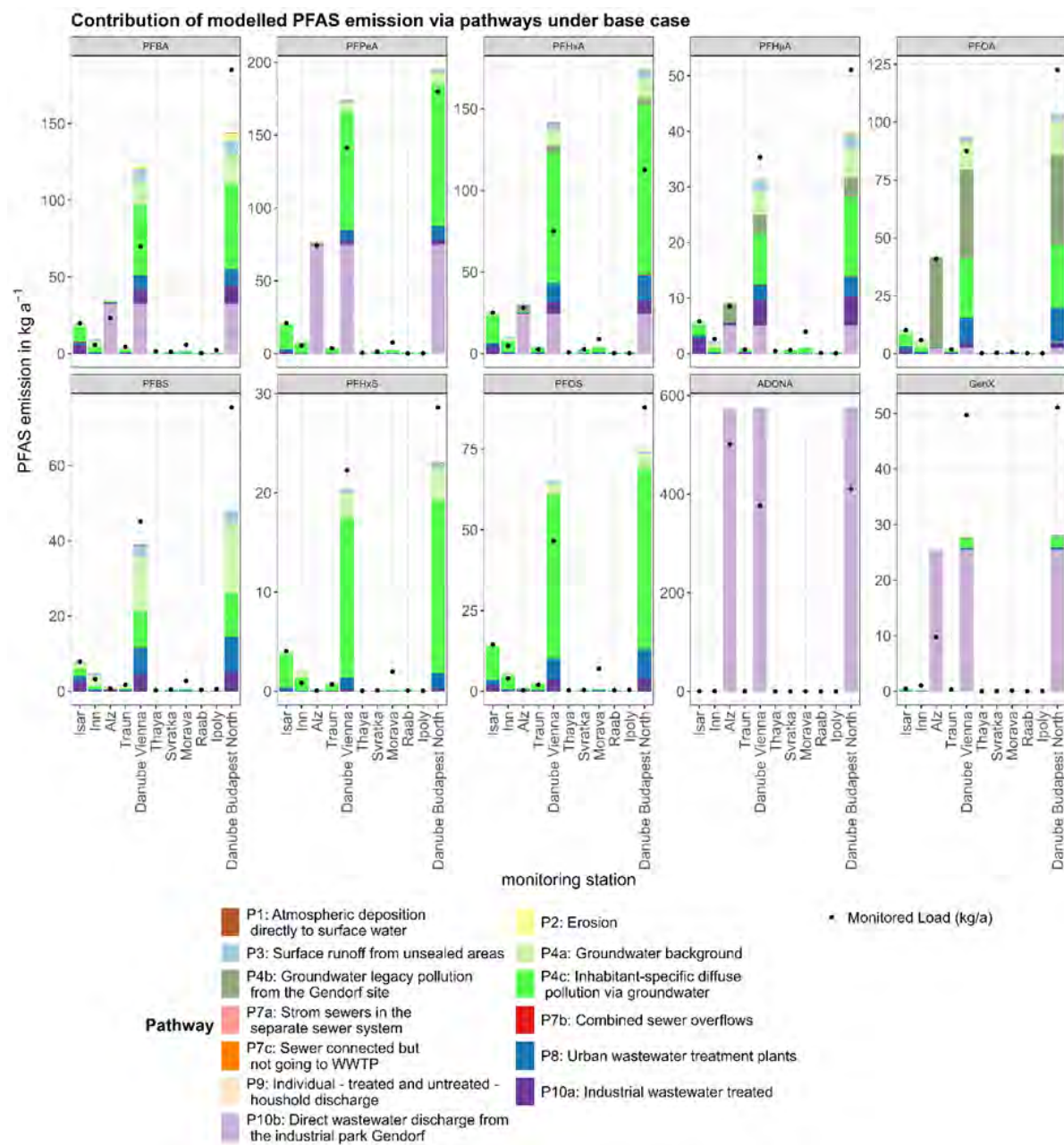


Figure 4.13.: Modelled contribution of different emission pathways to loads of 10 single PFAS at outlets of 11 sub-catchments for different PFAS. Black dots indicate the river load calculated from observed concentrations and river discharge.

Using the validated models for the upper Danube Basin, a risk map has been drawn showing the risk of exceedance of thresholds from EU legislation. Figure 4.14 shows a base variant of the model results. The worst-case and best-case variants of these calculations, which account for the uncertainties in emission modelling, can be found in Annex D.

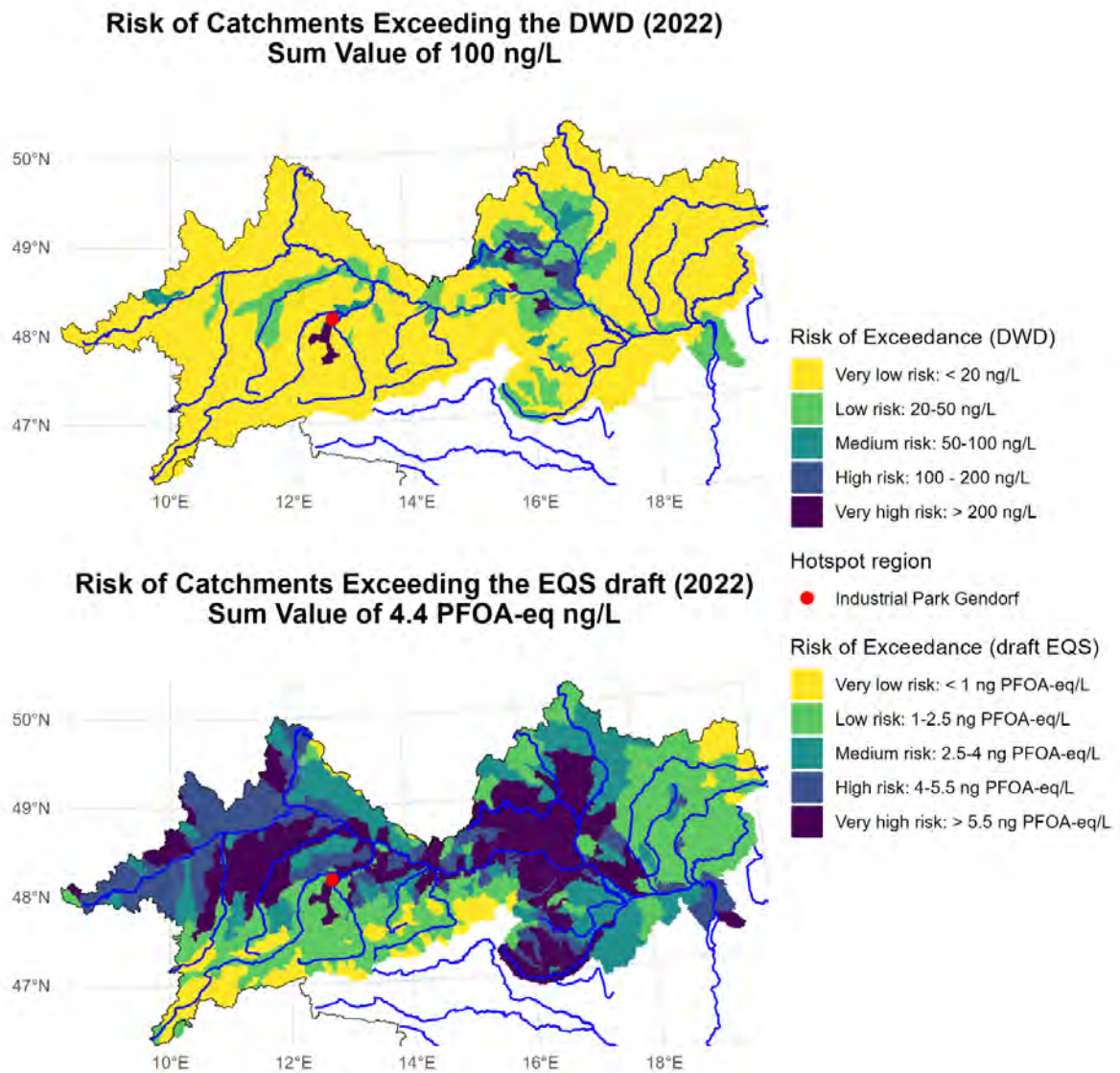


Figure 4.14.: Risk of exceedance of drinking water standards (upper picture) and proposed (E)QS (lower picture) for sum of PFAS in the rivers of the upper Danube catchments.

PFAS sum parameters from EU Drinking Water Directive (Figure 4.14 upper part, EU DWD) and (E)QS as proposed for the new groundwater and environmental quality standard directive (Figure 4.14 lower part, EC COM(2022) 540 final) have been used for assessment. In both cases, the sums have been calculated from the 10 parameters where quantitative modelling was possible. Figure 4.14 uses a risk ranking schema based on defined concentration ranges from very low to very high risk of exceedance of the (E)QS of both approaches. The results indicate that the risk of exceedance of the thresholds set by the EU DWD is very low or low in most of the surface waters in the upper Danube Basin and therefore for bank filtrate taken from these rivers. The situation is completely different for the proposed values of the groundwater and

environmental quality standard directive, where the risk of exceedance is medium to very high in many regions of the catchment.

4.6.3. Bank filtration models

Generic bank filtration model

In this subsection we describe the application of the generic bank filtration (section 4.4.2) model to different sites to explore the viability of less data-intensive models for early phase risk assessment. There are 3 riverbank filtration sites within the case study (Vienna, Budapest–Tahi, and Budapest–Surány) where attenuation of bank filtrate is simulated. Measurements at the 3 sites for 28 PFAS in the river Danube and in the riverbank filtrate were obtained from Obeid et al. (2023). At all 3 sites 10 PFAS substances (PFBA, PFPeA, PFHxA, PFHpA, PFOA, PFBS, PFHxS, PFOS, GenX, and ADONA) were measured above limit of quantification in the river and in groundwater. However, at the Budapest–Surány site, PFOA, PFOS, and GenX had higher concentrations at the well than in the river, indicating an additional inland source of Obeid et al. (2023). These substances were therefore excluded.

Table 4.4 presents the parameters used to model the three case studies. The K_{oc} values used in the study are representative for medium coarse sand aquifers with low clay content. Log K_{oc} for each substance was set to values based on 1:10 soil water ratio from batch sorption studies as presented in an extensive study by Nguyen et al. (2020). Organic carbon content (f_{OC}) was determined from sediment samples taken at Vienna and Budapest sites. The sites have similar f_{OC} contents and particle size distributions (AGES 2024). To determine C/C_0 , the median concentration for all measured PFAS substances in the sampled wells was divided by the median values measured in the river Danube at Vienna or Budapest. In Vienna, the median was limited to a sample well with information available regarding hydraulics. When porosity or velocity parameters were not given from a source, hydraulics were estimated through the Darcy’s law. Field measurements in Vienna showed that clogging occurs at the river bank and infiltration is likely to occur in the middle of the river where there is less obvious clogging (Obeid et al. 2023). The distance for the Vienna site was set to reflect this flow hypothesis.

Table 4.4.: Vienna and Budapest model parameters for the gBf model.

Parameters	Vienna		Budapest - Tahi		Budapest - Surany	
Model type	BTC	Heatmap	BTC	Heatmap	BTC	Heatmap
Porosity	0.15 ⁷		0.3 ⁸		0.3 ⁸	
Density solids [g/cm ³]	2.7		2.7		2.7	
f_{OC} [g/g] ¹	0.002		0.002		0.002	
Log K_{OC} [-]	1.0 – 2.9 ²	0.1 – 6	1.0 – 2.9 ²	0.1 – 6	1.0 – 1.9 ²	0.1 – 6
Half-life [d]	500 – 2000	1 – 2000	500 – 2000	1 – 2000	500 – 2000	1 – 2000

Parameters	Vienna		Budapest - Tahi		Budapest - Surany	
Model type	BTC	Heatmap	BTC	Heatmap	BTC	Heatmap
Long. dispersion [m]	10		10		10	
Velocity [m/d]	21 ⁶		2.14 ⁸		1.38 ⁸	
Distance [m]	141 ⁴		60 ⁵		228 ⁵	
Time of Travel [d]	7 ⁶		28 ⁸		165 ⁸	
C/C ₀ [-] ³	0.93		0.73		0.8	

¹ Sediment analyses from 11–12 m depth (Vienna) and 91.42 m above Baltic sea level (Budapest) (AGES 2024); ² Log K_{oc} from batch experiments for measured compounds at site from Nguyen et al. (2020); ³ median concentration reduction calculated from Obeid et al. (2023); ⁴ distance from middle of Danube River to the sample well from Obeid et al. (2025); ⁵ Distance from production well to the river bank (Nagy-Kovács et al. 2019); ⁶ calculated by Darcy's Law. (2019); ⁷ Derx et al. (2021); ⁸ Model results and values from the small-scale model.

Using the parameters from Table 4.4, the gBF model simulated attenuation of PFAS at each case study site. Figure 4.15 presents heat maps and breakthrough curves for the Vienna, Budapest-Tahi, and Budapest-Surány case study sites.

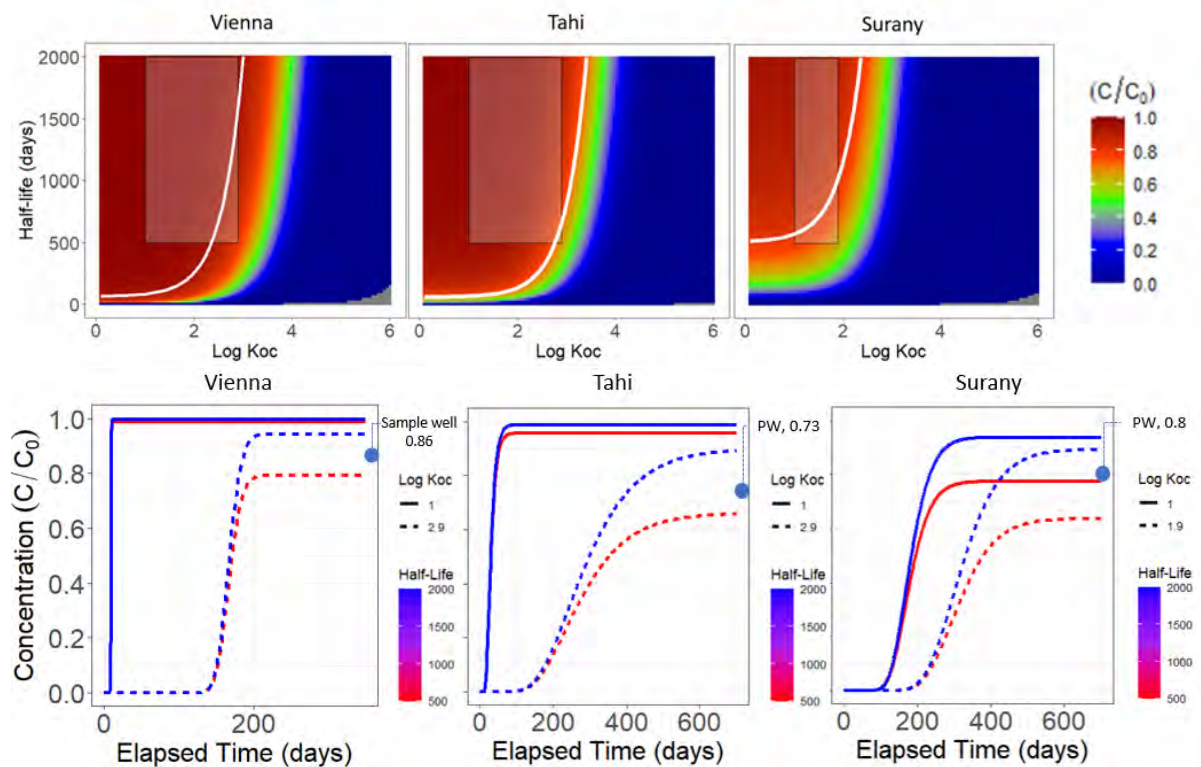


Figure 4.15.: Attenuation heatmaps (above) and breakthrough curves (below) simulated by the generic bank filtration model at Vienna and Budapest (Tahi, Surány) case study sites. For the heatmap, the black framed rectangle shows parameter range representative of PFAS substances observed at site; the white line indicates median measured concentrations at site. Measured median C/C_0 values for PFAS are shown on the breakthrough curve as blue dots. PW = Pumping well.

When comparing the simulated concentration with measured concentrations (white line in the heatmaps), for the considered PFAS substances the white line intersects the box representing the behaviour expected for PMT substances. There is a reasonably good match between observation and simulation at all three sites. Looking at the heatmap for Vienna, the PMT box indicates an expected concentration of $0.8 - 1 C/C_0$. The measured $C/C_0 = 0.93$ falls in this range and corresponds to a $\text{Log } K_{oc} > 2$ and half-life between 500 to 1500 days. Due to the low time of travel (7 days) at the site, substance breakthrough at Vienna occurs faster than at the other case study sites.

At Budapest-Tahi, the dominant travel time is 28 days and the PMT box indicates an expected concentration of $0.68 - 1 C/C_0$. Here, the weakest fit is observed, with only a small range of overlap with the measured range ($C/C_0 = 0.73$) is visible at the highest $\text{Log } K_{oc}$ (slightly less than 2.9) - and lowest half-life values (500 – 600 days).

Budapest-Surány has the longest travel time of the three sites (165 days). At Surány, the box indicates an expected concentration of $0.65 - 1 C/C_0$ of the PFAS compounds. The measured $C/C_0 = 0.8$ corresponds to 1 to 1.9 $\text{Log } K_{oc}$ (the full parameter range) and a half-life between 600 and 1000 days.

By applying a model needing only basic knowledge of the hydraulic situation and transport properties, this study demonstrates that it is possible to realistically simulate mass concentrations with a simple and generic bank filtration model. Measured C/C_0 was found to overlap the PMT box at the sites in each model. Therefore, applying a simple and straightforward model is a viable solution for data scarce sites and early phase assessments.

3D numerical flow and transport models

For Vienna and Budapest, a 3D numerical approach was followed for the bank filtration (BF) modelling. For Vienna, being a small-scale system with well-defined boundary conditions, the groundwater flow model and the reactive transport model have the same extent. The Budapest sites, however, are part of the larger groundwater system of Szentendre, with no well-defined hydrological boundaries nearby except for the Danube river. Therefore, a regional groundwater flow model needed to be constructed, in order to derive (time-varying) boundary conditions for local cut-out models. More details on the construction of this regional model, encompassing the whole of Szentendre Island is given in Annex F. Also, a streamline schematization of the (steady-state) flow patterns in the cut-out models is given in Annex F.

The two cut-outs of the regional model both have an extent of around 1 x 1 km and encompass the surroundings of the pumping wells (PW) Tahi 1-5 and Surány 12 as well as several monitoring wells (MW). The localized cut-outs allow for higher resolution and more detail than would be practical for the entire island (having a modelled area of 56 km²). Danube levels and pumping rates vary in the models on a daily time basis. The PWs are modelled as they appear in reality (as a single vertical shaft with 5 horizontal adits in a star shape), which could affect the flow regime and thus PFAS transport characteristics. In Vienna, only MWs are present.

The calibration of the 3D physically-distributed models¹ was done for the period of 2022-2024, which was the monitoring period in Budapest and Vienna. Calibration was performed in measured heads in the PWs and all MWs within each model. The calibration resulted in horizontal hydraulic conductivities (K) of 5-40 m/day in sand and 307-537 m/day in gravel for Surány, 18-48 m/day in sand and 256-300 m/day in gravel for Tahi, and an average of 26 m/day for the heterogeneous soil in Vienna. The Surány model calibration shows good results for MW1 and MW2, and reasonable results for the PW after the reconstruction, which ended in June 2022 (Table 4.5). In Tahi, the simulated values in MW2, PW and MW3 are reasonable. Unfortunately, no reliable z-coordinate for MW1 was available, so this MW was discarded. For Vienna, a better fit with the measurements was reached than for the Budapest sites, presumably due to better defined boundary conditions and the absence of pumping wells.

A one-site kinetic model was employed for the reactive transport modelling of the same 10 PFAS considered in the catchment scale models (Groot et al. 2025). Of these 10 compounds, 5 have been studied in natural soil column tests at TU Wien and modelled in Hydrus 1D (Simunek et al. 2013) with the same type of reactive model as employed here (one-site kinetic sorption). The obtained transport parameter values for these 5 PFAS were then applied here (Table 4.6). The parameter values for the remaining 5 compounds were obtained by means of a

¹For the Budapest cut-out models this is a second calibration step, as the regional model encompassing them has also been calibrated, see Annex F.

Table 4.5.: Mean Absolute Error (MAE, in m) and R^2 for all monitored wells in both cut-out models.

	Surány						Tahi			Vienna		
	MW1	MW2	MW3	PW	MW4	MW5	MW2	PW	MW3	MW1	MW3	MW4
MAE (m)	0.31	0.28	0.17	0.37	0.25	0.08	0.27	0.25	0.26	0.06	0.06	0.05
R^2 (-)	0.84	0.85	0.95	0.98	0.95	0.99	0.89	0.90	0.87	0.98	0.97	0.97

Table 4.6.: Sorption characteristics for the 10 modelled PFAS, using Hydrus' 1-site chemical nonequilibrium sorption model.

	K_d (m ³ /kg)	Alpha (hr ⁻¹)		K_d (m ³ /kg)	Alpha (hr ⁻¹)
PFBA ^b	$3.85 \cdot 10^{-6}$	24	PFPeA ^a	$1.30 \cdot 10^{-5}$	24
PFHxA ^b	$1.76 \cdot 10^{-5}$	24	PFHpA ^b	$2.36 \cdot 10^{-5}$	24
PFOA ^a	$3.20 \cdot 10^{-5}$	24	PFBS ^b	$1.30 \cdot 10^{-5}$	24
PFHxS ^b	$2.54 \cdot 10^{-5}$	24	PFOS ^a	$7.50 \cdot 10^{-5}$	120
GenX ^b	$1.36 \cdot 10^{-5}$	24	ADONA ^a	$1.50 \cdot 10^{-5}$	24
6:2 FTS ^{b,c}	$2.20 \cdot 10^{-5}$	24			

^a values obtained by modelling column tests in natural soil (Obeid et al. 2023).

^b values obtained by regression based on molecular structure.

^c only modelled in the AC-1 scenarios.

statistical regression based on similarities to the studied species in terms of molecular structure (chain length, number of fluorine atoms, molar volume).

Just like river levels and pumping rates, PFAS concentrations in the Danube fluctuate daily in the model. However, because only monthly samples were available, it was not possible to use the monitoring data directly as input for the model's daily time steps. Therefore, daily input concentrations for each of the 10 PFAS were generated based on statistical variation during the monitoring period at each site (Groot et al. 2025).

In the Vienna model, model boundaries other than the Danube are no-flow and therefore no boundary concentrations need to be assigned to them. For the Budapest sites, all lateral boundaries are open and therefore need boundary concentrations. However, from the flow patterns given in Annex F it is apparent that the boundaries perpendicular to the Danube do not influence the PW's of interest, as water coming in from these boundaries flows to other PW's. The PW's of interest may receive water from the inland model boundary opposite from the river. There is no information about the PFAS concentrations that should be assigned to these boundaries. However, because the travel time of this water to the PW are very long (multiple decades), time in which a myriad of processes may decrease concentrations (sorption,

degradation, transformation), a concentration of 0 was assumed at the model boundaries for all 10 species. Behind the PW at both transects though, some substances were found to have locally elevated concentrations (especially PFOA, PFOS and Gen-X), presumably due to an unknown inland source. To accommodate for this, a daily concentration input was applied behind Surány MW4 and Tahi MW3. Additionally, because the 10 species of PFAS have been present in the environment for much longer than the calibration period, a “warm-up” period of at least 1 year was run for each scenario to obtain the initial spatial concentration distribution of each of the 10 PFAS.

At Tahi, the simulated median PFAS concentrations for the monitoring period show a good fit compared to the observed values (Figure 4.16). Most PFAS agree within ± 1 ng/L. Some substances (e.g. PFPeA, PFHxA and ADONA at Tahi) show too high modelled median groundwater concentrations, most likely due to the input concentrations in the Danube not fitting exactly to the measured values (Groot et al. 2025). A lack of variation can be seen when comparing observed to simulated concentrations. Likely, this is an effect of lack of temporal correlation in the randomly generated daily river input concentrations. Because daily river concentrations can have any value within the chosen statistical distribution, concentrations jump up and down from day to day. These concentrations mix in the groundwater, so that variability is reduced. In other words, there are no longer periods of low or high concentrations in the model, that most likely would have occurred in reality. However, due to monthly sampling, we have no information on this. Lastly, elevated background concentrations (e.g. of PFOA, PFOS, GenX in Surány) are not accurately simulated because of the little information available on these inland sources. After calibration, the model was run for the period 2015–2021, which represents the reference period for the scenario simulations. For this period, daily Danube PFAS concentrations were generated on the same statistical basis as for the monitoring period (see above, Groot et al. (2025)). Subsequently, scenarios were simulated, of which the results can be read in Section 4.6.4.

Differences between the small-scale and large-scale BF modelling

There are many differences worth noting between the Vienna (small-scale, ~ 10 m) and Budapest (large-scale, ~ 100 – 1000 m) sites. In Budapest, because of the pumping of drinking water wells, the sampled groundwater is a mix between water that has infiltrated a long time ago (possibly even from the other side of the Szentendre island) and water that has infiltrated recently from the nearby riverbank. In Vienna, the water infiltrates only from one side of the island and travels a shorter distance to the wells, leading to less mixing. Therefore, the groundwater represents more directly the PFAS concentrations in the Danube. This can be easily seen from Figure 26, where concentrations are more stable than in the Budapest sites. The shorter travel distances and simpler, unidirectional flow system make the Vienna case better defined with smaller uncertainties. This is reflected in the better calibration result (i.e. residuals between measured and modelled heads), as was shown in Table 4.5.

Another difference is the presence of a clogging layer in Vienna, which potentially increases effectiveness of the RBF system. However, as can be seen from Figure 4.16, PFAS concentrations do not significantly decrease from the river to the groundwater. This is because of the continuous influx of PFAS from the river, meaning that over time, an equilibrium developed between the river water and groundwater concentrations. Because of this continuous influx, the clogging

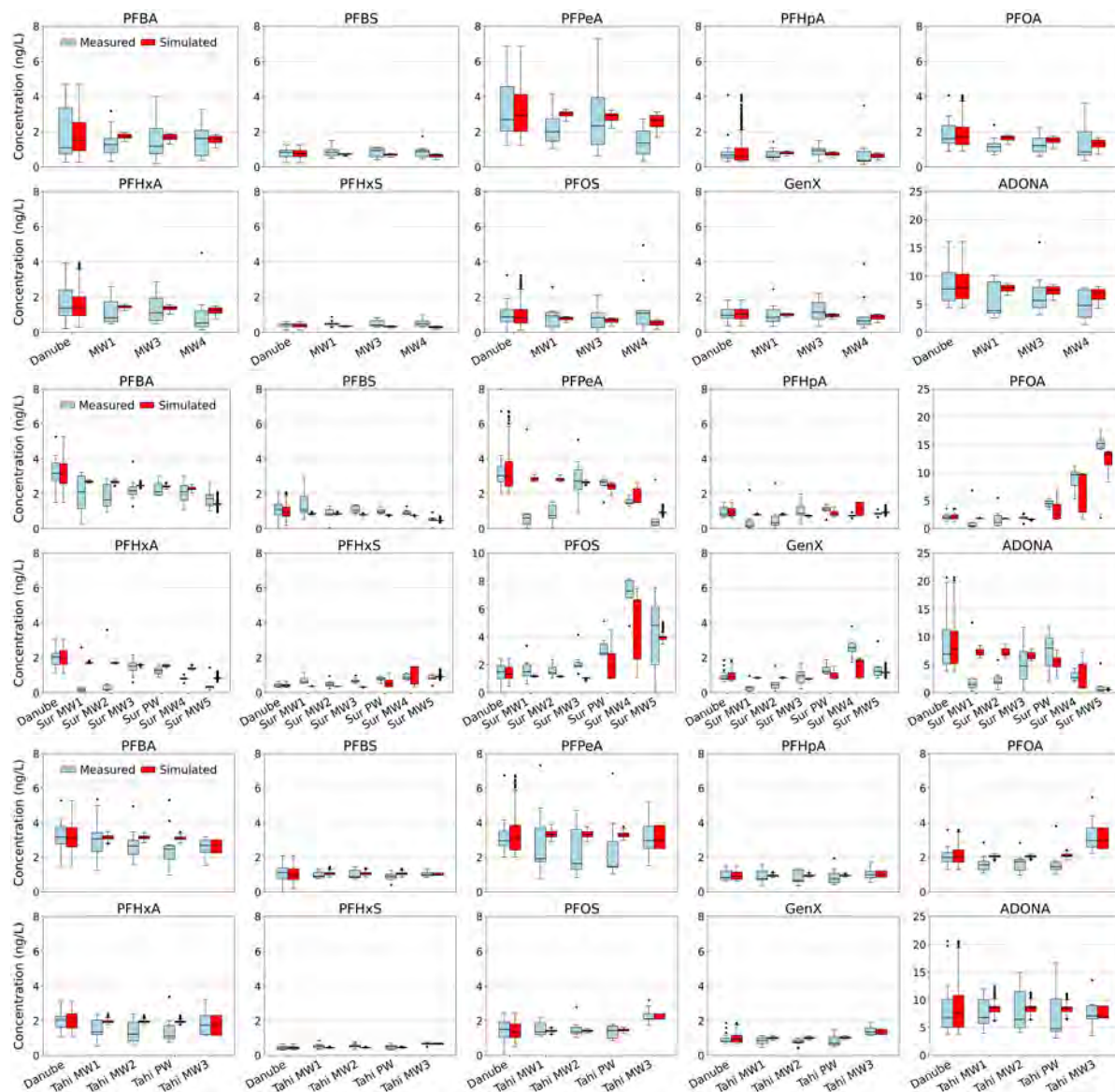


Figure 4.16.: Box plots of measured versus simulated concentrations of all 10 substances in monitoring wells (MWs) and the pumping well (PW) from 2022–2024 at Vienna (top), Surány (middle), and Tahi (bottom). The black line indicates the median, the boxes the quartiles and the whiskers represent the smallest and largest values within 1.5 times the inter-quartile range from the first and third quartiles. Dots represent outliers.

layer does not provide an extra barrier against PFAS contamination. However, in the case of a temporary influx (e.g. in the case of an accidental spill of a large amount of PFAS), it might prove valuable. More on this can be read in section 4.6.4. Despite these systemic differences between these sites, in terms of modelling approach they can be treated similarly and the chosen 3D numerical approach is appropriate for both. The monitoring data, which do not provide information on the reactive behaviour of PFAS, also do not justify the use of separate modelling approaches for the two scales in order to get the most information from the modelling exercise.

4.6.4. Model train application for scenario assessment

Scenarios assessed with the model train are not intended to be realistic predictions of future development, as this was not feasible with the available data and models. Instead, the scenarios are intended to show how hypothetical situations would be reflected in model results, and what kind of questions could be answered by the model train if future developments were better known.

Table 4.7 gives an overview on scenario assumptions of changes in the upper Danube catchment to be assessed with the model train prepared for the catchment – river – riverbank filtration – drinking water interaction. As reference situation we use the period 2015–2021, for which most recent multiyear hydrological information was available for the whole catchment.

As for the main PFAS point source in the catchment, the 3M PFAS production in Gendorf, the company announced the phase out of PFAS production in 2025, the ending of the point source emission stemming from this production is implemented in a Baseline Scenario (BL) which is otherwise unchanged compared to the emissions in the reference situation. Also, the diffuse emissions from the Gendorf site stay unchanged. Further on, the BL scenario is used to show effects of contrasting climatic conditions in the catchment. It assumes hydrological conditions of the year 2013 as an example for a wet year or a “pre-climate change situation” (low flow Q_{95} at Vienna: about 1500 m³/s, as compared to the long term average low flow Q_{95} of 950 m³/s) and it assumes hydrological conditions of the year 2018 as an example of the dry year or a “post climate change situation” (low flow Q_{95} at Vienna: about 700 m³/s as compared to the long term average low flow Q_{95} of 950 m³/s) in the catchment.

The scenario “accidental spill” (AC) assumes a fire close to the city of Linz upstream of the bank filtration sites at Vienna and Budapest, leading to a spill in the river of PFAS contained in the firefighting foam. In this scenario two contrasting recipes are assumed for firefighting foams, an old one based on PFOS and a newer one based on 6:2 FTS. In both cases, “worst case” assumptions for the spill have been made to visualize what might happen in an extreme situation. The spill is tracked on its way down river Danube and its impact on bank filtered water is assessed. Again, two contrasting hydrological conditions in the catchment controlling the water flow and PFAS transport are shown as sub-scenarios.

Water pollution control scenarios assume two levels of action to reduce PFAS emissions in the catchment and again two contrasting flow regimes. The first level of water pollution control, implemented in scenario “WPC1”, is addressing current environmental emissions via wastewater treatment plants (WWTP) and is assuming advanced quaternary treatment with activated carbon at all WWTPs with more than 10,000 p.e. (population equivalents). The second level of

Table 4.7.: Overview of scenario assumptions to calculate potential changes of PFAS concentrations in river Danube and bank filtration wells at Vienna and Budapest.

Scenario group	Scenario	Climate/ river discharge	PFAS produc- tion Gendorf	Legacy pollution	Acciden- tal spill	Advanced waste water treatment	PFAS use re- striction
Reference period (Ref)		based on historical data (2015– 2021)	Yes	current situation	No	No change	No change
Baseline (BL)	BL-pre- climate change	hydrology 2013	No	current situation	No	No change	No change
	BL- post- climate change	hydrology 2018	No	current situation	No	No change	No change
Accidental Spill (AC)	AC1- high flow	high-flow period starting 2013-01-09	No	current situation	Spill near Linz, new “6:2 FTS foam”	No change	No change
	AC1- low flow	low-flow period starting 2018-07-11	No	current situation		No change	No change
	AC2- high flow	high-flow period starting 2013-01-09	No	current situation	Spill near Linz, old “PFOS new foam”	No change	No change
	AC2- low flow	low-flow period starting 2018-07-11	No	current situation		No change	No change
Water pollution control I (WPC1)	WPC1- pre	hydrology 2013	No	current situation	No	activated carbon at WWTP > 10k PE	No change
	WPC1- post	hydrology 2018	No	current situation	No		No change
Water Pollution Control II (WPC2)	WPC2- pre	hydrology 2013	No	Groundwater remedia- tion at hot spots	No	activated carbon at WWTP > 10k PE	Restriction to essential use concept
	WPC2- post	hydrology 2018	No		No		

water pollution control, implemented in scenario “WPC2”, addresses the much more challenging task of remediation of legacy pollution from contaminated sites and a source control strategy based on the concept of an essential use for PFAS (PFAS may only be used in products where their application is considered as “essential”). More details on the assumptions for the different scenarios can be found in Annex G.

An overview of the modelling results of scenarios is shown in Table 4.8. As in Figure 4.14, a risk-ranking schema based on defined concentrations ranges from very low to very high risk for exceedance of the QS for the PFAS sum parameter from the EU Drinking Water Directive (EU DWD) or the QS (quality standard) included in the proposal for a new groundwater directive and the EQS (environmental quality standard) included in the proposal for a new environmental quality standard directive (EC COM(2022) 540 final) have been used for assessment. Again, sums have been calculated from the 10 parameters where quantitative modelling was possible.

The risk of exceedance of the quality standards of the DWD is very low in most of the scenarios. An exception is the accidental spill scenario (AC) with its sub-scenarios. Assuming a spill with the newer 6:2 FTS based firefighting foam would only cause a medium or low risk of exceedance of the sum of PFAS in river Danube for few days. The effect of bank filtration would lower this risk for drinking water abstraction by flattening the peak of the spill by retardation and mixing processes. The example of the spill with the old PFOS-based foam clearly indicates the risk that would have been provoked by such a spill. Depending on flow conditions, a high or very high risk of exceedance of drinking water standards would have been expected in river Danube at Vienna and Budapest for some days. Again, the effect of bank filtration would have reduced the risk for exceedance of quality standards depending on the flow time in the groundwater being significantly higher at water abstraction wells in Surány than in Tahi or at the control well at Vienna (the later one not used for water abstraction).

The risk of exceeding the (E)QS for PFOA-eq as proposed for a new groundwater and environmental quality standard directive is much higher than in the DWD case. While the closure of the 3M Gendorf production site and the implementation of further water protection control measures (WPC1 and WPC2) would lead to a reduction of the risk of exceedance of the EQS in the Danube, this risk might increase again in case of hydrological conditions causing a reduced flow in the river. A reduction of the risk for exceedance of the proposed QS for the sum of PFOA-eq in groundwater as effect of bank filtration is insignificant for all scenarios, as this QS is calculated as average over the whole year and the retardation of bank filtration can reduce peak pollution, but does not hinder PFAS to distribute on a longer run. In contrast, inland pollution from the Danube Island at Budapest Surány may even contribute to the risk of exceedance of QS in groundwater in case of low water levels in river Danube and higher shares of contribution from inland water to the abstraction wells.

Table 4.8.: Estimated concentrations and risk of exceedance of (E)QS in river Danube at Vienna and Budapest and after bank filtration for different scenarios for the 10 PFAS evaluated. Maximum concentrations (ng/L) were reported for the DWD, average concentrations (ng PFOA-eq/L) for the (E)QS.

Scenario	Σ PFAS ₁₀ DWD (EU DWD)					Σ PFAS ₁₀ PFOA-eq draft (E)QS (EC COM(2022) 540 final)				
	Vienna		Budapest			Vienna		Budapest		
	Danube	BF	Danube	Tahi	Surány	Danube	BF	Danube	Tahi	Surány
Ref	36.8	19.9	41.0	26.6	24.6	5.2	3.2	6.3	6.3	8.5
BL-pre-cc	11.5	5.4	12.4	21.3	27.1	3.0	1.6	3.8	4.6	11.2
BL-post-cc	17.7	8.4	18.8	14.3	20.9	5.2	2.9	6.4	6.4	11.6
AC1-hf	for 5 days	6.5	for 5 days	18.2	for 92 days	average	2.2 (>365 days)	average	4.3 (205 days)	9.1 (209 days)
AC1-lf	for 5 days	10.0	for 5 days	for 25 days	for 32 days	average	3.7 (>365 days)	average	6.8 (>365 days)	9.8 (>365 days)
AC2-hf	for 3 days	8.1	for 8 days	for 27 days	for 144 days	average	4.4 (175 days)	average	9.0 (253 days)	11.7 (>365 days)
AC2-lf	for 9 days	15.9	for 9 days	for 68 days	for 142 days	average	8.3 (212 days)	average	10.7 (304 days)	13.2 (>365 days)
WPC1-pre	10.8	5.0	11.5	18.4	27.7	2.7	1.5	3.5	3.9	10.4
WPC1-post	16.7	7.9	17.5	13.5	20.1	4.9	2.7	5.9	5.9	9.3
WPC2-pre	6.8	3.1	7.2	11.1	27.6	1.7	0.9	2.1	2.9	9.7
WPC2-post	10.5	5.0	10.9	9.2	18.2	3.3	1.8	3.9	3.9	8
		Very low risk: < 20 ng Σ PFAS ₁₀ /L						Very low risk: < 1 ng PFOA-eq/L		
		Low risk: 20–50 ng Σ PFAS ₁₀ /L						Low risk: 1–2.5 ng PFOA-eq/L		
		Medium risk: 50–100 ng Σ PFAS ₁₀ /L						Medium risk: 2.5–4 ng PFOA-eq/L		
		High risk: 100–200 ng Σ PFAS ₁₀ /L						High risk: 4–5.5 ng PFOA-eq/L		
		Very high risk: >200 ng Σ PFAS ₁₀ /L						Very high risk: > 5.5 ng PFOA-eq/L		

For the BF modelling, water flow boundary conditions (including daily river fluctuations as well as pumping rates) for the pre-climate change situations were taken from the year 2013, and for

the post-climate change situation from the year 2018 (see Annex G for more information). Table 14 shows that generally, the post-climate change (post-cc) scenarios predict higher ΣPFAS_{10} and ΣPFAS_{10} PFOA-equivalents concentrations as compared to the pre-climate change (pre-cc) scenarios. This means that according to this modelling study, climate change will generally increase health risks with regards to PFAS. This happens mostly because of the predicted increased length and severity of low-flow periods, which in turn increase river concentrations due to reduced dilution. However, when compared to the reference period (Ref), the post-cc baseline (BL) scenario predicts a decrease in PFAS concentrations in almost all cases. This is because the effects of climate change are counteracted by the reduction in industrial activity, especially the imminent closing of the PFAS production at Gendorf, which will lead to a very reduced PFAS load, particularly because of a reduction in ADONA emissions. Moreover, if water pollution control measures are implemented (WPC1 and WPC2), a definitive reduction in concentrations compared to the reference period is predicted, even for the post-cc situation. However, it is important to note that even in this scenario, risk levels for many areas are medium or higher according to the proposed (E)QS guidelines (EC COM(2022) 540 final). In terms of current DWD (EU DWD), only scenario WPC2 predicts a very low risk level at all three areas, although this depends on the contribution of contaminated background water.

In Vienna, the ΣPFAS_{10} as well as ΣPFAS_{10} PFOA-equivalents concentrations decrease from the river Danube to the bank filtered (BF) water in all scenarios. This is due to mixing with ambient groundwater and sorption of PFAS to the aquifer material, leading to very low risk levels in all scenarios according to the current DWD. This has two further causes: (1) no inland background contamination is present, and (2) the riverbed at the Vienna BF site has a high degree of clogging. The effects of the first cause are evident, the second cause leads to reduced infiltration of river water into the aquifer. According to the thresholds in the draft of the (E)QS, risk levels are predicted to be low or medium in Vienna, but very high for the accidental spill of old AFFFs (AC-2), which will be elaborated upon below.

In Budapest, PFAS concentrations are higher in groundwater than in river water in many of the simulated scenarios. This is due to mixing with inland groundwater from behind the PWs, shown to be contaminated (notably with PFOS, PFOA and GenX). The mixing ratio between river and ambient groundwater depends on water levels in the river Danube, the PWs and the background groundwater, which vary from day to day. This is why for the exact same river concentrations, different results can be observed in Surány versus Tahi, and this is also why the pre-cc and post-cc scenarios lead to different mixing ratios and thus, in some cases, to surprising results. For example, at Tahi, post-cc scenarios lead to a decrease of the ΣPFAS_{10} concentrations from river to groundwater, while pre-cc scenarios lead to an increase. In terms of ΣPFAS_{10} PFOA-equivalents, the groundwater at Tahi has the same exact concentration as the river concentration in all post-cc scenarios, showing that in these scenarios, the groundwater is almost exclusively affected by the river water. This shows the importance of discovering, monitoring and possibly treating inland background contamination, as well as studying the hydrological conditions at RBF sites.

The results of the accidental spill (AC) scenarios are shown in Figure 4.17 to Figure 4.19 in more detail. The spills are assumed to happen over a period of 7 days, leading to a relatively short spike in PFAS concentrations in the river Danube at Vienna and Budapest. Because the spill is assumed to enter the river Danube in Linz, Austria, the levels at Vienna are higher than at Budapest. Furthermore, the peak concentrations for the low flow (lf) scenarios are higher than

for the high flow (hf) scenarios, due to a decrease in discharge in the river Danube, leading to reduced dilution. So, if a spill happens during low flow conditions, 4 times higher concentrations can be expected than during high flow conditions. Lastly, a spill of new AFFFs (AC-1) leads to about 10-15 times lower peak $\Sigma 10$ PFAS concentrations and about 40-100 times lower $\Sigma 10$ PFOA-equivalents than old AFFFs (AC-2) in river water.

In groundwater, these effects are somewhat attenuated (depending on the local hydrological situation) but still noticeable. The groundwater concentrations ultimately depend on the specific background concentration, transport time and subsurface characteristics at each well. These results can support water management during a PFAS spill event, as they can be used to make a quick estimate of the severity of the situation based on circumstantial information.

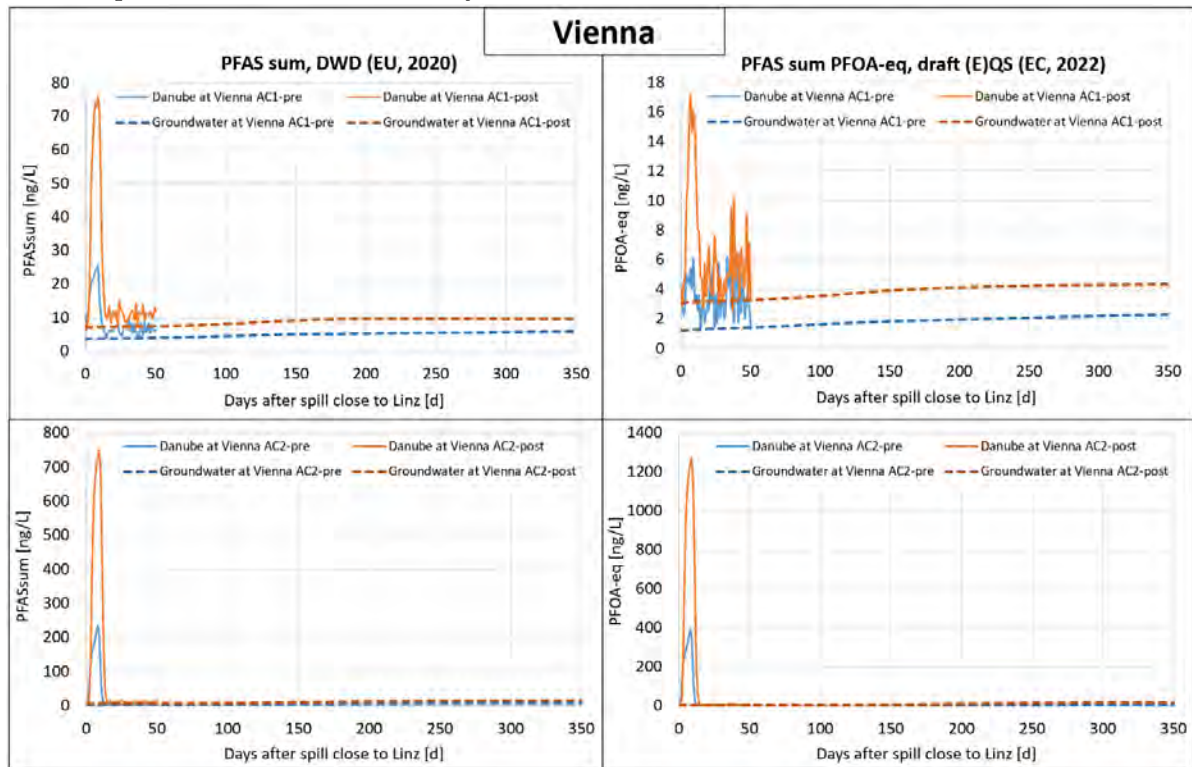


Figure 4.17.: Development of a PFAS-peak from an accidental spill with new AFFF (top) and old AFFF (bottom) into river Danube close to Linz observed at the bank filtration site at Vienna. River concentrations in solid lines, groundwater concentrations in dotted lines.

At the site in Vienna, it takes multiple months for the PFAS spill to infiltrate into the groundwater, during which dispersion leads to a flattening of the concentration peak. The riverbank at this site is so clogged that there is a 3-meter gradient between the water level in the Danube and the water level in the first groundwater monitoring well (1 m into the riverbank). This means that barely any water is able to flow through, which, together with sorption processes, leads to such extreme flattening of the peak. This is also the reason why PFAS concentrations do not cross the threshold of higher risk levels as defined in the current DWD in any spill scenario here (as can also be seen in Table 4.8), showing that although a clogged riverbank is not necessarily effective in regular situations (as discussed in section 4.6.3), it does prove a highly potent barrier in case of a temporary increase in river concentrations. Still,

groundwater PFAS concentrations do rise and peak after around 300 days. For the proposed (E)QS, AC1 results in low and medium risks for pre-cc and post-cc situations, respectively, while AC2 results in very high-risk levels for both cases. It is clear that the groundwater will be of such low quality for at least a year, and the best estimate is, that it will take at least three years for concentrations to return to the pre-spill levels, possibly longer.

At Tahi, the concentrations of ΣPFAS_{10} and ΣPFAS_{10} PFOA-equivalents start increasing in the PW after about 25 days for the pre-cc scenarios and after about 50 days for the post-cc scenarios. This difference occurs because of the lower river level in the post-cc scenarios, leading to a lower gradient and thus slower groundwater flow. In the pre-cc scenarios, the increase of PFAS concentrations between 200 and 250 days after the spill does not happen due to infiltration of river water, but due to a sudden increase in the gradient between the pumping well and the monitoring well No. 3 due to falling water levels in both the river Danube and the pumping well, leading to an influx of PFAS from the inland source of contamination. This happens in all scenarios (not just the AC scenarios), highlighting the importance of a thorough understanding of the hydrogeological situation at the site of interest.

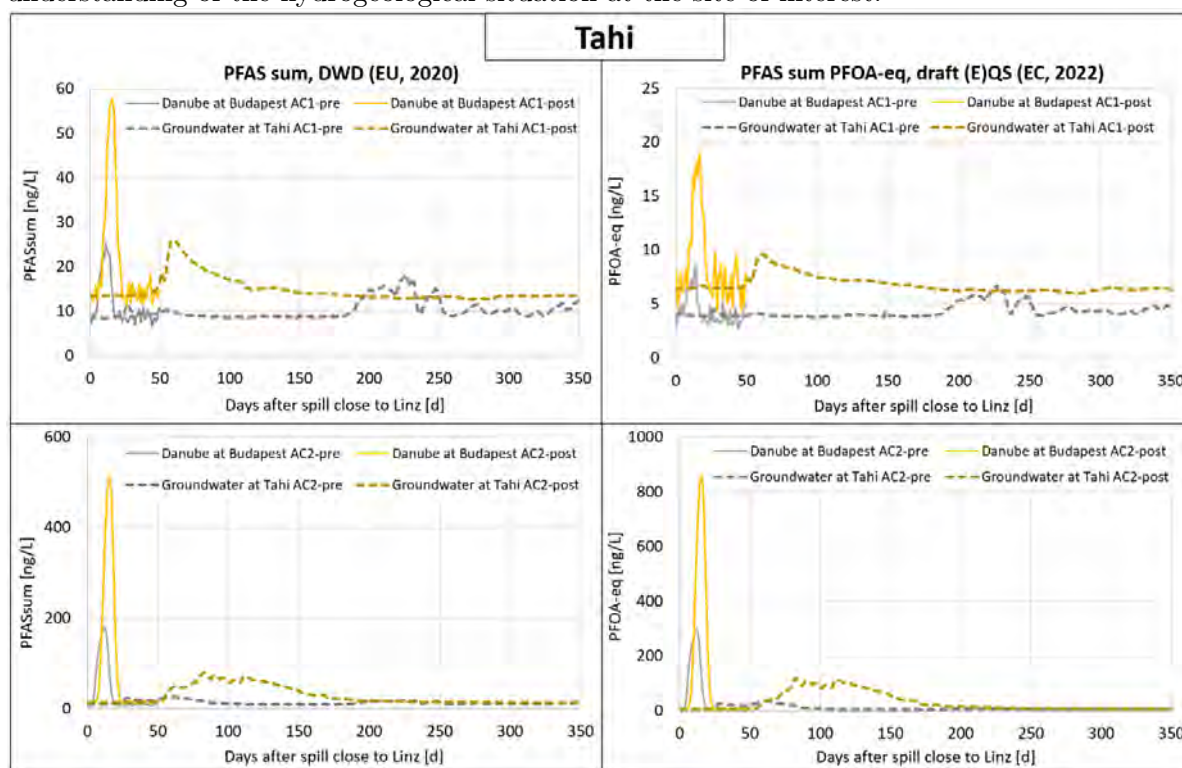


Figure 4.18.: Development of a PFAS-peak from an accidental spill with new AFFF (top) and old AFFF (bottom) into river Danube close to Linz observed at the bank filtration site at Tahi, Budapest. River concentrations in solid lines, groundwater concentrations in dotted lines.

Even though the effect is not as pronounced as in Vienna, mixing and sorption processes lead to a reduction and dispersion of the PFAS peaks at Tahi as well. This has the positive effect of a reduced maximum concentration compared to the river. The negative effect is that the PFAS concentrations in the pumping well are elevated for a longer time period. In practical terms, this means that the water does not meet the quality criteria for drinking water during

this time. As can be expected, risk levels are elevated higher and for a longer time if the spill contains old AFFF (AC-2) and if the flow conditions are lower (post-cc) (Table 4.8). Another interesting finding is that for the AC-1 scenarios, the ΣPFAS_{10} is higher than the ΣPFAS_{10} PFOA-equivalents, but for the AC-2 scenarios, this is the other way around. This is due to the high concentration of PFOS in old AFFFs, which has a high relative potency factor (RPF) due to its toxicity.

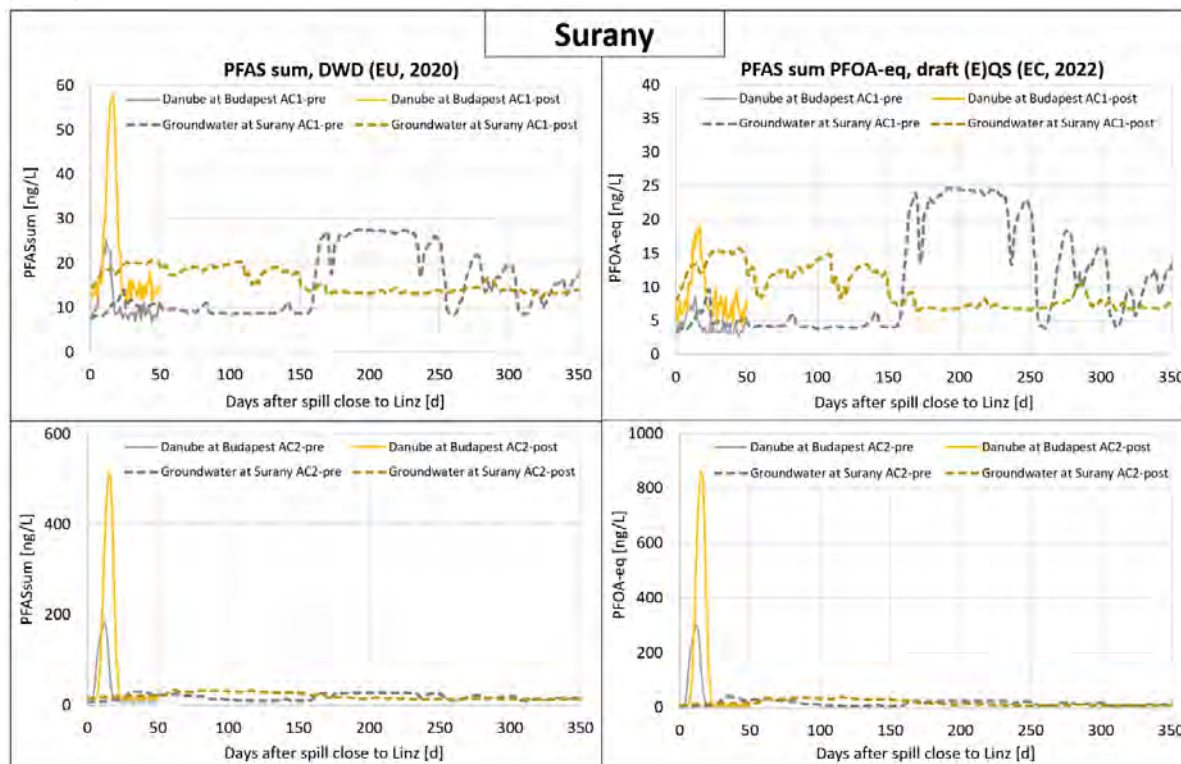


Figure 4.19.: Development of a PFAS-peak from an accidental spill with new AFFF (top) and old AFFF (bottom) into river Danube close to Linz observed at the bank filtration site at Surány, Budapest. River concentrations in solid lines, groundwater concentrations in dotted lines.

Due to Surány's close proximity to Tahi, the PFAS peak in the river Danube was assumed to be the same. However, there are two important differences between Tahi and Surány. First, the hydrological situation is different, as the Surány pumping well is located further away from the riverbank and has a different pumping schedule than the Tahi pumping well. Generally, it can be stated that due to this difference, the spill has a smaller effect on groundwater concentrations in Surány than in Tahi, simply because less river water reaches the Surány pumping well. Second, the background contamination is a lot more pronounced at Surány, with higher concentrations of PFOS, PFOA and GenX. In the pre-cc scenarios, the significant increase in PFAS concentrations between 170 and 300 days after the spill is due to an increase in pumping rate, leading to a higher gradient between the background water and thus an influx of contaminated water. The same happens in the post-cc scenarios between 10 and 150 days after the spill. These effects are so pronounced that they tend to obscure the effects of the spill on the groundwater.

However, the spill can be seen to influence pumping well PFAS concentrations in the pre-cc scenarios after about 25 days after the spill. Compared to the effects of the background contamination, the peak is small in the AC-1 scenarios, reaching a concentration of 14 ng/L Σ PFAS₁₀ and 10 ng/L Σ PFAS₁₀ PFOA-equivalents, but in the AC-2 scenarios it reaches 30 ng/L Σ PFAS₁₀ and 40 ng/L Σ PFAS₁₀ PFOA-equivalents, the latter being almost ten times the proposed threshold in the (E)QS. In the AC-2 post-cc scenarios, as the spill reaches the PW at the same time as the background contamination, these effects are conjoined and lead to 35 ng/L Σ PFAS₁₀ and 40 ng/L Σ PFAS₁₀ PFOA-equivalents concentrations as well.

To conclude, PFAS risk levels are predicted to be highest and remain high the longest in Surány, followed by Tahi and finally Vienna. The differences between the sites are quite large for some of the spill scenarios and were found to deviate from the hypotheses due to the complex interactions of PFAS concentrations infiltrating from the river on the one hand and PFAS contributions from the background water on the other. This shows the importance of surveying the hydrological situation at the site of interest, including possible inland sources of PFAS.

Key messages of Danube Case Study

The Gendorf chemical park on the River Alz and diffuse inputs from urban areas are the main sources/pathways of per- and polyfluorinated carboxylic acids (PFCA) with a chain length of up to 8 C for the Danube River upstream of Budapest. For per- and polyfluorinated sulfonic acids (PFSA) with a chain length of up to 8 C, the diffuse urban inputs predominate. A large part of these emissions is due to legacy pollution (contaminated soil and groundwater from former fire-fighting foam use or old municipal landfills), which will persist even if strict source control for PFAS is implemented. Municipal and industrial WWPT effluents together contribute with a share of up to 25% of the total emissions of both PFAS groups. For the PFOA substitutes ADONA and Gen X, the Gendorf chemical park is the only relevant source that could be identified in the region.

Except for some small tributaries, the surface waters in the Danube Basin upstream of Budapest, including the Danube itself show a very low or low risk of exceeding the threshold for drinking water of the EU drinking water directive of 100 ng l⁻¹ for the sum of 20 PFAS. This is of relevance in case that surface waters are used as drinking water source via bank filtration. There is a high to very high risk of exceeding the European Commission's proposed quality standard for surface and groundwater of 4.4 ng l⁻¹ PFOA toxicity equivalents as a sum of 24 PFAS in the Danube upstream of Budapest and in most of its tributaries. These risks may be reduced by massive efforts to implement water pollution control measures (including groundwater remediation in hot spot areas). The risk might even increase if low effort is made to control water pollution and the Danube's flow is reduced due to the effects of climate change.

Abstraction via bank filtration shows hardly any impact on PFAS concentrations in the groundwater flow from rivers to the abstraction wells in case of continuous inputs. Adsorption/desorption seem to reach an equilibrium after

long-term operation. For some of the “old” PFAS compounds (PFOA and PFOS) in the Budapest case, even higher values are observed inland from the pumping wells, which is attributed to unknown sources and leads to a reduction in water quality. In the case of peak concentrations in the Danube due to accidental spills, bank filtration processes can significantly reduce their impact on groundwater by retardation and mixing processes.

The application of model train combining the MoRE and the PPM emission models demonstrated the capabilities of such a complementary approach. Both models proved capable of predicting the instream concentration of 10 different PFAS based on emission estimates, with similar results in terms of pathway contributions and risk assessment in the catchment. Based on their specific strengths, both models contributed to the scenario assessment, with MoRE being better able to calculate water protection scenarios and the PPM model showing its main advantages in providing high temporal resolution results for accidental spill scenarios. The results of both models provide the input to bank filtration modelling in a sequential combination of the model train.

A 3D numerical reactive transport model is the best choice for modelling the fate and transport of PFAS in a bank filtration setting. This is also true in situations where a steady-state approach is warranted, as the 3D cut-out models run sufficiently fast, so that computation time is not an issue. At the same time, the 3D numerical approach overcomes several conceptual shortcomings of the 1D approach, i.e. it can include (transverse) mixing and dispersion and (by extension) can better handle nonlinear (sorption) processes. For situations in which the complex dynamic surface water - groundwater is important, a transient 3D approach is indispensable.

4.7. Limitations and outlook

4.7.1. Emission and in-stream modelling

Danube catchment models

The investigations in the Danube case study focused on PFAS as highly relevant group of vPvM chemicals in context of industrial chemicals or more generally speaking contaminants of emerging concern. Emissions from legacy pollution at contaminated site (e.g. fire-fighting foam application, old municipal landfills) have been identified as highly relevant even in the context of a large catchment. Quantification of emissions from these sources is hampered by the lack of sufficient data and information.

The identification of local hotspot of PFAS pollution due to training grounds for firefighting in context of airports or not, is only at a starting point with some single cases being localized in the catchment. Many more are expected to pop up. Quantification of PFAS-releases from single hot spots is still not robust enough to be used for extrapolation to other cases. The data set on PFAS concentrations in landfill leachate has been improved during this project. The problem is

the absence of a harmonized inventory on old municipal landfills including information on size, age and type on an international level. Country inventories show too large inconsistencies to be used as basis for emission estimates.

Due to this incompleteness in understanding and/or data it was not possible to directly quantify these emissions based on a pathway orientated (Tier 3) or sources orientated (Tier 4) approach. These emission pathways therefore have been quantified only using the riverine orientated (Tier 2) approach (using inhabitant specific emission factors derived via back calculation from measured in-stream loads). Further efforts in administration and research to provide better inventories and emission factors could significantly improve emission modelling on regional scale.

Another major shortcoming, specifically in the context of application of a source orientated (Tier 4) approach, is absence of robust openly available information on PFAS production, import and export resulting in use volumes of PFAS on national and EU-level. There is an urgent need for major efforts to provide this information, as it is decisive for sound environmental exposure assessment not only for surface and ground water.

Modelling results reported here include 10 PFAS substances. Another 10 could be modelled but could not be validated on in-stream concentrations, as the empirical basis is missing because values of these PFAS were mostly below the analytical limits of quantification. Among these latter ten were PFAS like PFDA and PFNA with high relative potency (implying high potential risk at low concentrations) and therefore of high importance in risk assessment of exceeding environmental quality standards based on PFOA-toxicity equivalents. It is known that the wider group of PFAS includes thousands of substances beyond the ones discussed here. The information on these remaining substances is insufficient for assessments like those presented here. A reproducible and standardised analytical parameter for “total PFAS” or even “total toxicity of PFAS” could be a very helpful in this context to address relevant PFAS in a combined way, if limits of quantifications are sufficiently low.

The scientific knowledge about the fate of PFAS in the environment is still limited. This includes their distribution between different phases (air, water, solids) and the transformations of so called “precursors” into stable “end products” like PFOA, PFOS and others. In frame of this project 6:2 FTS (mainly from WWTP effluents) and N-EtFOSA (mainly from landfill leachate) as precursors have been included into the emission, fate and transport model. Still transformation of 6:2 FTS in the environment is matter of high uncertainty. Further research is needed in this respect to improve emission, fate and transport modelling. Emission models on catchment scale would highly benefit from better understanding of the leaching behaviour of PFAS from contaminated soils and the extent of local groundwater pollution due to the application of fire-fighting foams or to the presence of municipal landfills as presented in chapter 3.

Models in the urban setting of Berlin

A number of simplifications and assumptions were made for the modelling of emissions into Berlin's water bodies, which reduce the accuracy of the representation of hydraulic and substance processes and thus of the model. By extrapolating average concentrations to monthly loads, it is possible to draw conclusions about the long-term pollution situation of a water body,

but it is not possible to assess pollution peaks in the water body. Extreme precipitation events and the temporal distribution of inputs and loads are not mapped. Depending on the topography of the sewer system, the sedimentation and remobilisation of pollutants in the sewers, the characteristics of the stormwater runoff can vary considerably. This further limits the transferability of the concentrations measured at the two sampling sites in Berlin to the entire Berlin sewer system. On the other hand, it must be mentioned that the input concentrations for the load calculations sometimes have very high standard deviations and correspondingly high uncertainties are propagated in the model.

Besides the limitations regarding the emissions, the modelling of PMT substances in surface water has a number of additional limitations: (i) The schematisation of the Berlin surface water system ignores a number of details, such as the precise location of the wastewater treatment plants, smaller canals and others. (ii) It is assumed that the flow field is constant, whereas storm events but also daily variations in the sewage outflows will influence the flow in the water system. (iii) Perhaps more importantly, the modelling makes simplifying assumptions about the behaviour of the PMT substances in the water and the sediment. In addition, some of the parameters that influence this behaviour, notably the concentration of particulate matter and its settling velocity, had to be estimated based on general understanding.

4.7.2. Bank filtration models

Generic bank filtration model (gBF)

The generic bank filtration model provides a practical tool to roughly estimate to which extent wells could be affected by chemicals from the river site after bank filtration. The model only requires some basic information on the local situation (soil material, flow length) and physio-chemical information (degradation, sorption) of the respective chemical. Results could be used as screening tool for locations that might be affected by specific chemicals.

Main limitations can be summarised as follows: (i) For dynamic systems with large temporal and spatial variations this tool is suitable only to a very limited degree. (ii) The gBF model does not account for transformation products, transformation rates, and different geochemical conditions. (iii) In case of pumping wells, the gBG model does not consider the distribution of travel times of the water pumped, thus ignoring the mixing of water with different travel times and concentrations.

3D numerical flow and transport models

In general, the further elaborated BF models are important because of their ability to simulate transient conditions, as well as model more detailed reactive processes (such as one-site kinetic sorption, which was employed here). This is especially important in scenarios such as an accidental spill, in which transient river conditions can have a significant effect on the amount of PFAS infiltrating into the riverbank.

The monitoring data on the BF sites do not provide information on the reactive behaviour of the PFAS, other than the apparent absence of significant transformation, decay or permanent sorption. This is due to the fact that the breakthrough of the PFAS (the full passage of the

contaminant front and any tailing there may have been in the past due to spreading processes like sorption and dispersion) is already complete. This will not be unique to the sites of this case study. Particularly valuable would be monitoring during a (preferably prolonged) period of changing river PFAS concentrations, as that would give information on how the PFAS actually moves through the subsurface. The occasions for this (e.g. during the emergence of a substance, or during an accident/spill) will – hopefully – be very rare and/or hard to identify and act upon. The modelling of the column experiments showed that sorption of PFAS can be rather complicated, and each type of PFAS has a different behaviour with varying rates of sorption and de-sorption. This is only moderately captured by the one-site kinetic sorption model employed here, as it was clear from the column experiments that this type of model generally mis-represents peak transport time by about 10-15% and overestimates tailing. However, because peak concentrations can be simulated very accurately, this model was chosen here. More complex sorption models (such as two-site nonequilibrium and attachment-detachment sorption models) simulate PFAS breakthrough more accurately and could be used in the future, but as of now the functionality for these models does not exist in iMOD-WQ, so prospective users have to code these reactions themselves using the User-Defined Reactions (UDR) package

In the 3D approach used in the current study, the modelling codes MODFLOW-2005 and MT3DMS modeling codes were used, as implemented in the iMOD modelling framework. Recently, a new version of MODFLOW, MODFLOW6, has become available, with greatly enhanced functionalities. It fully integrated groundwater flow and solute transport. An important new feature is the possibility to use unstructured grids. This allows the user to increase the model resolution in areas where that matters the most and decrease it where detail is not as important or not warranted by a lack of data. The case of bank filtration can particularly benefit from unstructured grids, as model detail can be added around the production wells and between the wells and the river. In the hinterland, a lower resolution can be chosen to limit calculation times. At the moment of this writing MODFLOW6 still lacks functionalities regarding complex reactive transport phenomena, but the expectation is that this will become available soon.

5. Discussion and conclusions

5.1. Background and scope of the guidance document

Models are used in exposure assessments for two main reasons. The first reason is to complement monitoring data: it is often impractical or prohibitively expensive to monitor the environmental exposure at all times and along all exposure pathways and routes for all relevant chemicals. In this context, modelling can assist in mapping the temporal and spatial variability of exposure, exposure pathways and exposure routes. Further, modelling can be used to test hypotheses: can the known sources along the known pathways actually account for the measured exposure along the known exposure routes? If the answer is no, then the underlying conceptual framework needs to be reconsidered. A second rationale for using models is to assess potential future developments. Will the proposed mitigation measure prove effective in achieving the required exposure reduction? Or will the intended introduction of a new chemical result in adverse human health effects? Or will climate change interfere with exposure pathways, and how?

The scope of this document is to provide guidance for applications of models with specific focus on model trains for exposure assessment for persistent, mobile and toxic chemicals (PMTs) as part of environmental risk assessment related to surface and groundwaters. This document, based on the PROMISCES project results, explains the basic concepts of specific models and how best to use them in model trains, in the frame of a tiered approach. The term “model train” is used for a combination of stand-alone models to cover complex situations involving multiple environmental spheres such as atmosphere, lithosphere, hydrosphere, biosphere, and anthroposphere, as well as their interfaces. The intention is to inform users and interested stakeholders on what needs to be considered for the application of different methods, what can be expected and what cannot. The guidance document is written in terms of concepts rather than software/actual models.

It focuses on basic ideas, information requirements, concepts of implementation, basic physical background, and on the comparison of different approaches to quantify processes by single models, as well as on the role of single models in the context of a model train. It presents (i) “screening level” models for the assessment of regional exposure of groundwater from soil pollution and for the assessment of general exposure of air, soil and water at local, regional or global scales, with less detail than more targeted approaches, (ii) spatial and temporal explicit approaches for the identification of pollution plumes in the soil groundwater-continuum and (iii) model train applications for the catchment – river – river bank filtration – drinking water continuum.

Exposure of surface water and groundwater to PMTs depends on use patterns and environmental fate of the chemicals. Emission, fate and transport models incorporate driving factors into documented algorithms. The extent to which a substance persists in surface waters can for

instance be calculated with the “SimpleBox - Aquatic Persistence Dashboard” based on physical-chemical characteristics. The approach presented to derive generic risk limits for soils shows that, depending on regional variations in geo(hydro)logical conditions, the high mobility of some PFAS could lead to strict requirements for materials applied on soil.

5.2. Pollution plumes in the soil-groundwater continuum

For the soil-groundwater continuum, a novel model train coupling 1D-Hydrus, MODFLOW and MT3DMS to simulate PFAS fate and transport at watershed scale is presented. The model train accounts for the main physical, chemical and biological processes controlling the fate and transport of PFAS at this scale. For sorption and degradation reactions, several algorithms can be used allowing to select the most appropriate according to PFAS molecular properties and the characteristics of the simulated domain. A modelling framework describing the main steps required to build a model train has been also elaborated to facilitate the work of future modellers. Examples of the model train capabilities have been provided for two case studies, a PluriMetric Pilot experiment and a AFFF-polluted aquifer. The results of these modelling applications highlight the key role of identifying correctly the main physical and chemical processes controlling fate and transport of PFAS in the studied domain to build robust conceptual models. To increase model robustness, a thorough model calibration approach must be conducted, preferentially using time series measurements of PFAS concentration in pore solution in different locations of the contaminated site.

Moreover, based on the results provided by the two simulated case studies, the key role of the unsaturated zone in the transfer and long-term migration of PFAS has been confirmed. If possible, a high frequency monitoring of PFAS concentration in the pore solution of the unsaturated zone should be performed as a sharp migration front can occur in this zone. For a broad range of PFAS sorption reactions in the unsaturated zone are expected to occur onto the soil-water and air-water interfaces, implying that PFAS sorption evolves according to water content. Therefore, numerical formalism more complex than linear isotherm needs to be used in the model developed for the soil-groundwater continuum, nonlinear and nonideal formalism should be used. Considering the key role of capillary fringe displacement on PFAS transport in the unsaturated zone, the model train seems very efficient to perform PFAS simulations as it can describe explicitly water flow and solute transport at the interface between unsaturated and saturated zones avoiding the main pitfall encountered in other numerical architecture.

5.3. Modelling of the catchment – river – riverbank filtration – drinking water continuum

In the context of model applications for exposure assessment in the catchment – river – riverbank filtration – drinking water continuum, the guidance document demonstrates that the combination of stand-alone models in model trains expands the scope that can be covered. Model trains can combine individual models either in a complementary way or in a sequence. A complementary combination may either compare models of different complexity to find out which level of complexity (and associated effort) is needed to answer which questions or compare different

models with their different strengths and weaknesses in parallel to assess uncertainties, and/or use models for scenario evaluation according to their specific capabilities.

The application of a model train incorporating the emission models MoRE and PPM demonstrated the capabilities of such a complementary approach based on the case of the Upper Danube catchment. Both models proved capable of predicting the instream concentration of 10 different PFAS based on emission estimates and produced with similar results in terms of exposure levels, pathway contributions and risk assessment of exceedance of drinking water or environmental quality standards in the surface water bodies of the catchment. Based on their specific strengths, both models contributed to the scenario assessment including climate scenarios, with MoRE being better able to represent scenarios with water protection measures and the PPM showing its main advantages in providing high temporal resolution results for accidental spill scenarios.

A complementary application of a model train for comparing models with different levels of complexity for fate and transport modelling of bank filtration is presented for the Danube case study and related bank filtration sites. A 3D numerical reactive transport model proves to be the best choice for modelling the fate and transport of PFAS in a bank filtration setting. This is also true in situations where a steady-state approach is warranted, as the 3D cut-out models run sufficiently fast, so that computation time is not an issue. At the same time, the 3D numerical approach overcomes several conceptual shortcomings of the 1D approach, i.e. it can include (transverse) mixing and dispersion and (by extension) can better handle nonlinear (sorption) processes. For situations in which the complex dynamic interaction between surface water and groundwater is important, a transient 3D approach is indispensable.

The results of the model train application combining the MoRE and the PPM emission models also provided the input to bank filtration modelling in a sequential combination of the model train for the upper Danube catchment. Such a sequential combination facilitates a broader application in terms of content and a combination of approaches at different spatial resolutions. Scenarios including catchment related aspects as water pollution control measures, climate scenarios and their impacts on exposure of surface waters have been combined with scenario assessment at bank filtration sites and the risk of exceedance of limit values for groundwater or drinking water. The Berlin case demonstrates a sequential model train by combining an emission model of the city with a fate and transport model of the city's surface waters.

Main challenges for future improvements of exposure assessment for PFAS on catchment scale are:

- the high relevance of legacy pollution from the use of fire-fighting foams or from old municipal landfills. Regarding the former, there is a need for more and better understanding of the extent of local groundwater pollution due to these applications (strongly linked to studies on the soil-groundwater continuum) and improved identification of contaminated sites. For landfills, the main challenges are related to the lack of a harmonised inventory of old municipal landfills, including information on size, age and type at international level.
- the lack of robust, openly available information on the production, import-export and therefore use volumes of PFAS at national and EU level. A major effort is urgently needed

to provide this information, as it is decisive for sound environmental exposure assessment, not only for surface water and groundwater.

- the huge number of PFAS, including thousands of substances beyond the ones discussed in this document. A reproducible and standardised analytical parameter for “total PFAS” or even for “total toxicity of PFAS” could be a very helpful in this context to address relevant PFAS in a combined way, if limits of quantifications are sufficiently low.
- the limited scientific knowledge about the fate of PFAS in the environment. This includes knowledge of their partitioning between different phases (air, water, solids) and the transformations of so called “precursors” into stable “end products” like PFOA, PFOS and short chain substances.

Bibliography

- AGES (2024). *Analysis of soil parameters on behalf of the TU Vienna - Analysis orders 23142348-001 and 23142348-002*. Österreichische Agentur für Gesundheit und Ernährungssicherheit GmbH (AGES) (cit. on pp. 91, 92).
- Anderson, R. H., G. C. Long, R. C. Porter, and J. K. Anderson (2016). “Occurrence of select perfluoroalkyl substances at U.S. Air Force aqueous film-forming foam release sites other than fire-training areas: Field-validation of critical fate and transport properties”. In: *Chemosphere* 150, pp. 678–685. ISSN: 0045-6535. DOI: 10.1016/j.chemosphere.2016.01.014 (cit. on p. 47).
- Bakker, M., V. Post, C. D. Langevin, J. D. Hughes, J. T. White, J. J. Starn, and M. N. Fienen (Sept. 2016). “Scripting MODFLOW Model Development Using Python and FloPy”. en. In: *Groundwater* 54.5, pp. 733–739. ISSN: 0017-467X, 1745-6584. DOI: 10.1111/gwat.12413 (cit. on p. 58).
- Bakker, M., V. Post, C. D. Langevin, J. D. Hughes, J. White, J. Starn, and M. N. Fienen (2024). *FloPy: Python package for creating, running, and post-processing MODFLOW-based models*. Github code repository. DOI: 10.5066/F7BK19FH. URL: <https://github.com/modflowpy/flopy> (visited on 12/13/2024) (cit. on p. 58).
- Bear, J. (1979). *Groundwater hydraulics*. New York: McGraw-Hill (cit. on p. 75).
- Beegum, S., J. Šimůnek, A. Szymkiewicz, K. Sudheer, and I. M. Nambi (2018). “Updating the Coupling Algorithm between HYDRUS and MODFLOW in the HYDRUS Package for MODFLOW”. en. In: *Vadose Zone Journal* 17.1, p. 180034. ISSN: 1539-1663. DOI: 10.2136/vzj2018.02.0034 (cit. on p. 44).
- Behnisch, P., A. Sosnowska, E. Mombelli, and J. Kuckelkorn (2024). *PROMISCES Deliverable D1.5 – Set of novel QSAR models/grouping/read-across and in vitro bioassay approaches predicting relevant toxicological endpoints for PFAS/iPM(T) chemicals*. Tech. rep. version 2. DOI: 10.3030/101036449. URL: https://promisc.es.eu/Results/_/D1.5.pdf (cit. on p. 6).
- BWB (2024). “Unpublished measurement data from wastewater treatment plants, Berlin” (cit. on p. 79).
- Chorus, I. and M. Zessner (2021). “Assessing and controlling the risk of cyanobacterial blooms: Nutrient loads from the catchment”. eng. In: *Toxic Cyanobacteria in Water*. 2nd ed. United Kingdom: CRC Press, pp. 433–503. ISBN: 978-0-367-53332-8. DOI: 10.1201/9781003081449-7 (cit. on p. 68).
- Collenteur, R., G. Brunetti, and M. Vremec (2019). *Phydrus: Python implementation of the HYDRUS-1D unsaturated zone model* (cit. on p. 58).
- EC COM(2019)640 final (Dec. 2019). *Communication from the Commission to the European Parliament, the European Council, the Council, the European Economic and Social Committee and the Committee of the Regions: The European Green Deal*. en. Publisher: Publications Office of the European Union. URL: <https://op.europa.eu/en/publication-detail/-/publication/b828d165-1c22-11ea-8c1f-01aa75ed71a1/language-en> (visited on 01/15/2025) (cit. on p. 21).

- DELTARES (2025). *D-Emissions, Water quality and aquatic ecology modelling suite, Assessment tool for the emitted pollution at catchment scale, user manual*. Version 7.00. URL: https://content.oss.deltares.nl/delft3d/D-Emissions_User_Manual.pdf (cit. on p. 70).
- Derx, J., J. Komma, P. Reiner, J. Vierheilig, D. Savio, R. Sommer, A. K. T. Kirschner, C. Frick, R. Linke, A. H. Farnleitner, and A. P. Blaschke (2021). “Using hydrodynamic and hydraulic modelling to study microbiological water quality issues at a backwater area of the Danube to support decision-making”. en. In: *Österreichische Wasser- und Abfallwirtschaft* 73.11-12, pp. 482–489. ISSN: 0945-358X, 1613-7566. DOI: 10.1007/s00506-021-00797-7 (cit. on p. 92).
- EU DWD. *Directive (EU) 2020/2184 of the European Parliament and of the Council of 16 December 2020 on the quality of water intended for human consumption (recast)*. URL: <https://eur-lex.europa.eu/eli/dir/2020/2184/oj/eng>. (Cit. on pp. 15, 87, 90, 100–102).
- European Commission (EC) (2012). *Common Implementation Strategy for the Water Framework Directive (2000/60/EC) Guidance Document No. 28 Technical Guidance on the Preparation of an Inventory of Emissions, Discharges and Losses of Priority and Priority Hazardous Substances*. eng. Tech. rep. European Commission (EC). DOI: 10.2779/2764. URL: <https://data.europa.eu/doi/10.2779/2764> (visited on 01/15/2025) (cit. on pp. 67, 68).
- EC C(2022) 9383 final (2022). *ANNEXES to the Commission Delegated Regulation amending Regulation (EC) No 1272/2008 as regards hazard classes and criteria for the classification, labelling and packaging of substances and mixtures*. Reference information missing. URL: <https://environment.ec.europa.eu/system/files/2022-12/Annexes%20to%20the%20Delegated%20Regulation.pdf> (cit. on p. 28).
- EC COM(2020) 98 final (July 2020). *Communication from the Commission to the European Parliament, the Council, the European Economic and Social Committee and the Committee of the Regions – A new Circular Economy Action Plan for a cleaner and more competitive Europe*. en. Publisher: Publications Office of the European Union. URL: <https://op.europa.eu/en/publication-detail/-/publication/d33bd445-1930-11eb-b57e-01aa75ed71a1/language-en> (visited on 01/15/2025) (cit. on p. 21).
- EC COM(2022) 540 final (2022). *Proposal For A Directive Of The European Parliament And Of The Council amending Directive 2000/60/EC establishing a framework for Community action in the field of water policy, Directive 2006/118/EC on the protection of groundwater against pollution and deterioration and Directive 2008/105/EC on environmental quality standards in the field of water policy*. URL: https://environment.ec.europa.eu/publications/proposal-amending-water-directives_en (visited on 10/26/2022) (cit. on pp. 16, 17, 87, 90, 100–102).
- EC COM(2021) 400 final (Oct. 2021). *Opinion of the European Economic and Social Committee on the communication from the Commission to the European Parliament, the Council, the European Economic and Social Committee and the Committee of the Regions – Pathway to a Healthy Planet for All – EU Action Plan: ‘Towards Zero Pollution for Air, Water and Soil’*. en. (OJ C, C/105, 04.03.2022, p. 143). URL: <https://eur-lex.europa.eu/legal-content/EN/TXT/?uri=CELEX:52021AE2629> (visited on 01/15/2025) (cit. on p. 21).
- ECHA (2024). *REACH Registration Dossier: 6:2 fluorotelomer sulfonamide alkylbetanin*. URL: <https://chem.echa.europa.eu/100.047.300> (cit. on p. 29).
- EFSA, C., D. Schrenk, M. Bignami, L. Bodin, J. K. Chipman, J. del Mazo, B. Grasl-Kraupp, C. Hogstrand, et al. (2020). “Risk to human health related to the presence of perfluoroalkyl substances in food”. en. In: *EFSA Journal* 18.9. EFSA Panel on Contaminants in the Food Chain (EFSA CONTAM Panel). ISSN: 1831-4732. DOI: 10.2903/j.efsa.2020.6223 (cit. on p. 37).

- 2000/60/EC. *DIRECTIVE 2000/60/EC OF THE EUROPEAN PARLIAMENT AND OF THE COUNCIL of 23 October 2000 establishing a framework for Community action in the field of water policy*” or, in short, the *EU Water Framework Directive*. URL: <http://data.europa.eu/eli/dir/2000/60/oj>. (Cit. on p. 66).
- European Chemical Agency (ECHA) (2016). *Guidance on information requirements and chemical safety assessment Chapter R.16: Environmental Exposure Estimation. Version 3.0 February 2016*. en. ECHA. DOI: 10.2823/515110. URL: https://echa.europa.eu/documents/10162/17224/information_requirements_r16_en.pdf/ (cit. on p. 28).
- Fuchs, S., M. Kaiser, L. Kiemle, S. Kittlaus, S. Rothvoß, S. Toshovski, A. Wagner, R. Wander, T. Weber, and S. Ziegler (Mar. 2017). “Modeling of Regionalized Emissions (MoRE) into Water Bodies: An Open-Source River Basin Management System”. en. In: *Water* 9.4, p. 239. ISSN: 2073-4441. DOI: 10.3390/w9040239. URL: <https://www.mdpi.com/2073-4441/9/4/239> (visited on 12/13/2024) (cit. on p. 70).
- Goedecke, M., L. Haag, and J. H. Gerstenberg (2019). *Wasserhaushaltsmodell Berlin ABIMO 3.2 - Handreichung für Anwendende Technische Anleitung zur Aufbereitung von Datengrundlagen sowie Dokumentation von Methoden und Berechnungsergebnissen des auf Berliner Verhältnisse angepassten blockbezogenen Niederschlags - Abflussmodell ABIMO der Bundesanstalt für Gewässerkunde, 2006 bis 2019* (cit. on p. 79).
- Groot, H., A. Sosnowska, W. Peijnenburg, J. Meesters, A. Wintersen, V. Zhiteneva, N. Devau, J. Valstar, et al. (2025). “PROMISCES D2.3 Toolbax fate & transport modelling of PMTs in the environment”. in preparation. DOI: 10.3030/101036449. URL: <https://cordis.europa.eu/project/id/101036449/results> (cit. on pp. 21, 94–96).
- Gupta, H. V., H. Kling, K. K. Yilmaz, and G. F. Martinez (2009). “Decomposition of the mean squared error and NSE performance criteria: Implications for improving hydrological modelling”. In: *Journal of Hydrology* 377.1-2, pp. 80–91. ISSN: 00221694. DOI: 10.1016/j.jhydrol.2009.08.003 (cit. on p. 16).
- Handl, S., E. Mayr, and R. Perfler (June 2017). “Brunnenmonitoring – Beurteilung von Einflussfaktoren auf die Leistungsfähigkeit bei Uferfiltratbrunnen”. de. In: *Österreichische Wasser- und Abfallwirtschaft* 69.5, pp. 240–246. ISSN: 1613-7566. DOI: 10.1007/s00506-017-0385-0. URL: <https://doi.org/10.1007/s00506-017-0385-0> (visited on 01/15/2025) (cit. on p. 65).
- Harbaugh, A. W. (2005). “MODFLOW-2005 : the U.S. Geological Survey modular ground-water model—the ground-water flow process”. en. In: *Techniques and Methods*. Number: 6-A16. ISSN: 2328-7055. DOI: 10.3133/tm6A16. URL: <https://pubs.usgs.gov/publication/tm6A16> (visited on 01/15/2025) (cit. on p. 78).
- Held, T. and M. Reinhard (2020). *Remediation management for local and wide-spread PFAS contaminations*. en. Umweltbundesamt. URL: <https://www.umweltbundesamt.de/en/publikationen/remediation-management-for-local-wide-spread-pfas> (visited on 01/15/2025) (cit. on p. 58).
- Høisæter, Å., A. Pfaff, and G. D. Breedveld (2019). “Leaching and transport of PFAS from aqueous film-forming foam (AFFF) in the unsaturated soil at a firefighting training facility under cold climatic conditions”. In: *Journal of Contaminant Hydrology* 222, pp. 112–122. ISSN: 0169-7722. DOI: 10.1016/j.jconhyd.2019.02.010 (cit. on p. 58).
- Hughes, J. D., C. D. Langevin, S. R. Paulinski, J. D. Larsen, and D. Brakenhoff (2023). “FloPy Workflows for Creating Structured and Unstructured MODFLOW Models”. en. In: *Groundwater* 62.1, pp. 124–139. ISSN: 1745-6584. DOI: 10.1111/gwat.13327 (cit. on p. 58).

- ITRC (2015). *Integrated DNAPL Site Characterization and Tools Selection (ISC-1)*. URL: https://projects.itrcweb.org/DNAPL-ISC_tools-selection/ (cit. on p. 77).
- Li, L., A. Sangion, F. Wania, J. M. Armitage, L. Toose, L. Hughes, and J. A. Arnot (Dec. 2021). “Development and Evaluation of a Holistic and Mechanistic Modeling Framework for Chemical Emissions, Fate, Exposure, and Risk”. In: *Environmental Health Perspectives* 129.12. Publisher: Environmental Health Perspectives, p. 127006. DOI: 10.1289/EHP9372. URL: <https://ehp.niehs.nih.gov/doi/10.1289/EHP9372> (visited on 01/15/2025) (cit. on p. 24).
- Liu, M., E. Saracevic, S. Kittlaus, T. Oudega, A. Obeid, Z. Nagy-Kovács, B. László, N. Krlovic, Z. Saracevic, G. Lindner, G. Rab, J. Derx, O. Zoboli, and M. Zessner (2023). “PFAS-Belastungen im Einzugsgebiet der oberen Donau”. de. In: *Österreichische Wasser- und Abfallwirtschaft* 75.9, pp. 503–514. ISSN: 1613-7566. DOI: 10.1007/s00506-023-00973-x (cit. on p. 79).
- Lyu, X., F. Xiao, C. Shen, J. Chen, C. M. Park, Y. Sun, M. Flury, and D. Wang (2022). “Per- and Polyfluoroalkyl Substances (PFAS) in Subsurface Environments: Occurrence, Fate, Transport, and Research Prospect”. en. In: *Reviews of Geophysics* 60.3, e2021RG000765. ISSN: 1944-9208. DOI: 10.1029/2021RG000765 (cit. on p. 47).
- Meesters, J.A.J. (2024). *PROMISCES D2.6 : An improved SimpleBox model for improved environmental risk assessment and life cycle impact assessment*. DOI: 10.3030/101036449 (cit. on pp. 28, 29, 31, 32).
- Nagy-Kovács, Z., J. Davidesz, K. Czihat-Mártonné, G. Till, E. Fleit, and T. Grischek (Feb. 2019). “Water Quality Changes during Riverbank Filtration in Budapest, Hungary”. en. In: *Water* 11.2, p. 302. ISSN: 2073-4441. DOI: 10.3390/w11020302 (cit. on p. 92).
- Neumann, M. and I. Schliebner (Nov. 2019). *Protecting the sources of our drinking water: The criteria for identifying persistent, mobile and toxic (PMT) substances and very persistent and very mobile (vPvM) substances under EU Regulation REACH (EC) No 1907/2006*. en. Umweltbundesamt. URL: <https://www.umweltbundesamt.de/en/publikationen/protecting-the-sources-of-our-drinking-water-the> (cit. on pp. 76, 77).
- Nguyen, T. M. H., J. Bräunig, K. Thompson, J. Thompson, S. Kabiri, D. A. Navarro, R. S. Kookana, C. Grimison, C. M. Barnes, C. P. Higgins, M. J. McLaughlin, and J. F. Mueller (Dec. 2020). “Influences of Chemical Properties, Soil Properties, and Solution pH on Soil–Water Partitioning Coefficients of Per- and Polyfluoroalkyl Substances (PFASs)”. en. In: *Environmental Science & Technology* 54.24, pp. 15883–15892. ISSN: 0013-936X, 1520-5851. DOI: 10.1021/acs.est.0c05705 (cit. on pp. 91, 92).
- Obeid, A. A., T. J. Oudega, O. Zoboli, C. Gundacker, A. P. Blaschke, M. Zessner, E. Saracevic, N. Devau, et al. (2023). “The occurrence and persistence of PFAS at riverbank filtration sites in the Upper Danube basin”. de. In: *Österreichische Wasser- und Abfallwirtschaft* 75.9-10, pp. 515–527. ISSN: 0945-358X, 1613-7566. DOI: 10.1007/s00506-023-00974-w (cit. on pp. 91, 92, 95).
- Obeid, A. A., T. J. Oudega, O. Zoboli, C. Gundacker, A. P. Blaschke, M. Zessner, E. Saracevic, N. Devau, et al. (2025). “The effect of different molecular physicochemical properties on PFAS transport and sorption behaviour in saturated porous media”. In preparation (cit. on p. 92).
- Oudega, T. J., A. A. Obeid, N. Devau, O. Zoboli, C. Gundacker, A. P. Blaschke, M. Zessner, E. Saracevic, et al. (2024). “PFAS transport and retention during riverbank filtration and in saturated columns”. In: *River Basins Conference, Budapest*. DOI: 10.3311/rb2024 (cit. on p. 73).

- EUSES 2024 (2024). *Presentation on theme: "USES guia del USES 4.0. EUSES (European Union System for the Evaluation of Substances) Multimedia*. URL: <https://slideplayer.com/slide/4857718/> (visited on 01/15/2025) (cit. on p. 26).
- SimpleBox Website (2024). <http://www.rivm.nl/SimpleBox> (cit. on p. 27).
- Schepens, M., J. te Biesebeek, J. Hartmann, N. van der Aa, R. Zijlstra, and P. Boon (2023). *Risk assessment of exposure to PFAS through food and drinking water in the Netherlands*. Tech. rep. Rijksinstituut voor Volksgezondheid en Milieu RIVM. DOI: 10.21945/RIVM-2023-0011. URL: <https://rivm.openrepository.com/handle/10029/626814> (visited on 01/15/2025) (cit. on p. 37).
- Schumacher, F. (2023). *BIBER (Berechnungs- und Informationssystem Berliner Oberflächengewässer) Stationäre Berechnung der Wasserstands- und Durchflussverhältnisse im Berliner Gewässersystem bei niedrigen (MNQ) und mittleren (MQ) Durchflüssen*. Tech. rep. Ingenieurbüro für Wasser und Umwelt (cit. on p. 80).
- Simunek Jirka, J., M. Šejna, and M. Van Genuchten (Jan. 2013). *The HYDRUS-1D Software Package for Simulating the One-Dimensional Movement of Water, Heat, and Multiple Solutes in Variably-Saturated Media*. (Cit. on pp. 78, 94).
- Smits, J. G. C. and J. K. L. van Beek (July 2013). "ECO: A Generic Eutrophication Model Including Comprehensive Sediment-Water Interaction". en. In: *PLOS ONE* 8.7. Publisher: Public Library of Science, e68104. ISSN: 1932-6203. DOI: 10.1371/journal.pone.0068104. URL: <https://journals.plos.org/plosone/article?id=10.1371/journal.pone.0068104> (visited on 01/15/2025) (cit. on p. 70).
- Sosnowska, A., T. Puzyn, W. Peijnenburg, and P. Wassenaar (2024). *PROMISCES Deliverable D2.1 - Toolbox improved in silico models for identification of PMT properties*. Tech. rep. QSARLab and RIVM. DOI: 10.5281/zenodo.14800915. URL: https://promisces.eu/Results/_/D2.1.pdf (cit. on pp. 25, 29, 30).
- Swartjes, F. A., ed. (2011). *Dealing with Contaminated Sites: From Theory towards Practical Application*. en. Dordrecht: Springer Netherlands. ISBN: 978-90-481-9757-6. DOI: 10.1007/978-90-481-9757-6. URL: <https://link.springer.com/10.1007/978-90-481-9757-6> (visited on 01/15/2025) (cit. on p. 34).
- Szabó, B., M. Weynants, and T. K. D. Weber (Jan. 2021). "Updated European hydraulic pedotransfer functions with communicated uncertainties in the predicted variables (euptfv2)". English. In: *Geoscientific Model Development* 14.1. Publisher: Copernicus GmbH, pp. 151–175. ISSN: 1991-959X. DOI: 10.5194/gmd-14-151-2021. URL: <https://gmd.copernicus.org/articles/14/151/2021/> (visited on 01/15/2025) (cit. on p. 36).
- Togola, A., E. Saracevic, T. Hensel, B. Idjaton, and F. Zietzschmann (2024). *PROMISCES Deliverable D1.3 – Methods for global organic fluorinated content (TOP, TOF/AOF/EOF) for relevant matrices*. Tech. rep. DOI: 10.3030/101036449. URL: <https://cordis.europa.eu/project/id/101036449/results> (cit. on p. 6).
- US EPA, O. (2024). *CompTox Chemicals Dashboard*. en. Data and Tools. URL: <https://www.epa.gov/comptox-tools/comptox-chemicals-dashboard> (visited on 01/15/2025) (cit. on pp. 29, 30).
- Verbruggen, E., P. Wassenaar, and C. Smit (2017). *Water quality standards for PFOA : A proposal in accordance with the methodology of the Water Framework Directive 2017-0044*. RIVM. DOI: 10.21945/RIVM-2017-0044. URL: <http://hdl.handle.net/10029/620918> (cit. on pp. 37, 39).

- Vermeulen, P. T. M., G. M. C. M. Janssen, and T. Kroon (2024). “Efficient Model Calibration Using Submodels”. en. In: *Water Resources Research* 60.11. ISSN: 1944-7973. DOI: 10.1029/2023WR036441 (cit. on p. 78).
- Verseveld, W. J. van, A. H. Weerts, M. Visser, J. Buitink, R. O. Imhoff, H. Boisgontier, L. Bouaziz, D. Eilander, M. Hegnauer, C. ten Velden, and B. Russell (Apr. 2024). “Wflow_sbm v0.7.3, a spatially distributed hydrological model: from global data to local applications”. English. In: *Geoscientific Model Development* 17.8, pp. 3199–3234. ISSN: 1991-959X. DOI: 10.5194/gmd-17-3199-2024 (cit. on p. 70).
- Wang, Z., G. W. Walker, D. C. G. Muir, and K. Nagatani-Yoshida (Mar. 2020). “Toward a Global Understanding of Chemical Pollution: A First Comprehensive Analysis of National and Regional Chemical Inventories”. en. In: *Environmental Science & Technology* 54.5, pp. 2575–2584. ISSN: 0013-936X, 1520-5851. DOI: 10.1021/acs.est.9b06379 (cit. on p. 24).
- West, M. R., B. H. Kueper, and M. J. Unga (Mar. 2007). “On the Use and Error of Approximation in the Domenico (1987) Solution”. en. In: *Groundwater* 45.2, pp. 126–135. ISSN: 0017-467X, 1745-6584. DOI: 10.1111/j.1745-6584.2006.00280.x (cit. on p. 75).
- Wicke, D., A. Matzinger, and P. Rouault (2015). *Abschlussbericht Relevanz organischer Spurenstoffe im Regenwasserabfluss Berlins*. Tech. rep. Kompetenzzentrum Wasser Berlin (cit. on p. 79).
- Wintersen, A., L. Oste, R. van der Meiracker, P. van Breemen, G. Roskam, and J. Spijker (2020). *Verschil in uitloging van PFAS uit grond en bagger*. Tech. rep. Rijksinstituut voor Volksgezondheid en Milieu (RIVM). DOI: 10.21945/RIVM-2020-0102. URL: <https://rivm.openrepository.com/handle/10029/623865> (visited on 01/15/2025) (cit. on p. 39).
- Zheng, C. and P. Wang (Dec. 1999). *MT3DMS: A modular three-dimensional multispecies transport model for simulation of advection, dispersion, and chemical reactions of contaminants in groundwater systems; documentation and user's guide*. Tech. rep. Contract report SERDP-99-1. Vicksburg, Mississippi, USA: United States Army Engineer Research and Development Center, p. 220 (cit. on p. 78).

A. Substance properties to be used in the SB-AP Dashboard

Authored by: Johannes AJ Meesters

Dutch National Institute for Public Health and Environment (RIVM)

Table A.1.: Derived biodegradability rate constants in water based on REACH Registration Dossier Information

Substance short name and CAS number	Degradability Test	Description(s) of test outcome(s)	Interpreted minimum degrada- tion rate constant ($\log(\text{s}^{-1})$)	Interpreted maximum degrada- tion rate constant ($\log(\text{s}^{-1})$)	Registration dossier
cC604 CAS: 1190931- 27-1	OECD 301 A	No significant degradation after 28-day DOC Die-Away Test	Log (1/100 years) = - 9.5 $\log(\text{s}^{-1})$	Log (-ln(1- 0.001)/28 days) = - 9.38 $\log(\text{s}^{-1})$	ECHA 2022b
6:2 FTSA CAS: 27619-97-2	OECD 301 B	After 28 days of incubation, the substance degradation reached a maximum mean of 42%	Log (-ln(1- 0.42)/28 days) = - 6.65 $\log(\text{s}^{-1})$	Log (-ln(1- 0.42)/28 days) = - 6.7 $\log(\text{s}^{-1})$	ECHA 2019
PFBS CAS: 375-73-5	Read across from structural analogue Potassium- 1,1,2,2,3,3, 4,4,4- nonafluoro- butane-1- sulphonate, CAS 29420-49-3	Given 14% degradation after 28 days, the structural analogue is not readily biodegradable according to OECD criteria	Log (-ln(1- 0.14)/28 days) = - 7.2 $\log(\text{s}^{-1})$	Log (-ln(1- 0.14)/28 days) = - 7.2 $\log(\text{s}^{-1})$	ECHA 2018b

Substance short name and CAS number	Degradability Test	Description(s) of test outcome(s)	Interpreted minimum degradation rate constant ($\log(s^{-1})$)	Interpreted maximum degradation rate constant ($\log(s^{-1})$)	Registration dossier
NFBS CAS: 68298-12-4	Activated 18-day sludge test on parent compound and potential metabolites	Only 4% of parent compound was available after 18 days of sterile sludge application. 2 % of parent compound was available after viable sludge application, but also 19 % of potential metabolites	$\log(-\ln(1-0.04)/18 \text{ days}) = -7.58 \log(s^{-1})$	$\log(-\ln(1-0.21)/18 \text{ days}) = -6.81 \log(s^{-1})$	ECHA 2021b
6:2 FTOH CAS: 647-42-7	OECD 301 B and OECD 301 D	In one replicate of the OECD 301 B test the biodegradation came to a maximum of 21% after 28 days. In another replicate the biodegradation remained at a level of 0%. In the OECD 301 D test, the degradability was on average 5 % after 28 days.	$\log(-\ln(1-0.05)/28 \text{ days}) = -7.67 \log(s^{-1})$	$\log(-\ln(1-0.21)/28 \text{ days}) = -7.0 \log(s^{-1})$	ECHA 2021a
ADONA CAS: 919005-14-4	OECD 301 B	The 28-day biodegradation of substance was found to be 6%	$\log(-\ln(1-0.001)/28 \text{ days}) = -9.38 \log(s^{-1})$	$\log(-\ln(1-0.06)/28 \text{ days}) = -7.59 \log(s^{-1})$	ECHA 2022a
FTSAAm CAS: 80475-32-7	OECD 301 B; OECD 306	The test item attained 13 % biodegradation after 28 days in OECD 301 B and 8% in OECD 306	$\log(-\ln(1-0.08)/28 \text{ days}) = -7.46 \log(s^{-1})$	$\log(-\ln(1-0.13)/28 \text{ days}) = -7.24 \log(s^{-1})$	ECHA 2018a
6:2 FTAB CAS: 34455-29-3	OECD 301 F	0% biodegradation after 28 days	$\log(1/100 \text{ years}) = -9.5 \log(s^{-1})$	$\log(-\ln(1-0.001)/28 \text{ days}) = -9.38 \log(s^{-1})$	ECHA 2024

Table A.2.: Collection minimum and maximum dissociation constants for selected substances

Substance	CAS Number	Min pKa	Max pkA	Reference
cC604	1190931-27-1	-1.96	46.5	US EPA 2024c
6:2 FTSA	27619-97-2	1.23	1.23	US EPA 2024b
PFBS	375-73-5	-1.61	-1.61	US EPA 2024f
NFBS	68298-12-4	-8.47	8.21	US EPA 2024e
6:2 FTOH	647-42-7	9.74	9.74	US EPA 2024d
ADONA	919005-14-4	-0.22	-0.22	US EPA 2024a
FTSAAm	80475-32-7	7.05	7.05	US EPA 2024g
6:2 FTAB	34455-29-3	4.78	4.78	ECHA 2024

References

- ECHA (2018a). *REACH Registration Dossier 6:2 fluorotelomer sulfonamide aminoxide*. Consulted October 2024. European Chemical Agency. URL: <https://chem.echa.europa.eu/100.072.233> (cit. on p. 122).
- ECHA (2018b). *REACH Registration Dossier Perfluorobutane sulfonic acid*. Consulted October 2024. European Chemical Agency. URL: <https://chem.echa.europa.eu/100.006.176> (cit. on p. 121).
- ECHA (2019). *REACH Registration Dossier 6:2 Acid sulfonic fluorotelomer*. Consulted October 2024. European Chemical Agency. URL: <https://chem.echa.europa.eu/100.044.149> (cit. on p. 121).
- ECHA (2021a). *REACH Registration Dossier 3,3,4,4,5,5,6,6,7,7,8,8,8-tridecafluorooctan-1-ol*. Consulted October 2024. European Chemical Agency. URL: <https://chem.echa.europa.eu/100.010.435> (cit. on p. 122).
- ECHA (2021b). *REACH Registration Dossier N-Methyl perfluorobutane sulfonamide*. Consulted October 2024. European Chemical Agency. URL: <https://echa.europa.eu/de/registration-dossier/-/registered-dossier/32215/1/1> (cit. on p. 122).
- ECHA (2022a). *REACH Registration Dossier 2,2,3-trifluoro-3-[1,1,2,2,3,3-hexafluoro-3-(trifluoromethoxy)propoxy]propanoic acid*. Consulted October 2024. European Chemical Agency. URL: <https://chem.echa.europa.eu/100.221.098> (cit. on p. 122).
- ECHA (2022b). *REACH Registration Dossier Acetic acid, 2,2-difluoro-2-[[2,2,4,5-tetrafluoro-5-(trifluoromethoxy)-1,3-dioxolan-4-yl]oxy]-, ammonium salt (1:1)*. Consulted October 2024. European Chemical Agency. URL: <https://chem.echa.europa.eu/100.207.411> (cit. on p. 121).
- ECHA (2024). *REACH Registration Dossier 6:2 fluorotelomer sulfonamide alkylbetanin*. Consulted October 2024. European Chemical Agency. URL: <https://chem.echa.europa.eu/100.047.300> (cit. on pp. 122, 123).

- US EPA (2024a). *CompTox Chemicals Dashboard 4,8-Dioxa-3H-perfluorononanoic acid*. Consulted October 2024. United States Environmental Protection Agency. URL: <https://comptox.epa.gov/dashboard/chemical/details/DTXSID40881350> (cit. on p. 123).
- US EPA (2024b). *CompTox Chemicals Dashboard 6:2 Fluorotelomer sulfonic acid*. Consulted October 2024. United States Environmental Protection Agency. URL: <https://comptox.epa.gov/dashboard/chemical/details/DTXSID6067331> (cit. on p. 123).
- US EPA (2024c). *CompTox Chemicals Dashboard Ammonium perfluoro[(5-methoxy-1,3-dioxolan-4-yl)oxy]acetate*. Consulted October 2024. United States Environmental Protection Agency. URL: <https://comptox.epa.gov/dashboard/chemical/details/DTXSID00882626> (cit. on p. 123).
- US EPA (2024d). *CompTox Chemicals Dashboard Fluorotelomer alcohol 6:2*. Consulted October 2024. United States Environmental Protection Agency. URL: <https://comptox.epa.gov/dashboard/chemical/details/DTXSID5044572> (cit. on p. 123).
- US EPA (2024e). *CompTox Chemicals Dashboard N-(Methyl)nonafluorobutanesulfonamide*. Consulted October 2024. United States Environmental Protection Agency. URL: <https://comptox.epa.gov/dashboard/chemical/details/DTXSID1071373> (cit. on p. 123).
- US EPA (2024f). *CompTox Chemicals Dashboard Perfluorobutanesulfonic acid*. Consulted October 2024. United States Environmental Protection Agency. URL: <https://comptox.epa.gov/dashboard/chemical/details/DTXSID5030030> (cit. on p. 123).
- US EPA, O. (2024g). *N,N-Dimethyl-3-((perfluorohexyl)ethylsulfonyl)aminopropanamine N-oxide - Chemical Details*. URL: <https://comptox.epa.gov/dashboard/chemical/details/DTXSID80880983> (visited on 01/30/2025) (cit. on p. 123).

B. PluriMetric Pilot experiments

Authored by: Nicolas Devau¹ and Johan Valstar²

¹BRGM, French Geological Survey, 2 avenue Claude Guillemin, Orléans France

²Deltares, Boussinesqweg 1, Delft, the Netherlands

B.1. Key concepts to simulate PFAS fate and transport in SGW continuum

As stated in the main text, a solid knowledge on the processes controlling PFAS migration in SGW continuum is required. Four main types of processes have been identified in literature. These processes are highly non-linear and inter-related, leading to complex dynamic system. A broad range of mathematical formalisms and equations have already been used to simulate these processes. A short overview of these processes and the main type of equations are described below.

B.1.1. Transport processes

Due to their high solubility most of the PFAS are migrating as soluble species. Therefore, both advective and dispersive transport processes are controlling PFAS mobility in porous media. Advective process is strongly related to the water flow velocity in a porous media. Advective process is mainly vertical in the unsaturated zone. The flow rate is first dependent on boundary conditions, i.e. effective recharge and water table depth for the top and bottom of the SGW continuum, respectively. Then, water flow rate in such variably saturated system is also controlled by the structure of the pore network as well as the water content. In saturated conditions, water flow is both horizontal and vertical and is controlled by changes in hydraulic head, storage capacity and the effective permeability of the solid materials. Dispersion processes are related to the structure of the pore connection and throat pore size. In unsaturated conditions, vertical dispersivity is predominant while longitudinal and transversal dispersivity can affect PFAS migration in saturated conditions. Note that diffusion processes could also affect PFAS mobility, notably at the vicinity of solid phase explaining kinetic of sorption processes onto the SWI and AWI. In unsaturated conditions, the Richards equation is usually used as it has been broadly demonstrated to be efficient to simulate water flow in variably saturated conditions. This equation is highly nonlinear and needs to be solved using soil water functions such as unsaturated hydraulic conductivity function and water retention curve. Several functional forms have been developed. In saturated conditions, the standard Darcy laws coupled

to the continuity equation is used. For solute transport, the standard advection-dispersion equation (ADE) is suitable to describe solute transport in a porous medium.

Due to their molecular structure consisting of both an ionic hydrophilic moiety and hydrophobic moiety, many PFAS acts as surfactants or surface-active agents. In highly contaminated sites, surface tension reduction due to PFAS adsorption onto the SWI and AWI can reduce solution surface tension and contribute to the unsaturated flow of water and transport of contaminants in the SGW continuum. Furthermore, flow of solution with high PFAS concentration in porous media can lead to production of foam in the pore network. This foam can modify the pore connectivity, modifying the effective porosity as well as saturated and unsaturated permeability. Surface tension-driven flow is simulated by using modified version of the soil water functions as well as an equation to simulate dependence of the surface tension on the PFAS concentration.

B.1.2. Sorption reactions onto SWI

Adsorption of PFAS can occur on many different geosorbents. Adsorption at solid-water interface (SWI) is dictated by multiple forces acting between the PFAS and the surface of the geosorbent, which includes covalent bonding, hydrophobic bonding, hydrogen bonding, electrostatics interactions, non-polar attractions and solvation and desolvation processes. Nature and magnitude of these forces are determined by the complicated interplay between physicochemical properties of PFAS and the properties of the solid and aqueous phases of the soil. Additional properties need to be also taken into account to determine adsorption properties of soils or sediments such as the pore volume, the ratio between micropore/mesopore, particle diameter and surface area. Last, kinetic of the PFAS sorption reaction could be neglected in most of the model developed to simulate fate and transport of PFAS, except for models dedicated to simulating PFAS migration on very short time scales (less than a few hours). The main type of equations used to describe PFAS sorption onto the SWI is the linear sorption isotherm relying on a partition coefficient. Nevertheless, several experiments in controlled conditions demonstrated that PFAS sorption onto the SWI is non-ideal and non-linear, suggesting that non-linear sorption isotherm should be used instead such as Freundlich or Langmuir isotherm. First-order equation has been also developed to simulate a kinetically controlled sorption reaction. According to the multiplicity of the sorption reactions with the various geosorbent that can be found in soil and solid materials of unsaturated and saturated zone, a density-distribution approach based on fractional-derivative equations considering both instantaneous and kinetic reactions have been also developed.

B.1.3. Sorption reactions onto AWI

Many PFAS are surface-active agents with their molecular structure consisting of both and ionic hydrophilic moiety and hydrophobic moiety. As surfactants, these substances will seek out and accumulate at environmental interfaces in order according to thermodynamic laws. Indeed, PFAS sorption onto hydrophobic interface is driven by hydrophobic forces, reaching to minimize Gibbs energy. Among the various hydrophobic interface that can be encountered in porous media, fluid-fluid interface such as air-water interface (AWI) plays a key role considering is ubiquity in most of the variably-saturated porous media as well as the extent of the AWI area. In some specific contaminated site such as firefighting training sites, entrapped residual fuels

and solvents were also present in the vadose zone. They can provide an additional hydrophobic interface favouring PFAS accumulation onto them. Current research has focused mainly on the sorption of anionic PFAS under environmental conditions (e.g. PFCAs and PFSAAs) at the AWI. The partition at the AWI for both PFCAs and PFSAAs decreases with increasing PFAS concentrations, suggesting a non-linear behaviour (Guo et al. 2020). This result is in line with the greater retardation of PFOA under a lower input concentration in unsaturated sand packed columns (Lyu et al. 2018). Furthermore, for a given PFAS type, the values of the partition coefficient are greater for the long chain PFAS compared to the shorter chain substances (Silva et al. 2019). Solution chemistry, cation type in aqueous solution and pH affects sorption of PFAS at the AWI. A broad range of equations has been also developed to simulate sorption reaction onto the AWI from empirical form to more physical-based. The simpler equations are empirically predicting changes in surface of the AWI according to saturation of porosity, then using this surface as input parameter in a non-linear isotherm. Soil-water retention curves relying on air-water surface tension and capillary pressure are used in the physically based equations to simulate changes in surface of air-water interface according to saturation of porosity. As for sorption reaction onto the SWI, density-distribution approach based on fractional-derivative equations is used to simulate PFAS sorption onto the AWI, assuming that there is too much inter-related processes involved that could not be clearly distinguished.

B.1.4. Degradation and transformation reactions

Many PFAS are recalcitrant and stable under natural environmental conditions, which imply that they have ever-lasting impacts on the environment (Naidu et al. 2020). However, under certain natural conditions, some PFAS may be partially degraded or transformed to other PFAS forms. In a natural porous media, some long chain length PFAS may be transformed or degraded into different shorter chain PFAS or into PFAS with different functional groups (e.g. carboxylic acid and phosphate esters). According to literature data, full degradation reactions of PFAS into inorganic components (e.g. CO_2 , SO_4^{2-} and F^-) do not occur in environmental conditions. PFAS transformations/degradations reactions are mediated either by abiotic chemical reactions (e.g. hydrolysis) or microbial activities (aerobic/anaerobic redox reactions mediated by microbial activities). For example, under natural conditions, FTOH may degrade into polyfluoralkyls acids (PFAAs) (Bolan et al. 2021), with efficiency of this process decreasing from aerobic to anoxic to anaerobic conditions. Most of the degradation/transformation reactions are rate-limited and depends on several factors such as the nature and concentration of PFAS in pore solutions and sorbed onto solid phases microbial community, physical and chemical properties of the pore solution, water content and temperature (Naidu et al. 2020). Single and double-first order equations are commonly used to describe PFAS degradation processes.

B.2. Extended description of the PMP experiment

The PMP is a plurimetric tank with a length of 5.2 m, a width of 3.6 m and a thickness of 3 m. This tank has been filled with a man-made geomedia. This geomedia has been produced by mixing sand material (92% w/w), organic matter issued from urban green waste compost (3% w/w) and clay material containing clay minerals and oxides (2% w/w). The design of the experiment has been selected to be as close as possible to a real aquifer. The water table depth

was kept stable at 1m depth below the surface of the PMP. Therefore, the thicknesses of the unsaturated and saturated zones were of 1 m and 2 m, respectively. Furthermore, controlled water flow and mass transport boundary conditions are maintained during the duration of the experiment. Concerning water flow, three boundary conditions have been fixed. Two boundary conditions in the saturated zone: a hydraulic barrier on one side of the PMP maintaining a constant hydraulic head and a pumping well located on the opposite side. The pumping rate is maintained at a constant flow rate of $4 \times 10^{-2} \text{ m}^3/\text{h}$ during all the duration of the experiment to maintain steady-state conditions in the saturated zone. The two other sides of the PMP have no flow boundary conditions. Pressure transducers are connected to the pumps providing water in the hydraulic barrier to maintain constant hydraulic head at 1 m depth below the surface. Water recharge and PFAS injection was performed at the top of the PMP using a sprinkler system deployed on a square of 2.25 m^2 allowing imbibition of the unsaturated zone. The surface of the infiltration square corresponds to nearly 10% of the total surface at the top of the PMP. The infiltration square is located closer to the side of the PMP where hydraulic head (1.5 m between the center of the square and this side of the PMP) is kept constant than the pumping well (the center of the square is 3 m downstream of the pumping well).

The AFFF used during the PMP experiment mainly contains PFAS with 8 carbon chain length. The main PFAS found in the AFFF are 6:2 FTSA, 6:2 FTAB and 6:2 FTSAam (1525.0 mg/L, 3409.0 mg/L, 780 mg/L, respectively) and, in a lesser extent, PFHxA, 8:2 FTSA, 4:2 FTSA and 10:2 FTSA (8.9 mg/L, 3.8 mg/L, 3.4 mg/L, 1.7 mg/L). Other chemical compounds as also part of the AFFF formulation such as polyethylene glycol or ionic salts (SO_4^{2-} and NH_4^+). This AFFF formulation is similar to the one reported in literature for products developed since 2000. Homogeneity and stability of the product has been assessed by performing multiple sampling and analysis on the stored mother solution.

The monitoring set up in PMP is based on probes and sampling device allowing us to the monitor water table depth, soil moisture and soil water potential in the vadose zones as well as sample water in vadose and saturated zones. The water table level has been monitored by using automatic pressure transducer installed in 9 piezometers. Capillary pressure and water content in the vadose zone has been monitored using 15 tensiometers and 15 TDR. To collect water samples, 80 suctions cups were positioned along the main flow lines in different locations in the PMP and at different depths from -0.5m to -2.5m. Water samples were also collected in the 9 piezometers. Sensors and probes are distributed according to a regular grid at the surface and in the depth of the PMP. This grid has been selected to ensure robust calculations of PFAS distribution in the PMP at the end of the experiment. The following physical/chemical properties have been measured on all the water samples: pH, redox, temperature, electrical conductivity. On a more limited number of samples, additional analyses have been conducted, bromide concentrations and total organic fluoride concentrations. On a subset of these latter samples, targeted PFAS analyses have been done to quantify the concentration of each PFAS present in the AFFF. More details concerning the protocol used to perform these chemical analyses can be found in WP1 deliverables.

The experiment was designed to reproduce a real AFFF contamination of a SGW continuum. More precisely, PFAS migration from the infiltration square at the top of the PPM to the pumping well located 3m downstream via vertical solute transport through the unsaturated zone and horizontal solute transport in the saturated zone was targeted. This migration pattern has been indeed encountered in several real AFFF contaminated site. The experiment has been

conducted during 11 months, with specifically 8 months dedicated to monitor PFAS migration. During this time length, the experiment has been divided in the three following stage to achieve this goal:

- **Baseline stage.** This stage was devoted to acquiring a baseline of the PMP prior to AFFF contamination. The flow rate in the saturated zone was kept at the fixed value aforementioned. Weekly recharge events were performed by infiltrating 120L of PFAS-free water on the infiltration square at the top of the PMP. The time length for this stage is 2.5 months (from mid-February 2024 to mid-April 2024). Prior to this stage, a stabilisation stage of 4 months was applied. A sampling campaign has been conducted at the beginning and the end of this stage. Water was sampled in all sampling points in the PMP.
- **PFAS infiltration stage.** This stage was conducted during three weeks (from mid-April 2024 to mid-May 2024). A diluted solution of AFFF (3% w/w) was infiltrated from the injection square. The total volume of input solution is equal to 1.6 m³. This volume has been selected to reach PFAS concentration in pore solution and sorbed PFAS concentrations in the range of the concentrations measured in highly contaminated sites mentioned in literature. To prevent saturation of the unsaturated zone, the total volume of diluted AFFF solution was infiltrated in 14 infiltration periods. During each infiltration period, 120 L of diluted AFFF solution was infiltrated during 3h. A non-reactive tracer (Br) was also added to the input solution to characterize the transport properties of the PMP during PFAS migration. The flow rate in the saturated zone is maintained at the value fixed in the first stage. A monitoring campaign was conducted after each PFAS injection step at the sampling points located below the infiltration square and in its vicinity.
- **PFAS leaching stage.** This stage was performed to induce PFAS migration from the infiltration square to the unsaturated and saturated zones as it can be induced by natural recharge on a real AFFF-contaminated. During this stage, PFAS-free water was infiltrated on a weekly basis during 5 months (from mid-May to October 2024) in the injection square. The infiltrated volume is equal to 120L. Each week, water samples were collected in all sampling points in the PMP.

The prior step before building a model of the PMP experiment was to conduct a comprehensive interpretation of the results, notably in-depth data analyses. This prior step before building the model is a cornerstone to be able to build a correct conceptual model of the PMP experiment. The following conclusions were drawn based on the results obtained from the measured parameters during the experiment:

- The concentrations in PFAS are lower in pore water in both unsaturated and saturated zones than in the diluted AFFF solution. In the pore solution, the decrease is more marked for 6:2 FTAB and 6:2 FTSAam than for 6:2 FTSA. This latter compound has become predominant in the dissolved PFAS (in the input solution, 6:2 FTAB is predominant). The magnitude of the decrease is, in mean during all the experiment, equal to 50%, 78%, 98% for 6:2 FTSA, 6:2 FTAB and 6:2 FTSAam, respectively. These decreases of PFAS concentrations in the pore water suggest that sorption reactions onto the AWI and SWI had a strong impact on PFAS migration in the unsaturated zone. In the saturated zone, in addition to the sorption reactions, dilution of the high PFAS pore solution coming

from the unsaturated zone below the infiltration square by the PFAS-free pore solution injected in the PMP to maintain groundwater flow can also explained the decrease of PFAS concentration in the saturated zone

- The affinity of the 3 main PFAS to the AWI and/or SWI differs. Based on their affinity to these two interfaces, the PFAS compounds can be ranked as following 6:2 FTSAam > 6:2 FTAB > 6:2 FTSA, Hence, the residence time in the geomeia is lower for 6:2 FTSA than 6:2 FTAB and even more for 6:2 FTSAam. This interpretation is supported by the fact that 6:2 FTSA and 6:2 FTAB have been measured in pore solution during all the experiment. In the sampling points located downstream of the infiltration square in the saturated zone, only 6:2 FTSA had been found in pore water. Concentrations of 6:2 FTSAam were close to null in pore water in both unsaturated and saturated zones during all the experiment.
- In all the sampling points, concentrations of 6:2 FTSA change with time according to a similar pattern. This pattern can be divided into three periods: concentration of 6:2 FTSA is close to null, then an increase of the concentration is measured followed by a decrease of the concentration. The duration of each one of these periods as well as the magnitude of the increase or decrease vary according to the locations in space and depth of the sampling points. These results highlight that inter-related processes including advection-dispersion and sorption reactions onto the SWI and/or AWI as well as mixing between water with different PFAS concentration impact the change in 6:2 FTSA concentrations during the experiment.
- For the 6:2 FTSA breakthrough curves measured in the sampling points below the infiltration square (in both unsaturated and saturated zone), 6:2 FTSA concentration increased drastically during the infiltration stage. The higher concentrations were measured in the sampling points located just below the capillary fringe in the saturated zone, illustrating that 6:2 FTSA is mainly stored in this transition zone between the unsaturated and saturated zone. Then, the PFAS concentration decreases at the start of the leaching phase. The decrease was more marked in the sampling points located in the saturated zone than unsaturated zone, suggesting that a higher amount of 6:2 FTSA was sorbed in this latter zone. To explain this trend, a hypothesis that sorption reactions onto the AWI had played a key role in 6:2 FTSA fate and transport in the unsaturated zone during the experiment can be claimed. The intensity of the sorption seems higher in the upper part of the unsaturated zone than in the deeper part.
- As the distance between the infiltration square and the sampling point increases, the time delay between the start of the diluted AFFF infiltration and the rising of 6:2 FTSA concentration in the pore water increases. Furthermore, the increase is lower in the sampling points located far from the infiltration square. These results suggest that reactive processes seem to play a lower role than transport processes as the distance between the infiltration square increases.
- The trends of the breakthrough curves measured for 6:2 FTAB and 6:2 FTSAam were similar to the one aforementioned for 6:2 FTSA but the rising of the concentration was lower. Based on these results, one can hypothesis that the same physical and chemical processes have controlled the fate and transport of 6:2 FTSA, 6:2FTAB and 6:2 FTSAam

during the experiment only the magnitude of the processes, notably sorption reactions onto the SWI and/or AWI had differed.

- No significant changes in the concentrations of the PFAS resulting from the degradation reaction of the precursors contained in the diluted AFFF solution infiltrated at the top of the PMP have been measured, suggesting that no degradation reactions occurred during the experiment. These results are in line with previous experimental results obtained either on laboratory conditions or on real AFFF-contaminated sites.
- Interpretations of the breakthrough curves measured for the non-reactive tracer in the sampling points located below the infiltration square indicate that evaporation process occurs during the PFAS-infiltration and -leaching stages. This hypothesis needs to be formulated to explain the increase of Br concentration in the pore water above the value of the infiltrated solution.
- The hydraulic properties in the unsaturated and saturated zones below the infiltration square change drastically during the PFAS-infiltration and -leaching stages as indicated by the measurements of water content and capillary pressure from few centimetres below the surface to 3 m depth. This change can be explained by foam formation during diluted AFFF infiltration stage. Although infiltration flow rate was maintained low to prevent foam formation, foam had still been produced in pore network during this stage. By expanding, the PFAS-induced foam had modified the connection between the pores, leading to create preferential flow lines in the soil column below the infiltration square. This change in pore network is in line with the quick increase of PFAS concentration in sampling point located both in the unsaturated and saturated zones below the infiltration square. PFAS-induced foam seems stable with time the capillary pressure and water content in response to the infiltration with the same water rate are identic during and after AFFF-infiltration stage.
- AFFF infiltration in the geomeia seems also to change hydraulic properties in the unsaturated and saturated zones, notably permeability. In the unsaturated zone, changes in capillary pressure and water content in response to water infiltration were faster during and after AFFF infiltration stages compared to measurements perform during the baseline stage. In the saturated zone, interpretations of AFFF infiltration on hydraulic properties are more difficult to characterize but are also suspected.

B.3. Hydraulic, solute transport and reactive properties for simulations of the CS#6

Table B.1.: Hydraulic properties for each layer of the 1D-vertical model and groundwater flow models

Layers	Qr	Qs	Alpha (m^{-1})	n	Ks (m/day)	l
1D-Hydrus Layer 1	0.045	0.38	14.5	2.68	0.31	0.5

Layers (thickness)	Q _r	Q _s	Alpha (m ⁻¹)	n	K _s (m/day)	l
1D-Hydrus Layer 2	0.045	0.38	14.5	2.68	0.41	0.5
1D-Hydrus Layer 3	0.045	0.38	14.5	2.68	0.41	0.5
1D-Hydrus Layer 4	0.045	0.25	14.5	2.68	0.41	0.5
1D-Hydrus Layer 5	0.045	0.2	14.5	2.68	0.41	0.5
1D-Hydrus Layer 6	0.045	0.2	14.5	2.68	0.41	0.5
MODFLOW/MT3DMS Layer 1 below infiltration square	-	0.2	-	-	0.31	-
MODFLOW/MT3DMS Layers 2-10 below infiltration square	-	0.2	-	-	0.31	-
MODFLOW/MT3DMS Layer 1 outside infiltration square	-	0.38	-	-	0.31	-
MODFLOW/MT3DMS Layers 2-10 outside infiltration square	-	0.38	-	-	0.31	-

Table B.2.: Solute transport and reactive properties for each layer of the 1D-vertical model and groundwater flow models

Layers	Bulk density (kg/m ³)	Disp. L (m)	Disp. T. (m)
1D-Hydrus Layer 1	1700	0.2	-
1D-Hydrus Layer 2	1700	0.2	-
1D-Hydrus Layer 3	1700	0.2	-
1D-Hydrus Layer 4	1700	0.1	-
1D-Hydrus Layer 5	1700	0.05	-
1D-Hydrus Layer 6	1700	0.05	-
MODFLOW/MT3DMS Layer 1 below infiltration square	1700	0.05	0.05
MODFLOW/MT3DMS Layers 2-10 below infiltration square	1700	0.05	0.05

Layers (thickness)	Bulk density (kg/m ³)	Disp. L (m)	Disp. T. (m)
MODFLOW/MT3DMS Layer 1 outside infiltration square	1700	0.2	0.2
MODFLOW/MT3DMS Layers 2-10 outside infiltration square	1700	0.2	0.2

Table B.3.: Model parameters for 6:2 FTSA sorption reactions for each layer of the 1D-vertical model and groundwater flow models

Layers	Fract.	K _L (g/m ³)	Nu (g/m ³)	Alpha (d ⁻¹)
1D-Hydrus Layer 1	0.5	2.2x10 ⁻⁵	0.07	0.45
1D-Hydrus Layer 2	0.5	1.4x10 ⁻⁵	0.07	0.15
1D-Hydrus Layer 3	0.5	1.1x10 ⁻⁵	0.07	0.1
1D-Hydrus Layer 4	0.5	1.0x10 ⁻⁸	0.07	0.1
1D-Hydrus Layer 5	0.5	1.0x10 ⁻⁸	0.07	0.1
1D-Hydrus Layer 6	0.5	1.0x10 ⁻⁸	0.07	0.1
MODFLOW/MT3DMS Layer 1 below infiltration square	-	1.0x10 ⁻⁸	0.07	-
MODFLOW/MT3DMS Layers 2-10 below infiltration square	-	1.0x10 ⁻⁸	0.07	-
MODFLOW/MT3DMS Layer 1 outside infiltration square	-	1.0x10 ⁻⁸	0.07	-
MODFLOW/MT3DMS Layers 2-10 outside infiltration square ()	-	1.0x10 ⁻⁸	0.07	-

Table B.4.: Model parameters for 6:2 FTAB sorption reactions for each layer of the 1D-vertical model and groundwater flow models

Layers	Fract.	K_L (g/m ³)	Nu (g/m ³)	Alpha (d ⁻¹)
1D-Hydrus Layer 1	0.5	5.0x10 ⁻⁵	0.07	0.45
1D-Hydrus Layer 2	0.5	1.9x10 ⁻⁵	0.07	0.25
1D-Hydrus Layer 3	0.5	1.1x10 ⁻⁵	0.07	0.2
1D-Hydrus Layer 4	0.5	1.0x10 ⁻⁷	0.07	0.2
1D-Hydrus Layer 5	0.5	1.0x10 ⁻⁷	0.07	0.2
1D-Hydrus Layer 6	0.5	1.0x10 ⁻⁷	0.07	0.2
MODFLOW/MT3DMS Layer 1 below infiltration square	-	1.0x10 ⁻⁷	0.07	-
MODFLOW/MT3DMS Layers 2-10 below infiltration square	-	1.0x10 ⁻⁷	0.07	-
MODFLOW/MT3DMS Layer 1 outside infiltration square	-	1.0x10 ⁻⁷	0.07	-
MODFLOW/MT3DMS Layers 2-10 outside infiltration square	-	1.0x10 ⁻⁷	0.07	-

Table B.5.: Model parameters for 6:2 FTSAam sorption reactions for each layer of the 1D-vertical model and groundwater flow models

Layers	Fract.	K_L (g/m ³)	Nu (g/m ³)	Alpha (d ⁻¹)
1D-Hydrus Layer 1	0.5	1.0x10 ⁻⁴	0.07	0.85
1D-Hydrus Layer 2	0.5	9.5x10 ⁻⁵	0.07	0.45
1D-Hydrus Layer 3	0.5	5.1010 ⁻⁵	0.07	0.4
1D-Hydrus Layer 4	0.5	1.0x10 ⁻⁶	0.07	0.4
1D-Hydrus Layer 5	0.5	1.0x10 ⁻⁶	0.07	0.4
1D-Hydrus Layer 6	0.5	1.0x10 ⁻⁶	0.07	0.4

Layers (thickness)	Fract.	K_L (g/m ³)	Nu (g/m ³)	Alpha (d ⁻¹)
MODFLOW/MT3DMS Layer 1 below infiltration square	-	1.0x10 ⁻⁶	0.07	-
MODFLOW/MT3DMS Layers 2-10 below infiltration square	-	1.0x10 ⁻⁶	0.07	-
MODFLOW/MT3DMS Layer 1 outside infiltration square	-	1.0x10 ⁻⁶	0.07	-
MODFLOW/MT3DMS Layers 2-10 outside infiltration square	-	1.0x10 ⁻⁶	0.07	-

B.4. Simulations of the spatial and temporal pattern of the non-reactive tracer concentration during the PMP experiment

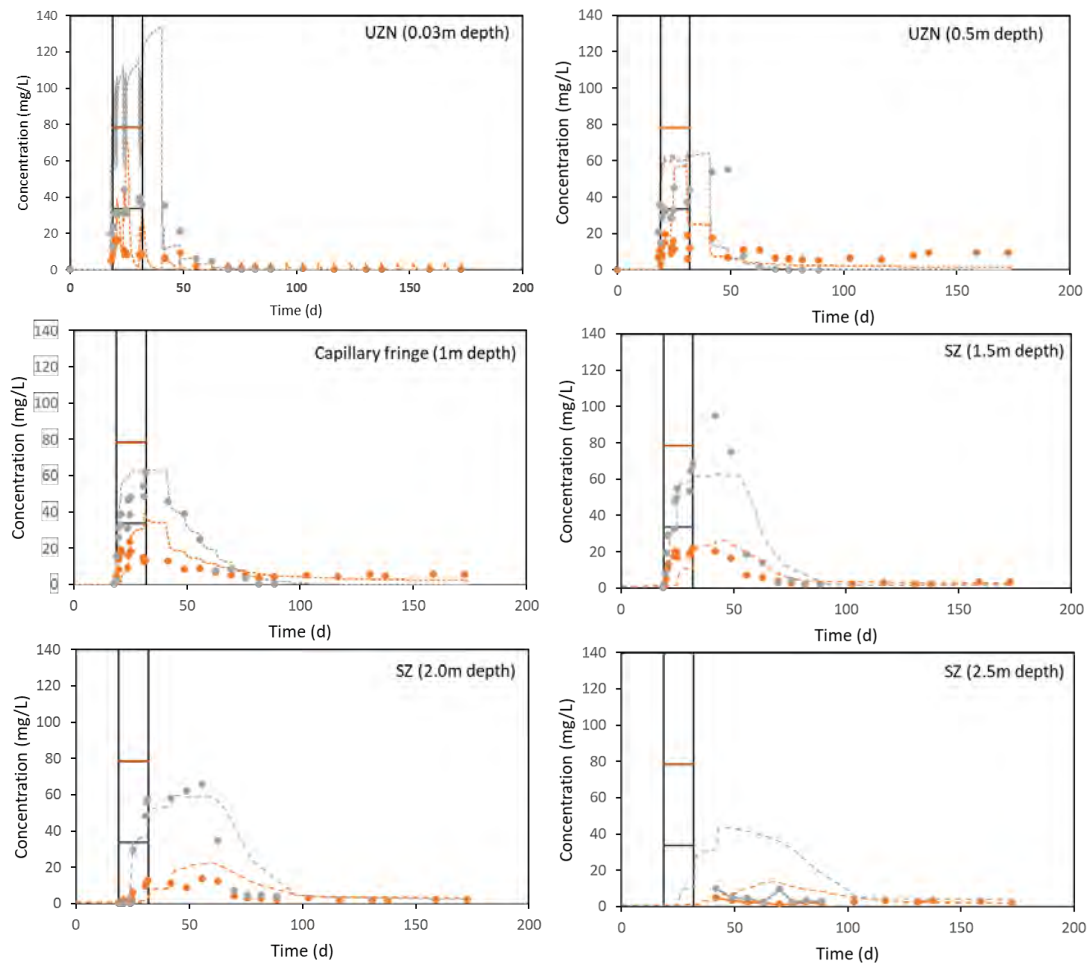


Figure B.1.: Measured and simulated concentrations in bromide (grey) and total organic fluoride (orange) over time in pore solution at five depths (0.03 m, 0.5 m, 1 m, 1.5 m, 2.0 m and 2.5 m depth) in the unsaturated and saturated zones below the infiltration square during the PMP experiment. Concentrations are expressed in mgF/L. Lines represent simulated concentrations over time while dots represent measured concentrations.

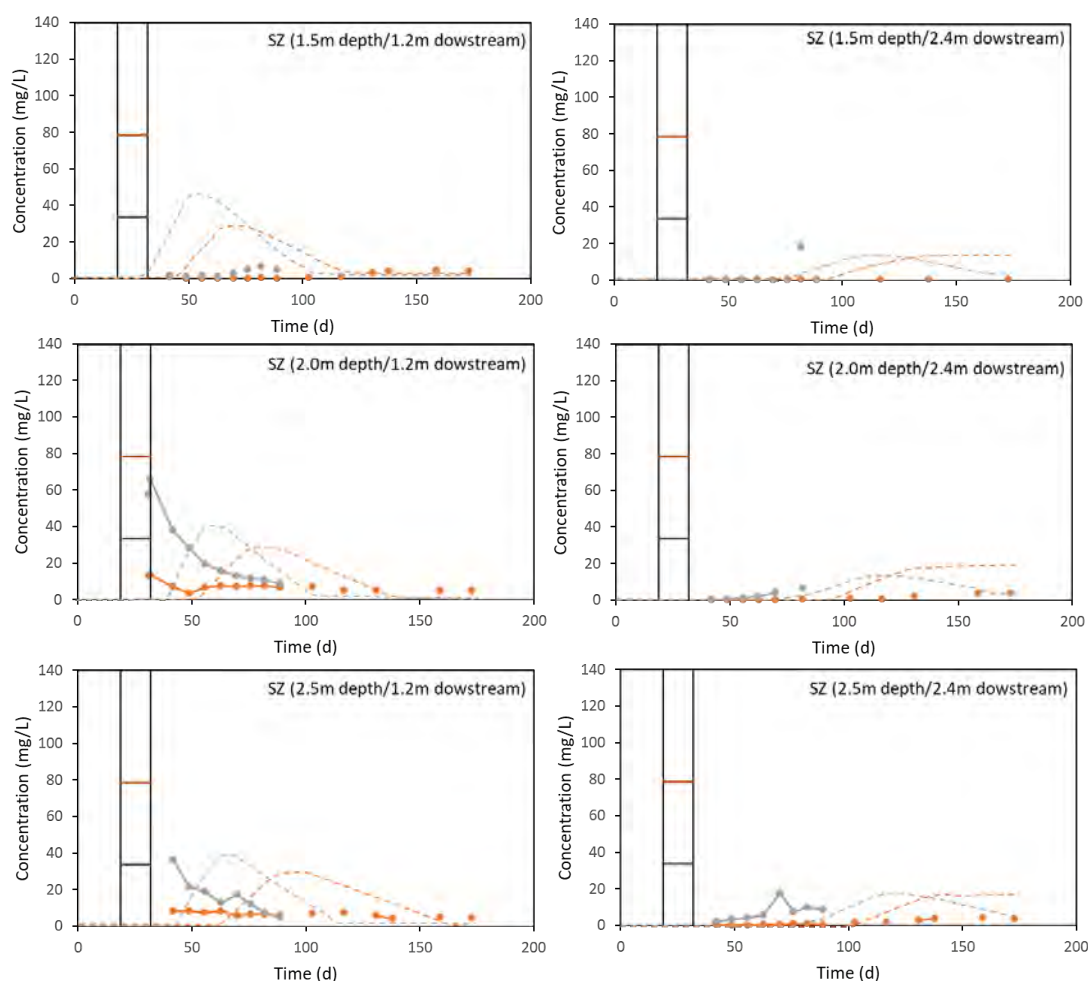


Figure B.2.: Measured and simulated concentrations in bromide (grey) and total organic fluoride (orange) over time in pore solution at three depths (1.5 m, 2.0 m and 2.5 m depth) in the saturated zone in two locations (1.2 m and 2.4 m far from the centre of the infiltration square) downstream to the infiltration square in the main flow path during the PMP experiment. Concentrations are expressed in mgF/L. Lines represent simulated concentrations over time while dots represent measured concentrations.

References

Bolan, N., B. Sarkar, M. Vithanage, G. Singh, D. C. W. Tsang, R. Mukhopadhyay, K. Ramadass, A. Vinu, et al. (2021). "Distribution, behaviour, bioavailability and remediation of poly- and per-fluoroalkyl substances (PFAS) in solid biowastes and biowaste-treated soil". In: *Environment International* 155, p. 106600. ISSN: 0160-4120. DOI: 10.1016/j.envint.2021.106600. (Visited on 01/15/2025) (cit. on p. 127).

- Guo, B., J. Zeng, and M. L. Brusseau (Feb. 2020). “A Mathematical Model for the Release, Transport, and Retention of Per- and Polyfluoroalkyl Substances (PFAS) in the Vadose Zone”. en. In: *Water Resources Research* 56.2, e2019WR026667. ISSN: 0043-1397, 1944-7973. DOI: 10.1029/2019WR026667. URL: <https://agupubs.onlinelibrary.wiley.com/doi/10.1029/2019WR026667> (visited on 01/28/2025) (cit. on p. 127).
- Lyu, Y., M. L. Brusseau, W. Chen, N. Yan, X. Fu, and X. Lin (July 2018). “Adsorption of PFOA at the Air–Water Interface during Transport in Unsaturated Porous Media”. In: *Environmental Science & Technology* 52.14. Publisher: American Chemical Society, pp. 7745–7753. ISSN: 0013-936X. DOI: 10.1021/acs.est.8b02348 (cit. on p. 127).
- Naidu, R., P. Nadebaum, C. Fang, I. Cousins, K. Pennell, J. Conder, C. J. Newell, D. Longpré, et al. (Aug. 2020). “Per- and poly-fluoroalkyl substances (PFAS): Current status and research needs”. In: *Environmental Technology & Innovation* 19, p. 100915. ISSN: 2352-1864. DOI: 10.1016/j.eti.2020.100915. URL: <https://www.sciencedirect.com/science/article/pii/S2352186420307495> (visited on 01/15/2025) (cit. on p. 127).
- Silva, J. A. K., W. A. Martin, J. L. Johnson, and J. E. McCray (June 2019). “Evaluating air-water and NAPL-water interfacial adsorption and retention of Perfluorocarboxylic acids within the Vadose zone”. In: *Journal of Contaminant Hydrology* 223, p. 103472. ISSN: 0169-7722. DOI: 10.1016/j.jconhyd.2019.03.004 (cit. on p. 127).

C. Large scale investigations in CS#7 AFFF-polluted aquifer

Authored by: Laura del Val Alonso¹, Johan Valstar², Sonia Jou¹, Carme Bosch¹, Manuel Martínez^{1,3}

¹Eurecat, Plaça de la Ciència 2 - 08243 – Manresa, Catalonia, Spain

²Deltares. Boussinesqweg 1, Delft, the Netherlands

³Universitat Rovira i Virgili, Mechanical Engineering Department, Av. Països Catalans 26, 43007, Tarragona, Spain

C.1. Conceptual model

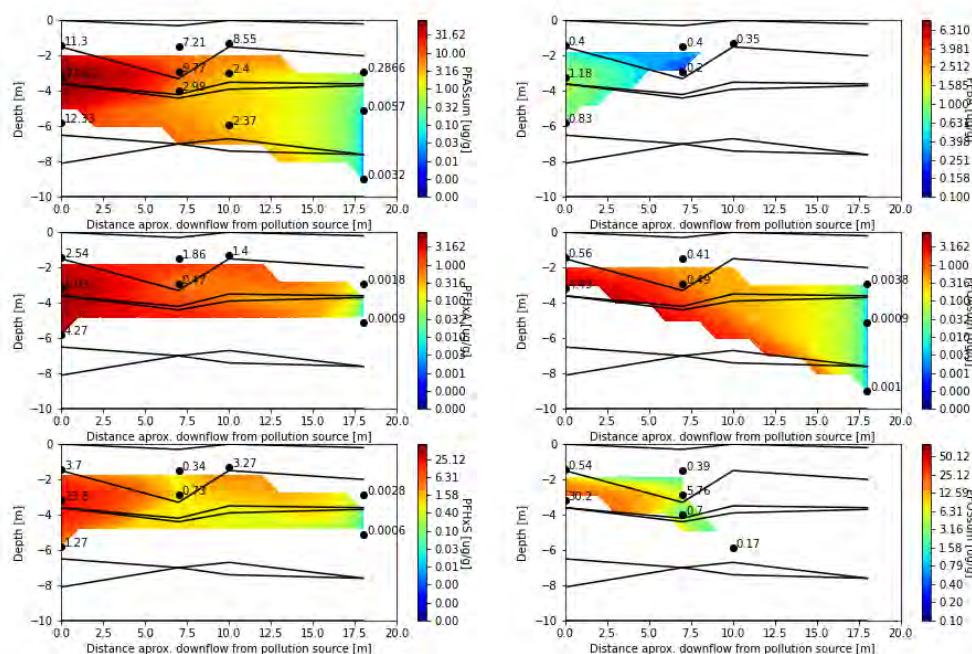


Figure C.1.: Concentrations of most abundant PFAS in the soil matrix. Black lines represent contact between different lithologies

HYDRUS1D and MODFLOW/MT3D model train was tested at field scale, in Case Study 7. This case study consists in a relatively pristine aquifer polluted exclusively by aqueous film forming foams (AFFF) periodically released in fire-fighting training activities. This is a relevant case study for future replication, as many PFAS polluted sites in Europe are related to fire extinguishing activities (i.e. airports, Goldenman et al. 2019). Moreover, the fact that it is exclusively polluted by PFAS, makes it ideal for the study of the PFAS sorption and migration patterns.

The aquifer is composed by alluvial and colluvial Quaternary sediments (10 m depth), which lay unconformably over the bedrock (fractured granodiorite and granite). The main groundwater bearing unit is formed by the detrital sediments and weathered bedrock with relatively high hydraulic conductivity due to intergranular porosity. Groundwater depth at the site ranges between 5.5 to 6.0 m. Six boreholes were installed to perform the characterization and remediation of the site. Further information about the site can be found in the PROMISCES Deliverable D2.2 – *Characterization of PFAS and chlorinated solvent contamination in two aquifers in Spain* (López de Alda et al. 2025).

PFAS pollution in soil and groundwater were characterised at the beginning of the project, in Autum 2021, before any remediation activity took place. Soil data (Figure C.2) reflects how PFAS infiltrate below the source (MW01 on the left, at $x = 0$) and are retained at the sandy silt sediments between -2 and -4 meters. PFAS concentrations in groundwater (Figure C.3) follow a similar pattern, although they peak at MW02, 7.5 m downgradient from MW01.

The most abundant PFAS at this site are PFBA, PFPeA, PFHxA, PFOA, PFHxS, PFOS and 6:2 FTS. 6:2 FTS has a complex degradation pathway under natural conditions that leads to PFBA, PFHxA and PFPeA (Held and Reinhard 2020). Therefore, we assume concentrations of these three are the results of the full degradation of 6:2 FTS close to the source. The other three PFAS (PFOA, PFOS, PFHxS), are known to be undegradable under natural conditions, so we assumed they are only affected by sorption processes. From these PFOS is the one showing higher concentrations in both solid and liquid phases Therefore, it was chosen for the modelling.

Data outside the polluted site and the project implementation period is very scarce, forcing us to simplify the model geometry and scope. To analyse the fate and transport of PFAS, we did a 2D vertical cross-sectional model. The model reflects the average flow path of groundwater flowing downhill through the polluted site towards the nearby river. The exact location of the site is not shown due to confidentiality issues.

C.2. Model set-up

Fate and transport of PFAS were modelled in two steps following the proposed model train. The unsaturated zone was model with *HYDRUS 1D* (*Phydrus*), while the saturated zone was modelled with *MODFLOW/MT3D* (*FloPy*).

A 1D vertical transport model was set up with *Phydrus* (Python library to run HYDRUS 1D, Collenteur et al. 2019) for the unsaturated zone below the source (foams were applied between MW01 and MW04). Initial hydraulic parameters were obtained from soil samples. This includes hydraulic permeabilities, porosities and the bulk density of the soil. PFOS transport parameters

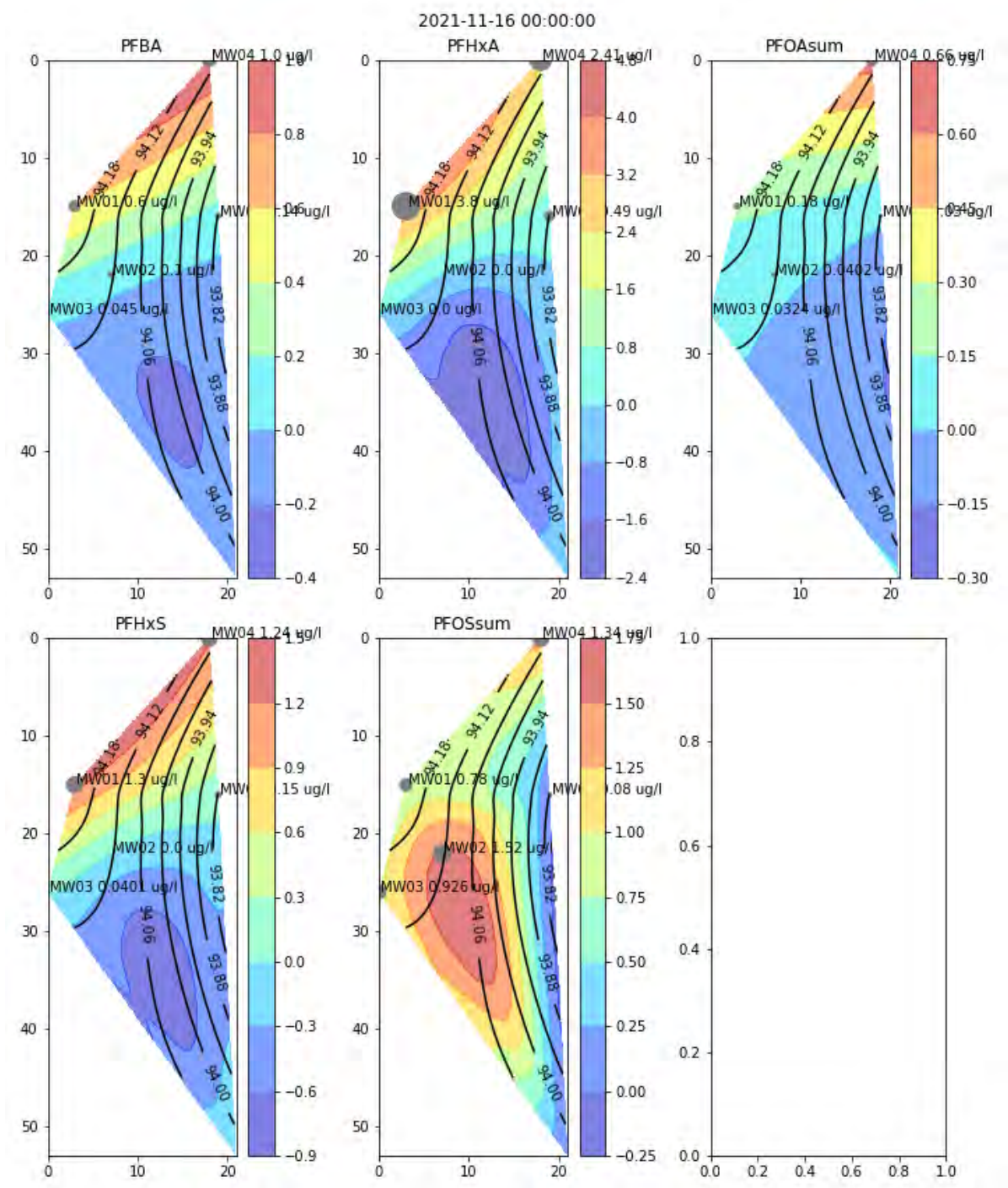


Figure C.2.: Interpolation of PFAS concentration groundwater represented in a map view of the site. Black isolines represent the piezometric heads. Borehole locations are represented by a dot, which size correlates with the total concentration of each type of PFAS, specified in the label.

were obtained during batch and column experiments (K_d and diffusivity). Rainfall data was facilitated by MeteoCat for a nearby meteo station. The vertical 600 cm domain was divided in 5 zones: anthropic fill (160 cm), fine silty sands (200 cm), gravels (120 cm), fine silty sands (30 cm) and gravels (90 cm). As in many cases, information on the quantity of product used in each firefighting event and its frequency was not available. Therefore, we assumed two events per month, in which 20,000 L of diluted foaming products were estimated to be used (based on the amount of water used for extinguishing a car on fire). An estimate of PFOS concentrations in foaming products can be obtained from Høisæter et al. (2019).

A 2D vertical transport fully saturated model was set in *FloPy* (Python library to run MODFLOW6 models, Hughes et al. 2023) to model flow and transport in the saturated zone. The model is 700 m long and around 14 m depth (Figure C.3). The top boundary is the average piezometric level. A constant head boundary was prescribed at the left side (up-gradient), and a drain boundary was set at the river location, while the bottom was assumed impermeable. At the top, a recharge flux boundary condition was set using the bottom leachate of the unsaturated zone model. Three lithologies were defined, a high permeable sandy layer, a lower permeability weathered granite and a very low permeability granite layer at the bottom. Initial values for the hydraulic conductivity of the site were obtained from the slug tests performed during the characterization phase.

Both models were run over a period of 2146 days (starting in January 2016 ending in November 2021 when the field campaign took place). HYDRUS1D model, run previously 1200 days to reach a stationary state with annual average precipitation and evapotranspiration values. Hydraulic conductivities (K), linear sorption coefficients (K_d) and the PFOS input concentration through the top boundary, were calibrated by roughly matching the measured field data.

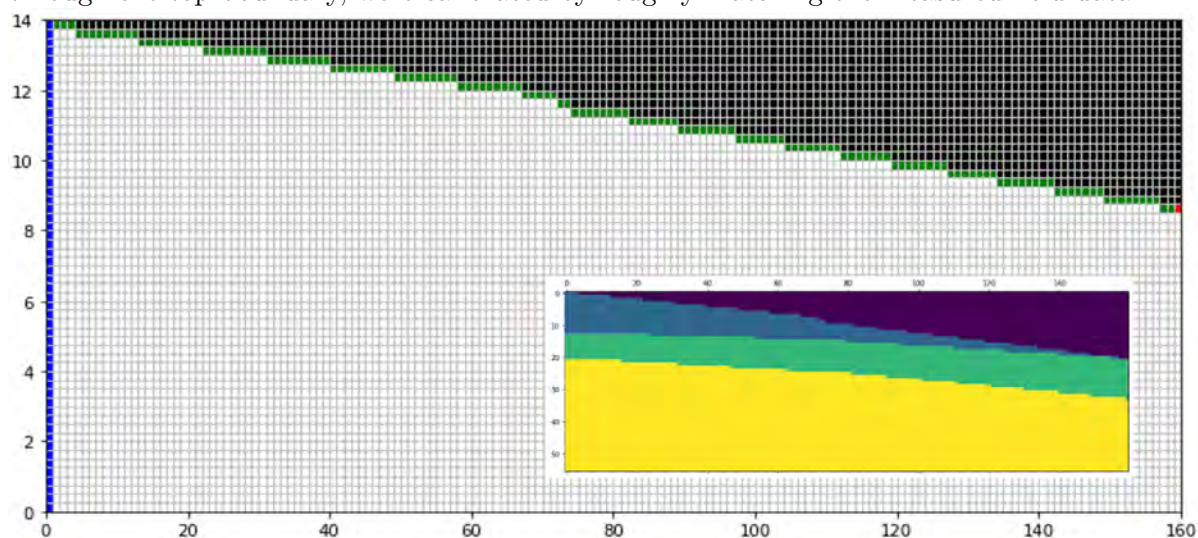


Figure C.3.: Geometry of the 2D vertical transport model of the fully saturated zone. Blue cells represent the upper gradient BC (Constant Head), green cells represent the top BC (Recharge) and the red cell represent the location of the river, set as Drain BC. Black cells are inactive cells. Small graph represents the distribution of hydraulic conductivities.

Table C.1.: Calibrated parameters for the unsaturated and saturated models.

Model layers (HYDRUS1D)	K (cm/day)	Kd (cm ³ /g)	Model layers (MOD- FLOW/MT3D)	K (m/day)	Kd (m ³ /g)
Anthropic fill	20000	0.001	Anthropic fill	1	$6 \cdot 10^{-7}$
Buffer layer (10 cm)	200	0.03	Buffer layer (10 cm)	1	$6 \cdot 10^{-7}$
Fine silty sands	20	0.6	Fine silty sands	0.1	$6 \cdot 10^{-7}$
Buffer layer (10 cm)	200	0.03			
Rounded gravels	20000	0.001			
Buffer layer (10 cm)	200	0.03			
Fine silty sands	20	0.3			
Buffer layer (10 cm)	200	0.03			
Rounded gravels	20000	0.001			

C.3. Results from the unsaturated zone model

We could roughly reproduce the distribution of sorbed PFOS concentrations in the soil profile (Figure C.4c). The model results reflect the high PFOS concentrations we found in the fine silty sandy layer between 150 and 350 cm depth. Concentrations of PFOS in liquid phase show a front advancing during the approximately first 500 days, which then stabilizes in an average concentration around $1 \cdot 10^{-7}$ mmol/cm³, that oscillates following seasonal recharge patterns.

Leachate fluxes through the bottom boundary are a result of the precipitation, the high evapotranspiration rates and the periodic pollution influxes (Figure C.5b). Periodicity of the training events is smoothed out through the profile resulting in oscillating leachate concentrations at the bottom boundary which also patterns reflect seasonal cycles (Figure C.5d). During summer the entire soil profile gets dry, increasing concentration of PFOS in the liquid phase.

Calibrated hydraulic conductivities are larger than those measured in the field (0.03–100 cm/day), while linear sorption coefficients are slightly smaller, than those measured in the lab (2.7 cm³/g) (Table C.1). Moreover, input concentrations had to be reduced from values described by Høisæter et al. (2019) (100,000 µg PFOS/L in diluted product) in 4 orders of magnitude to match the concentrations in liquid phase. These deviations from the expected value do not come as a surprise. Hydraulic conductivities were estimated from soil samples, which may not be fully representative from the complete profile. Linear sorption coefficients may be overestimating sorption, since they were obtained with isotherms that did not reach saturation, and PFOS does not behave linearly (McGarr et al. 2023). This may explain why we needed to lower the Kd values to match observed sorbed concentrations. And finally, since we do not have information about the training events, we cannot be sure literature data is representative of the case study. Besides, we know, from talks with the firemen, that the frequency we used in the model is the

worst-case scenario, and that not in all training events AFFF foams were used. Therefore, it is likely that PFOS release to the soil was smaller.

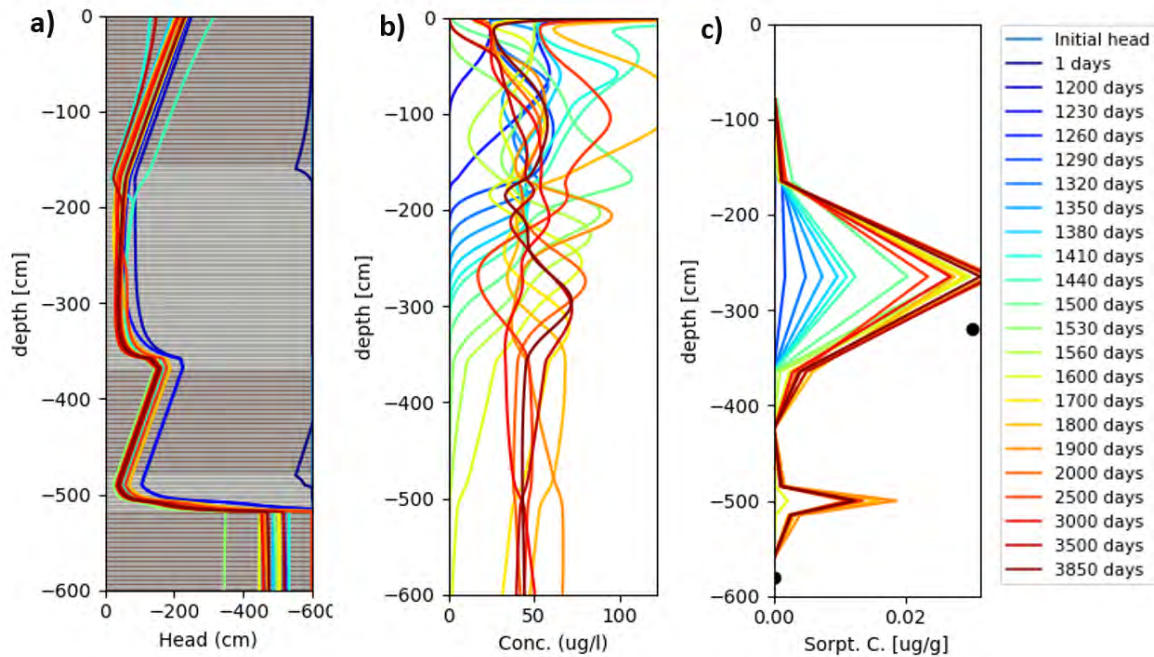


Figure C.4.: Vertical distribution of main HYDRUS 1D modelled variables in the unsaturated profile: a) Head in cm and distribution of materials. b) Evolution of PFOS concentrations in liquid phase. c) Lines represent modelled sorbed concentration over time for each layer, while black dots represent measured PFOS concentrations in soil at the field site.

C.4. Results from fully saturated model

Leachate fluxes from the unsaturated zone model were introduced in the fully saturated model at the cell representing the horizontal location of the pollution source. The unsaturated zone model was also run without pollution events, just with the rain and evapotranspiration data, to estimate effective recharge for the rest of the active top boundary cells of the saturated model.

Time-dependent head data was not available for the site before remediation took place. Moreover, there are no observation piezometers from the local water agency within a reasonable distance to the site. Therefore, hydraulic permeabilities measured in the field during the characterization phase were used to parameterize the model.

Concentrations measured during autumn 2021, which also do not provide information about temporal evolution of PFOS, were used to roughly calibrate transport parameters aiming to reproduce the downgradient spatial distribution of PFOS (Figure C.6). To compare observed and modelled data, modelled concentrations were vertically averaged, assuming that the field samples are a mix of the water entering the screened interval of the monitoring well.

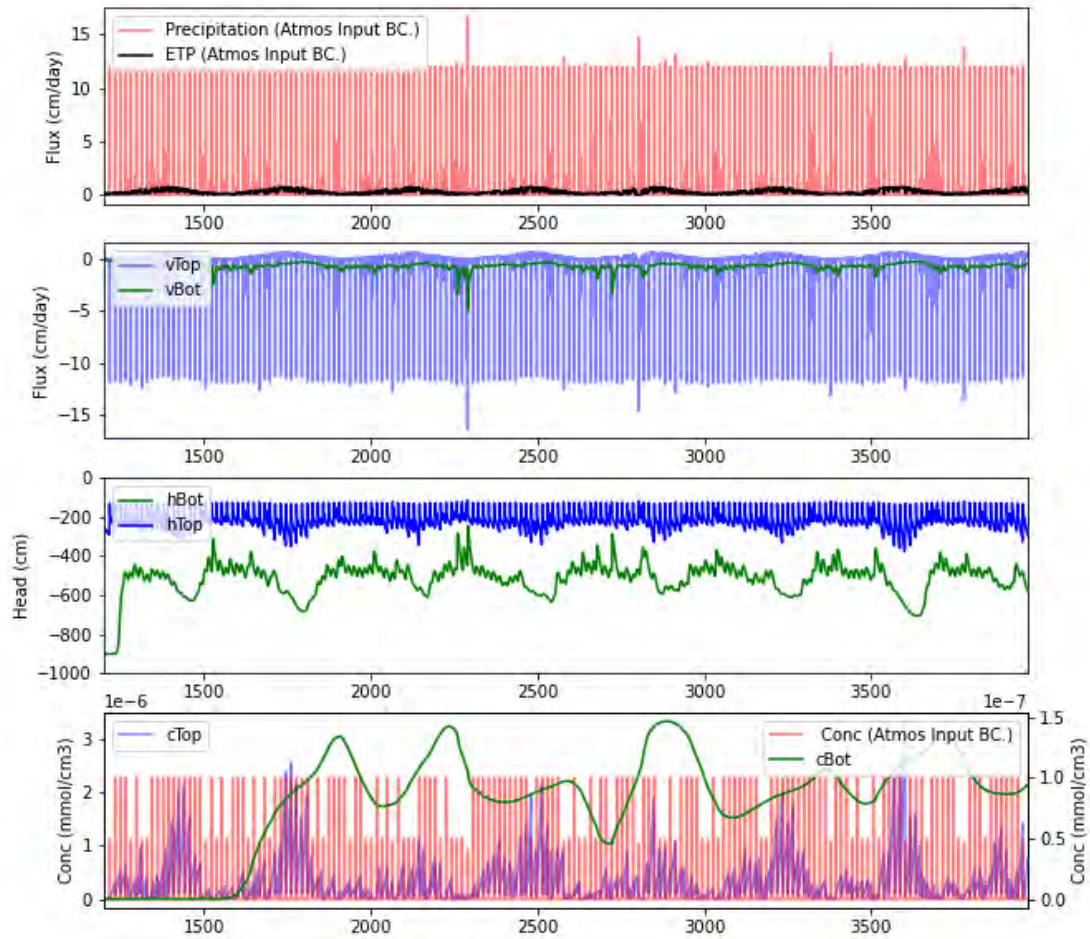


Figure C.5.: Fluxes and heads at top and bottom boundaries. a) Precipitation from Fogars de la Selva meteo station plus the estimated infiltration during each firefighting training event. The potential evapotranspiration (ETP) estimated with Hargreaves. b) Fluxes through top (vTop-blue) and bottom (vBot - green) boundaries. c) Head at top (hTop) and bottom (hBot) boundaries. d) Concentration at top boundary (cTop – left axis). Concentration imposed at the atmospheric boundary condition (Conc) and concentration existing the bottom boundary (cBot).

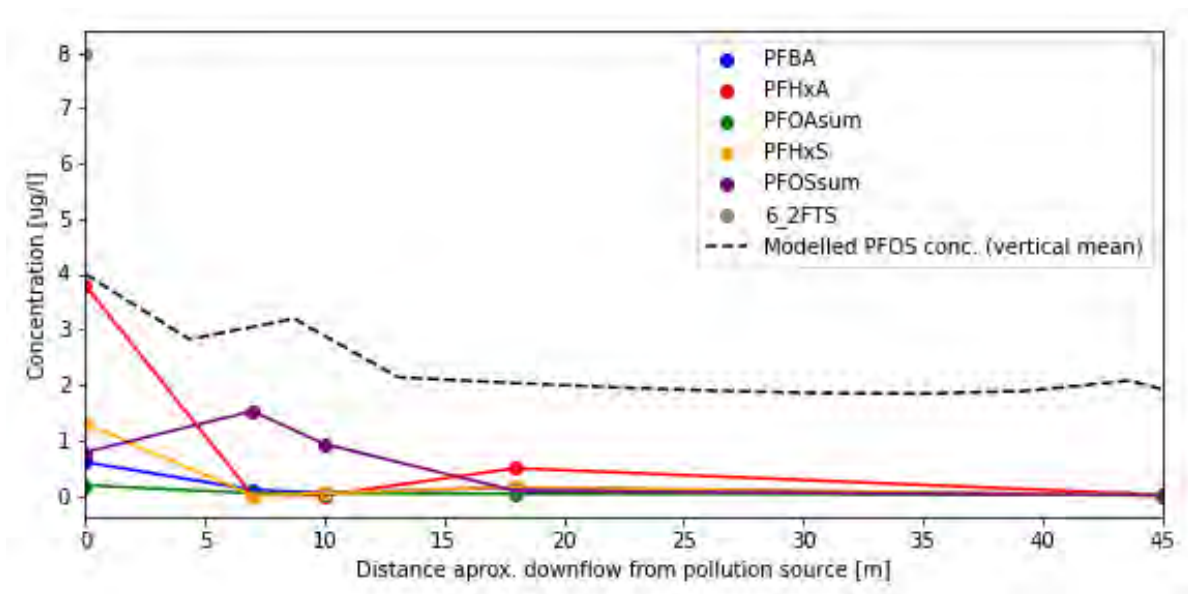


Figure C.6.: Downgradient (from the source) distribution of most abundant PFAS at the site. Data obtained during a sampling campaign in autumn 2021. Dashed line represents modelled concentrations of PFOS.

Modelled PFOS concentrations in groundwater (Figure C.6) are in the order of magnitude of observed ones, though still higher. Oscillations in the concentration of the recharge flux at the source are reflected as higher concentration pulses in the downflowing plume (Figure C.7). They can also be observed as little peaks downflow from the source in Figure C.6.

Time zero represents the moment in which PFOS are release for the first time at the surface. It takes them around a year to reach the groundwater level. From there, it takes around 2 years to reach the river (Figure C.8).

C.5. Conclusions

The modelling approach presented here combines *HYDRUS1D* and *MODFLOW/MT3D* to model PFAS fate and transport from the source at the soil surface, to the exfiltration point, in a downgradient river. The model uses a simple linear sorption to approximate observed PFOS concentration in soil and liquid phases. Based on the model a rough estimation of the time for the PFOS plume to reach the river was obtained.

The presented modelling approach simplifies the behaviour of PFAS. In reality, sorption at the soil matrix does not have a linear isotherm. Moreover, sorption at the air-water interface, which is very relevant for some PFAS, is not incorporated in the Hydrus-1D code. Therefore, this sorption process can only be incorporated by la constant sorption isotherm. As long as the ratio of the soil-water content to the area of the water air interface remains constant, this approximation is acceptable. Moreover, any more complex isotherm will need better data to estimate the isotherm parameters. The complexity of the model should go in line with the

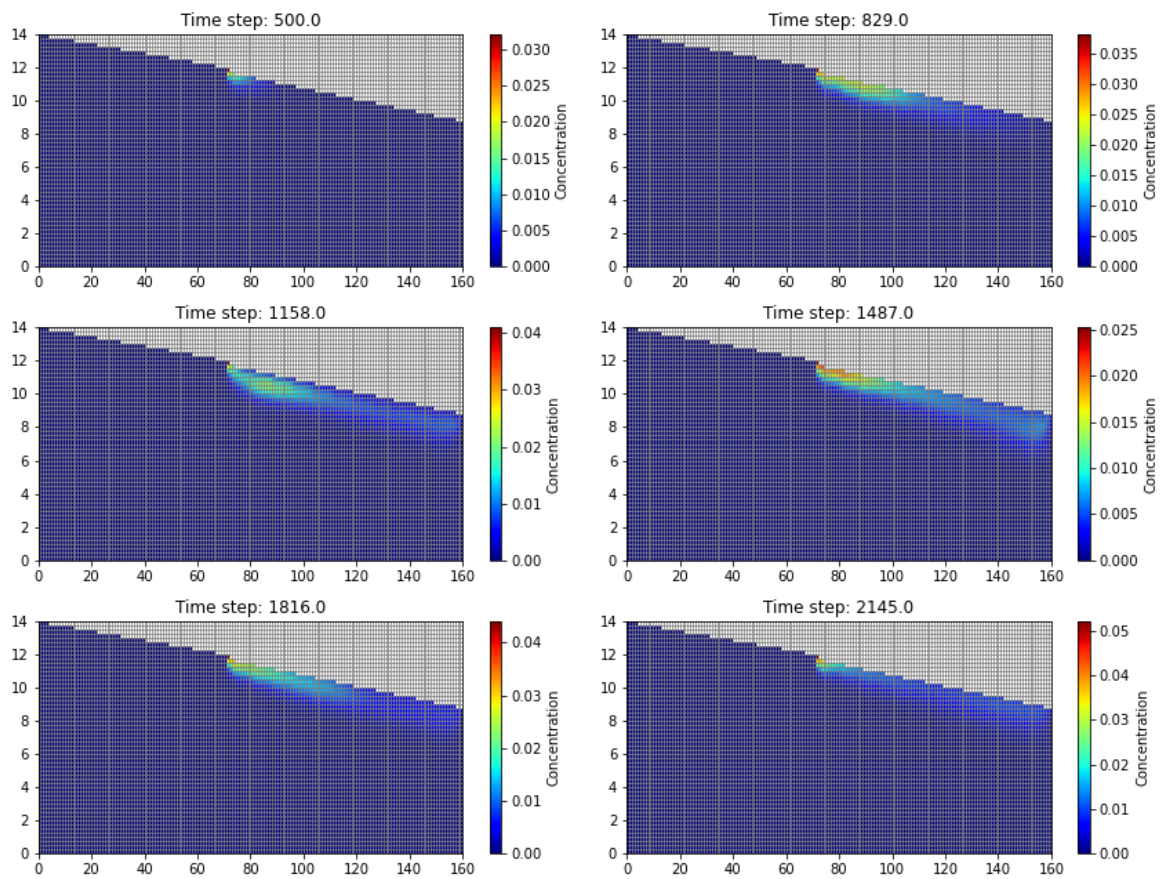


Figure C.7.: PFOS concentration distribution at 6 modelled times (days). Concentrations in g/m³.

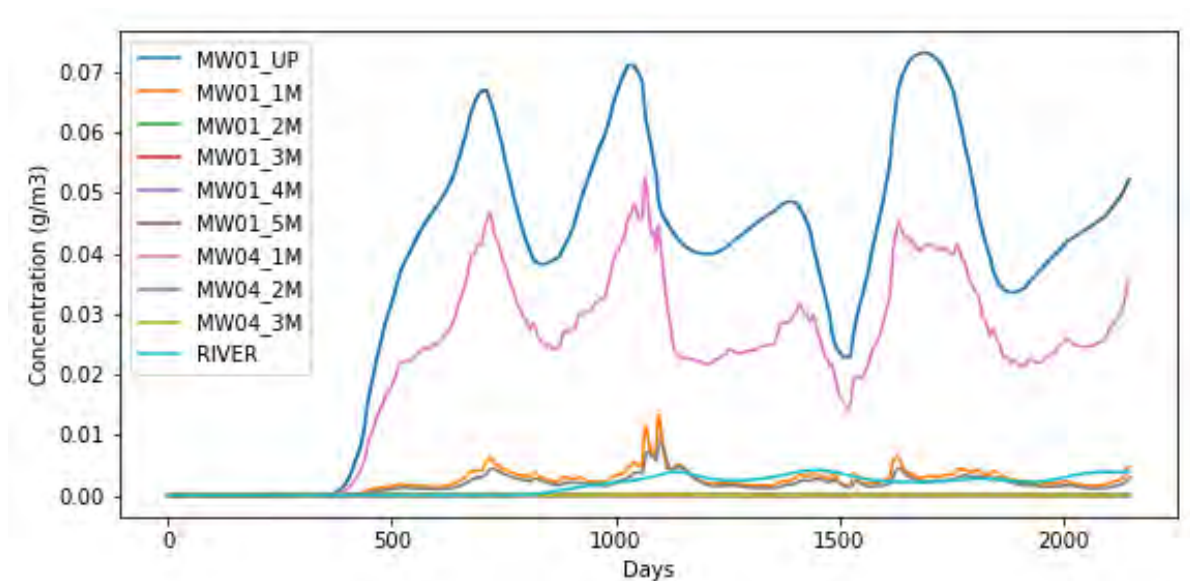


Figure C.8.: Evolution of concentrations of PFOS in groundwater at different depth for the two boreholes close to the source and for the river

amount and quality of the available data. In the absence of lots of data, the combination of *HYDRUS1D* and *MODFLOW/MT3D*, through their Python tools, could be a good starting point for modelling the fate and transport of PFAS.

In an optimal situation, in which sufficient spatial and temporal coverage of the data is available, the main limitations of this approach are, (a) the lack of a real coupling between both models, and (b) the lack of the incorporation of the process of adsorption of PFAS at the air-water interface in *Hydrus-1D*. The effect of temporal changes in the water content on the ratio of adsorbed and dissolved PFAS is therefore not described correctly. This assumes the fringe zone does not move, neglecting the contribution of draining and rewatering cycles in the transport of PFOS towards the groundwater. This is an important process for PFAS transport, as they are substances that concentrate at the interface between air and water.

References

- Collenteur, R., G. Brunetti, and M. Vremec (2019). *Phydrus: Python implementation of the HYDRUS-1D unsaturated zone model* (cit. on p. 140).
- Goldenman, G., M. Fernandes, M. Holland, T. Tugran, A. Nordin, C. Schoumacher, and A. McNeill (Mar. 2019). *The cost of inaction*. en. 2019:516. TemaNord. Copenhagen: Nordic Council of Ministers. ISBN: 978-92-893-6065-4. DOI: 10.6027/TN2019-516. URL: <http://urn.kb.se/resolve?urn=urn:nbn:se:norden:org:diva-5514> (visited on 01/28/2025) (cit. on p. 140).
- Held, T. and M. Reinhard (2020). *Remediation management for local and wide-spread PFAS contaminations*. en. Umweltbundesamt. URL: <https://www.umweltbundesamt.de/en/publikationen/remediation-management-for-local-wide-spread-pfas> (visited on 01/15/2025) (cit. on p. 140).

- Høisæter, Å., A. Pfaff, and G. D. Breedveld (2019). “Leaching and transport of PFAS from aqueous film-forming foam (AFFF) in the unsaturated soil at a firefighting training facility under cold climatic conditions”. In: *Journal of Contaminant Hydrology* 222, pp. 112–122. ISSN: 0169-7722. DOI: 10.1016/j.jconhyd.2019.02.010 (cit. on pp. 142, 143).
- Hughes, J. D., C. D. Langevin, S. R. Paulinski, J. D. Larsen, and D. Brakenhoff (2023). “FloPy Workflows for Creating Structured and Unstructured MODFLOW Models”. en. In: *Groundwater* 62.1, pp. 124–139. ISSN: 1745-6584. DOI: 10.1111/gwat.13327 (cit. on p. 142).
- López de Alda, M., M. Llorca, M. Farré, A. Cano López, V. Matamoros Mercadal, L. Fernández Rojo, and C. Bosch (2025). *PROMISCES, D2.2 – Characterization of PFAS and chlorinated solvent contamination in two aquifers in Spain*. in preparation. DOI: 10.3030/101036449. URL: <https://cordis.europa.eu/project/id/101036449/results> (cit. on p. 140).
- McGarr, J. T., E. G. Mbonimpa, D. C. McAvoy, and M. R. Soltanian (May 2023). “Fate and Transport of Per- and Polyfluoroalkyl Substances (PFAS) at Aqueous Film Forming Foam (AFFF) Discharge Sites: A Review”. en. In: *Soil Systems* 7.2, p. 53. ISSN: 2571-8789. DOI: 10.3390/soilsystems7020053 (cit. on p. 143).

D. Catchment Model MoRE for the upper Danube basin

Authored by: Meiqi Liu¹, Steffen Kittlaus¹, Matthias Zessner¹

¹TU Wien, Institute of Water Quality and Resource Management, Karlsplatz 13, Vienna, Austria

D.1. Overview

This Annex provides an overview of the regionalized emission model (MoRE) developed as part of Case Study 2 in the PROMISCES project, along with the final results generated from this model. We applied the model to a spatial scale that covers the Upper Danube basin, from its source to the city of Budapest.

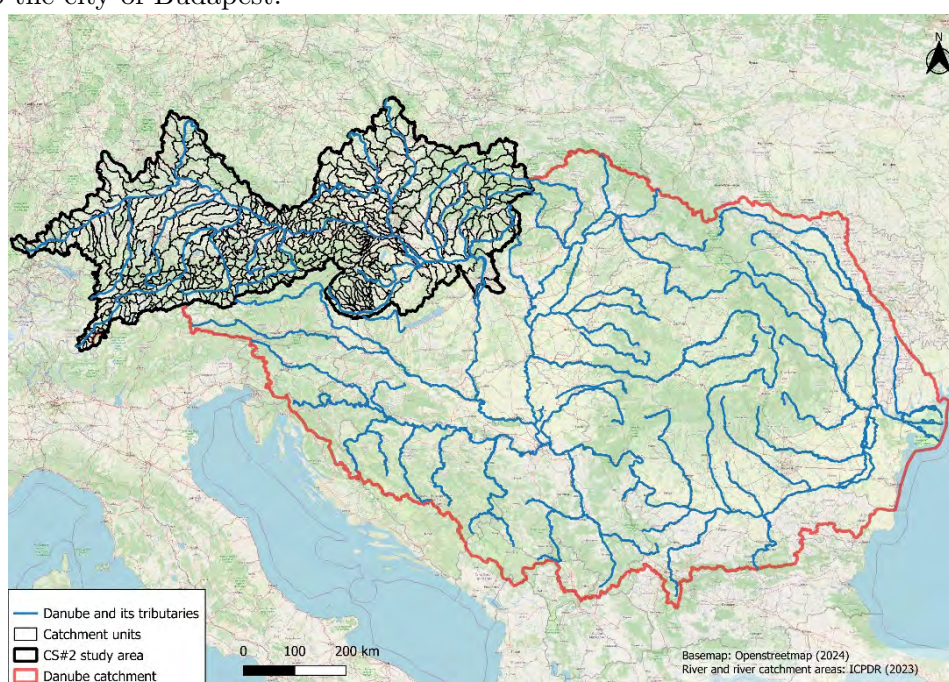


Figure D.1.: Overview map showing the Danube catchment (outlined in red) and the case study #2 area–Upper Danube catchment (outlined in black), including smaller catchment units.

D.2. Modelled PFASs

In PROMISCES Case Study 2, the focus of the MoRE model is on per- and polyfluoroalkyl substances (PFASs), a group of synthetic chemicals widely used in various household and industrial applications (Glüge et al. 2020).

Based on the results of the monitoring campaign conducted under Subtask 2.2.4 – *Large catchment scale monitoring*, we selected a total number of 18 PFAS substances as input to the model. In addition, surface water monitoring data from selected river gauges provided the opportunity to validate the model.

Table D.1.: List of modelled PFAS substances. The substance groups are classified according to the EPA Method 1633 (EPA 2024)

Short Name	Substances	CAS No.	Substance Group
PFBA	Perfluorobutanoic acid	375-22-4	short-chain Perfluoroalkyl carboxylic acids
PFPeA	Perfluoropentanoic acid	2706-90-3	short-chain Perfluoroalkyl carboxylic acids
PFHxA	Perfluorohexanoic acid	307-24-4	short-chain Perfluoroalkyl carboxylic acids
PFHpA	Perfluoroheptanoic acid	375-85-9	short-chain Perfluoroalkyl carboxylic acids
PFOA	Perfluorooctanoic acid	335-67-1	long-chain Perfluoroalkyl carboxylic acids
PFNA	Perfluorononanoic acid	375-95-1	long-chain Perfluoroalkyl carboxylic acids
PFDA	Perfluorodecanoic acid	335-76-2	long-chain Perfluoroalkyl carboxylic acids
PFBS	Perfluorobutane sulfonic acid	375-73-5	short-chain Perfluoroalkyl sulfonic acids
PFPeS	Perfluoropentane sulfonic acid	2706-91-4	short-chain Perfluoroalkyl sulfonic acids

Short Name	Substances	CAS No.	Substance Group
PFHxS	Perfluorohexane sulfonic acid	355-46-4	short-chain Perfluoroalkyl sulfonic acids
PFOS	Perfluorooctane sulfonic acid	1763-23-1	long-chain Perfluoroalkyl sulfonic acids
PFNS	Perfluorononane sulfonic acid	68259-12-1	long-chain Perfluoroalkyl sulfonic acids
PFDS	Perfluorodecane sulfonic acid	335-77-3	long-chain Perfluoroalkyl sulfonic acids
FTSA62	6:2 Fluorotelomer sulfonic acid	27619-97-2	Fluorotelomer sulfonic acids
ADONA	4,8-Dioxa-3H-perfluorononanoic acid	919005-14-4	Per- and Polyfluoroether carboxylic acids
GenX	Hexafluoropropylene oxide dimer acid	13252-13-6	Per- and Polyfluoroether carboxylic acids
PFOSA	Perfluorooctanesulfonamide	754-91-6	Perfluorooctane sulfonamides
NEtFOSAA	N-ethyl perfluorooctanesulfonamidoacetic acid	2991-50-6	Perfluorooctane sulfonamidoacetic acids

D.3. Modelled Pathways

The MoRE model system was originally designed as a pathway-oriented tool to simulate the input of substances into surface waters (Fuchs et al. 2017). In the PROMISCES project, we adapted the MoRE model to include PFASs and identified potential critical pathways for PFAS emissions, following the guidelines of the EU Guidance Document No.28 (European Commission (EC) 2012). For general details, please refer to section 4.2 of the main text of the guidance document. Overall, the model includes eight pathways, with the groundwater (P4), urban sewer system (P7) and industrial direct emitter (P10) pathways further divided into several sub-pathways. In addition to the base model and scenarios built on its setup, we also implemented a version of the model that accounts for groundwater diffuse pollution from landfills and aerodromes that might conduct fire-fighting activities. Results related to this version are not included in this document, but available in the exported SQLite model. For further information, please refer to the PROMISCES Toolbox document (Groot et al. 2025).

Table D.2.: List of pathways with abbreviations and corresponding numbers as referenced in the European Comission (EC) (2012) document, modelled in this study.

Number	Abbreviation	Description of the pathway
P1	AD	Atmospheric deposition directly to surface water
P2	ER	Erosion
P3	SR	Surface runoff from unsealed areas
P4a	GW	Groundwater background
P4b	LS	Groundwater legacy pollution from the Gendorf site
P4c	DU	Inhabitant-specific diffuse pollution via groundwater
P7a	US_ss	Strom sewers in the separate sewer system
P7b	US_cso	Combined sewer overflows
P7c	US_oss	Sewer connected but not going to WWTP
P8	WWTP	Urban wastewater treatment plants
P9	US_nss	Individual - treated and untreated - household discharge
P10a	ID	Industrial wastewater treated
P10b	ID_Gendorf	Direct wastewater discharge from the industrial park Gendorf

D.4. Basic Model Setup

The model encompasses 526 sub-catchments, with an average area of 354 ± 352 km², and operates on an annual temporal resolution. The base model covers the period from 2015 to 2021, which is defined as the "reference period." For scenario setups, the years 2013 and 2018 were selected to represent baseline years for pre- and post-climate change situations, respectively. For detailed setup on scenarios, please refer to the Annex of this guidance document on Model Scenarios.

Hydrological input parameters for the model were derived from the Wflow model developed by Deltares (Verseveld et al. 2024), with enhanced resolution achieved by combining precipitation data from the scaled SPARTACUS dataset GeoSphere Austria (2020) and the ERA5 dataset (Hersbach et al. 2023). Other basic input data were sourced from various open databases or directly requested from local authorities.

PFAS-specific input data were collected from the Subtask 2.2.4 monitoring activities, and from the DHm3c inventory (Kittlaus et al. 2023). Since many concentration data points were below the limit of quantifications (LOQ), the regression on order statistics (ROS) (Helsel 2012) method was applied to help more accurate estimation on summary statistics. When the data met the requirements for the ROS method (more than 3 detects and more than 20% detected),

the 25th, 50th and 75th percentiles were calculated to represent best-, base- and worst-case variants. For concentration data not meeting these requirements, 0 values were used as input to the best- and base-case variants, while LOQ value was applied for worst-case variant. For detailed information on the model, please refer to the Toolbox document (Groot et al. 2025).

D.5. Approach for Validating the Model

D.5.1. Substances Selection

Ten PFAS compounds were selected for model validation, as these substances typically have recorded concentrations in the rivers above the LOQ and substance-specific input data meet the requirement for calculation using ROS method. This allows for meaningful comparisons between observed and modelled data.

Table D.3.: List of PFAS substances selected for validation.

Short Name	Substances	CAS Number	Substance Group
PFBA	Perfluorobutanoic acid	375-22-4	short-chain Perfluoroalkyl carboxylic acids
PFPeA	Perfluoropentanoic acid	2706-90-3	short-chain Perfluoroalkyl carboxylic acids
PFHxA	Perfluorohexanoic acid	307-24-4	short-chain Perfluoroalkyl carboxylic acids
PFHpA	Perfluoroheptanoic acid	375-85-9	short-chain Perfluoroalkyl carboxylic acids
PFOA	Perfluorooctanoic acid	335-67-1	long-chain Perfluoroalkyl carboxylic acids
PFBS	Perfluorobutane sulfonic acid	375-73-5	short-chain Perfluoroalkyl sulfonic acids
PFHxS	Perfluorohexane sulfonic acid	355-46-4	short-chain Perfluoroalkyl sulfonic acids
PFOS	Perfluorooctane sulfonic acid	1763-23-1	long-chain Perfluoroalkyl sulfonic acids
ADONA	4,8-Dioxa-3H-perfluorononanoic acid	919005-14-4	Per- and Polyfluoroether carboxylic acids
GenX	Hexafluoropropylene oxide dimer acid	13252-13-6	Per- and Polyfluoroether carboxylic acids

Additionally, transformations of typical precursors were considered, including the conversion of N-EtFOSAA to PFOS (Wen et al. 2018), and 6:2 FTS to PFPeA and PFHxA (Méndez et al. 2022). This was achieved by counting the emission from precursor compounds to the transformed compounds proportionally, during the calculation of inhabitant-specific emission factors. For more information, please check the section Calculation of Inhabitant-Specific Emission Factor.

The model results were validated through in-stream loads and concentrations. Overall, among the 11 surface-water monitoring sites in Subtask 2.2.4 (shown in Figure D.2), 2 were selected for calibrating inhabitant-specific emission factors, while the remaining 9 sites were used for model validation.

Two performance metrics, the Nash-Sutcliffe Efficiency (NSE) and Kling-Gupta Efficiency (KGE) were applied to assess the model performance.

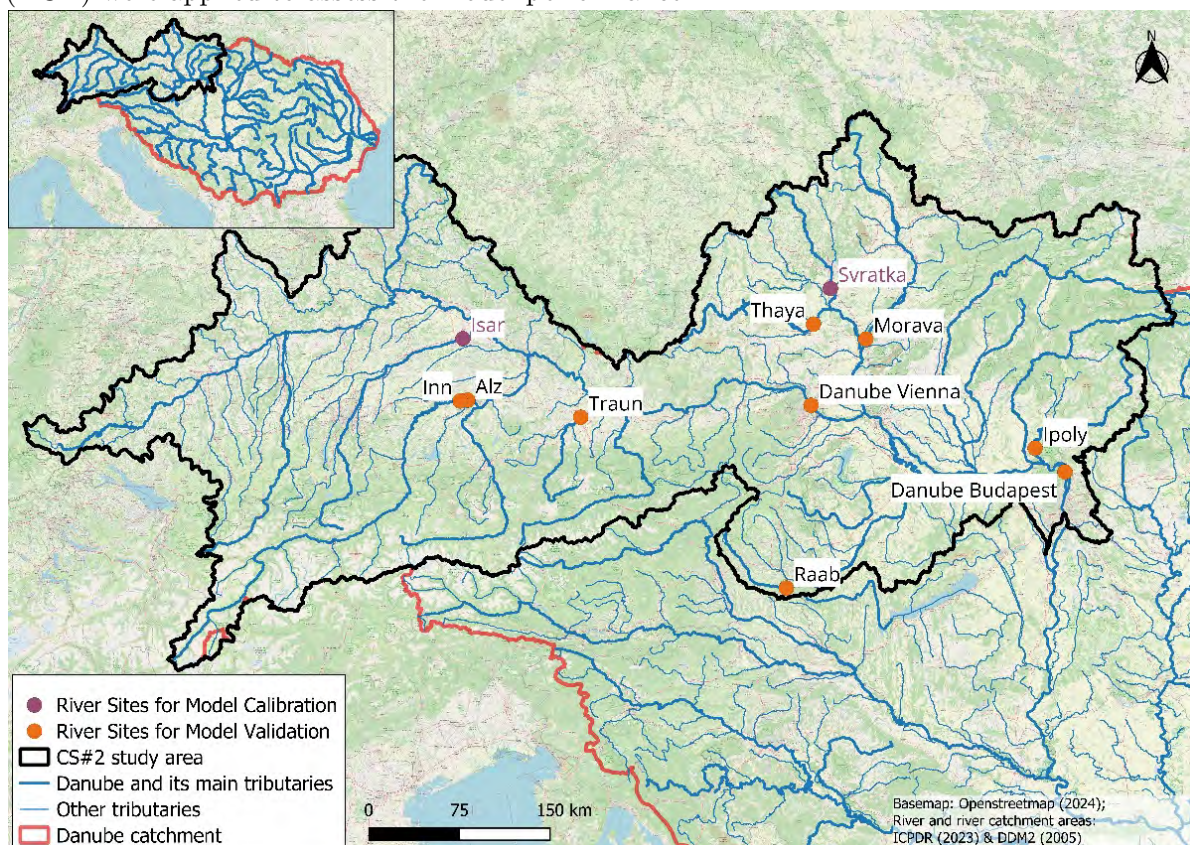


Figure D.2.: Map of surface water monitoring sites in subtask 2.2.4.

D.5.2. Nash-Sutcliffe Efficiency (NSE)

The Nash-Sutcliffe Efficiency (NSE) is a normalized statistic that determines the relative magnitude of the residual variance compared to the measured data variance (Nash and Sutcliffe 1970) . Its formula is shown as:

$$NSE = 1 - \frac{\sum_{i=1}^n (O_i - P_i)^2}{\sum_{i=1}^n (O_i - \bar{O})^2}$$

Where O_i are the observed values, P_i are the modelled values, and \bar{O} is the mean of the observed values.

The NSE value ranges from $-\infty$ to 1, with 1 being a perfect match between the model and observed data, 0 indicates that the model predictions are as good as using the mean of the observed data.

D.5.3. Kling-Gupta Efficiency (KGE)

The Kling-Gupta Efficiency (KGE) is an index that incorporates the correlation, bias and variability ratio to provide a more balanced view of model performance (Gupta et al. 2009) . Its formula is shown as:

$$KGE = 1 - \sqrt{(r - 1)^2 + (\beta - 1)^2 + (\gamma - 1)^2} \quad (D.1)$$

Where r is the Pearson correlation coefficient between simulated and observed data, β is the ratio of the means (bias), γ is the ratio of the standard deviations (variability).

The KGE value ranges from $-\infty$ to 1, with 1 being a perfect match between the model and observed data.

Performance Indication

In the sections below, we will use the following ranges for both NSE and KGE values to indicate the model performance:

- [0.75, 1]: very good performance
- [0.5, 0.75]: good performance
- [0.25, 0.5]: satisfactory performance
- $[-\infty, 0.25]$: unsatisfactory performance

D.5.4. Calculation of Inhabitant-specific Emission Factor

The model pathway “P4c - DU: Inhabitant-specific diffuse pollution via groundwater” was developed using the followed formula:

Inhabitant-specific Diffuse Emission via Groundwater =

Number of Inhabitants \times PFAS Inhabitant-specific Emission Factor

In this formula, the number of inhabitants was part of the basic input data to the model, while the inhabitant-specific emission factor for each PFAS was calculated using an R-programming script first (Team 2024), then input to the model as constant values.

Initially, the model was run in base-variant setup, with all pathways in Table D 2 excepts for the P4c - DU pathway. The results on emission values were then fetched at two calibration sites: Isar and Svatka.

Table D.4.: Inhabitant-specific emission factors for calibration sites Isar and Svatka.

PFAS	EF_{Isar}	EF_{Svatka}	unit
PFBA	2.96	0.86	mg/(inh · a)
PFPeA	5.25	1.48	mg/(inh · a)
PFHxA	5.18	2.59	mg/(inh · a)
PFHpA	0.59	0.63	mg/(inh · a)
PFOA	1.66	0	mg/(inh · a)
PFBS	0.62	0.17	mg/(inh · a)
PFHxS	1.04	0.06	mg/(inh · a)
PFOS	3.27	0.26	mg/(inh · a)
ADONA	0.02	0	mg/(inh · a)
GenX	0.11	0.02	mg/(inh · a)

Next, adjustments were made to count for precursor transformations. The emission from N-EtFOSAA was transferred 100% to PFOS, and the emission from 6:2 FTS was distributed with 50% converting to PFPeA and 50% to PFHxA.

Furthermore, the total emission (including upstream catchments) for each PFAS was divided by the total inhabitants (including upstream catchments) at two sites. Moreover, a $\pm 20\%$ variance was applied to represent best- and worst-case variants. Negative emission factor values were replaced by 0.

The emission factors derived from the Isar calibration site were used for catchment units in the upper part of the study area, where the climate is more wet and a higher level of economic development was prevailing for some decades. This includes all catchment units in Germany, Austria, and some small catchment in the Alpine region from Italy, Switzerland and Slovenia.

Emission factors from Svatka calibration site were applied to catchment units located in the downstream part of the study area, where the climate is relatively drier. This includes all catchment units in Czech Republic, Slovakia and Hungary.

D.6. Model Validation

This section shows the model validation results, based on the base-case variant.

D.6.1. Discharge, area-specific

The basic hydrological data, such as precipitation, evapotranspiration and net discharge, originated from the Wflow model. These data were used for further calculations of the catchment water balance. At the end of water balance algorithm, the total runoff and gross discharge (including upstream) for each catchment were calculated by the model. Figure D 3 shows a comparison between the gross discharge generated by the model and the monitored discharge data from official gauges at each monitoring site.

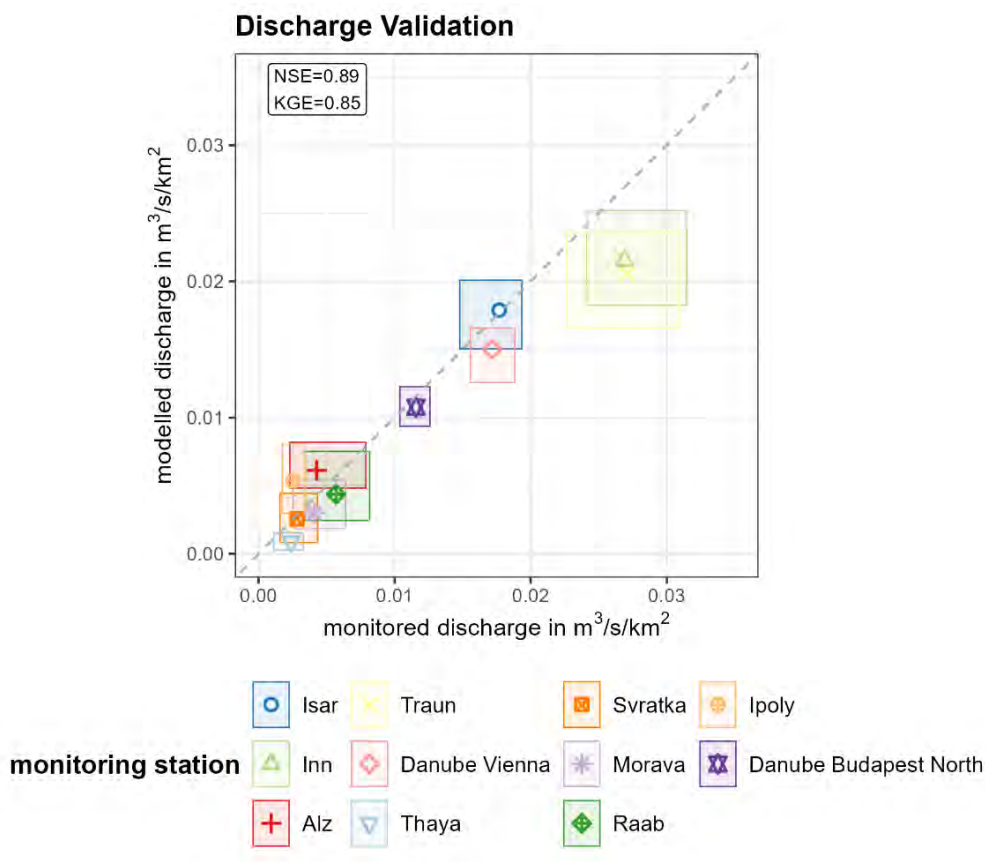


Figure D.3.: Validation graph of the modelled and observed discharge value at each monitoring sites, in area-specific form.

D.6.2. Load, area-specific

One of the final outputs from the model is total emission of each PFAS from individual catchment units. The model further calculated the cumulative load at the outlet of each catchment, which includes emissions from all upstream units.

In Subtask 2.2.4, a monitoring campaign was conducted between April 2022 and September 2023. The monitored concentrations at each surface-water monitoring site were processed using the ROS method, following the same approach as for the model input concentration data. The median values for each PFAS were then multiplied by the average discharge from official gauges over the reference period (2015–2021).

Due to high PFAS emissions in the Alz catchment, two versions of validation graphs are presented below: one including all validation sites, and one excluding the Alz site.

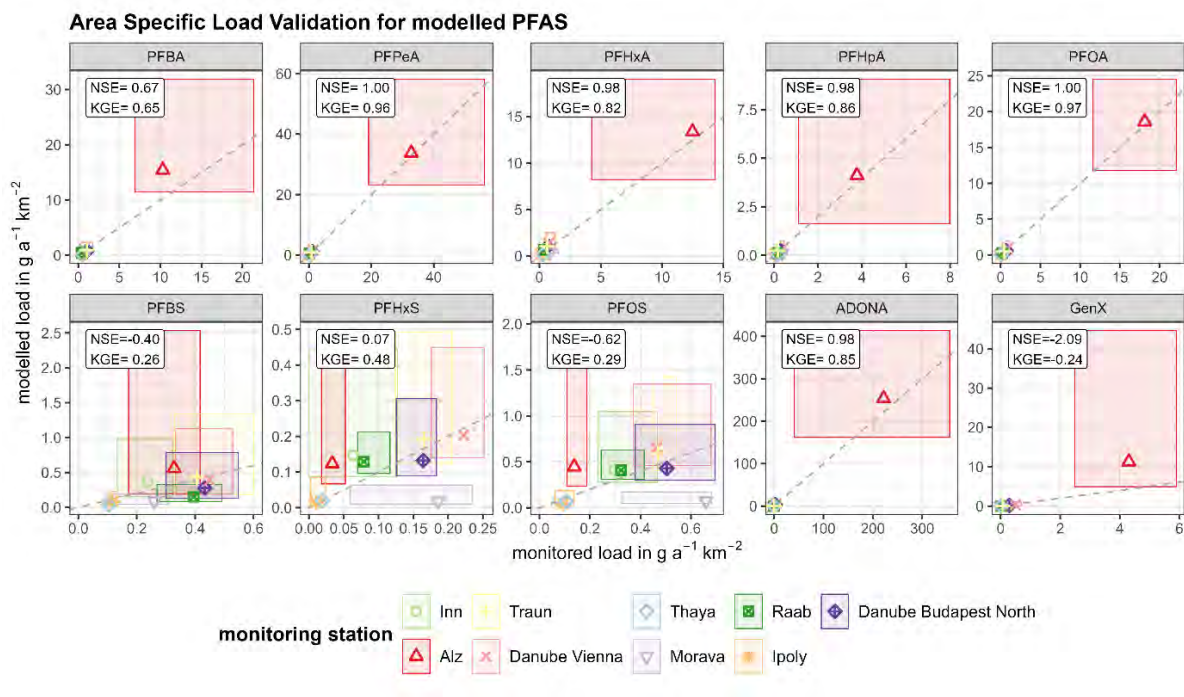


Figure D.4.: Validation graph of the modelled load and monitored load for selected PFAS at each validation sites, in area-specific form.

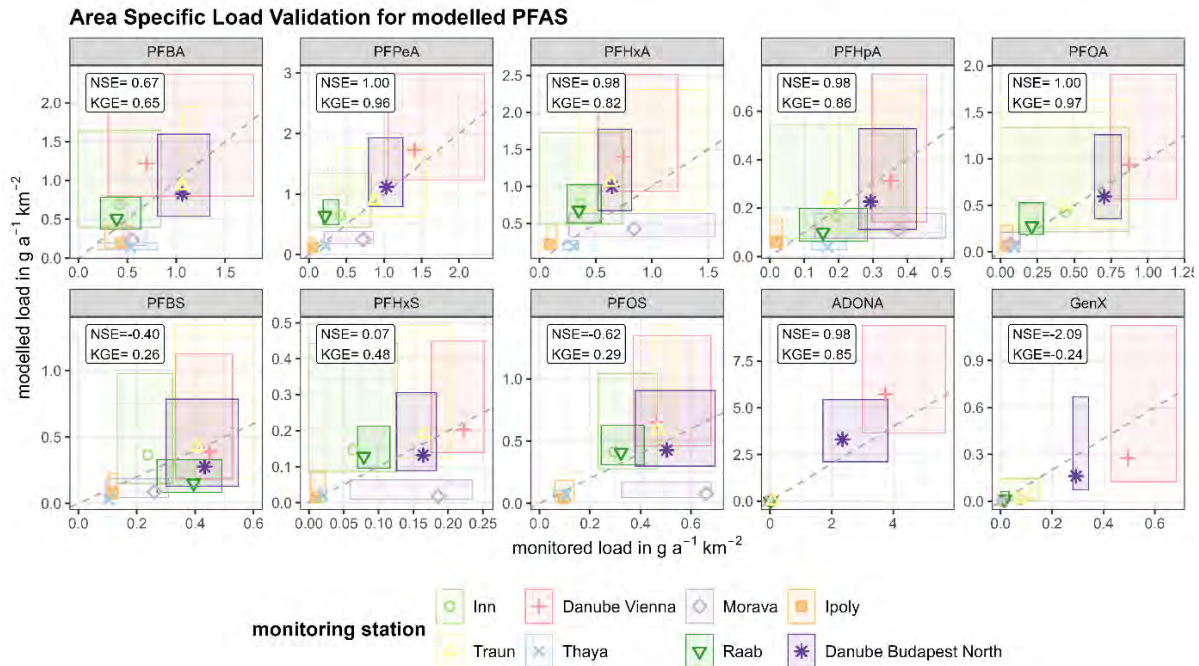


Figure D.5.: Validation graph of the modelled load and monitored load for selected PFAS at each validation sites excepts for Alz, in area-specific form.

D.6.3. Concentration

Concentrations for each PFAS were calculated in MoRE by dividing the modelled cumulative load by the modelled gross discharge at the outlet of each catchment. These values were then validated with in-stream monitored concentrations collected in Subtask 2.2.4. Due to the high PFAS concentrations in the Alz river, two versions of validation graphs are presented below: one including all validation sites, and one excluding the Alz site.

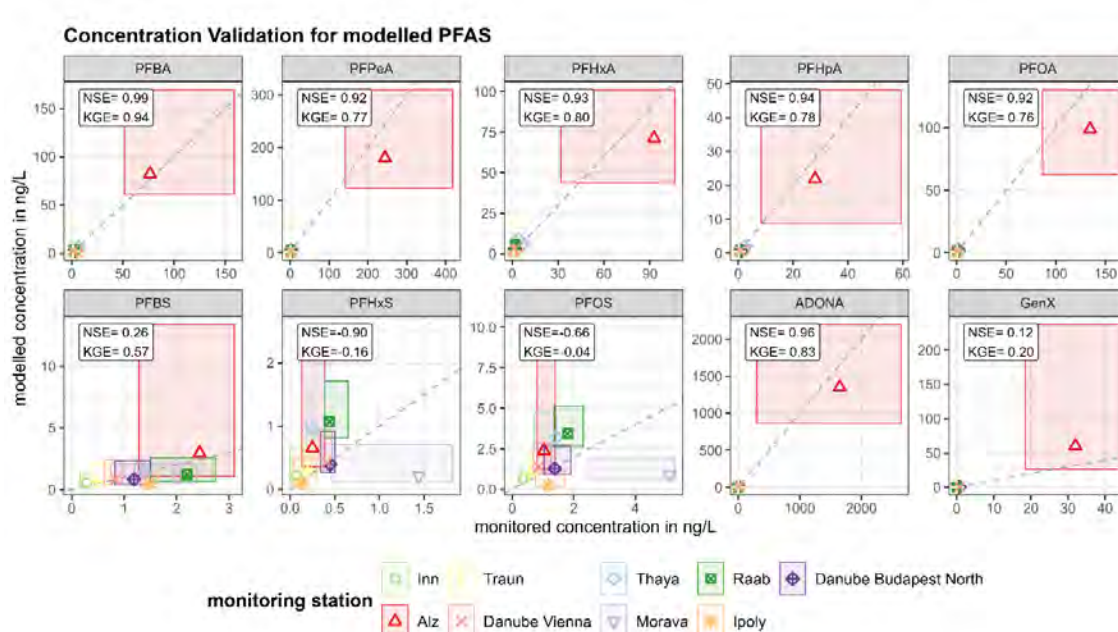


Figure D.6.: Validation graph of the modelled concentrations and monitored concentrations for selected PFAS at each validation sites.

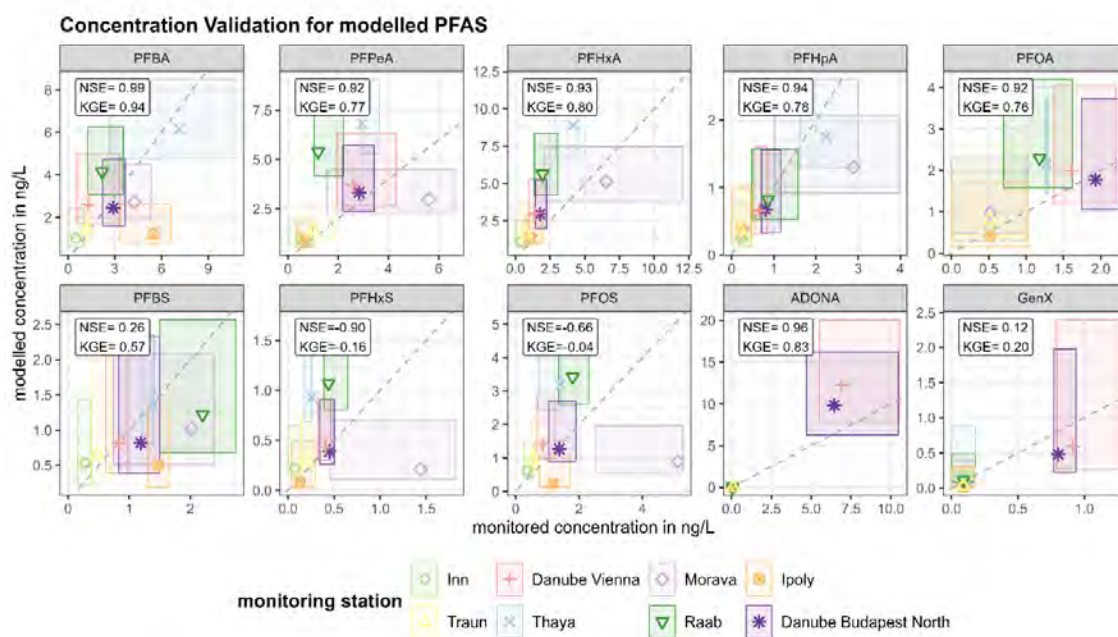


Figure D.7.: Validation graph of the modelled concentrations and monitored concentrations for selected PFAS at each validation sites excepts for Alz.

D.6.4. Sum of PFASs

Using the modelled concentrations for selected PFAS substances, two summed PFAS values were then calculated via a R-script, according to the standards provided in the Drinking Water Directive (EU 2020) and the drafted Environmental Quality Standard (EC COM(2022) 540 final).

For the DWD sum value, the sum of 10 selected PFAS was calculated through direct addition, expressed in ng/L. For the drafted EQS sum value, each PFAS was assigned with a relative potency factor (RPF), with PFOA used as a reference (RPF = 1). A weighted sum was then calculated in PFOA-equivalent ng/L.

To account for the effects of precursor transformations, the same approach was applied to the monitored concentrations data. Specifically, the concentrations of N-EtFOSAA was added to the level of PFOS, while half of the 6:2 FTS concentration was added to PFPeA and the other half to PFHxA.

Due to the high concentrations in the Alz river, two versions of validation graphs are presented: one including all validation sites (Figure D.8), and one excluding the Alz site (Figure D.9).

Table D.5.: Relative potency factors for the selected PFAS (drafted EQS (EC COM(2022) 540 final)).

PFAS	CAS number	Relative Potency Factor (RPF)
PFBA	375-22-4	0.05
PFPeA	2706-90-3	0.03
PFHxA	307-24-4	0.01
PFHpA	375-85-9	0.505
PFOA	335-67-1	1
PFBS	375-73-5	0.001
PFHxS	355-46-4	0.6
PFOS	1763-23-1	2
GenX	13252-13-6	0.06
ADONA	919005-14-4	0.03

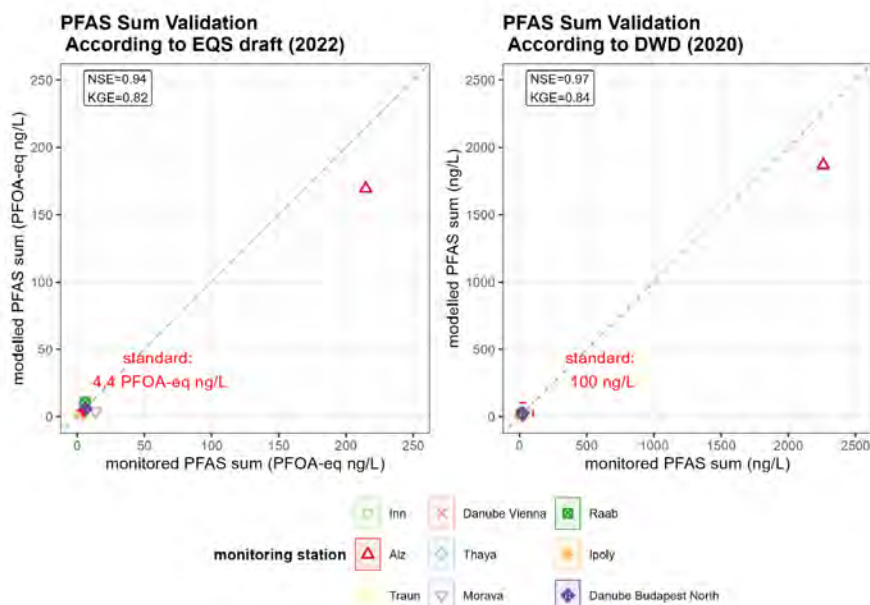


Figure D.8.: Validation graph of the PFAS-sum calculated according to DWD (EU 2020) and drafted EQS (EC COM(2022) 540 final) using the modelled concentrations and monitored concentrations at each validation sites.

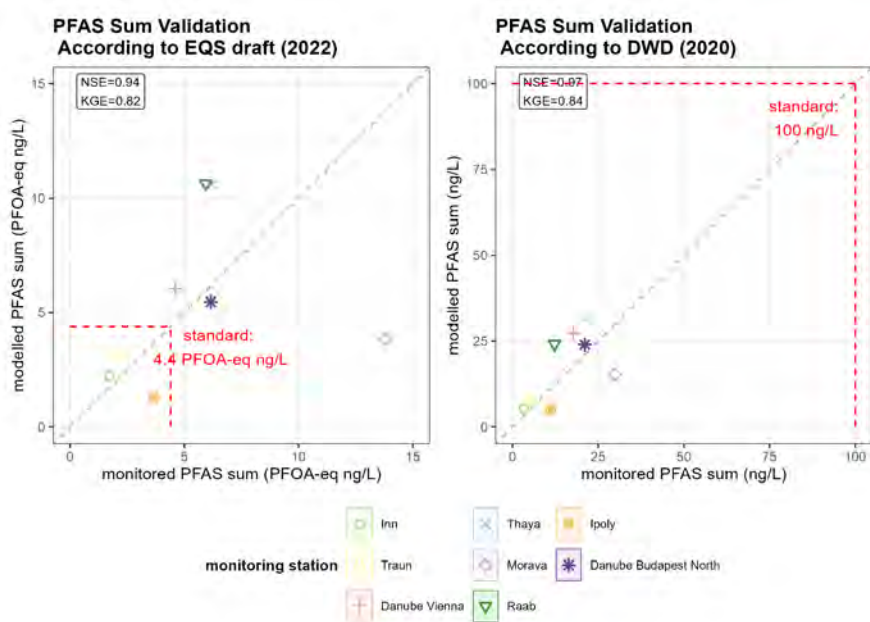


Figure D.9.: Validation graph of the PFAS-sum calculated according to DWD (EU 2020) and drafted EQS (EC COM(2022) 540 final) using the modelled concentrations and monitored concentrations at each validation site excepts for Alz.

D.7. Modelled Pathway Contribution

This section shows the modelled results from the base-case variant, for each modelled pathway (Table D.2) and PFAS substances. Emissions (including upstream catchments) and concentrations at each validation sites were retrieved from the model. These results are then displayed in bar charts, either as absolute values or as proportional values compared to the loads or concentrations derived from monitoring data.

D.7.1. Loads, absolute value

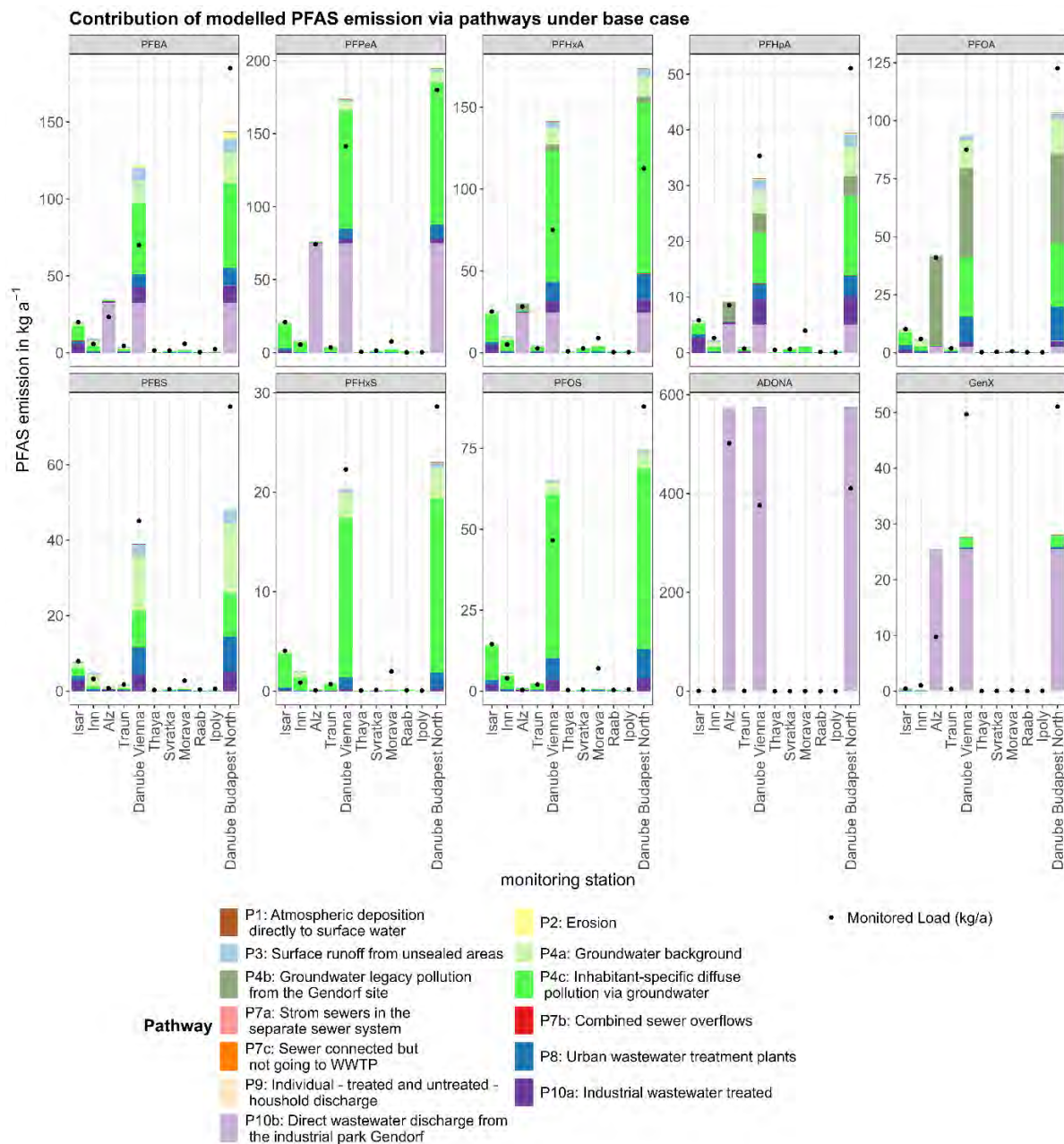


Figure D.10.: Modelled PFAS emission from each pathway shown in cumulative form in absolute amount. Black dots indicate the load calculated from monitored data.

D.7.2. Loads, proportion to the total value

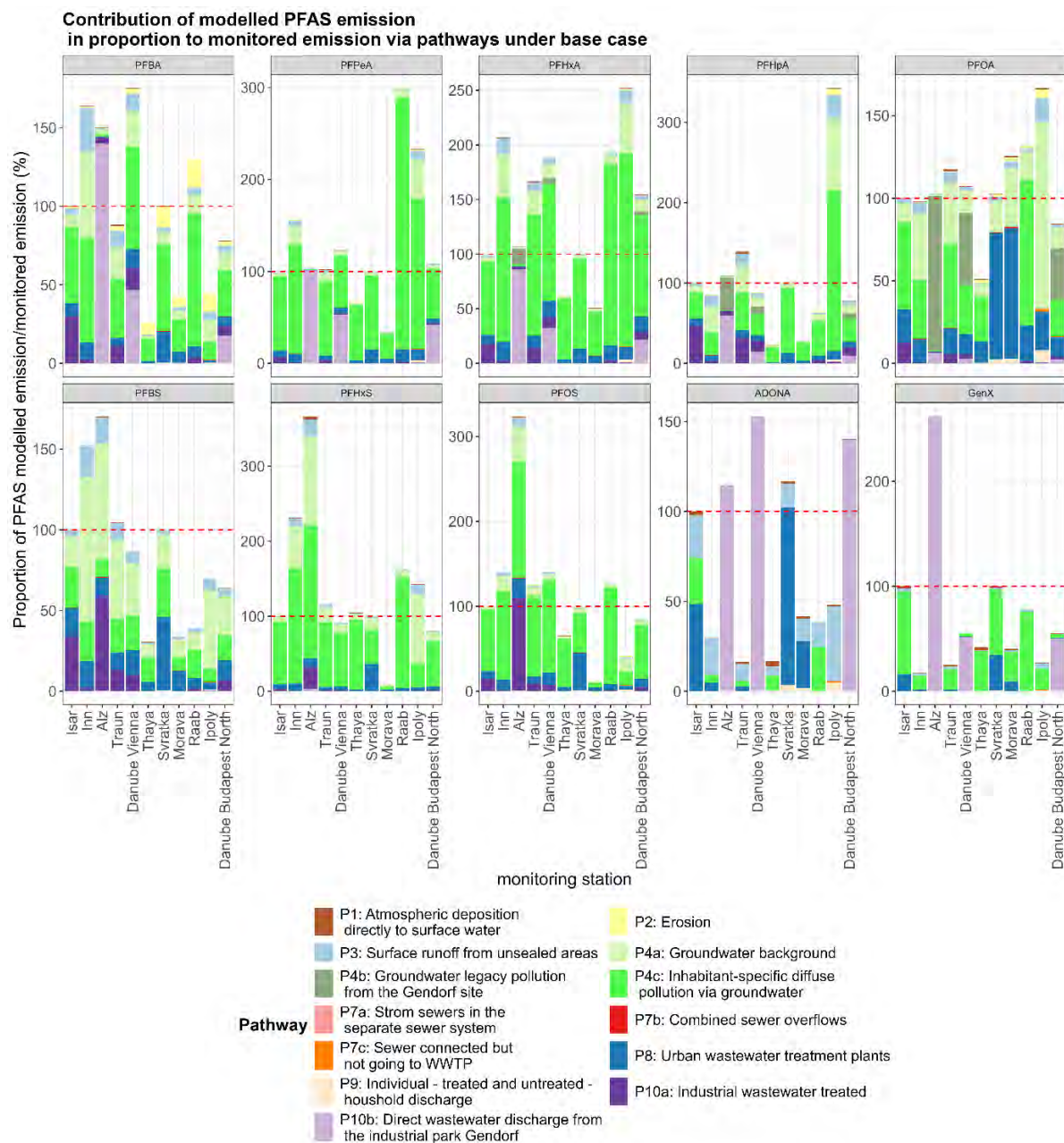


Figure D.11.: Modelled PFAS emission from each pathway shown in proportional form compared to the load calculated from monitored data. Red dashed lines indicate the level of monitored river load, set as 100%.

D.7.3. Concentrations, absolute value

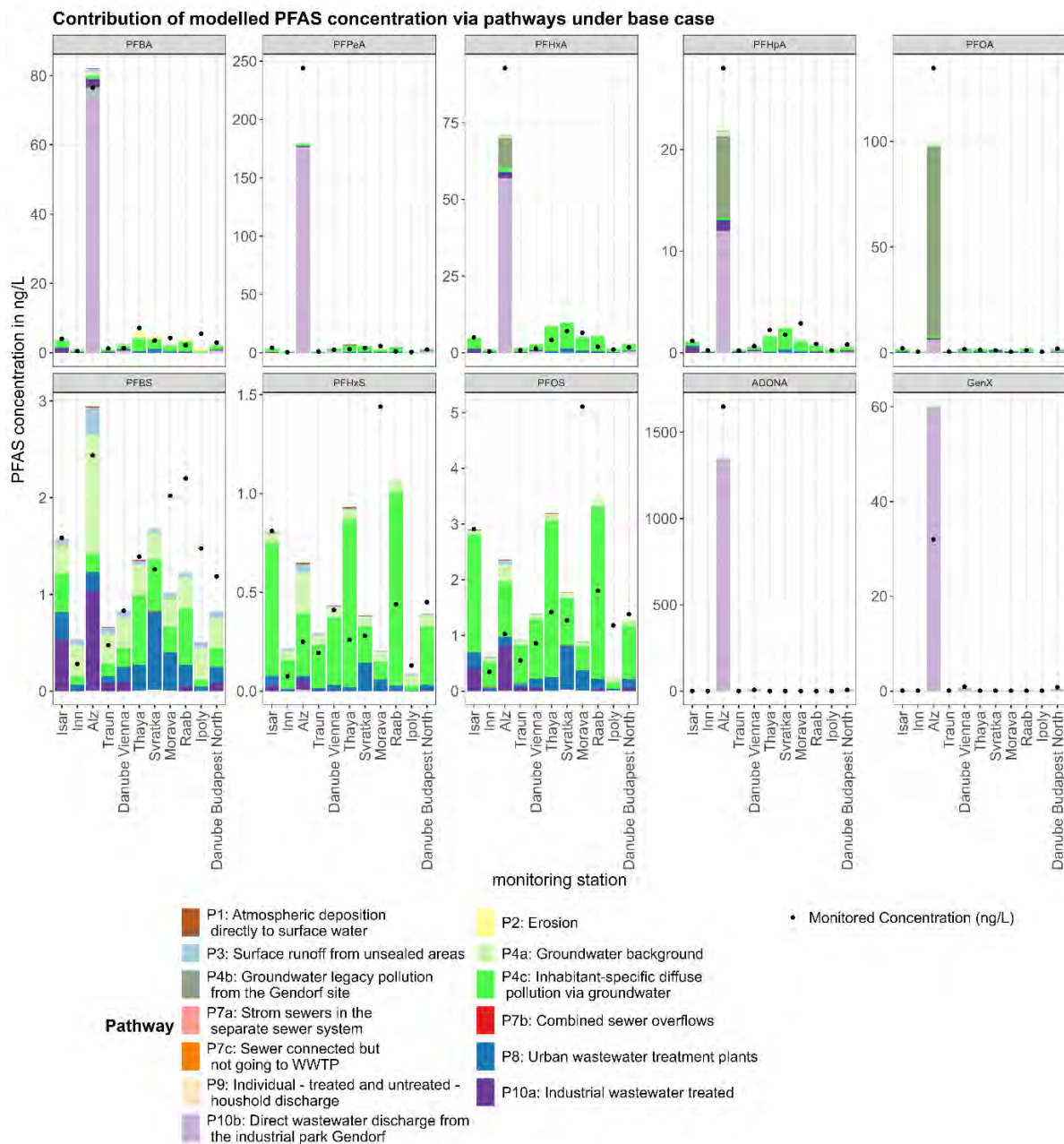


Figure D.12.: Modelled PFAS concentrations from each pathway shown in cumulative form in absolute amount. Black dots indicate the river concentrations monitored at each site.

D.7.4. Concentrations, proportional to the observed value

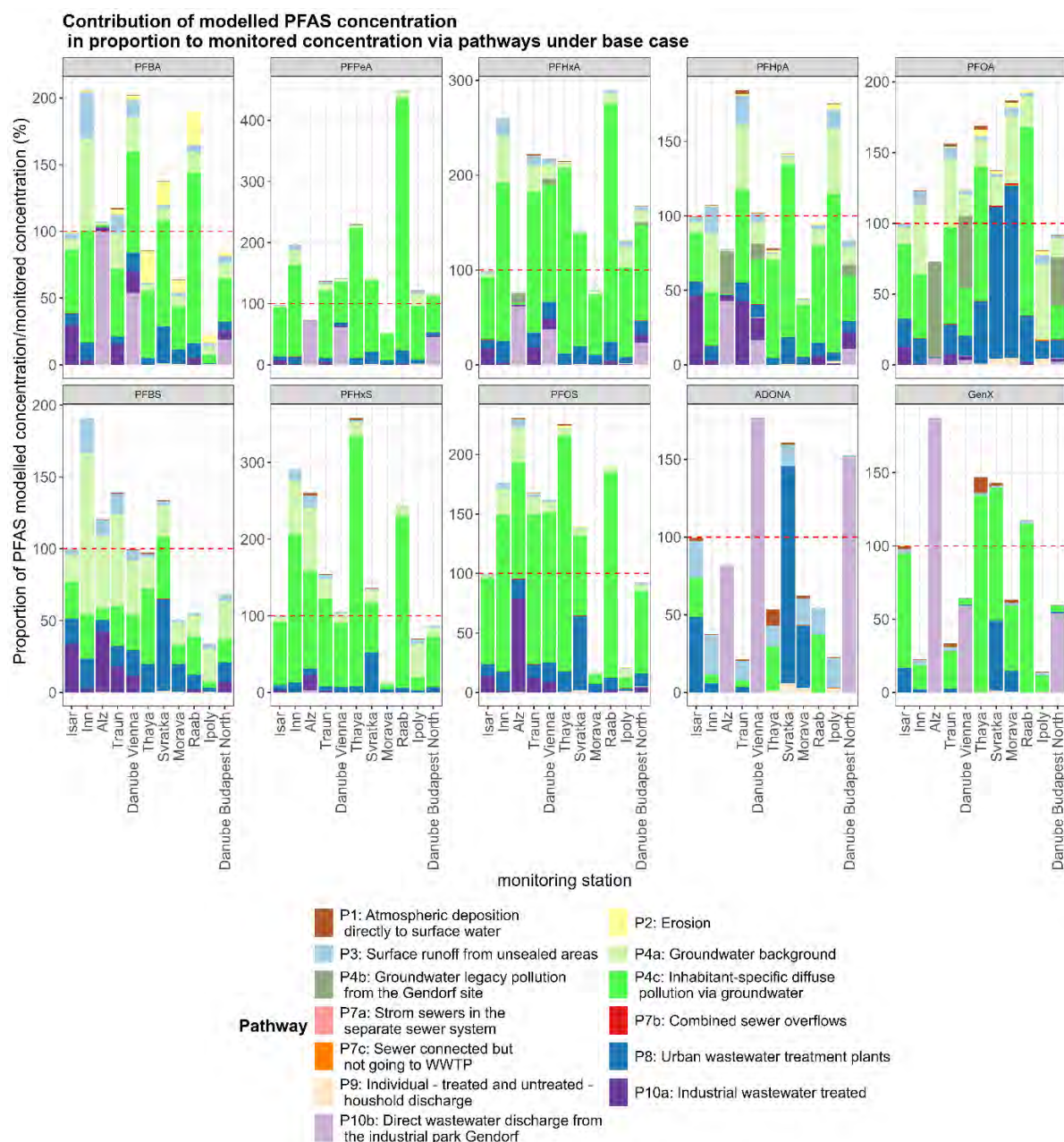


Figure D.13.: Modelled PFAS concentrations from each pathway shown in proportional form compared to the river concentrations monitored at each validation site. Red dashed lines indicate the level of monitored river concentrations, set as 100%.

D.8. Risk Maps

PFAS sums were calculated from the modelled concentrations at all catchment units, following the DWD (EU 2020) and drafted EQS (EC COM(2022) 540 final) methods. As the model

could not cover all PFAS substances listed by each standard, only 10 selected PFAS substances were counted for summation. Additionally, the risk levels of river PFAS-sum levels exceeding the guideline values provided by these two standards were assessed.

For EU (2020), with a standard level of 100 ng/L peak concentration for a sum of 20 PFAS, risk levels were classified as:

- $\Sigma\text{PFAS}_{10} < 20 \text{ ng/L}$: very low risk
- $20 \text{ ng/L} < \Sigma\text{PFAS}_{10} < 50 \text{ ng/L}$: low risk
- $50 \text{ ng/L} < \Sigma\text{PFAS}_{10} < 100 \text{ ng/L}$: medium risk
- $100 \text{ ng/L} < \Sigma\text{PFAS}_{10} < 200 \text{ ng/L}$: high risk
- $\Sigma\text{PFAS}_{10} > 200 \text{ ng/L}$: very high risk

For the drafted EQS (EC COM(2022) 540 final), with an annual average standard level of 4.4 ng PFOA-equivalent/L for a sum of 24 PFAS, risk levels were classified as:

- $\Sigma\text{PFAS}_{10} < 1 \text{ ng PFOA-eq/L}$: very low risk
- $1 \text{ ng PFOA-eq/L} < \Sigma\text{PFAS}_{10} < 2.5 \text{ ng PFOA-eq/L}$: low risk
- $2.5 \text{ ng PFOA-eq/L} < \Sigma\text{PFAS}_{10} < 4 \text{ ng PFOA-eq/L}$: medium risk
- $4 \text{ ng PFOA-eq/L} < \Sigma\text{PFAS}_{10} < 5.5 \text{ ng PFOA-eq/L}$: high risk
- $\Sigma\text{PFAS}_{10} > 5.5 \text{ ng PFOA-eq/L}$: very high risk

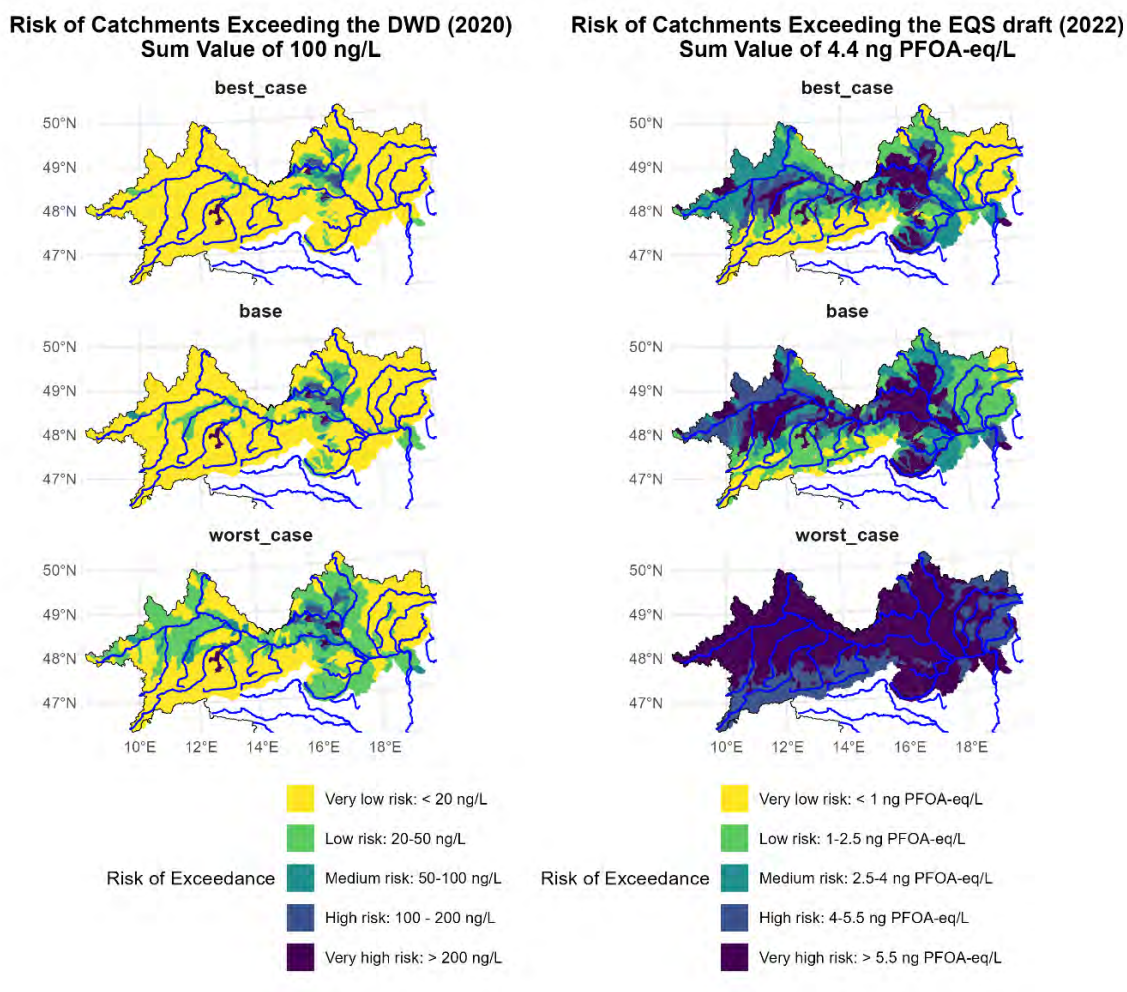


Figure D.14.: Map of risks of model catchments exceeding the standard levels of PFAS-sum for DWD (EU 2020) and drafted EQS (EC COM(2022) 540 final).

D.9. Acknowledgements

The authors thank Jos van Gils, Erwin Meijers, Devanshi Pathak, H  l  ne Boisgontier, Corine ten Velden and Sebastian Hartgring from Deltares for providing hydrological information and for the exchanges on methods and results of the watershed modelling tasks.

References

European Commission (EC) (2012). *Common Implementation Strategy for the Water Framework Directive (2000/60/EC) Guidance Document No. 28 Technical Guidance on the Preparation of an Inventory of Emissions, Discharges and Losses of Priority and Priority Hazardous*

- Substances*. eng. Tech. rep. European Commission (EC). DOI: 10.2779/2764. URL: <https://data.europa.eu/doi/10.2779/2764> (visited on 01/15/2025) (cit. on pp. 152, 153).
- EC COM(2022) 540 final (2022). *Proposal For A Directive Of The European Parliament And Of The Council amending Directive 2000/60/EC establishing a framework for Community action in the field of water policy, Directive 2006/118/EC on the protection of groundwater against pollution and deterioration and Directive 2008/105/EC on environmental quality standards in the field of water policy*. URL: https://environment.ec.europa.eu/publications/proposal-amending-water-directives_en (visited on 10/26/2022) (cit. on pp. 162, 163, 168–170).
- EPA (Jan. 2024). “Method 1633 Analysis of Per- and Polyfluoroalkyl Substances (PFAS) in Aqueous, Solid, Biosolids, and Tissue Samples by LC-MS/MS”. en. In: URL: <https://www.epa.gov/system/files/documents/2024-01/method-1633-final-for-web-posting.pdf> (cit. on p. 151).
- EU (Dec. 2020). *Directive (EU) 2020/2184 of the European Parliament and of the Council of 16 December 2020 on the quality of water intended for human consumption (recast) (Text with EEA relevance)*. en. URL: <http://data.europa.eu/eli/dir/2020/2184/oj/eng> (visited on 11/11/2024) (cit. on pp. 162, 163, 168–170).
- Fuchs, S., M. Kaiser, L. Kiemle, S. Kittlaus, S. Rothvoß, S. Toshovski, A. Wagner, R. Wander, T. Weber, and S. Ziegler (Mar. 2017). “Modeling of Regionalized Emissions (MoRE) into Water Bodies: An Open-Source River Basin Management System”. en. In: *Water* 9.4, p. 239. ISSN: 2073-4441. DOI: 10.3390/w9040239. URL: <https://www.mdpi.com/2073-4441/9/4/239> (visited on 12/13/2024) (cit. on p. 152).
- GeoSphere Austria (2020). *SPARTACUS v2.1 Tagesdaten*. DOI: 10.60669/M6W8-S545 (cit. on p. 153).
- Glüge, J., M. Scheringer, I. T. Cousins, J. C. DeWitt, G. Goldenman, D. Herzke, R. Lohmann, C. A. Ng, X. Trier, and Z. Wang (2020). “An overview of the uses of per- and polyfluoroalkyl substances (PFAS)”. en. In: *Environmental Science: Processes & Impacts* 22.12, pp. 2345–2373. ISSN: 2050-7887, 2050-7895. DOI: 10.1039/D0EM00291G. URL: <http://xlink.rsc.org/?DOI=D0EM00291G> (visited on 08/17/2022) (cit. on p. 151).
- Groot, H., A. Sosnowska, W. Peijnenburg, J. Meesters, A. Wintersen, V. Zhiteneva, N. Devau, J. Valstar, et al. (2025). “PROMISCES D2.3 Toolbox fate & transport modelling of PMTs in the environment”. in preparation. DOI: 10.3030/101036449. URL: <https://cordis.europa.eu/project/id/101036449/results> (cit. on pp. 152, 154).
- Gupta, H. V., H. Kling, K. K. Yilmaz, and G. F. Martinez (2009). “Decomposition of the mean squared error and NSE performance criteria: Implications for improving hydrological modelling”. In: *Journal of Hydrology* 377.1-2, pp. 80–91. ISSN: 00221694. DOI: 10.1016/j.jhydrol.2009.08.003 (cit. on p. 156).
- Helsel, D. R. (2012). *Statistics for censored environmental data using Minitab and R*. en. 2nd ed. Wiley series in statistics in practice. OCLC: ocn748290711. Hoboken, N.J: Wiley. ISBN: 978-0-470-47988-9 (cit. on p. 153).
- Hersbach, H., B. Bell, P. Berrisford, G. Biavati, A. Horányi, J. Muñoz Sabater, J. Nicolas, C. Peubey, et al. (2023). *ERA5 hourly data on single levels from 1940 to present. Copernicus Climate Change Service (C3S) Climate Data Store (CDS)*. en. DOI: 10.24381/cds.adbb2d47. URL: <https://cds.climate.copernicus.eu/datasets/reanalysis-era5-single-levels?tab=overview> (visited on 01/29/2025) (cit. on p. 153).
- Kittlaus, S., A. Clement, M. K. Kardos, K. M. Dudás, N. Weber, O. Zoboli, and M. Zessner (Mar. 2023). *Inventory of hazardous substance concentrations in different environmental*

- compartments in the Danube river basin*. eng. DOI: 10.48436/xwve4-h7v43. URL: <https://researchdata.tuwien.at/records/xwve4-h7v43> (visited on 01/29/2025) (cit. on p. 153).
- Méndez, V., S. Holland, S. Bhardwaj, J. McDonald, S. Khan, D. O’Carroll, R. Pickford, S. Richards, C. O’Farrell, N. Coleman, M. Lee, and M. J. Manefield (2022). “Aerobic biotransformation of 6:2 fluorotelomer sulfonate by *Dietzia aurantiaca* J3 under sulfur-limiting conditions”. eng. In: *The Science of the total environment* 829, p. 154587. ISSN: 1879-1026. DOI: 10.1016/j.scitotenv.2022.154587 (cit. on p. 155).
- Nash, J. E. and J. V. Sutcliffe (Apr. 1970). “River flow forecasting through conceptual models part I — A discussion of principles”. In: *Journal of Hydrology* 10.3, pp. 282–290. ISSN: 0022-1694. DOI: 10.1016/0022-1694(70)90255-6. URL: <https://www.sciencedirect.com/science/article/pii/0022169470902556> (visited on 01/29/2025) (cit. on p. 155).
- Team, R. C. (2024). *R: The R Project for Statistical Computing*. URL: <https://www.r-project.org/> (visited on 01/29/2025) (cit. on p. 157).
- Verseveld, W. J. van, A. H. Weerts, M. Visser, J. Buitink, R. O. Imhoff, H. Boisgontier, L. Bouaziz, D. Eilander, M. Hegnauer, C. ten Velden, and B. Russell (Apr. 2024). “Wflow_sbm v0.7.3, a spatially distributed hydrological model: from global data to local applications”. English. In: *Geoscientific Model Development* 17.8, pp. 3199–3234. ISSN: 1991-959X. DOI: 10.5194/gmd-17-3199-2024 (cit. on p. 153).
- Wen, B., Y. Pan, X. Shi, H. Zhang, X. Hu, H. Huang, J. Lv, and S. Zhang (Nov. 2018). “Behavior of N-ethyl perfluorooctane sulfonamido acetic acid (N-EtFOSAA) in biosolids amended soil-plant microcosms of seven plant species: Accumulation and degradation”. In: *Science of The Total Environment* 642. TLDR: The results are the first to reveal N-EtFOSAA accumulation in plants and degradation in soil-plant microcosms, and showed that the root protein and lipid contents explain 85.0% of the variation in root N-TfOSAA levels., pp. 366–373. ISSN: 0048-9697. DOI: 10.1016/j.scitotenv.2018.06.073. URL: <https://www.sciencedirect.com/science/article/pii/S0048969718321442> (visited on 01/29/2025) (cit. on p. 155).

E. PROMISCES watershed model for PM substances (PPM)

Authored by: Erwin Meijers, Devanshi Pathak, H  l  ne Boisgontier, Corine ten Velden,
Sebastian Hartgring, Jos van Gils

Deltares. Boussinesqweg 1, Delft, the Netherlands

E.1. Introduction

In the PROMISCES project, Work Package 2, a model train application was set up for the Danube catchment upstream of Budapest (see Section 4.6 of the main text). The model train applied consisted of the MoRE and PPM models for assessing sources and pathways of the emissions in the catchment as well as the in-stream fate and transport of PFAS. At selected bank filtration drinking water abstraction sites, a 1D streamtube approach with advective-dispersive-reactive transport along flowlines through the groundwater system to the abstraction well(s) was set up, as well as a 3D physically-distributed reactive transport model (MT3DMS) for the groundwater system of the Budapest island. As a basis for the groundwater transport models (both the 1D streamline and the 3D approach) a 3D dynamic MODFLOW model was constructed. The MoRE model was driven by simulated hydrology data abstracted from the Wflow model component of the PPM.

This annex provides a description of the PPM model. It consists of three components:

1. The Wflow distributed hydrological modelling framework (Verseveld et al. 2024)
2. The D-Emissions (EM) emission modelling framework (DELTARES 2025a)
3. The D-WaterQuality (WQ) water quality modelling framework (DELTARES 2025b; Smits and Beek 2013).

Hydrological processes are represented on a regular fine grid of cells with their own physical characteristics (elevation, soil, land use and land cover). Meteorological forcing data are used to calculate the generation of runoff and infiltration, which is then routed through the catchment river system, taking into account the presence of natural lakes and reservoirs. The routing process accounts for both surface and subsurface flows. Snow related processes are included. The Wflow framework also offers a component to calculate erosion and sediment delivery to the river network (Boisgontier and Gils 2020).

The EM and WQ model components both make use of the Delft3D-WAQ open source water system modelling software¹. This software offers a range of numerical solution techniques for the mass balance equation/advection-diffusion equation as well as comprehensive mass balance output. These features are used for simulating PFAS emissions, representing different compartments of the techno-sphere (e.g. paved surfaces, wastewater and stormwater collection and treatment) and the terrestrial system. The emission modelling component follows a source-oriented approach as much as possible, see Section 4.2 of the main text. The same software is used to represent in-stream processes for PFAS.

E.2. Methods

E.2.1. General

In this project, 10 PFAS substances were modelled. Additionally, NtFOSAA was modelled as a precursor of PFOS. Table E.1 provides a list of these substances. The model domain was the Danube River Basin upstream of the city of Budapest in Hungary.

The modelling approach is distributed in space and in time. It was based on the Danube Hazard m³c project (Kovacs et al. 2023). In that project, modelling was performed with a daily timestep for the lumped sub-catchments schematization and hydrology provided by the European scale E-Hype model (Hundecha et al. 2016) for 2003–2013. In the current project, modelling was performed on a rectangular grid. The hydrology was calculated using the Wflow distributed modelling framework (Verseveld et al. 2024) for the period 2011–2022. The emission modelling approach is based on the related Water Framework Directive Common Implementation Strategy Guidance Document (European Commission (EC) 2012).

PFAS modelling relied on monitoring data collected in various environmental and man-made compartments (including surface water, wastewater, soil, groundwater and atmospheric deposition), collected by TU Wien. These data stem from the period 2013–2024 and include pre-existing data next to data collected within the PROMISCES project.

PFAS sources within the catchment were characterised using the above monitoring database. For the sake of creating input data, all values below limit of quantification (LOQ) were initially replaced by the LOQ.

E.2.2. Hydrological modelling

The Wflow software package is able to simulate several hydrological processes (Figure E.1). A distinction can be made between vertical processes, which are contained within each cell in the model, and lateral processes, describing the fluxes between the cells. The following processes are included:

- Precipitation and evapotranspiration
- Interception and infiltration

¹<https://oss.deltares.nl/web/delft3d>

Table E.1.: List of modelled PFAS substances

Substance acronym	Substance name	CAS number
ADONA	ADONA	958445-44-8
GenX	2,3,3,3-tetrafluoro-2-(heptafluoropropoxy)propionic acid	13252-13-6
NEtFOSAA	N-Ethylperfluorooctane sulfonamidoacetic acid	2991-50-6 or 2991-51-7
PFBA	Perfluorobutanoic acid	375-22-4
PFBS	Perfluorobutane sulfonic acid	375-73-5
PFPeA	Perfluoropentanoic acid	2706-90-3
PFHxA	Perfluorohexanoic acid	307-24-4
PFHxS	Perfluorohexane sulfonic acid	355-46-4
PFHpA	Perfluoroheptanoic acid	375-85-9
PFOA	Perfluorooctanoic acid	335-67-1
PFOS	Perfluorooctane sulfonic acid	1763-23-1

- Snowfall, accumulation in glaciers and snowmelt
- Storage in reservoirs and Lakes

The area of application is the Danube catchment upstream of Budapest, covering larger parts of Germany, Austria, Czech Republic, Slovakia and Hungary and small parts of Switzerland, Italy, Slovenia and Poland (Figure E.2). The outlet of the catchment is at 47.23 °N and 18.91 °E. The model resolution is 0.0166 degrees ($\sim 1500 \cdot 1500$ m) and the cell count is 81,217.

Data processing to build the model is supported by the HydroMT (Hydro Model Tools) package, that includes GIS, hydrological, statistical and plotting methods needed for rapidly building inter-connected environmental models (Eilander and Boissongontier 2022). Input data for the hydrology model include spatial data such as elevation from MERIT Hydro (Yamazaki et al. 2019), soil properties from Soilgrids (Hengl et al. 2017), landcover data from VITO 2015 (Buchhorn et al. 2020) and MODIS LAI (Myneni 2015), reservoirs and lakes from GRanD (Lehner et al. 2011) and HydroLAKES (Messenger et al. 2016). Considering the large domain, the hydrological model was prepared using global data and parametrisation (direct estimates from literature and pedo-transfer functions) to get a first good estimate of all model parameters (Imhoff et al. 2020).

Daily ERA5 re-analysis data were selected for spatio-temporal model forcing data (C3S 2017). This dataset includes precipitation, which is directly used, and temperature, incoming radiation and pressure which is used to determine the potential evapotranspiration using the method from De Bruin. The ERA5 dataset has a resolution of 31 km and is used for the period 2010–2022.

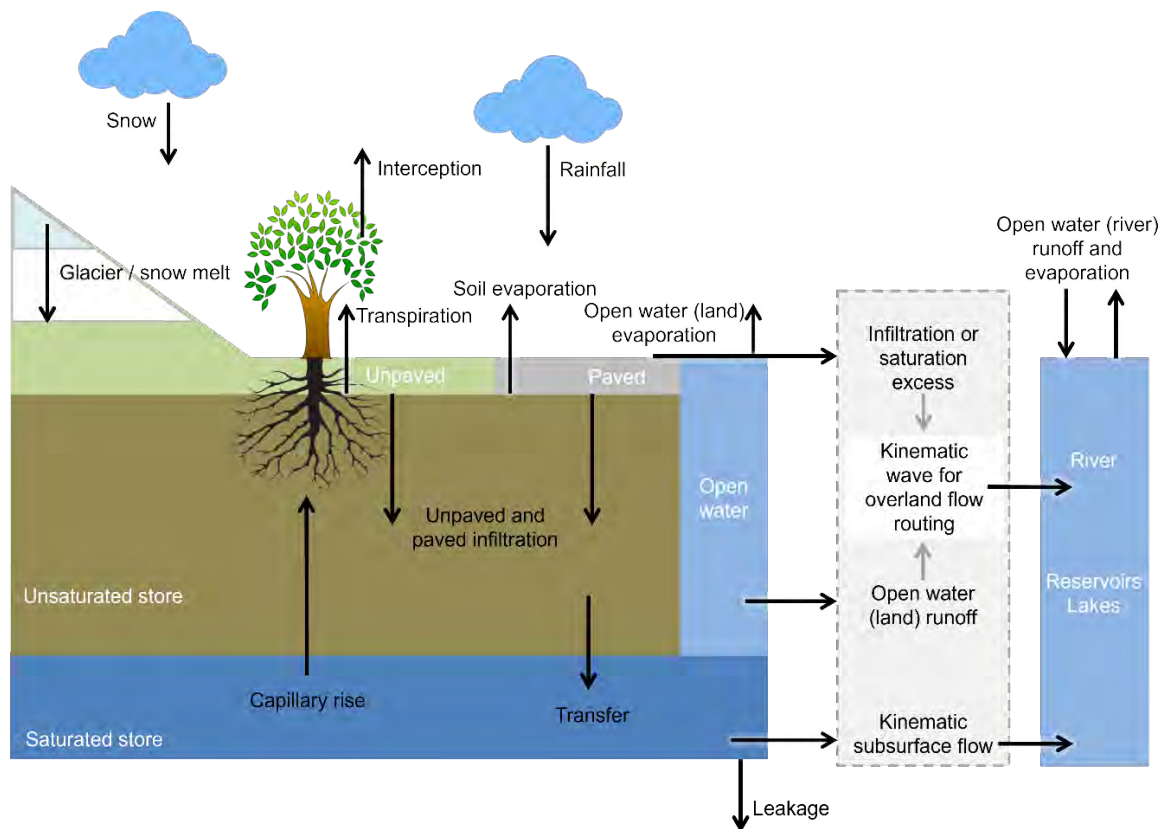


Figure E.1.: Schematic overview of hydrological processes included in the Wflow model of the upper Danube catchment.

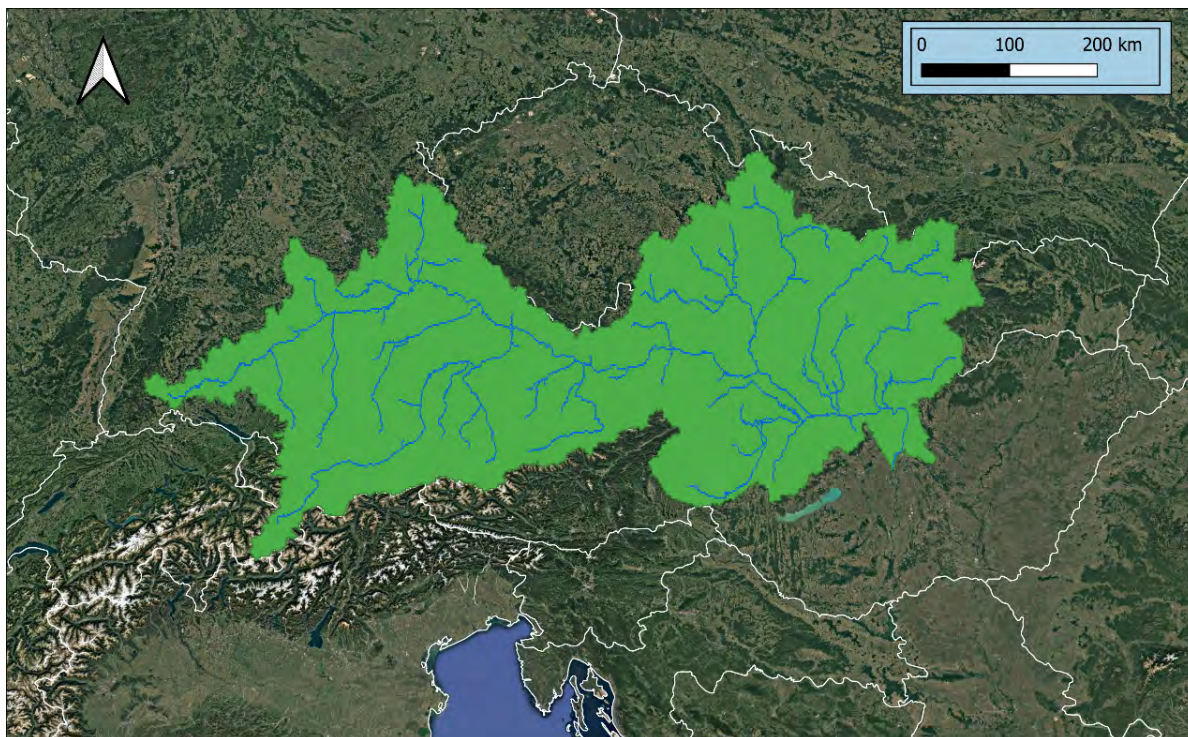


Figure E.2.: Model domain.

For the Austrian part of the domain, the higher resolution SPARTACUS dataset (Hiebl and Frei 2018) was added, see Figure E.3. In order to benefit from the higher resolution without compromising the earlier calibration using ERA5 forcing only, the Spartacus precipitation was scaled to reproduce the ERA5 totals at the level of sub-catchments.

Wflow features different options for river routing. The kinematic wave approach (KW) performs well in steep-sloped areas, often upstream in the catchment. In flat areas or for large waves (floods) the local-inertial method with one-dimensional sub-grid floodplain attenuation (FP) tends to better describe wave attenuation and celerity. In this model the FP method was used.

E.2.3. Emission modelling: sources of PFAS

The following sources of PFAS were included in the modelling:

- Atmospheric deposition
- Industry point sources
- Domestic wastewater
- Diffuse sources in urban areas

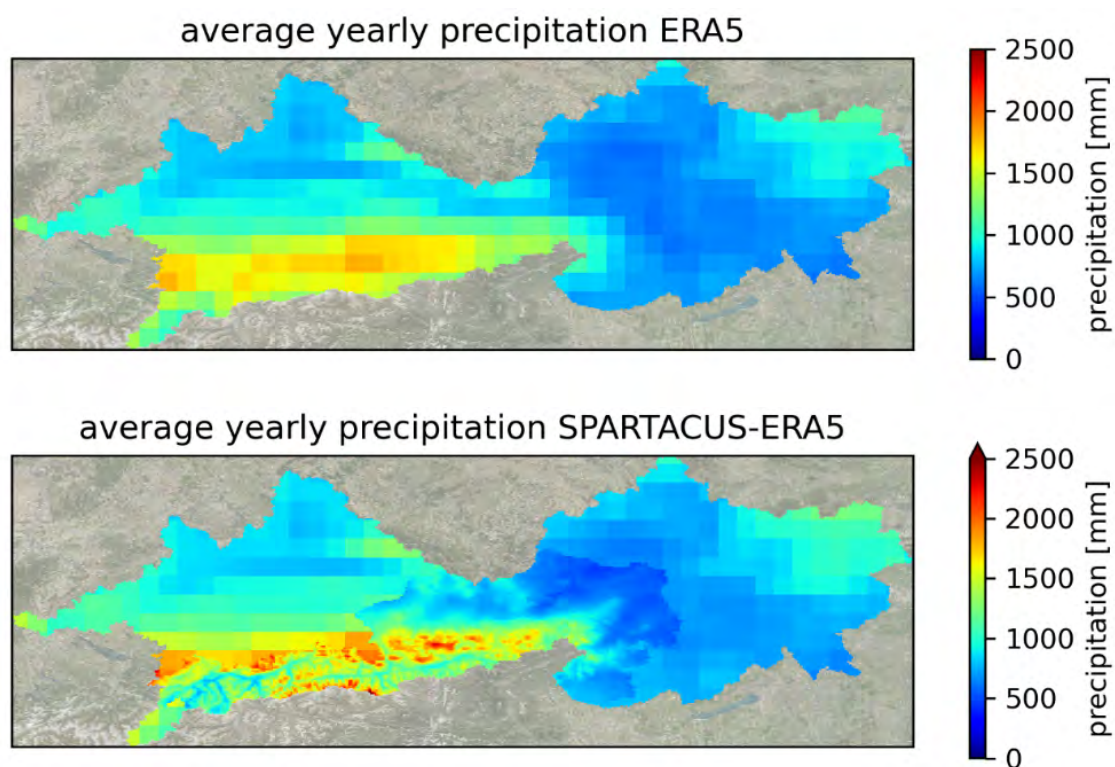


Figure E.3.: Comparison of ERA5 annual precipitation (top) and blended Spartacus-ERA5 annual precipitation (bottom).

Table E.2.: Substance specific median concentrations, emission factors (EF) or loads considered to characterise some of the PFAS emission sources. S1 = source 1 for atmospheric deposition, S2 = source 2 for domestic wastewater and S3 = source 3 for PFAS hotspot at Gendorf chemical park. The factors considered to characterise the rest of the sources are explained in the text.

PFAS substance	S1 median concentration (ng L ⁻¹)	S2 median concentration (ng L ⁻¹)	S2 EF (kg cap ⁻¹ d ⁻¹)	S3 Point source (kg d ⁻¹)
GenX	0.278	0.000295	$8.85 \cdot 10^{-11}$	0.0699
NEtFOSAA	0.54	0.00072	$2.16 \cdot 10^{-10}$	0
ADONA	0.36	0.000815	$2.45 \cdot 10^{-10}$	1.5728
PFBA	2.71	0.005	$1.50 \cdot 10^{-9}$	0.0893
PFBS	0	0.004	$1.20 \cdot 10^{-9}$	0
PFHpA	2	0.002	$6.00 \cdot 10^{-10}$	0.014
PFHxA	2	0.006	$1.80 \cdot 10^{-9}$	0.0664
PFHxS	0	0.0005	$1.50 \cdot 10^{-10}$	0
PFOA	0.35	0.005	$1.50 \cdot 10^{-9}$	0.0071
PFOS	0.15	0.00395	$1.19 \cdot 10^{-9}$	0
PFPeA	2	0.004	$1.20 \cdot 10^{-9}$	0.2058

All sources are expressed as the product of an Activity Rate (AR) and an Emission Factor (EF). Every source is allocated to an initial receptor from where its releases are routed through different environmental and man-made compartments towards the surface waters.

Basic information to quantify the sources was a population density map (Schiavina et al. 2019) and a settlement type map (Pesaresi et al. 2019).

Atmospheric deposition Atmospheric deposition was defined as a concentration in rainfall (EF, g m⁻³) multiplied with the actual rainfall (AR). The initial receptors for atmospheric deposition are automatically arranged in the model as paved surface, unpaved surface or surface water based on the land use of the receiving grid cells. A constant median concentration (ng L⁻¹) in spatially and temporally varying rainfall was used across the entire catchment area (Table E.2). For PFBS and PFHxS, the median value had to be replaced by zero, as the original value caused a strong build up in soils and a corresponding strong increase of these PFAS reaching surface waters from soils by surface and subsurface runoff. For both substances, > 95% of analyses were reported below the LOQ.

Domestic wastewater To characterise emissions from domestic wastewater, we used population as the AR. EFs were derived using observations (median concentrations) in WWTP effluents

(Table E.2) and per capita wastewater production. The amount of sewage (wastewater + stormwater) produced per capita was estimated based on country data compiled in Kovacs et al. (2023) at 300 L cap⁻¹ d⁻¹. The initial receptor for this source is domestic wastewater, which is seen as a separate compartment in the modelling approach. It is noted that normally influent data would have to be used to characterize the per capita load to wastewater, as effluent data would already be affected by treatment and their use would lead to an underestimation of the EF. For the persistent PFAS this argument is not valid as they are not removed during conventional treatment. Some PFAS are reported to show higher concentrations in effluents than in influents, due to the transformation of so-called precursors. This transformation is implicitly included in the EF's derived from effluent concentrations.

Direct industrial discharge TU Wien provided the data about industry locations, type (e.g. chemical, food production, paper, electronic, etc.) and their corresponding annual water discharge. In TU Wien monitoring database, information about the types of industries for some monitoring samples in the wastewater compartment were available. Using this information, we derived median effluent concentrations for industry types for all PFAS substances. For industry types with no monitoring data, we used minimum effluent concentration value from the list of median effluent concentrations of all industry types. Direct discharges from each industry (kg d⁻¹) to surface water were derived by multiplying industry-type specific median effluent concentration and annual discharge.

Diffuse sources in urban areas It is expected that there are various sources of PFAS especially in urban areas. These are for example landfills, areas where PFAS containing fire-fighting foams were used (either for practicing or during true incidents) and smaller industrial sites where PFAS are used for various purposes. The data to realistically represent these distributed sources of PFAS are hard to collect. For this reason, a proxy for this source was used. This proceeded as follows:

- The source was assumed proportional to the weighed population number in each urban cell.
- The weight factor is related to the country GDP as in van Gils et al. (2020) .
- The source strength is then aggregated over sub-catchments (the sub-catchments used in the MoRE model) and expressed as an area specific value.
- The area-specific source strength in each sub-catchment is expressed relative to the model wide area-specific source strength. This provides a ratio >1.0 in strongly urbanized sub-catchments and a ratio <1.0 in less urbanized sub-catchments. In a sub-catchment without any urban cells, this ratio is 0.0.
- The source is then introduced as a spatially variable concentration in soils, equal to the median soil concentration in the monitoring data, multiplied with the ratio of area specific sub-catchment source strength over basin wide source strength.

The result is illustrated in Figure E.4. This picture clearly shows the population centers Munich, Brno, Vienna and Budapest. For the actual median soil concentrations used, reference is made to Table E 8.



Figure E.4.: Spatially variable initialization of the concentration of PFOA in top soils.

PFAS hotspot: Gendorf chemical park in Germany Gendorf chemical park in the Alz river sub-catchment is a known source of high effluent discharge (Kittlaus et al. 2022). To address these high emissions from the Gendorf chemical park in the Alz river sub-catchment, we provide point source emissions at this site separately (Table E.2). Direct discharges for PFCAs and alternative substances (GenX and ADONA) in surface water at the Gendorf site were calculated using the observed median effluent concentrations from the Gendorf Wastewater treatment plant and its annual discharge ($2,835,000 \text{ m}^3 \text{ y}^{-1}$ for central plant Gendorf).

E.2.4. Emission modelling: wastewater and stormwater pathways of PFAS to surface waters

Input parameters related to wastewater management infrastructure were derived from a combination of sources (Table E.3). The majority of the parameters in Table E.3 were specified based on settlement type-dependent, country-scale estimates derived from the ICPDR inventory (Table E.4). Additionally, *FrRainSew*, the parameter representing the fraction of stormwater intercepted by sewer systems, was also defined based on the type of settlement. We assumed that in urban areas, stormwater collection systems are nearly fully developed ($FrRainSew = 0.9$), whereas in rural areas, they are mostly absent ($FrRainSew = 0.1$).

Table E.3.: Data sources for wastewater management parameters

Name in model	Definition	Unit	Source
FrSewered	fraction wastewater intercepted by sewer systems	(-)	ICPDR inventories
FrRainSew	fraction stormwater intercepted by sewer systems	(-)	Own estimate
FrSeptic	fraction wastewater to septic tanks	(-)	ICPDR inventories
FComSew	fraction of combined sewers	(-)	Various sources
SewLeakage	Daily rainfall threshold for occurrence of combined sewer overflows	mm/day	Local P95 of daily rainfall during 2011–2022
FrTreat1	fraction wastewater primary treated	(-)	ICPDR inventories
FrTreat2	fraction wastewater secondary treated	(-)	ICPDR inventories
FrTreat3	fraction wastewater tertiary treated	(-)	ICPDR inventories

Table E.4.: Input values of wastewater management parameters derived from ICPDR inventory (Kovacs et al. 2023)

Cluster	FrSewered	FrSeptic	FrUnMan	FrTreat0	FrTreat1	FrTreat2	FrTreat3
AT_U	0.993	0.007	0.000	0.000	0.000	0.000	1.000
AT_R	0.995	0.005	0.000	0.000	0.000	0.001	0.999
CZ_U	0.952	0.048	0.000	0.000	0.000	0.012	0.988
CZ_R	0.915	0.085	0.000	0.000	0.000	0.136	0.864
DE_U	0.999	0.001	0.000	0.000	0.000	0.001	0.999
DE_R	0.999	0.001	0.000	0.000	0.000	0.043	0.957
HU_U	0.896	0.065	0.039	0.000	0.000	0.000	1.000
HU_R	0.764	0.193	0.043	0.000	0.000	0.000	1.000
SK_U	0.951	0.047	0.002	0.006	0.000	0.024	0.970
SK_R	0.680	0.309	0.012	0.002	0.005	0.140	0.852

_U: urban region, _R: rural region, AT: Austria, CZ: Czech Republic, DE: Germany, HU: Hungary and SK: Slovakia

To simulate combined sewer overflows, we defined *SewLeakage* parameter. This parameter represents a precipitation threshold (95th percentile). If the threshold is exceeded, the inflow to the Sew compartment is directly routed to Sfw compartment. The country-scale parameters representing the fraction of combined sewers (*fComSew*) and the fraction of isolated/incinerated sewage sludge (*FrSldgRem*) were derived from data summarized by Kovacs et al. (2023), see Table E.5.

Table E.5.: Input parameter values for FComSew and FrSldgRem

Country	Fraction of sewage sludge incinerated or isolated	Fraction of combined sewer systems
Austria	0.56	0.29
Czech Republic	0.11	0.70
Germany	0.65	0.43
Hungary	0.18	0.03 (Budapest: 0.62)
Slovakia	0.10	0.10
Slovenia	0.82	0.59

E.2.5. Emission modelling: environmental pathways of PFAS to surface waters

Soil compartment in the model was initialized by providing estimates of soil quality at the start of the model simulation. The initial soil concentrations were determined by calculating the median values for all substances using soil compartment monitoring data from the TU Vienna database. We observed that median concentrations in the soil compartment were influenced by the LOQ as several values in the soil compartment fell below the LOQ. Therefore, we calculated quality scores for soil concentration statistics by first assigning a score of 1 or 0 based on the presence or absence of variation between the 25th, 50th, 75th, and 90th percentiles, respectively. These scores were then averaged to provide an overall soil quality score for each PFAS substance (Table E.6). We found that all substances with zero quality score (except ADONA) overestimated surface water concentrations at the most downstream monitoring site, Budapest south. To address this, we reduced the initial soil concentration by 50% for these substances. In two cases, GenX and Adona, soil concentrations were further reduced to match the measured concentrations at the basin outlet.

Table E.6.: Soil quality scores for PFAS substances

PFAS substance	Soil quality score	Soil quality (mg kg ⁻¹)
GenX	0	0.00025 modified to $3.1 \cdot 10^{-5}$
NEtFOSAA	0.5	0.0002

PFAS substance	Soil quality score	Soil quality (mg kg ⁻¹)
ADONA	0	0.0005 modified to 0.0
PFBA	0	0.0005
PFBS	1	0.000007
PFHpA	1	0.000058
PFHxA	1	0.000034
PFHxS	0.5	0.000005
PFOA	1	0.000118
PFOS	1	0.000079
PFPeA	1	0.000097

The sediment module was activated along with the hydrology module to include soil bound transport of PFAS substances. Furthermore, we also activated partitioning in soils by initializing SetSoiKd process in the emission model to include sorption behaviour of PFAS substances. This process sets the fraction of the substance in the soil moisture using a soil partitioning coefficient (Kd). Kd explains the distribution of substance between the soil phase and soil solution, and influence the fate of substance. However, only limited data are available in literature about Kd values for PFAS substances. Kd (or soil organic carbon partition coefficient, Koc) values are often estimated based on octanol-water partition coefficient (Kow). We obtained Kd values for 12 PFAS substances from a RIVM study on difference in leaching of PFAS from soil and dredged material (Wintersen et al. 2020). These values were correlated with the Kow value from two sources namely EPA CompTox chemical dashboard (US EPA 2024) and QSAR modelling from within the PROMISCES project (Sosnowska et al. 2024). Both sources derived similar Pearson's correlation coefficients (Figure E.5). We used Kow values from QSAR model (derived within the same project) to predict Kd values for the rest of the substances.

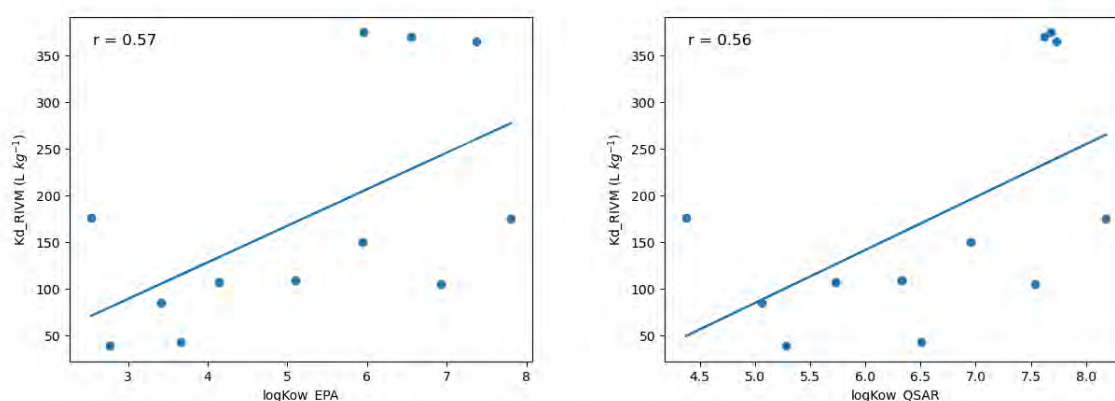


Figure E.5.: Linear regression plots to predict soil Kd values using EPA and QSAR model data

E.2.6. Water quality modelling: in-stream processes

The in-stream water quality model includes the downstream transport and dilution of PFAS emitted to surface waters. Fine sediment particles mobilized from soils and delivered to the stream network are also transported downstream and are allowed to settle in the stream network (van Gils et al. 2024). The PFAS are undergoing sorption to these particles following equilibrium partitioning parameterized by the partition coefficients reported earlier. The fraction of the PFAS sorbed to particles is thus retained in the stream network. In addition, the transformation of precursors into end product PFAS is included in one case: the precursor NEtFOSAA is transformed into end product PFOS. The half-life of NEtFOSAA in surface waters is set to 7.5 days (Rhoads et al. 2008).

E.3. Results

E.3.1. Simulated concentrations; model evaluation

Simulated concentrations of the 10 PFAS were compared to observed concentrations at 4 locations, as shown in Figure E.6. These four locations are all in the main Danube branch or in larger tributaries and can be briefly characterized as follows:

- “Inn”: a relatively pristine alpine tributary draining parts of Austria and Germany.
- “Isar”: a strongly urbanized tributary in Germany draining the Munich urban centre.
- “Morava”: a larger tributary draining a relatively dry part of the catchment mostly on Czech territory including the city of Brno.
- “Budapest”: the outlet of the basin that collects the water from all tributaries.

Figure E.7 to Figure E.10 show the simulated concentrations over a period of 11 years (2012–2022), as well as the observed concentrations from the 2022–2023. Note that the plots for all four stations use the same vertical scale for the 10 individual PFAS. This allows a visual perception of less polluted and more polluted sites. In all plots, the LOQ is indicated by a dashed line.

The plots show that for the majority of the 40 substance-station combinations, the model offers a reasonable representation of observed concentration levels and ranges.

E.3.2. Emission inventory

Figure E.11 provides the distribution of the emissions to surface waters over the modelled pathways P1-P10 (see main text, Section 4.2). This distribution varies significantly between individual PFAS. Dominant pathways are P3 (surface runoff), P4 (subsurface flow), P8 (WWTPs) and P10 (industry).

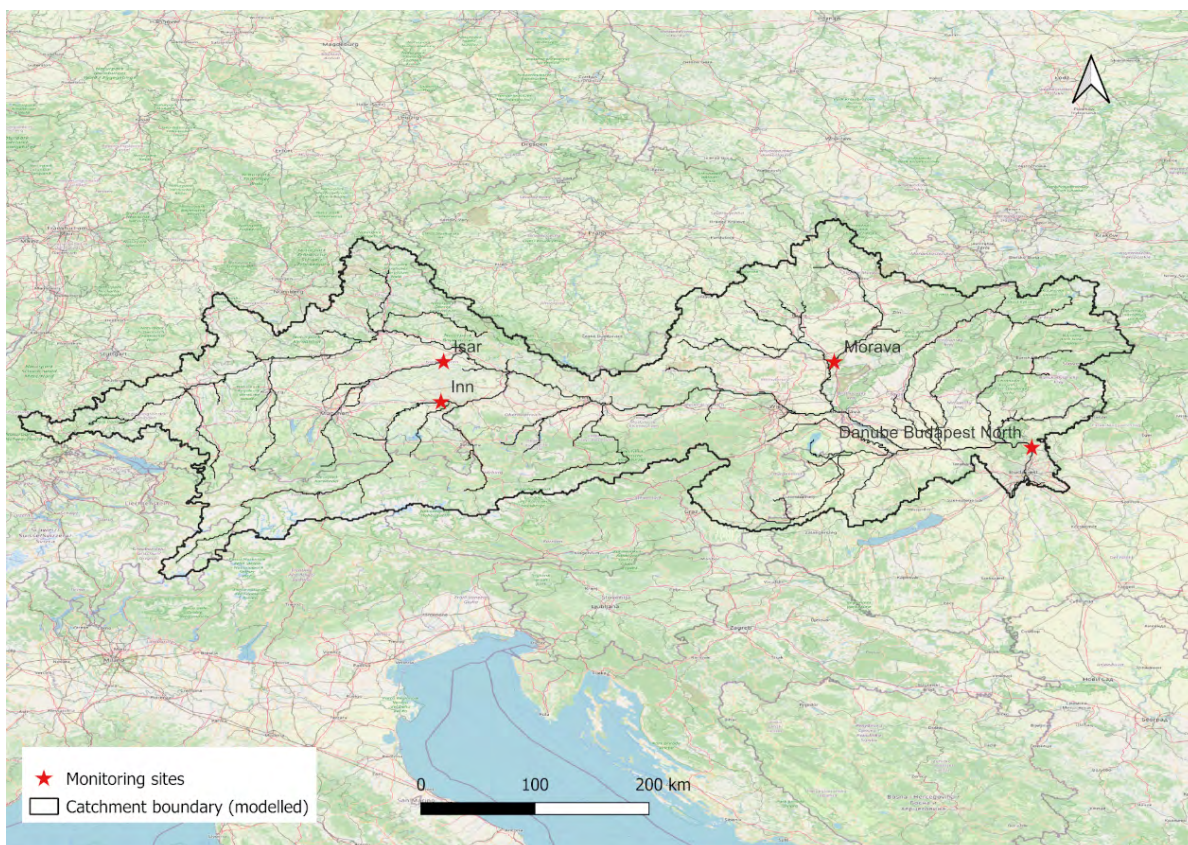


Figure E.6.: Location of specific monitoring sites considered for model evaluation

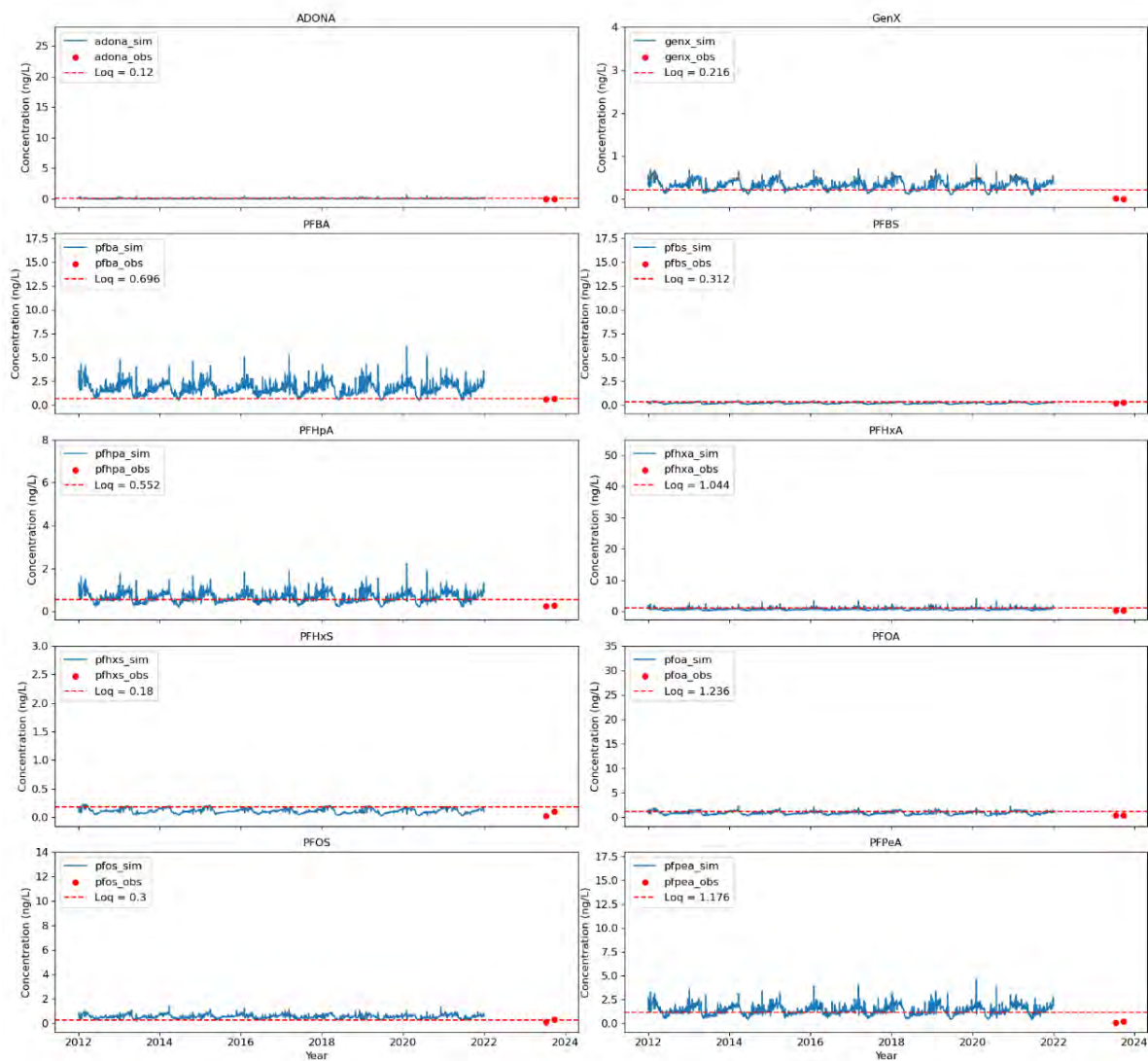


Figure E.7.: Modelled versus observed concentrations at the Inn monitoring site

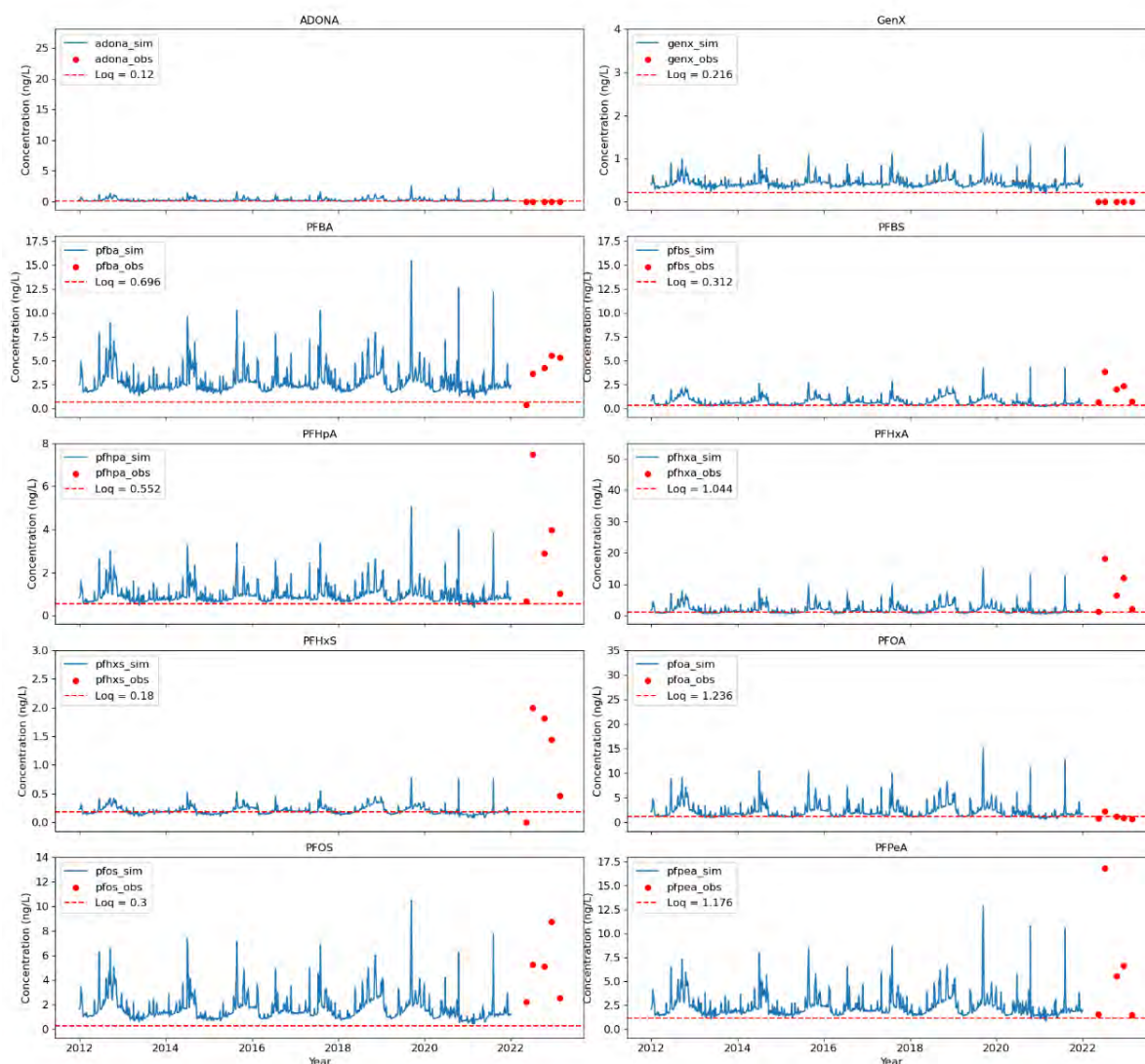


Figure E.8.: Modelled versus observed concentrations at the Morava monitoring site.



Figure E.9.: Modelled versus observed concentrations at the Isar monitoring site.

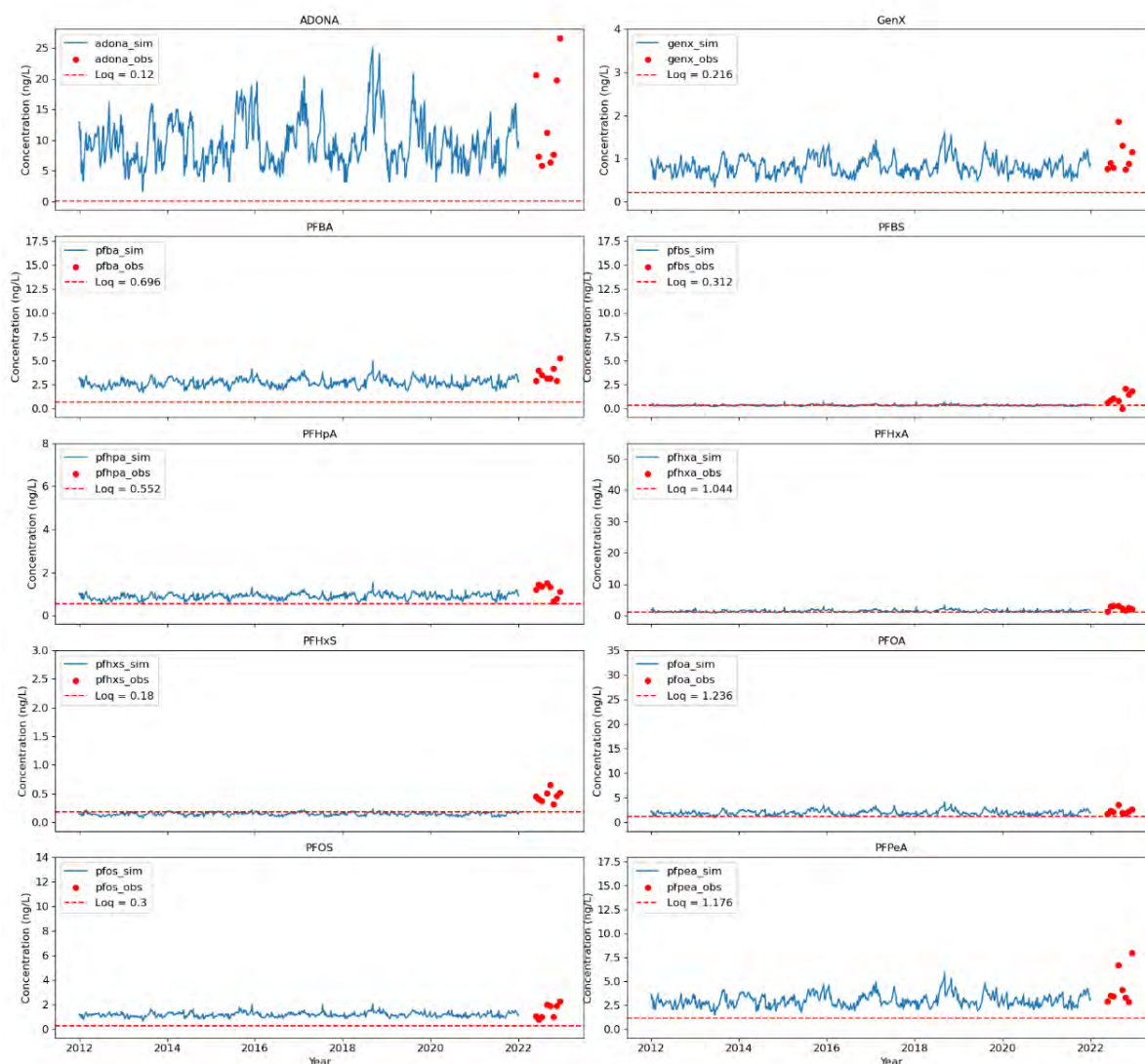
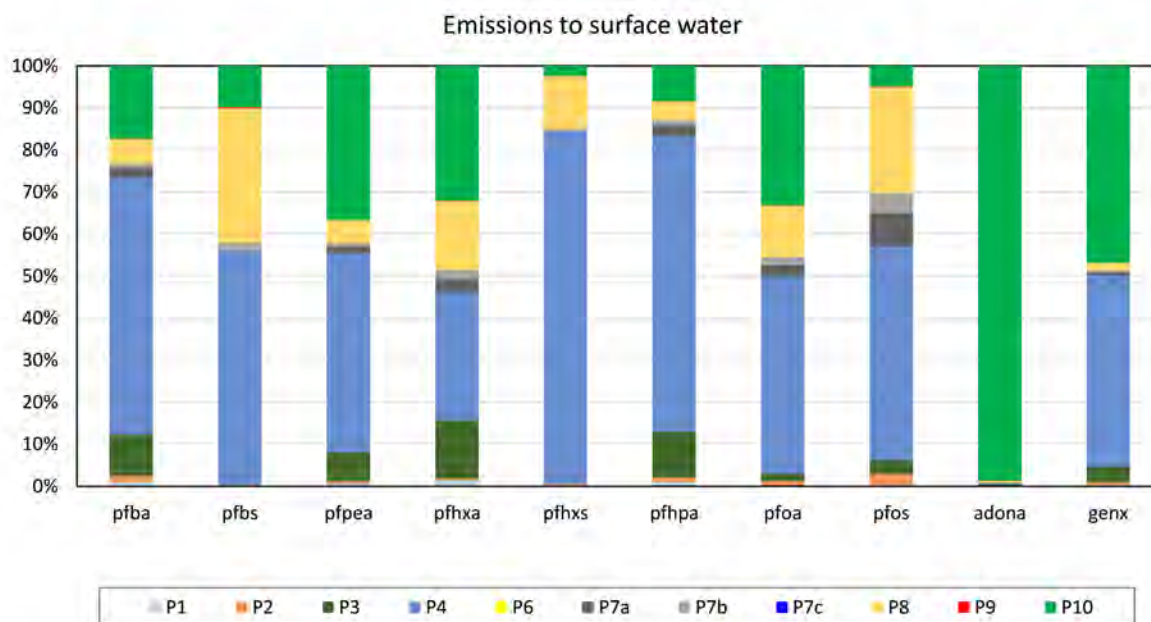


Figure E.10.: Modelled versus observed concentrations at the Budapest north monitoring site.

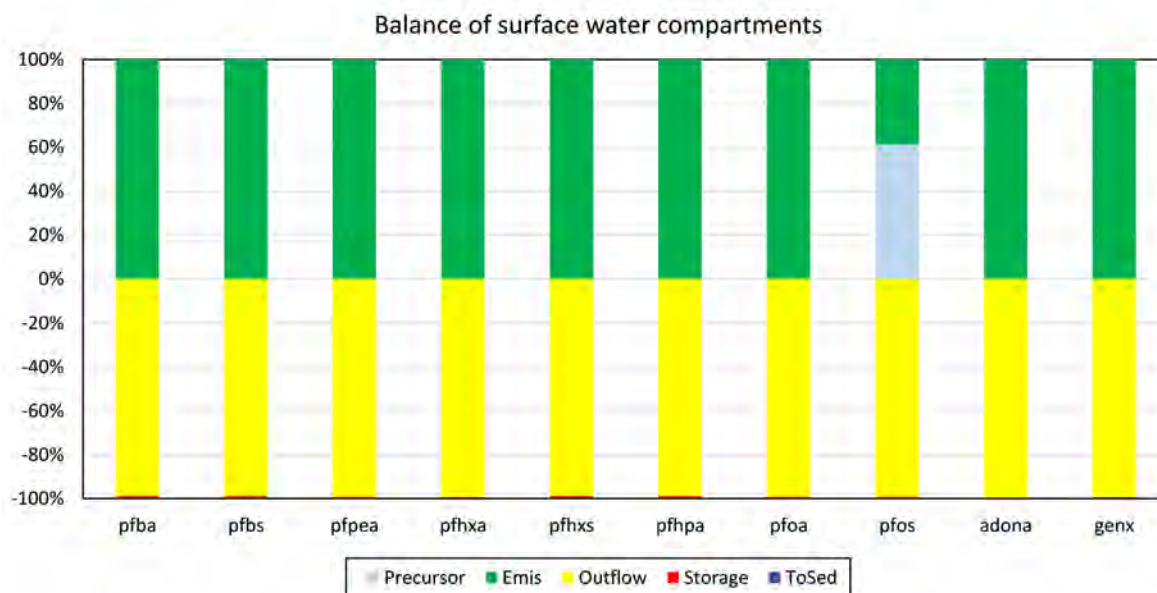


P1	Atmospheric deposition directly to surface water	P7	Storm water outlets (a) and combined sewer overflows (b) + unconnected sewers (c)
P2	Erosion	P8	Urban wastewater treated
P3	Surface runoff from unsealed areas	P9	Individual – treated and untreated – household discharges
P4	Interflow, drainage and groundwater	P10	Industrial wastewater treated
P5	n.a.	P11	Direct discharges from aquaculture, fisheries and other instream activities
P6	Surface runoff from sealed areas	P12	Natural background

Figure E.11.: Relative subdivision of total emissions aggregated over the Danube River catchment upstream of Budapest, averaged over simulated years 2012–2021.

E.3.3. Transport and fate in the river system

Figure E.12 shows the relative mass balance for the surface water compartment, aggregated over the whole domain. The balances are trivial for most simulated PFAS, with the total of emissions almost completely flowing out to the Middle Danube. The retention in aquatic sediments is in the order of 1% of the emissions for most PFAS. PFOS is the exception with about 60% of the outflow resulting from the precursor transformation.



“Precursor” = substance formed by transformation of precursor

“Emis” = emissions of substance

“Outflow” = mass flow via main Danube branch in a downstream direction

“ToSed” = retention/storage in aquatic sediments

Figure E.12.: Relative surface water compartment balances

E.3.4. Risk maps

The exposure of humans and the ecosystem have been tentatively calculated by evaluating:

- The sum of all modelled PFAS concentrations, that should not exceed 100 ng L⁻¹ to satisfy the Drinking Water Directive quality standard (Figure E.13).
- The sum of all modelled PFAS concentrations, weighed with their relative potency factor, the average value of which should not exceed 4.4 ng L⁻¹ PFOA eq. to satisfy the provisional WFD EQS (Figure E.14).

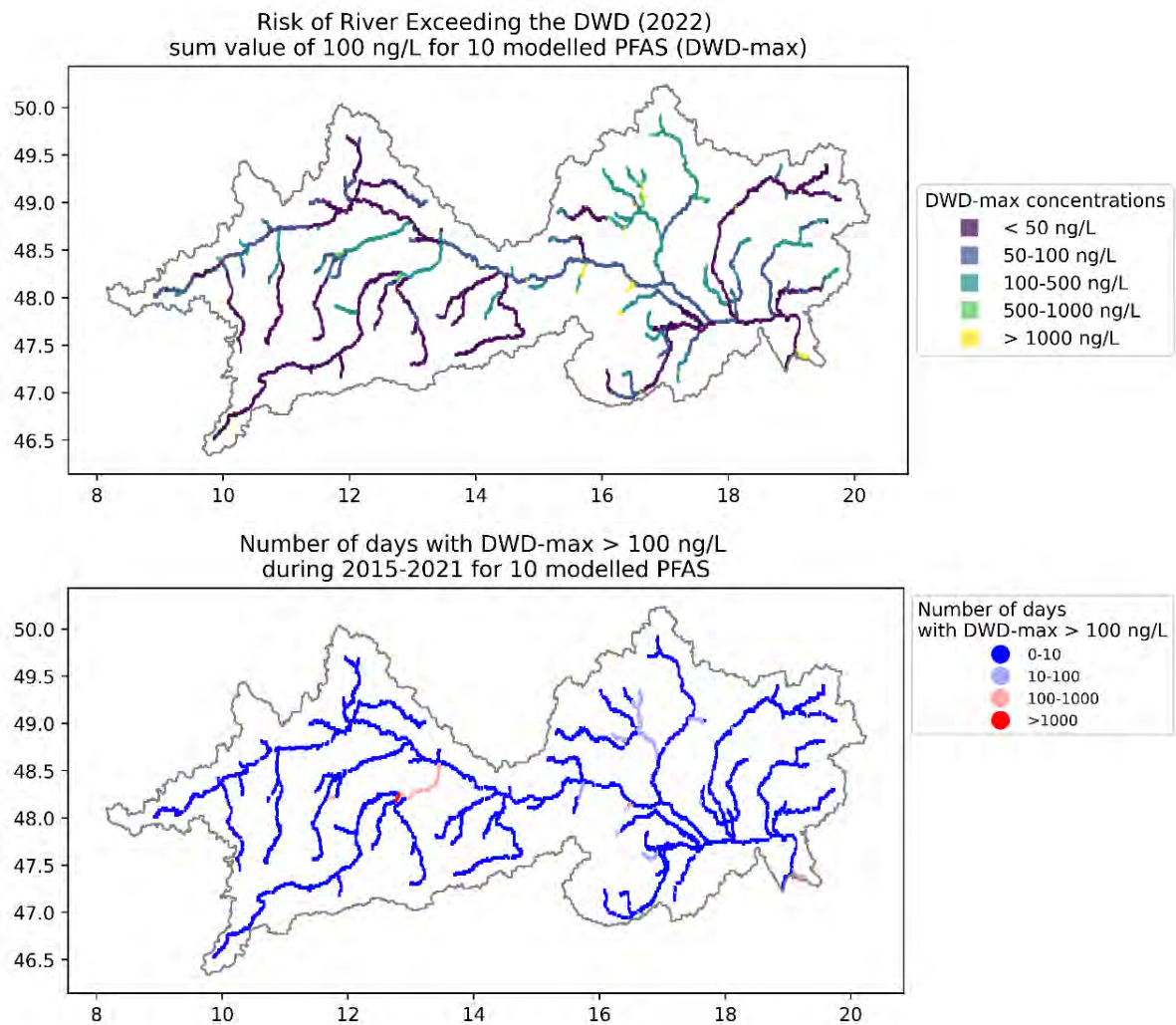


Figure E.13.: Maximum value of the sum of concentrations of 10 modelled PFAS (top) and the duration of exceedance of the 100 ng/L threshold included in the EU drinking water directive (DWD) (bottom).

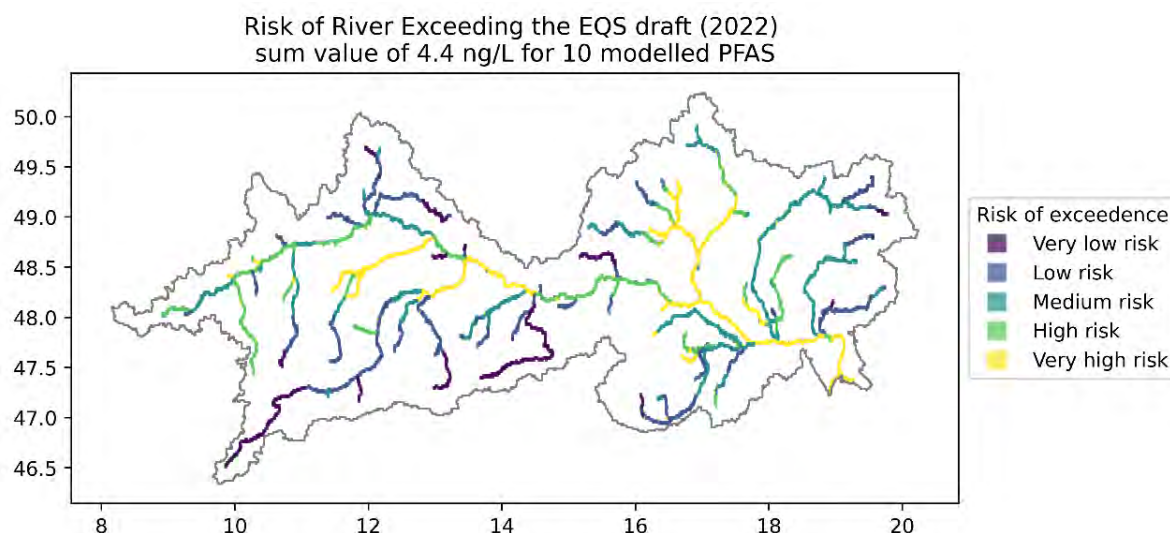


Figure E.14.: Risk of exceedance of the proposed EU Water Framework Directive environmental quality standard based on PFOA equivalent weighted concentrations of 10 PFAS

E.4. Acknowledgements

The authors thank Matthias Zessner, Steffen Kittlaus, Meiqi Liu and Thomas James Oudega of TU Wien for providing data and for the exchanges on methods and results of the watershed modelling tasks.

References

- Boisgontier, H. and J. van Gils (2020). “Physics-based basin-scale modelling of water quantity and sediment dynamics using wflow”. In: *Proceedings of the 22nd IAHR-APD Congress 2020*. Sapporo, Japan (cit. on p. 173).
- Buchhorn, M., B. Smets, L. Bertels, B. De Roo, M. Lesiv, N. E. Tsendbazar, M. Heold, and S. Fritz (2020). *Copernicus Global Land Service: Land Cover 100: collection 3: epoch 2015: Globe*. DOI: 10.5281/zenodo.3939038 (cit. on p. 175).
- Copernicus Climate Change Service (C3S) (2017). *ERA5: Fifth generation of ECMWF atmospheric reanalyses of the global climate*. URL: <https://cds.climate.copernicus.eu/cdsapp> (cit. on p. 175).
- DELTAES (2025a). *D-Emissions, Water quality and aquatic ecology modelling suite, Assessment tool for the emitted pollution at catchment scale, user manual*. Version 7.00. URL: https://content.oss.deltares.nl/delft3d/D-Emissions_User_Manual.pdf (cit. on p. 173).
- DELTAES (2025b). *D-Water Quality, Water quality and aquatic ecology modelling suite, Versatile water quality modelling in 1D, 2D or 3D systems including physical, (bio)chemical and biological processes, user manual*. Version 5.06. URL: https://content.oss.deltares.nl/delft3d4/Delft3D-WAQ_User_Manual.pdf (cit. on p. 173).

- European Commission (EC) (2012). *Common Implementation Strategy for the Water Framework Directive (2000/60/EC) Guidance Document No. 28 Technical Guidance on the Preparation of an Inventory of Emissions, Discharges and Losses of Priority and Priority Hazardous Substances*. eng. Tech. rep. European Commission (EC). DOI: 10.2779/2764. URL: <https://data.europa.eu/doi/10.2779/2764> (visited on 01/15/2025) (cit. on p. 174).
- Eilander, D. and H. Boisgontier (2022). *HydroMT, Automated and reproducible model building and analysis*. DOI: 10.5281/zenodo.6961871. URL: <https://github.com/Deltares/hydromt> (cit. on p. 175).
- Hengl, T., J. M. De Jesus, G. B. M. Heuvelink, M. Ruiperez Gonzalez, M. Kilibarda, A. Blagotić, W. Shangguan, M. N. Wright, X. Geng, B. Bauer-Marschallinger, et al. (2017). “SoilGrids250m: Global gridded soil information based on machine learning”. In: *PLoS ONE* 12.2. URL: <https://soilgrids.org> (cit. on p. 175).
- Hiebl, J. and C. Frei (2018). “Daily precipitation grids for Austria since 1961—development and evaluation of a spatial dataset for hydroclimatic monitoring and modelling”. In: *Theoretical and Applied Climatology* 132.1-2, pp. 327–345. ISSN: 0177-798X. DOI: \url{10.1007/s00704-017-2093-x}. URL: <https://www.zamg.ac.at/cms/en/research/climate/spatial-climate-datasets/spartacus> (cit. on p. 177).
- Hundecha, Y., B. Arheimer, C. Donnelly, and I. Pechlivanidis (2016). “A regional parameter estimation scheme for a pan-European multi-basin model”. In: *Journal of Hydrology: Regional Studies* 6, pp. 90–111. DOI: 10.1016/j.ejrh.2016.04.002 (cit. on p. 174).
- Imhoff, R. O., W. J. van Verseveld, B. van Osnabrugge, and A. H. Weerts (2020). “Scaling point-scale (pedo)transfer functions to seamless large-domain parameter estimates for high-resolution distributed hydrologic modeling: An example for the Rhine river”. In: *Water Resources Research* (cit. on p. 175).
- Kittlaus, S., M. Clara, J. van Gils, O. Gabriel, M. B. Broer, G. Hochedlinger, et al. (2022). “Coupling a pathway-oriented approach with tailor-made monitoring as key to well-performing regionalized modelling of PFAS emissions and river concentrations”. In: *Science of The Total Environment* 849, p. 157764 (cit. on p. 181).
- Kovacs, A., J. van Gils, S. Loos, O. Zoboli, M. Zessner, S. Kittlaus, N. Weber, et al. (2023). *Danube River Basin Scale Assessment Report, Annex to Output T3.2 of the DanubeHazard m3c project*. Vienna, Austria: International Commission for the Protection of the Danube River (cit. on pp. 174, 180, 182, 183).
- Lehner, B., C. Reidy Liermann, C. Revenga, C. Vörösmarty, B. Fekete, P. Crouzet, et al. (2011). “High-resolution mapping of the world’s reservoirs and dams for sustainable river-flow management”. In: *Global Dam Watch*. Available at <http://globaldamwatch.org/grand/> (cit. on p. 175).
- Messenger, M. L., B. Lehner, G. Grill, I. Nedeva, and O. Schmitt (2016). “Estimating the volume and age of water stored in global lakes using a geo-statistical approach”. In: *Nature Communications* 13603. DOI: 10.1038/ncomms13603. URL: <https://www.hydrosheds.org/page/hydrolakes> (cit. on p. 175).
- Myneni, R. (2015). *MODIS/Terra+Aqua Leaf Area Index/FPAR 4-Day L4 Global 500 m SIN Grid*. DOI: 10.5067/MODIS/MCD15A3H.006 (cit. on p. 175).
- Pesaresi, M., A. Florczyk, M. Schiavina, M. Melchiorri, and L. Maffenini (2019). *GHS settlement grid, updated and refined REGIO model 2014 in application to GHS-BUILT R2018A and GHS-POP R2019A, multitemporal (1975-1990-2000-2015), R2019A*. DOI: 10.2905/42E8BE89-54FF-464E-BE7B-BF9E64DA5218. URL: <http://data.europa.eu/89h/42e8be89-54ff-464e-be7b-bf9e64da5218> (cit. on p. 179).

- Rhoads, K. R., E. M.-L. Janssen, R. G. Luthy, and C. S. Criddle (2008). “Aerobic Biotransformation and Fate of N-Ethyl Perfluorooctane Sulfonamidoethanol (N-EtFOSE) in Activated Sludge”. In: *Environmental Science & Technology* 42.8, pp. 2873–2878. DOI: 10.1021/es702866c (cit. on p. 185).
- Schiavina, M., S. Freire, and K. MacManus (2019). *GHS population grid multitemporal (1975, 1990, 2000, 2015) R2019A*. DOI: 10.2905/42E8BE89-54FF-464E-BE7B-BF9E64DA5218. URL: <http://data.europa.eu/89h/0c6b9751-a71f-4062-830b-43c9f432370f> (cit. on p. 179).
- Smits, J. G. C. and J. K. L. van Beek (July 2013). “ECO: A Generic Eutrophication Model Including Comprehensive Sediment-Water Interaction”. en. In: *PLOS ONE* 8.7. Publisher: Public Library of Science, e68104. ISSN: 1932-6203. DOI: 10.1371/journal.pone.0068104. URL: <https://journals.plos.org/plosone/article?id=10.1371/journal.pone.0068104> (visited on 01/15/2025) (cit. on p. 173).
- Sosnowska, A., T. Puzyn, W. Peijnenburg, and P. Wassenaar (2024). *PROMISCES Deliverable D2.1 - Toolbox improved in silico models for identification of PMT properties*. Tech. rep. QSARLab and RIVM. DOI: 10.5281/zenodo.14800915. URL: https://promisc.es/Results/_/D2.1.pdf (cit. on p. 184).
- US EPA, O. (2024). *CompTox Chemicals Dashboard*. en. Data and Tools. URL: <https://www.epa.gov/comptox-tools/comptox-chemicals-dashboard> (visited on 01/15/2025) (cit. on p. 184).
- van Gils, J., H. Boigontier, L. Buckman, S. Weyrauch, T. Reemtsma, T. Barber, and K. Unice (2024). “Management-oriented modelling of tire and road wear particle fate & transport in the terrestrial and freshwater environment with a global perspective”. Submitted to *Science of the Total Environment* (cit. on p. 185).
- van Gils, J., L. Posthuma, I. T. Cousins, W. Brack, R. Altenburger, H. Baveco, et al. (2020). “Computational material flow analysis for thousands of chemicals of emerging concern in European waters”. In: *Journal of Hazardous Materials* 397, p. 122655. DOI: 10.1016/j.jhazmat.2020.122655 (cit. on p. 180).
- Verseveld, W. J. van, A. H. Weerts, M. Visser, J. Buitink, R. O. Imhoff, H. Boigontier, L. Bouaziz, D. Eilander, M. Hegnauer, C. ten Velden, and B. Russell (Apr. 2024). “Wflow_sbm v0.7.3, a spatially distributed hydrological model: from global data to local applications”. English. In: *Geoscientific Model Development* 17.8, pp. 3199–3234. ISSN: 1991-959X. DOI: 10.5194/gmd-17-3199-2024 (cit. on pp. 173, 174).
- Wintersen, A., L. Oste, R. van der Meiracker, P. van Breemen, G. Roskam, and J. Spijker (2020). *Verschil in uitloging van PFAS uit grond en bagger*. Tech. rep. Rijksinstituut voor Volksgezondheid en Milieu (RIVM). DOI: 10.21945/RIVM-2020-0102. URL: <https://rivm.openrepository.com/handle/10029/623865> (visited on 01/15/2025) (cit. on p. 184).
- Yamazaki, D., D. Ikeshima, J. Sosa, P. D. Bates, G. H. Allen, and T. M. Pavelsky (2019). “MERIT Hydro: A high-resolution global hydrography map based on latest topography datasets”. In: *Water Resources Research*. DOI: 10.1029/2019WR024873. URL: http://hydro.iis.u-tokyo.ac.jp/~yamada/MERIT_Hydro/ (cit. on p. 175).

F. Case Study #2: MODFLOW model of the Szentendre Island in Budapest

Authored by: Peter Vermeulen, Gijs Janssen

Deltares. Boussinesqweg 1, Delft, the Netherlands

As a hydrological basis for the transport modelling approaches (both the 1D and 3D approach) a regional groundwater flow model of the entire Danube island of Szentendre was constructed in MODFLOW (as implemented in the iMOD modelling framework (Vermeulen and Roelofsen 2024) and calibrated.

The geological basement of Szentendre Island consists of Tertiary marine sediments (Tard Clay). This formation is dominantly argillaceous silt; its thickness varies between 90 and 130 m. The basement is topped by fluvial gravels and sands of Pleistocene age. The immediate subsurface consists of hardly permeable formations such as muddy sands, soils and floodplain horizons with semi- consolidated shifting sand layers. In the watercourse of the Danube, the gravel and sand are covered by only a thin filtering layer, which clears the river water entering the porous sediments of physical and chemical as well as biological contaminants (Kármán et al. 2014).

The 3D MODFLOW model consists of 6 model layers of 2 to 4 m thickness and has a horizontal model resolution of 50×50 m. The subsurface model was constructed from available borehole information using Indicator Kriging. This was first done for model layers of 0.5 m thickness. To the different lithologies hydraulic conductivity values were assigned, which were later upscaled to the 6 MODFLOW model layers.

The model is encapsulated by the Danube river all around. Daily varying river water levels have been assigned. The Danube river is the only source for groundwater to the aquifers and this amount is strongly affected by the extraction wells along the Danube, see Figure F.1 (left). Strong inflows of $>50 \text{ m}^3/\text{d}/2500 \text{ m}^2$ appear at various locations. The computed groundwater levels show significant drawdowns to the extraction wells since there is no recharge from above, see Figure F.1. At a depth of 100 m+MSL (MSL stands for Mean Sea Level; the actual reference datum here is mBf which stands for mean Baltic sea level) the groundwater level is lower than 100 m+MSL at several locations. This causes the model to be dry and therefore those elements do not contribute to the groundwater flow. The largest drawdowns can be found at the south of the Danube island of Szentendre.

The model has been calibrated against head measurements in the period 2010–2024 on a daily base. Those measurements consist of both monthly and daily observations. For the calibration three types of parameters has been optimized:

- the horizontal permeability is subdivided into 6 categories of \log_{10} -values for permeability. So, one category describes permeability between 0.001 and 0.01 m/d and the next category those from 0.01 up to 0.1 m/d and so on;
- storage coefficient is subdivided into two categories, one for the specific yield and one for the storage coefficient;
- the riverbed resistance of the Danube is subdivided into 7 areas around the Danube island.

From the calibration it appeared that the most sensitive parameters are the horizontal permeability of 10 m/d and 100 m/d. The optimization increases this category with a factor of 4 and 2.5, respectively. The next most sensitive parameter category are the river resistances which were increased as well as decreased. Especially at the north- and northwest of the Danube island (including Tahi) the resistance is decreased (from 1 day to 0.75 days) and at the east side of the island (including Surány), decreased (from 1 to 10 days). The storage coefficients appeared to be of no significance in the calibration and have not been modified, i.e. they were kept at the initial estimates of (specific yield) 0.15 and (specific storage) 0.00001.

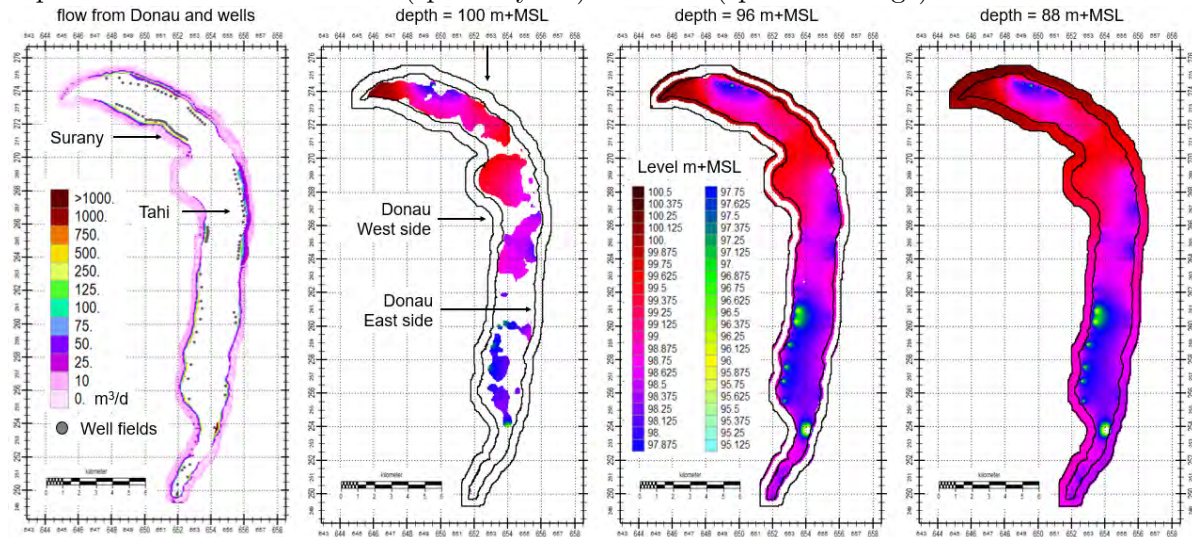


Figure F.1.: The first image on the left shows the layout of the Danube river and the volume of surface water (m^3/d) that flows into the subsoil. It also shows the location of the extraction wells, and particularly those for Surány and Tahi. The other images show the average computed groundwater levels at different depths.

The result after the calibration is given for four time series in Figure F.2. For the period February 2022 up to September 2023 a high-frequent monitoring program has been carried out. The model is well capable of reconstructing this highly frequent monitoring (Tahi MW2 and Surány MW2). The overall dynamics are well described, as well as the top levels (peaks). Lower groundwater levels are somewhat underestimated in the model. Two other measurement locations (F.13 and S_43.A) illustrate that the long-term behaviour of the model resembles the observations as well.

The overall statistics of the computed residuals between the computed groundwater levels and the measurements is given in Figure F.3. The overall average residual is 0.08 m; this value is actually minimized in the calibration and the histogram shows a pattern close to a normal

distribution. This is a direct result of the automatic calibration which minimizes the residual as a linear regression and strives to a minimal quadratic error. It indicates that the overall computed groundwater levels are slightly too high. Especially this is the case for Surány in which the groundwater levels are on average 0.5 m too high. It is important to notice that the residuals are computed on a 50 x 50 m resolution and observations directly in the extraction well are often lower than can be represented with the 50 x 50 m model, as they are influenced by a local cone of depression. This is apparently more the case for Surány than for Tahi. Excluding those observations from the statistics, the residuals of the regional model give a more accurate and fair representation of the model's performance. It is noteworthy that observation Tahi_MW1 gave a 1 m residual as Tahi_MW2 gave an almost perfect match, whereas the distance between both observations is less than 20 m. For this reasons Tahi_MW1 is left out of the statistics. The updated statistics are shown in the second row of Figure F.3. The overall residual, for the regional model, is now -0.13 m and the absolute residual 0.31 m. For Tahi and Surány the representative statistics improve as well.

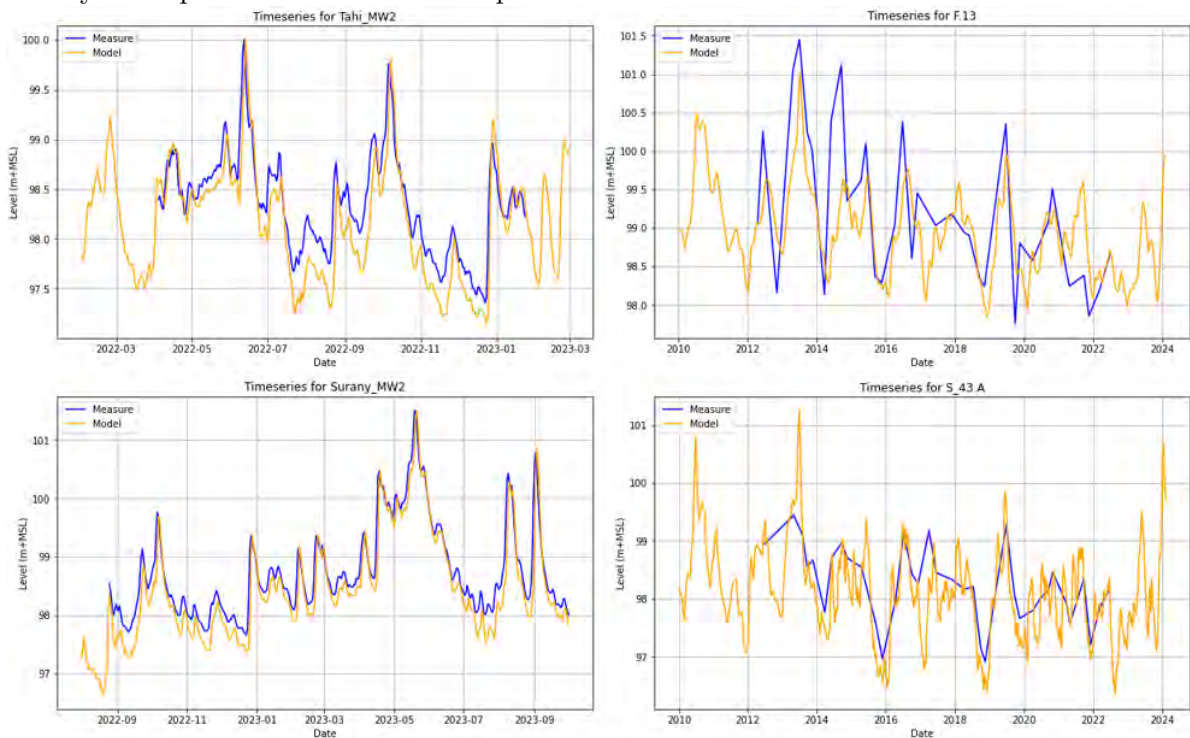


Figure F.2.: Showing timeseries of measured (blue) and computed (orange) groundwater levels (in mBf = local reference datum) for (top row) Tahi and (bottom row) Surány.

So, by excluding the local drawdown measurements (which are unrealistic to capture with the regional model), the statistics show that the regional model is actual very well capable of simulating the regional flow conditions. The regional groundwater flow model provides the data basis as well as the boundary conditions for two local cut-out models which are used to study the reactive PFAS transport during the bank filtration process. Those models run on a resolution of 5 x 5 m and can represent the local drawdown much better.

For insight in the flow situation, particle tracking has been performed on the two cut-out models for Tahi and Surány. Particles were released in the numerical flow field from all boundary conditions, and tracked until they reached their end destinations. The particles that ended in

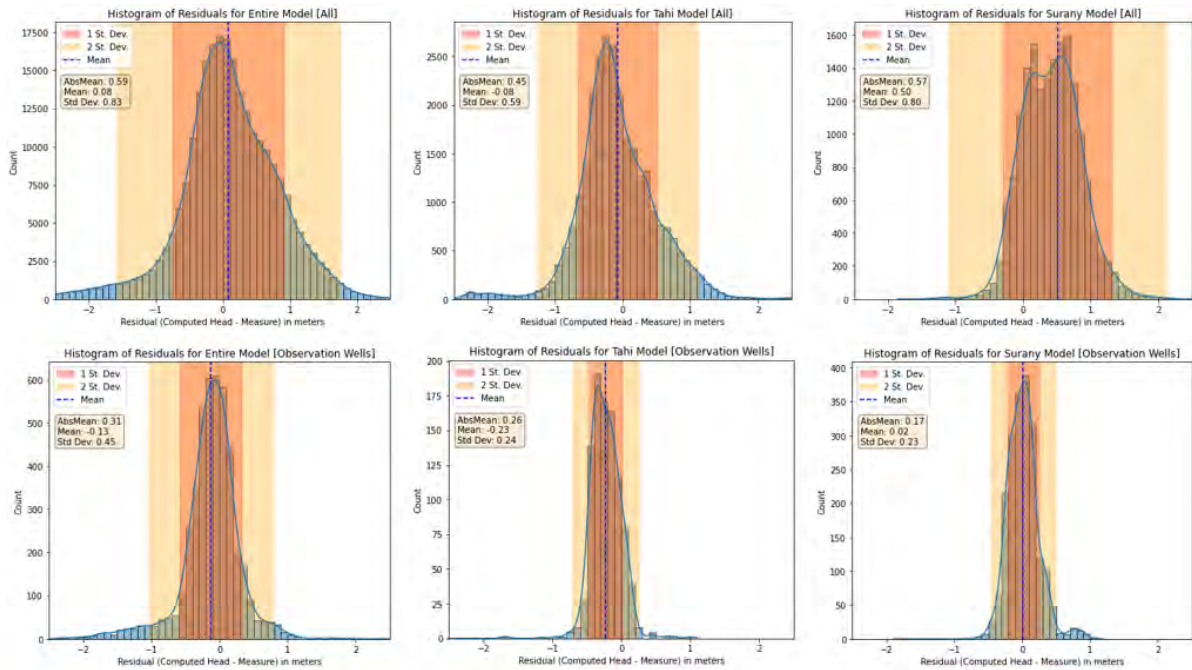


Figure F.3.: Showing the overall statistics of the residuals of the compute heads minus the measured heads. Upper row: including all measurements. Lower row: excluding the measurements at the pumping well locations. Left column: entire model. Middle column: extent of Tahi cut-out model. Right column: extent of Surány cut-out model.

the wells that are subject of this study (Tahi I. 5 and Surány 12) are visualised in Figure F.4.

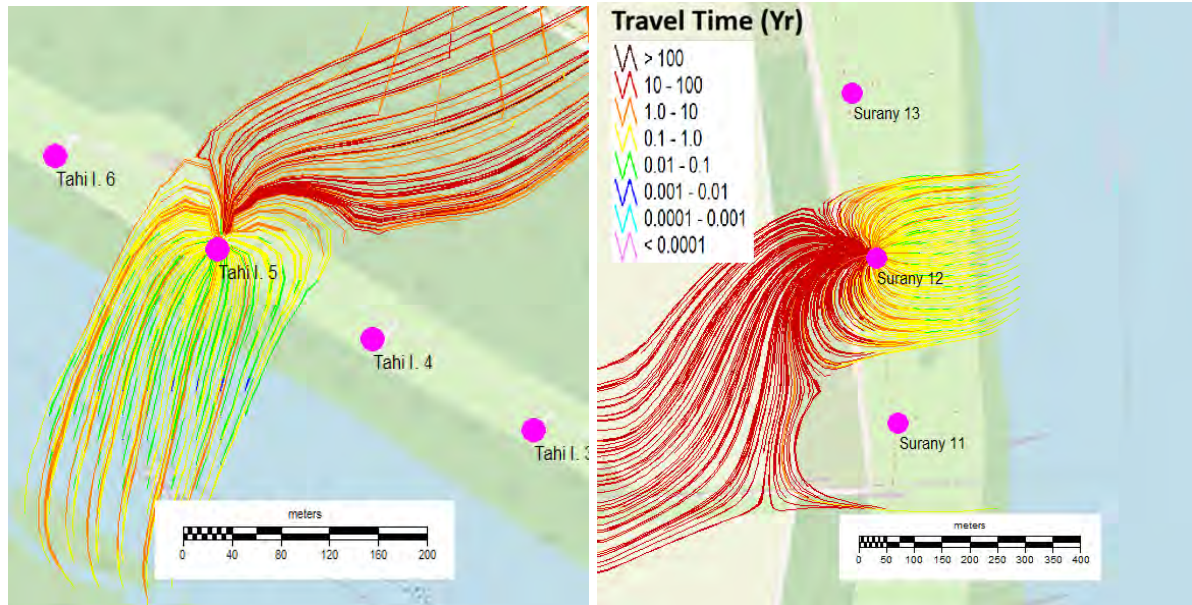


Figure F.4.: Schematized streamline pattern for the cut-out models, showing the flowlines ending in the investigated pumping wells Tahi1-5 (left) and Surány 12 (right). The legend shows the travel time from source (submodel boundary or river) to well. For reasons of clarity of the figures, only show a selection of the calculated streamlines is shown. The streamlines have been calculated for a longyear averaged steady-state situation (2012–2023).

Table F.1 presents some characteristics of the flow situation as derived from the streamline simulation. From the table it becomes apparent that for the Tahi well, only 5% of the pumped water does not originate from the nearby river bank, but from the cut-out model's boundaries. For Surány this contribution is a bit higher, i.e. 13%. For Tahi this indicates that the choice of model boundary concentrations (assumed zero here) will not significantly affect the results, if the assumption were to be incorrect. For Surány the contributions other than from the nearby river bank is something to keep in mind; however (very) long travel times are associated with these contributions (decades), thus still justifying assuming concentrations of zero associated to them.

Table F.1.: Characteristics of the flow situation as derived from the particle tracking simulations

	Tahi	Surány
Well flux (model input)	1698 m ³ /d	2289 m ³ /d
Total flux of streamlines	1698 m ³ /d	2274 m ³ /d
Total flux of streamlines from nearby river bank	1610 m ³ /d (95%)	1986 m ³ /d (87%)
Flux-weighted median travel time	28 days	165 days

References

- Kármán, K., P. Maloszewski, J. Deák, I. Fórizs, and C. Szabó (2014). “Transit time determination for a riverbank filtration system using oxygen isotope data and the lumped-parameter model”. In: *Hydrological Sciences Journal* 59.6, pp. 1109–1116. DOI: 10.1080/02626667.2013.808345 (cit. on p. 197).
- Vermeulen, P. and F. Roelofsen (2024). *IMOD User Manual*. Version 5.6.1. (Cit. on p. 197).

G. Scenario modelling for the upper Danube basin

Authored by: ¹Meiqi Liu, ²Thomas Oudega, ³Devanshi Pathak, ¹Steffen Kittlaus, ³Erwin Meijers, ²Ali Obeid, ³Hélène Boisgontier, ³Corine ten Velden, ³Sebastian Hartgring, ²Julia Derx, ³Jos van Gils and ¹Matthias Zessner

¹TU Wien, Institute for Water Quality and Resource Management, Austria

²TU Wien, Institute of Hydraulic Engineering and Water Resources Management, Austria

³ Deltares. Boussinesqweg 1, Delft, the Netherlands

G.1. General Considerations

The scenarios are not intended to be realistic predictions of future development, as predictions of future development are not available for many model inputs to model such realistic pathways. Instead, the scenarios are intended to show how hypothetical situations would be reflected in model results, and what kind of questions could be answered by the model train if future developments were better known.

- Scenarios are provided in the form of small stories.
- Based on the stories, assumptions are made regarding model inputs.
- Based on this scenario definition, it is documented which effects of a scenario were considered in the model and which effects were not considered (because not feasible or considered not relevant).
- Not every scenario needs to include the model train (some scenarios can be done with the bank filtration models only).
- Main scenarios contain sub-scenarios accounting for different hydrological conditions.

G.2. Reference situation

Emissions are modelled for the period 2015-2021 with the MoRE and PPM emission models for the upper Danube catchment. The hydrology of the models was derived from the W-FLOW model. Substance specific model input data were derived from monitoring data, mainly collected in 2022–2023.

Results of the MoRE model are reported as average of the 7 years modelling period in 3 model variants to account for input data uncertainty:

- best-case
- median-variant
- worst-case

All scenarios are based on the median variant; it can be assumed that uncertainty of the results for scenarios is at least as much as high as for the reference situation.

G.3. Baseline for Scenarios

The reference period model setup is used as the baseline for the scenarios, with the only change being that the PFAS production facility in Gendorf will close in 2025 and no further emissions from production are expected. However, emissions from the legacy contamination at the Gendorf site will continue to leach into rivers via groundwater.

For each scenario the impact of climate change on discharge is simulated as follows:

Changing climate conditions with changes in precipitation and temperature lead to changing flow conditions in rivers. Low flow periods are especially vulnerable to point source discharges as less dilution leads to higher concentrations in rivers. The changing climate may lead to changes in low flow periods or more severe low flow conditions (Laaha et al. 2016). As bank filtration sites are especially vulnerable to long periods of elevated concentrations the available historic flow data were investigated for a year which represents such critical conditions. As presented in Figure G.1, the year 2018 had a long duration of low flow but also significant high flow, while the year 2013 showed contrasting conditions with less extreme flows. Thus, the hydrological conditions of these years were chosen to represent pre-climate change (2013) and climate change (2018) conditions.

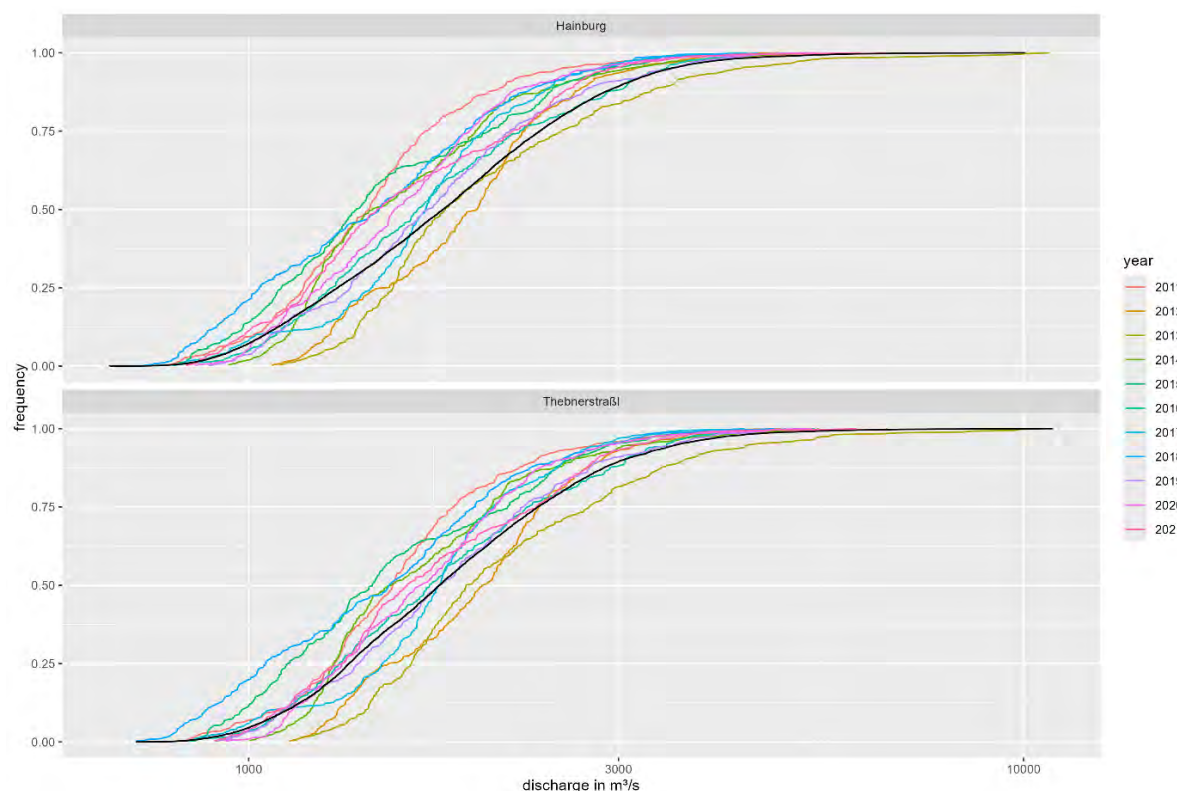


Figure G.1.: Evaluation of historic river gauge data at the Danube downstream of Vienna for critical flow conditions. The black line presents long-term average conditions (1977–2006 for Hainburg and 2000–2021 for Thebnerstraße).

G.3.1. Assumptions and implications for the models

The different hydrological conditions of pre-climate change and climate change were considered in the models without changing other variables in the model that could also be affected by a changing climate, e.g. concentration input data in pathways or per capita water consumption. Other variables that will change in the future, such as population density or PFAS use intensities, were also kept constant unless explicitly stated otherwise in the scenario description, as in most cases data availability is not sufficient to perform a reliable trend analysis on which to base predictions.

MoRE

The base model covers the period 2015–2021, and all scenarios are based on the median variant (base case) of this reference period. As the shutdown of PFAS production in the Gendorf facility was announced for 2025, this was included in the Baseline for all scenarios. Therefore, only the pathway P10b was removed from the model setup.

MoRE delivers mean annual concentrations and flows for the different hydrological conditions at the riverbank filtration sites.

PPM

The PPM model is a dynamic catchment water quality model that integrates PFAS emission sources and pathways. It is coupled with the W-FLOW hydrological model. The model setup covers the period from 2015 to 2021, providing time-series data of PFAS concentrations for this time frame at locations of interest. The PPM model is used to simulate elevation in PFAS concentrations at the riverbank filtration sites in response to the accidental spills at a location upstream.

RBF model

The RBF models took the output from the MoRe and PPM models to generate daily input concentrations for each scenario based on the delta-change compared to the reference period of the MoRe results (this is also the case for the WPC scenarios) (see Toolbox Chapter 6.2 for more information, Groot et al. 2025). The RBF models were then run for a pre- and post-climate change situation. In the latter, longer periods with reduced water levels may change the flow regime at bank filtration sites in Budapest and lead to increased impact from groundwater in the Danube Island, which shows elevated concentrations for some PFAS and lower concentrations for others.

The simulated concentrations in the PWs of Tahi and Surány in Budapest and in the farthest MW from the riverbank in Vienna, were processed to present for each scenario the resulting ΣPFAS_{10} and the ΣPFAS_{10} -PFOA-equivalent for the DWD and EQS guidelines, respectively.

G.4. Accidental spill scenario (AC)

Accidents happen. This scenario assumes a spill of PFAS into the Danube, based on the 2015 aqueous film forming foam (AFFF) spill in Port of Santos, Brazil (Pozo et al. 2022). In this event, a major chemical fire led to the discharge of 62000 L of AFFF into surface waters, over a 7-day period. The spill in this scenario is assumed to enter the Danube due to a large fire at the location of 48.277088, 14.349453 (WGS84), which is an industrial harbour area in Linz, Austria.

The scenario builds on the reference situation by adding especially high PFAS emissions for a limited time to the model. The question to be answered is: what would the effects of a spill like this be on the river Danube at Vienna and Budapest and the associated impact on the groundwater in Vienna and the abstraction wells of Budapest water works?

As the MoRE model with its annual time steps is not able to depict such an event, the PPM was used to model mixing and dilution in the Danube River to derive daily river concentrations at the bank filtration sites. The RBF model evaluated infiltration into the subsurface as well as subsequent transport to drinking water wells.

G.4.1. Sub scenarios: AC-highflow & AC-lowflow, old and new AFFFs

This scenario case was simulated for a high-flow (best-case) situation, as well as for a low-flow (worst-case) situation. AC-highflow was simulated starting in January 2013, and AC-lowflow will be simulated to start in July 2018.

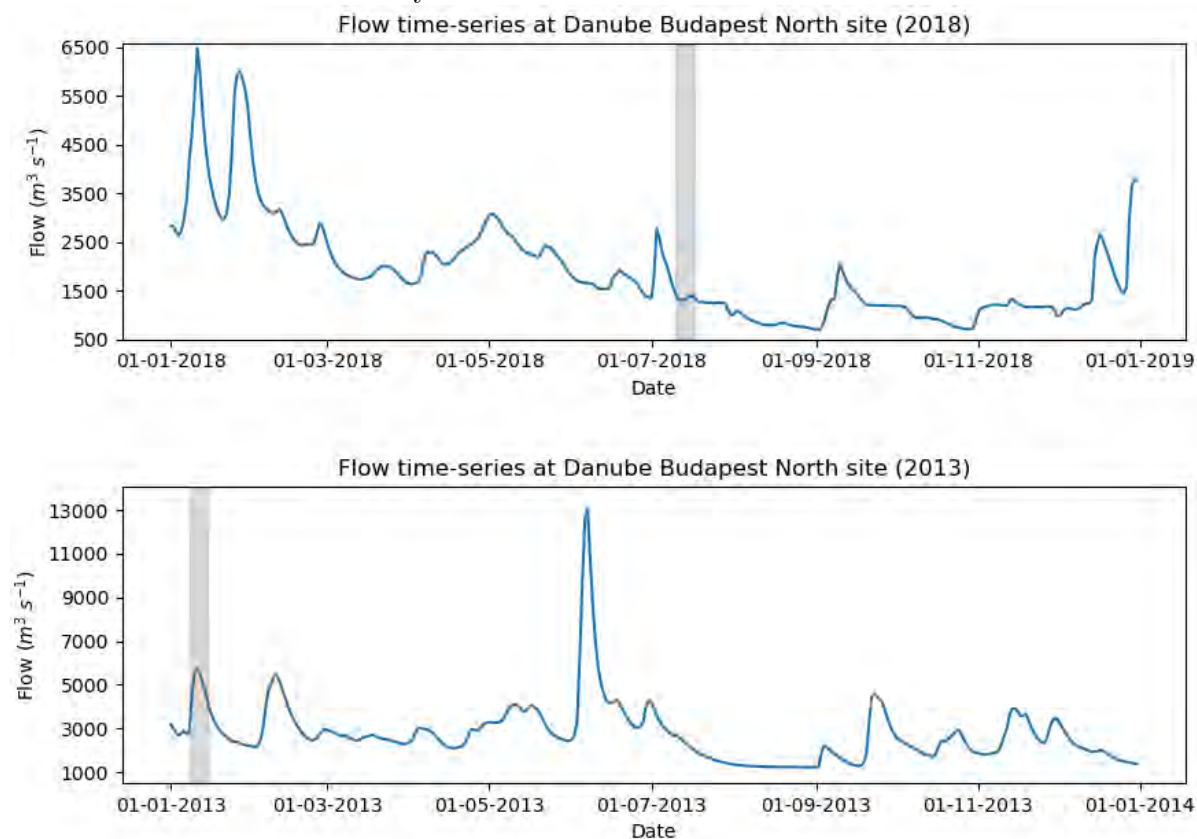


Figure G.2.: Flow time-series for AC-lowflow (2018) and AC-highflow (2013) scenarios, highlighting the spill period of 7 days

On top of that, two types of AFFFs were used: first, the older PFOS-based type that has been banned, and second, the newer type which is based on 6:2 FTS. Because the older foams are still in use on occasion (Jans and Berbee 2020; see also: Alaska DEC 2024), two accidental spills were simulated; one for each foam-type. This leads to four scenarios in total (Table G.1).

Because 6:2 FTS is not included in the list of 10 PFAS that are considered for the scenario analysis (and also not in the list of 24 PFAS used to calculate $\Sigma_{24}\text{PFOA}$ -equivalent PFAS according to EC COM(2022) 540 final, it will not be included directly in the interpretation of the results. However, 6:2 FTS is a precursor to other types of PFAS; here assumed to be PFHxS and PFPeA in equal ratio, with a transformation half-life of 3 days. Both of these substances are included in the Σ_{20} PFAS and the $\Sigma_{24}\text{PFOA}$ -equivalent PFAS, transformation processes were added in surface water modelling. In groundwater, because of the large travel times in comparison to the half-life of 6:2 FTS, transformation was assumed to be complete for all scenarios.

Table G.1.: Definition of sub scenarios for an accidental spill

	Scenarios with PFOS-based AFFF	Scenarios with 6:2 FTS-based AFFF
Scenarios for a high flow situation	1. AC-highflow + PFOS-based AFFF	2. AC-highflow + 6:2-FTS-based AFFF
Scenarios for a low flow situation	3. AC-lowflow + PFOS-based AFFF	4. AC-lowflow + 6:2-FTS-based AFFF

Table G.2.: AFFF composition. The new AFFF is an average of 8 modern AFFFs (Dauchy et al. 2017); the old AFFF composition is an average of 7 commercial AFFFs from 1992–2001 (Houtz et al. 2013)

New AFFF		Old AFFF	
Included PFAS	Concentration (mg/L)	Included PFAS	Concentration (mg/L)
6:2 FTSA	29	PFBS	71
6:2 FTSB	521	PFHxS	686
6:2 FtSaAM	67	PFOS	5643
<i>Total 6:2 FTS</i>	<i>617</i>	PFPeA	286
PFOS	5	PFHxA	114
		PFOA	100
Total PFAS:	622	Total PFAS:	6900

G.4.2. Assumptions and implications for the models

The composition of each foam-type was taken from the literature (Table G.2).

Table G.2 shows a 10 times higher concentration of total PFAS in the old AFFF as compared to the new AFFF. With 62000 litres spilled, this amounts to a total PFAS load of 37 kg for the new AFFFs (mostly 6:2 FTS), and 428 kg for the old AFFFs (mostly PFOS). This load was simulated to be discharged into the Danube River in 7 days.

For the RBF models, the spill output data of the PPM models was added on top of the background river concentrations of the BL scenarios to create the appropriate daily input concentrations for the Danube River.

G.4.3. Limitations

In reality, one cannot be certain of the PFAS compositions in Table G.2 (especially concerning the information that old AFFFs hold 10 times the amount of PFAS than new AFFFs), as the estimation of PFAS load from AFFFs presents a double limitation. The limitation is double because: first, the PFAS list is limited due to the list of targeted compounds by the studies from which the data were gathered, as these studies only target 20, 30, 40 PFAS, and hundreds of other non-targeted fluorochemical compounds might be present in AFFFs' formulations (Barzen-Hanson et al. 2017; D'Agostino and Mabury 2014). Total organofluorine contents quantified of AFFFs used in Canada ranged from 475 to 18000 mg F mL⁻¹ (Weiner et al. 2013). This is much more than any individual, or few individual PFAS that can be addressed here. The second limitation is in the limited list of 10 PFAS that is considered for this scenario, which does not always coincide with the PFAS measured by the studies. This means that the total PFAS in the new and old foams might be wildly different, but it does not necessarily mean that in reality one foam has more PFAS than the other. On top of this, one should be aware that literature studies' measurements of AFFF-composition are not always correct either. From Pozo et al. (2022): *"A ΣPFAS up to 3,200,000 µg/L were reported in concentrates of novel foams (Dauchy et al. 2017), which is 2000 times higher than the concentrations of ΣPFAS reported in this study. These results indicate that PFAS load reported in the major fire in Port of Santos may be underestimated, increasing the concern on the potential regional PFAS contamination."* However, for the purpose of this scenario, the estimations were considered sufficiently accurate.

G.5. Water pollution control 1 (WPC1)

Different measures could be implemented to reduce PFAS contamination in the Upper Danube Basin, which would address different pathways of surface water pollution and are associated with different time frames in respect to their effectiveness.

WPC1 focuses only on advanced wastewater treatment at municipal WWTP as it is proposed by the update of the Urban Waste Water Treatment Directive (EC COM(2022) 541 final). Currently the update of the Urban Waste Water Treatment Directive is negotiated on EU-Level. All WWTPs with > 100,000 p.e. (or > 150,000 p.e. according to more recent discussions) shall be equipped with a quaternary treatment for micro pollutant removal. A first version of the proposal focused on pharmaceuticals, for PFAS no elimination requirements but only monitoring is included. Smaller WWTP shall be equipped with a quaternary treatment in case of risk criteria (low dilution, not achieving the good status, impact on drinking water resources etc.).

This scenario assumes reduction of PFAS emissions from municipal waste water treatment according to technical possibilities for different PFAS-parameter. As ozonation has no clear effect on total PFAS, only activated carbon is relevant for PFAS and the scenario assumes solely implementation of activated carbon technology for all WWTP of > 10k p.e. Emissions via other pathways would stay unchanged. Requirements for CSO and rain water sewers will be revised as well in the new directive, but with less impact on PFAS emissions.

This scenario will be implemented using the MoRE emission model and concentrations at RBF sites will be fed into BF models.

This scenario will be combined with pre- and post-climate change hydrological conditions.

G.5.1. Assumptions and implications for the models

MoRE

A literature review was conducted to derive PFAS removal rates by typical application of activated carbon (as powdered activated carbon (PAC) or granulated activated carbon (GAC)) at municipal waste water treatment plants (Table G.3).

Based on this literature review the removal efficiency for all modelled compounds was estimated as presented in Table G.4.

Table G.4.: PFAS Removal efficiency assumed for activated carbon application on municipal WWTP.

PFBA	PFPeA	PFHxA	PFHpA	PFOA	PFBS	PFHxS	PFOS	ADONA	GenX
60%	60 %	60 %	60 %	60%	60%	60%	80%	20%	20%

This scenario assumes all WWTPs with >10,000 p.e. are upgraded with quaternary treatment. In addition to removing pathway P10b, removal efficiency for PFASs as given in Table G.4 were applied to emissions from pathway P8.

RBF-Models

Daily input concentrations were generated for the WPC scenarios in the same way as the BL scenarios (see above).

G.6. Water pollution control 2 (WPC2)

WPC2 scenario builds on the WPC1 scenario but assumes a much further going implementation of measures against diffuse PFAS emissions:

- banning of PFAS application for non-essential use
- groundwater remediation at hot spots of legacy pollution

A restriction proposal for PFAS was prepared by authorities in Denmark, Germany, the Netherlands, Norway and Sweden. It was submitted to ECHA on 13 January 2023. It aims to reduce PFAS emissions into the environment and make products and processes safer for people ECHA (2023). This ban of PFAS in many products could lead to a reduction of PFAS emissions from production and with certain time delay also consumptive use. This could reduce

Table G.3.: Removal efficiencies for PFAS reported in literature for adsorptive wastewater treatment steps. BV: Bed volumes

Technology	PFAS	Removal Efficiency	Data Source
GAC	PFOS	61% at 9700 BV	Inyang and Dickenson (2017)
	PFOA	35% at 9700 BV	
PAC	PFOS	6–52%	Mailler et al. (2015)
PAC	PFOS	53–92%, Median: 79%	Ulmer treatment; Rößler and Launay (2019)
	PFOA	31–77%, Median: 63%	
	PFBA	72–83%, Median: 81%	
	PFBS	41–75%, Median: 58%	
PAC	PFBA	Median: < 30% by 10 mg PAC/L, 30–60% by 20 mg PAC/L, < 30% by 30 mg PAC/L	Mannheim WWTP, Metzger et al. (2012)
	PFPeA	Median: < 30% by 10–30 mg PAC/L	
	PFHxA	Median: < 30% by 10–30 mg PAC/L	
	PFHpA	Median: < 30% by 10–20 mg PAC/L, 30–60% by 30 mg PAC/L	
	PFOA	Median: < 30% by 10 mg PAC/L, 30–60% by 20–30 mg PAC/L	
	PFBS	Median: < 30% by 10–30 mg PAC/L	
	PFHxS	Median: < 30% by 10 mg PAC/L, 30–60% by 20 mg PAC/L, < 30% by 30 mg PAC/L	
	PFOS	Median: < 30% by 10 mg PAC/L, 30–60% by 20 mg PAC/L, > 80% by 30 mg PAC/L	
	6:2 FTS	Median: < 30% by 10 mg PAC/L, 60–80% by 20 mg PAC/L, < 30% by 30 mg PAC/L	

emissions via point sources (WWPTs, PFAS-production sites) with some time delay, would not reduce diffuse pollution stemming from legacy contamination, but could reduce building up legacy pollution for the future.

Legacy pollution of PFAS is everywhere (soils, groundwater) but specifically hot spots (use of AFFF for firefighting or training, municipal landfills) are considered as potentially significant sources. To assess their impact on a regional catchment scale is still a challenge. Nevertheless, groundwater remediation at hot spots of legacy pollution will be a further challenge that could reduce pollution of river Danube on a long term run and could be considered in this scenario, even if in a best-case only semi-quantitative assessment will be possible.

In this scenario the catchment model will be used to calculate potential reductions of PFAS concentrations in river Danube at different time scales under assumption of different pollution control measure. Reduced concentrations in river Danube will serve as inputs for related changes of concentrations at the drinking water wells.

As in scenario WPC1 all municipal treatment plants with a capacity of >10k p.e. are equipped with activated carbon treatment.

G.6.1. Assumptions and implications for the models

MoRE

The restriction of PFAS application in many areas leads to reduced emissions from production, product application and disposal. An emission reduction of 70% is assumed. Thus, emissions via the pathways industrial direct dischargers, atmospheric deposition, sewer systems and urban waste water treatment plants (prior to advanced treatment) is cut by 70% (P1, P7a, P7b, P7c, P8 - prior to reduction by advanced treatment step, P10). The pathways “erosion”, “surface runoff from unsealed areas”, “groundwater background”, “groundwater legacy pollution from Gendorf” and “diffuse pollution from inhabitants” are considered unaffected by the ban of PFAS, as the reaction time of these systems might be very long.

The application of groundwater remediation technologies is implemented in the model following the assumptions, that 80 percent of contamination sites can be located, 60% of located contamination can be treated and treatment removes 80% of PFAS, resulting in an emission mitigation of 38%. This cut of emissions is applied to the pathways “groundwater background”, “groundwater legacy pollution from Gendorf” and “Inhabitant-specific diffuse pollution via groundwater” (P4a, P4b, P4c).

The reduction efficiency of emissions in municipal wwtp is assumed to be the same as in scenario WPC1.

RBF model

Daily input concentrations were generated for the WPC scenarios in the same way as the BL scenarios (see above). Background groundwater concentrations in Budapest were assumed to be 0, as a consequence of groundwater remediation.

G.7. Summary of Scenarios

Table G.5.: Summary of Scenarios

Scenario group	Scenario	Climate/ river dis- charge	PFAS produc- tion Gen- dorf	Legacy pollution	Accidental spill	Advanced treat- ment (PFAS)	PFAS use re- striction
Reference period (Ref)		based on his- torical data	Yes	current situation	No	No change	No change
Baseline (BL)	BL-pre- climate change	hydrology 2013	No	current situation	No	No change	No change
	BL- post- climate change	hydrology 2018	No	current situation	No	No change	No change
Accidental Spill (AC)	AC1- pre	hydrology 2013	No	current situation	foam 1, location 48.277088, 14.349453 (WGS84)	No change	No change
	AC1- post	hydrology 2018	No	current situation	foam 1, location 48.277088, 14.349453 (WGS84)	No change	No change
	AC2- pre	hydrology 2013	No	current situation	foam 2, location 48.277088, 14.349453 (WGS84)	No change	No change
	AC2- post	hydrology 2018	No	current situation	foam 2, location 48.277088, 14.349453 (WGS84)	No change	No change

Scenario group	Scenario	Climate/ river dis- charge	PFAS produc- tion Gen- dorf	Legacy pollution	Accidental spill	Advanced treat- ment (PFAS)	PFAS use re- striction
Water pollu- tion control I (WPCI)	WPC1- pre	hydrology 2013	No	current situation	No	activated carbon at WWTP >10k PE	No change
	WPC1- post	hydrology 2018	No	current situation	No	activated carbon at WWTP >10k PE	No change
Water Pollu- tion Control II (WPCII)	WPC2- pre	hydrology 2013	No	Ground water redama- tion at hot spots	No	activated carbon at WWTP >10k PE	Restriction to essential use concept
	WPC2- post	hydrology 2018	No	Ground water redama- tion at hot spots	No	activated carbon at WWTP >10k PE	Restriction to essential use concept

G.8. Scenario results

G.8.1. Scenario result presentation

Based on the modelled river and bank filtration concentrations the sum of 10 PFAS is calculated and compared to the threshold of 100 ng/L for the sum of 20 PFAS of the EU drinking water directive (DWD). The resulting risk quotient is classified into the following 5 classes:

- Very low risk: <20 ng/L
- Low risk: 20–50 ng/L
- Medium risk: 50–100 ng/L
- High risk: 100–200 ng/L
- Very high risk: >200 ng/L

Based on the modelled river and bank filtration concentrations for each of 10 PFAS the PFOA-equivalent concentration is calculated using weighting factors from the proposal for a new EU EQS directive (EC COM(2022) 540 final). Then the 10 PFAS are summed and compared to the

proposed AA-EQS of 4.4 ng PFOA-eq/L for 24 PFAS. The resulting risk quotient is classified into the following 4 classes:

- Very low risk: <1 ng PFOA-eq/L
- Low risk: 1–2.5 ng PFOA-eq/L
- Medium risk: 2.5–4 ng PFOA-eq/L
- High risk: 4–5.5 ng PFOA-eq/L
- Very high risk: >5.5 ng PFOA-eq/L

MoRE Model Scenario Results at Bank-Filtration sites

Scenario results generated by different models at two riverbank filtration sites, Danube Vienna and Danube Budapest North, will be presented together for comparison. Table G 6 and Table G 7 show the results from the MoRE model. For results from other models, please refer to the main text of the Guidance Document.

Modelled river concentrations at Danube Vienna and Danube Budapest North were retrieved, and PFAS sums at these validation sites were calculated according to the EU DWD and draft EQS (EC COM(2022) 540 final) methods for the selected 10 PFAS substances. These sums were compared with base-variant model results to calculate the percentage change from the reference period. The percentage changes were applied to the PFAS sums from monitoring data, generating adjusted values, which were then assigned with river risk levels as described in the “Risk Maps” section.

Scenario results of the bank filtration model

See Figure G.3.

References

- Alaska DEC (2024). *Aqueous Film Forming Foam (AFFF)*. Publication Title: Alaska Department of Environmental Conservation - Division of Spill Prevention and Response - Contaminated Sites Program - PFAS. URL: <https://dec.alaska.gov/spar/csp/pfas/firefighting-foam/> (cit. on p. 207).
- Barzen-Hanson, K. A., S. C. Roberts, S. Choyke, K. Oetjen, A. McAlees, N. Riddell, R. McCrindle, P. L. Ferguson, C. P. Higgins, and J. A. Field (2017). “Discovery of 40 Classes of Per- and Polyfluoroalkyl Substances in Historical Aqueous Film-Forming Foams (AFFFs) and AFFF-Impacted Groundwater”. eng. In: *Environmental science & technology* 51.4, pp. 2047–2057. ISSN: 1520-5851. DOI: 10.1021/acs.est.6b05843 (cit. on p. 209).
- D’Agostino, L. A. and S. A. Mabury (2014). “Identification of novel fluorinated surfactants in aqueous film forming foams and commercial surfactant concentrates”. eng. In: *Environmental science & technology* 48.1, pp. 121–129. ISSN: 1520-5851. DOI: 10.1021/es403729e (cit. on p. 209).

Table G.6.: Monitoring and modelled PFAS sum at two validation sites, Danube Vienna and Danube Budapest North, and relative changes compared to the monitoring PFAS-sum.

Site	Variant	ΣPFAS_{10} (ng L ⁻¹) DWD (2020)	ΣPFAS_{10} (ng PFOA- eq L ⁻¹) draft EQS (2022)	ΣPFAS change (%) DWD (2020)	ΣPFAS change (%) draft EQS (2022)
Danube Vienna	Monitoring data	17.5	4.3	-	-
	Base model - reference period	27.4	6.0	0	0
	Baseline - Pre-climate change	8.4	3.6	-69	-40
	Baseline - Post-climate change	13.0	6.1	-53	2
	WPC1 - Pre-climate change	7.8	3.3	-72	-45
	WPC1 - Post-climate change	12.2	5.7	-55	-5
	WPC2 - Pre-climate change	4.9	2.0	-82	-67
	WPC2 - Post-climate change	7.7	3.8	-72	-37
Danube Budapest North	Monitoring data	20.5	5.9	-	-
	Base model - reference period	24.0	5.5	0	0
	Baseline - Pre-climate change	8.3	3.3	-65	-40
	Baseline - Post-climate change	12.6	5.6	-48	2
	WPC1 - Pre-climate change	7.6	3.0	-68	-45
	WPC1 - Post-climate change	11.8	5.1	-51	-7
	WPC2 - Pre-climate change	4.8	1.9	-80	-65
	WPC2 - Post-climate change	7.4	3.3	-69	-40

Table G.7.: PFAS sum and risk at two validation sites, after applying relative changes calculated in Table G.6

Site	Variant	Adjusted PFAS sum (ng L ⁻¹) (DWD)	Adjusted PFAS sum (ng PFOA-eq L ⁻¹) (draft EQS)	Adjusted Risk (DWD)	Adjusted Risk (draft EQS)
Danube Vienna	Base model - reference period	17.5	4.3	Very low: < 20 ng/L	High: 4-5.5 ng PFOA-eq/L
	Baseline - Pre-climate change	5.4	2.6	Very low: < 20 ng/L	Medium: 2.5-4 ng PFOA-eq/L
	Baseline - Post-climate change	8.2	4.4	Very low: < 20 ng/L	High: 4-5.5 ng PFOA-eq/L
	WPC1 - Pre-climate change	4.9	2.4	Very low: < 20 ng/L	Low: 1-2.5 ng PFOA-eq/L
	WPC1 - Post-climate change	7.9	4.1	Very low: < 20 ng/L	High: 4-5.5 ng PFOA-eq/L
	WPC2 - Pre-climate change	3.1	1.4	Very low: < 20 ng/L	Low: 1-2.5 ng PFOA-eq/L
	WPC2 - Post-climate change	4.9	2.7	Very low: < 20 ng/L	Medium: 2.5-4 ng PFOA-eq/L
Danube Budapest North	Base model - reference period	20.5	5.9	Low: 20-50 ng/L	Very high: >5.5 ng PFOA-eq/L
	Baseline - Pre-climate change	7.2	3.5	Very low: < 20 ng/L	Medium: 2.5-4 ng PFOA-eq/L
	Baseline - Post-climate change	10.7	6	Very low: < 20 ng/L	Very high: >5.5 ng PFOA-eq/L
	WPC1 - Pre-climate change	6.6	3.2	Very low: < 20 ng/L	Medium: 2.5-4 ng PFOA-eq/L
	WPC1 - Post-climate change	10	5.5	Very low: < 20 ng/L	High: 4-5.5 ng PFOA-eq/L
	WPC2 - Pre-climate change	4.1	2.1	Very low: < 20 ng/L	Low: 1-2.5 ng PFOA-eq/L
	WPC2 - Post-climate change	6.4	3.5	Very low: < 20 ng/L	Medium: 2.5-4 ng PFOA-eq/L

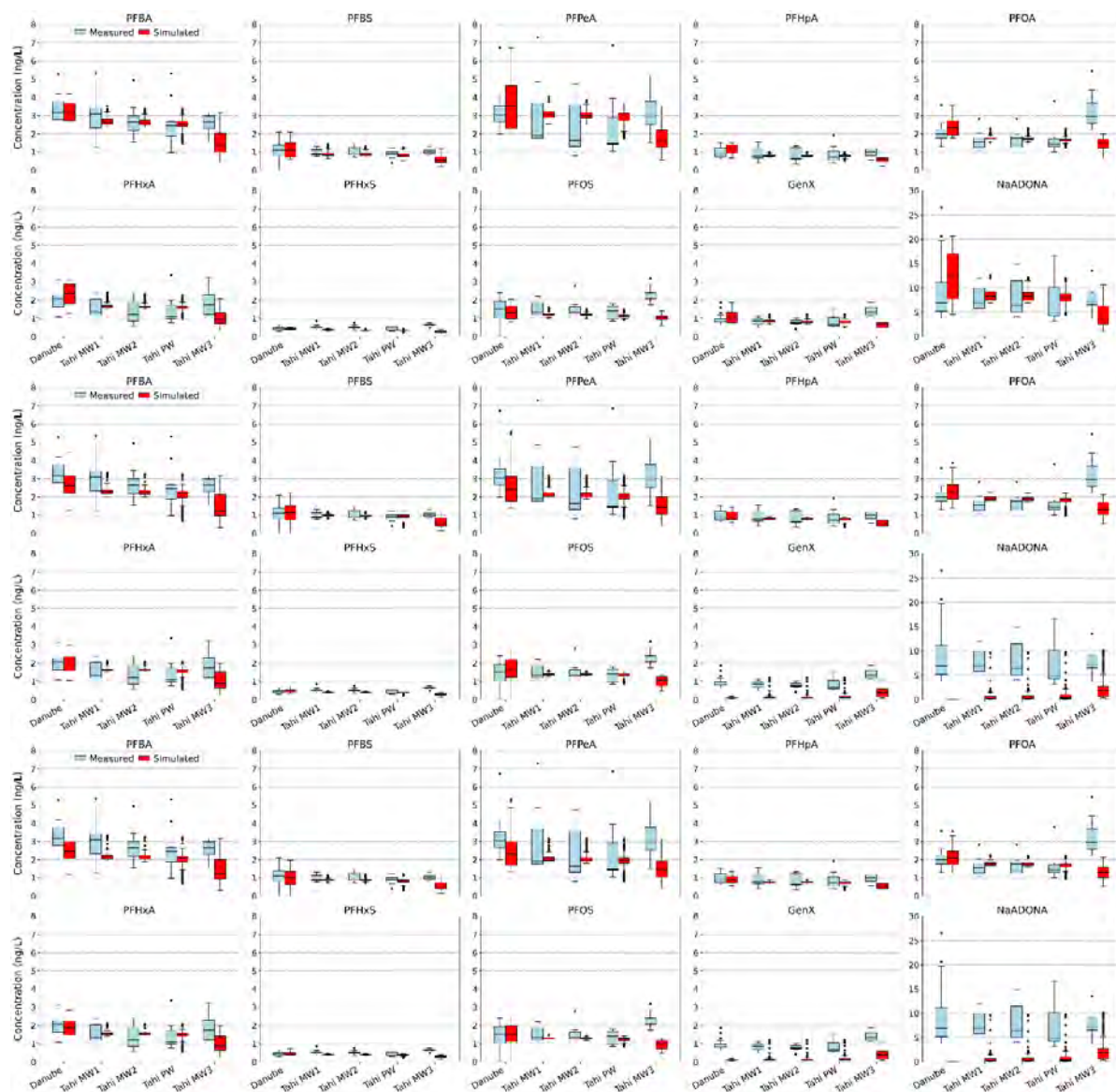


Figure G.3.: BF model results for reference period (top), scenario base line for post climate change conditions (middle) and scenario WPC1, post climate change (bottom)

- Dauchy, X., V. Boiteux, C. Bach, C. Rosin, and J.-F. Munoz (2017). “Per- and polyfluoroalkyl substances in firefighting foam concentrates and water samples collected near sites impacted by the use of these foams”. eng. In: *Chemosphere* 183, pp. 53–61. ISSN: 00456535. DOI: 10.1016/j.chemosphere.2017.05.056 (cit. on pp. 208, 209).
- EU DWD. *Directive (EU) 2020/2184 of the European Parliament and of the Council of 16 December 2020 on the quality of water intended for human consumption (recast)*. URL: <https://eur-lex.europa.eu/eli/dir/2020/2184/oj/eng>. (Cit. on p. 215).
- EC COM(2022) 540 final (2022). *Proposal For A Directive Of The European Parliament And Of The Council amending Directive 2000/60/EC establishing a framework for Community action in the field of water policy, Directive 2006/118/EC on the protection of groundwater against pollution and deterioration and Directive 2008/105/EC on environmental quality standards in the field of water policy*. URL: https://environment.ec.europa.eu/publications/proposal-amending-water-directives_en (visited on 10/26/2022) (cit. on pp. 207, 214, 215).
- ECHA (2023). *ECHA publishes PFAS restriction proposal*. European Chemical Agency. URL: <https://echa.europa.eu/-/echa-publishes-pfas-restriction-proposal> (visited on 01/30/2025) (cit. on p. 210).
- Groot, H., A. Sosnowska, W. Peijnenburg, J. Meesters, A. Wintersen, V. Zhiteneva, N. Devau, J. Valstar, et al. (2025). “PROMISCES D2.3 Toolbox fate & transport modelling of PMTs in the environment”. in preparation. DOI: 10.3030/101036449. URL: <https://cordis.europa.eu/project/id/101036449/results> (cit. on p. 206).
- Houtz, E. F., C. P. Higgins, J. A. Field, and D. L. Sedlak (2013). “Persistence of perfluoroalkyl acid precursors in AFFF-impacted groundwater and soil”. eng. In: *Environmental science & technology* 47.15, pp. 8187–8195. ISSN: 1520-5851. DOI: 10.1021/es4018877 (cit. on p. 208).
- Inyang, M. and E. R. V. Dickenson (2017). “The use of carbon adsorbents for the removal of perfluoroalkyl acids from potable reuse systems”. eng. In: *Chemosphere* 184, pp. 168–175. ISSN: 00456535. DOI: 10.1016/j.chemosphere.2017.05.161 (cit. on p. 211).
- Jans, A. C. H. and R. P. M. Berbee (2020). *Bronnen van PFAS voor het Nederlandse oppervlaktewater Onderzoek uitgevoerd in opdracht van IenW DGWB voor de Werkgroep Aanpak Opkomende Stoffen*. Tech. rep. Rijkswaterstaat (cit. on p. 207).
- Laaha, G., K. Haslinger, D. Koffler, J. Parajka, W. Schöner, A. Viglione, J. Zehetgruber, and G. Blöschl (2016). “Ein Drei-Standbeine-Ansatz zur Ermittlung zukünftiger Niederwasserabflüsse in Österreich”. In: *Österreichische Wasser- und Abfallwirtschaft* 68.1-2, pp. 54–57. ISSN: 0945-358X. DOI: 10.1007/s00506-015-0284-1 (cit. on p. 204).
- Mailler, R., J. Gasperi, Y. Coquet, S. Deshayes, S. Zedek, C. Cren-Olivé, N. Cartiser, V. Eudes, A. Bressy, E. Caupos, R. Moilleron, G. Chebbo, and V. Rocher (2015). “Study of a large scale powdered activated carbon pilot: Removals of a wide range of emerging and priority micropollutants from wastewater treatment plant effluents”. eng. In: *Water research* 72, pp. 315–330. ISSN: 1879-2448. DOI: 10.1016/j.watres.2014.10.047 (cit. on p. 211).
- Metzger, S., A. Rößler, and H. Kapp (2012). *Erweiterung des Klärwärks Mannheim um eine Adsorptionsstufe zur Verbesserung der Abwasserreinigung*. Tech. rep. Hochschule Biberach (cit. on p. 211).
- Pozo, K., L. B. Moreira, P. Karaskova, P. Přibyllová, J. Klánová, M. U. Carvalho, L. A. Maranhão, and D. M. Souza Abessa (2022). “Using large amounts of firefighting foams releases per- and polyfluoroalkyl substances (PFAS) into estuarine environments: A baseline study in Latin America”. eng. In: *Marine pollution bulletin* 182, p. 113938. ISSN: 1879-3363. DOI: 10.1016/j.marpolbul.2022.113938 (cit. on pp. 206, 209).

- EC COM(2022) 541 final (Oct. 26, 2022). *Proposal for a DIRECTIVE OF THE EUROPEAN PARLIAMENT AND OF THE COUNCIL concerning urban wastewater treatment (recast)*. URL: https://environment.ec.europa.eu/document/download/a936c2d5-2e3a-4eb1-a7c6-41ec98f3e72f_en?filename=Proposal%20for%20a%20Directive%20concerning%20urban%20wastewater%20treatment%20%28recast%29.pdf (cit. on p. 209).
- Rößler, A. and M. A. Launay (2019). “Durchführung von Vergleichsmessungen zur Spurenstoffelimination beim Ausbau von Kläranlagen um eine 4. Reinigungsstufe”. In: Place: Stuttgart Publisher: Kompetenzzentrum Spurenstoffe Baden-Württemberg, p. 48. URL: https://koms-bw.de/cms/content/media/2019_07_Abschlussbericht%20KomS_Vergleichsmessungen%20zur%20Spurenstoffelimination.pdf (cit. on p. 211).
- Weiner, B., L. W. Y. Yeung, E. B. Marchington, L. A. D’Agostino, and S. A. Mabury (2013). “Organic fluorine content in aqueous film forming foams (AFFFs) and biodegradation of the foam component 6:2 fluorotelomermercaptoalkylamido sulfonate (6:2 FTSAS)”. In: *Environ. Chem.* 10.6, p. 486. DOI: 10.1071/EN13128 (cit. on p. 209).